

Miniaturized Analytical Systems for Mass Spectrometry-Based Protein Studies

THÈSE N° 4507 (2009)

PRÉSENTÉE LE 30 OCTOBRE 2009

À LA FACULTÉ SCIENCES DE BASE

LABORATOIRE D'ÉLECTROCHIMIE PHYSIQUE ET ANALYTIQUE

PROGRAMME DOCTORAL EN CHIMIE ET GÉNIE CHIMIQUE

ÉCOLE POLYTECHNIQUE FÉDÉRALE DE LAUSANNE

POUR L'OBTENTION DU GRADE DE DOCTEUR ÈS SCIENCES

PAR

Mélanie ABONNENC

acceptée sur proposition du jury:

Prof. P. Vogel, président du jury
Prof. H. Girault, directeur de thèse
Prof. F. Foret, rapporteur
Prof. J. Peter-Katalinic, rapporteur
Prof. Ph. Renaud, rapporteur



ÉCOLE POLYTECHNIQUE
FÉDÉRALE DE LAUSANNE

Suisse
2009

À mes parents.

REMERCIEMENTS

Je tiens tout d'abord à adresser mes plus chaleureux remerciements à mon Professeur, Hubert Girault, qui m'a fait confiance en m'ouvrant les portes de son laboratoire afin d'accomplir ce travail de thèse. Je lui suis particulièrement reconnaissante pour la liberté qu'il m'a permis d'avoir dans mon travail, me permettant ainsi de gérer et mener à bien mes recherches comme je le souhaitais. Merci également pour tous ses encouragements et ses conseils concernant mon avenir.

Si j'en suis arrivée là aujourd'hui, c'est aussi grâce à différentes rencontres, toutes très enrichissantes. Mon parcours dans la recherche a débuté suite à ma rencontre avec le Dr. Alexandra Fuchs qui a encadré mon stage de Master, au sein du laboratoire Biopuces, au CEA de Grenoble, dirigé à l'époque par François Châtelain. Je les remercie de m'avoir orientée sur le chemin de l'Italie ainsi que de m'avoir encouragée à accomplir un doctorat. Je tiens à remercier tous mes anciens collègues et amis du laboratoire Biopuces et en particulier, Delphine Freida avec qui ce fut un immense plaisir de travailler. Merci également à Guillaume Colas, Maud Vernaz-Gris, Stéphanie Combe, Maxim Balakirev...

Mon aventure scientifique s'est ensuite poursuivie en Italie. Je voudrais adresser mes remerciements au Dr. Nicolò Manaresi qui m'a ouvert les portes de son entreprise, Silicon Biosystems, ainsi que pour ses nombreux encouragements. J'exprime ma profonde gratitude à tous mes anciens collègues et amis, les Drs. Luigi Altomare et Aldo Romani, et tous les doctorants et stagiaires de l'époque. Les apéritifs après le travail me manquent énormément ! Merci au Dr. Maximilian Sergio pour son amitié, pour tous les « debuggages » Linux, et pour m'avoir encouragée à venir à l'EPFL. Merci également à Tatiana, Antonio, « Pelato », Renato, Jaime, Enrique, Luca, Paul, Andrea, Bruno, Gianni, Martina, Monica...

Je remercie toutes celles et ceux sans qui cette thèse ne serait pas ce qu'elle est. Mes plus sincères remerciements vont donc à tous les chercheurs et membres du LEPA. Merci aux Drs. Jacques Josserand, Niels Lion, Jean-Marc Busnel, Gaëlle Proczek, Christophe Roussel

pour toutes nos discussions scientifiques ou autres, ainsi que pour leur amitié. J'ai une pensée particulière pour Gaëlle qui, en plus de son soutien, a eu le courage de relire ma thèse. Merci à tous mes collègues doctorants, Michel, Momo, Rahele, Meiqin, Imren, Reza, Anne-Laure, Brice, Hongyan, Peiyu, Yu, Liang, Fernando, Manuel, Astrid, et tous ceux que j'oublie. Je remercie également Valérie Devaud pour son amitié et surtout pour tous les conseils scientifiques et astuces qu'elle m'a donnés tout au long de ma thèse. Un grand merci à notre secrétaire Maria Szuman, ainsi qu'à Sandra Jeanneret, Anne-Lene Odegard, et à l'Ecole doctorale pour leur aide administrative durant ma thèse.

Je remercie également les membres de mon jury de thèse, les Professeurs F. Foret, J. Peter-Katalinic et Ph. Renaud pour avoir accepté de juger ce travail, ainsi que le Professeur P. Vogel pour avoir présidé mon jury de thèse.

Je tiens à saluer et remercier mes amis de toujours qui comptent beaucoup pour moi, Aurélie et Rémy, Belinda, Véronique, Claire ma binomette, Laëtitia, Marion...

Je voudrais finir ces remerciements en évoquant ma famille qui a toujours été présente dans les bons, comme dans les mauvais moments. Tout d'abord, je tiens à remercier mes parents pour m'avoir toujours encouragée dans mes choix aussi surprenants qu'ils puissent être parfois. Un immense merci à ma sœur, Isabelle, pour avoir toujours été à mes côtés et pour tous ses encouragements. Un grand merci aussi à Rose, Hamid, à mes beaux-parents Annick et Gérard, ainsi qu'à Claire et Grégory pour leur soutien. J'ai une pensée également pour mes grands-parents. Je n'oublie pas non plus mes nombreux cousin(e)s, tantes et oncles qui m'ont toujours motivée.

Je tiens à remercier de tout mon coeur Loïc pour son soutien, ses encouragements et sa patience. La thèse est une longue épreuve pour le thésard, mais également pour ceux qui l'entourent... Merci également pour toutes les discussions scientifiques très enrichissantes que nous avons pu avoir, ainsi que pour les heures passées à la re-lecture de ma thèse.

RÉSUMÉ

Les stratégies, actuellement mises en œuvre dans le domaine de la protéomique, reposent principalement sur le développement de méthodologies analytiques et instrumentales. Ainsi, parallèlement au développement d'analyses basées sur la détection par spectrométrie de masse (SM), il émerge des systèmes microfluidiques permettant entre autres de réaliser des analyses rapides et sensibles. Dans ce contexte, le présent travail de thèse s'intéresse au développement de systèmes analytiques miniaturisés pour l'analyse de protéines, notamment couplés à la SM.

Plusieurs approches ont été rapportées dans la littérature pour l'analyse de peptides tryptiques par SM et mettant en œuvre des marquages chimiques. Ces approches ont généralement pour but d'isoler spécifiquement des sous-classes par affinité, ou sont utilisées à des fins de quantification. En microfluidique, le flux est généralement laminaire, ce qui implique que le mélange, et par conséquent l'avancement de réaction, sont aussi contrôlés par la diffusion des réactifs. Ainsi, une étude par éléments finis de l'optimisation d'une réaction de marquage chimique dans un mélangeur-réacteur de type « sandwich » a été menée. Ce type de réacteur permet de mélanger deux solutions de réactifs, l'une de ces solutions étant « prise en sandwich » entre deux flux contenant le second réactif. Les simulations numériques effectuées ont souligné l'importance du positionnement du réactif présentant le plus faible coefficient de diffusion le long des parois du canal et ont montré que la diminution du débit des flux latéraux permet d'accroître le rendement de réaction grâce au profil parabolique du flux. Ces simulations rendent également compte de l'importance d'une telle optimisation dans le cas de réactions consécutives. Par ailleurs, les conclusions de cette étude sont directement applicables à des modifications chimiques de protéines dans un microcanal avant détection par SM.

Au vu des performances des microsystèmes d'infusion pour l'électrospray, une interface électrospray a été conçue par ablation laser. Dans un premier temps, le microsystème a été couplé avec succès à un montage CPL-SM et évalué par comparaison avec une source électrospray classique.

Afin de marquer spécifiquement les peptides élués par CPL directement sur le microsystème électrospray, une géométrie différente du mélangeur-réacteur de type « sandwich » a été

étudiée. Le mélangeur-électrospray conçu inclus une unité de mélange afin de perturber le flux et augmenter la réaction de marquage le long du microcanal. L'efficacité du mélangeur a été démontrée par microscopie par fluorescence et par le suivi de modification chimique de peptides par SM. Des études cinétiques ont également été menées par détection en SM. De plus, la modification en-ligne CPL-SM de peptides tryptiques cysteinés a permis une identification plus sûre et précise des protéines par « peptide mass fingerprinting » grâce à l'information fournie sur la séquence peptidique.

Ces dernières années, l'accent a été mis sur le développement d'unités analytiques miniaturisées. L'immobilisation de phases stationnaires fonctionnalisées dans un microcanal est communément utilisée afin d'isoler des peptides/protéines, de purifier, séparer un échantillon, ou pour effectuer des réactions. Dans ce contexte, les billes magnétiques apparaissent idéales par rapport à d'autres méthodes, notamment grâce à leur forte et réversible magnétisation, ainsi que les diverses fonctionnalisations de surface disponibles. Un microsystème incluant des rangées de pistes magnétiques de chaque côté du micro-canal a été réalisé afin de diriger le champs magnétique généré par des aimants permanents, vers des positions précises le long du micro-canal. Les billes s'organisent en multiples segments démontrant, à la fois numériquement et expérimentalement, une nette augmentation de la quantité de billes piégées, ce qui est favorable pour des applications de séparation par affinité.

En ce qui concerne les microsystèmes interfacés à la SM, la recherche s'oriente actuellement vers le développement de sources « multi-électrospray » pour des analyses à haut débit. Un microsystème avec plusieurs canaux parallèles a alors été développé. L'efficacité de ce microsystème pour l'analyse successive du contenu de six canaux, et la quantification relative des échantillons par SM, a été démontrée.

Les techniques douces d'ionisation ont révolutionné l'analyse des protéines par SM. Ainsi, contrairement à la majeure partie de ce travail qui traite de microsystèmes, cette dernière étude présente une nouvelle méthode d'ionisation ambiante, appelée ionisation par désorption sur membrane (M-DESI). Le principe est similaire à l'ionisation par désorption (DESI). Dans le cas du M-DESI, l'échantillon est désorbé à partir d'une membrane située dans l'axe entre la source électrospray et l'entrée du SM. Le concept a été validé par l'analyse de peptides et de protéines, offrant des perspectives pour la détection après séparation sur membrane.

Mots clés : Microfluidique, spectrométrie de masse, électrospray, ionisation par désorption, mélange, réaction, chimie analytique, protéine, protéomique.

ABSTRACT

Current proteomic strategies depend strongly on the development of analytical methodologies and instrumentation. In parallel to the development of mass spectrometry (MS) - based proteomic workflows, microfluidic devices emerged in this field as a flexible tool for rapid and sensitive protein studies. In this context, the present work focuses on the development of miniaturized analytical systems for protein studies, especially by electrospray ionization mass spectrometric detection.

Several approaches have been proposed to complement the mass spectrometric analysis of tryptic peptides using chemical tagging to isolate specific subclasses of proteins by affinity baits or for quantitation purposes. Optimization of a chemical tagging reaction in a sandwich mixer-reactor that consists of mixing two solutions providing the reactants in a channel, one central laminar flow being sandwiched between two outer flow solutions, was first investigated by finite-element method. The numerical simulations have highlighted the importance of positioning the reactant presenting the lowest diffusion coefficient close to the sidewall, as well as decreasing the outer flow velocities, to enhance a chemical reaction because of the parabolic flow profile across the microchannel. This optimization is even more relevant for consecutive reactions.

As infusion-based electrospray microchips are known to present great advantages in terms of sensitivity compared to standard ionization source, an ESI emitter microchip based on polymer photo-ablation was designed. First, the hyphenation of the chip in a LC-MS workflow was successfully achieved and evaluated by comparison with a standard pneumatically-assisted ESI source.

To perform enhanced on-chip post-column derivatization of peptides, a substitute design to the sandwich mixer-reactor was explored to improve reaction in a microchip before ESI – MS analysis. The electrospray micromixer chip includes a passive mixing unit to perturbate the flow along the microchannel. The mixing efficiency was demonstrated by fluorescence imaging, and on-chip chemical derivatization of peptides and kinetic studies before mass spectrometry were achieved. The on-line LC-MS derivatization of cysteinyl peptides was shown to provide a more confident and accurate protein identification by adding information on the peptidic sequence.

Within the development of electrospray microchips for mass spectrometry, many efforts have been put forward in the hyphenation of functional units. Immobilization of functionalized stationary phase in microfluidic systems is widely used to achieve protein or peptide isolation, sample cleaning, separation or reaction. In this context, magnetic beads have proven to be quite useful compared to other methods, such as immobilized packed beads or monoliths, because of their high and reversible magnetization, and various surface functionalization. A polymer microchip including a magnetic track array was designed to focus the magnetic field generated by permanent magnets towards precise locations along the microchannel. A multi-plug magnetic bead capture was obtained and a significant increase of bead capture efficiency was demonstrated both numerically and experimentally, which is beneficial for affinity separation applications, as example.

The research in microfluidic front-end devices for mass spectrometry is actually oriented to the development of multi-spray interfaces for high-throughput analysis. An electrospray microchip with a multi-track array was developed. The capability of the device to screen alternatively up to six samples and to perform relative quantification was assessed.

Soft ionization techniques have revolutionized the analysis of proteins by mass spectrometry. In contrast with the major content of the thesis dealing with microfluidic systems for protein analysis, the last chapter presents a novel ambient ionization method, so-called membrane-desorption electrospray ionization (M-DESI). The principle is similar to the desorption electrospray ionization (DESI) method. But, in the M-DESI approach the sample is desorbed directly from a mesh membrane positioned vertically and in-axis between the ESI emitter and the mass spectrometer inlet. Analysis of peptides and proteins was demonstrated as a proof-of-concept, offering great perspectives for detection after separation on membrane.

Keywords: Microfluidics, mass spectrometry, electrospray ionization, desorption ionization, mixing, reaction, analytical chemistry, protein, proteomics.

LIST OF ABBREVIATIONS

APCI	Atmospheric pressure chemical ionization
AP-MS	Atmospheric pressure mass spectrometry
APTDI	Atmospheric pressure thermal desorption ionization
ASAP	Ambient solid analysis probe
BLA	β -lactoglobulin A from bovine milk
BQ	Benzoquinone
BSA	Bovine serum albumin
CE	Capillary electrophoresis
CEC	Capillary electrochromatography
cICAT	Cleavable isotope-coded affinity tag
cIEF	Capillary isoelectric focusing
CRM	Charge residue model
DAPCI	Desorption atmospheric pressure chemical ionization
DAPPI	Desorption atmospheric pressure photo-ionization
DART	Direct analysis in real time
DBDI	Dielectric barrier discharge ionization
DESI	Desorption electrospray ionization
DeSSI	Desorption sonic spray ionization
DI	Desorption ionization
DIGE	Difference gel electrophoresis
DNA	Deoxyribonucleic acid
DTT	1,4-Dithio-DL-threitol
E-CTFE	Ethylene monochlor trifluor ethylene
EESI	Extractive electrospray ionization
ELDI	Electrospray laser desorption ionization
ELISA	Enzyme linked immunosorbent assay
EOF	Electroosmotic flow
ESI	Electrospray ionization

ETFE	ethylene tetrafluor ethylene
EWOD	Electrowetting-on-dielectric
FA	Formic acid
FD-ESI	Fused droplet electrospray ionization
FE	Finite elements
FT-ICR	Fourier transform ion cyclotron resonance
GE	Gel electrophoresis
HAPGDI	Helium atmospheric pressure glow discharge ionization
HGP	Human genome project
HPLC	High performance liquid chromatography
HUPO	Human proteome organisation
IA-CE	Immunoaffinity capillary electrophoresis
IC	Ion counts [counts·s ⁻¹]
ICAT	Isotope-coded affinity tag
iTRAQ	Isobaric tag for relative and absolute quantification
IEF	Isoelectric focusing
IEM	Ion evaporation model
IT	Ion trap
LAESI	Laser ablation electrospray ionization
LC	Liquid chromatography
MALDESI	Matrix - assisted laser desorption electrospray ionization
MALDI	Matrix - assisted laser desorption ionization
MB	Magnetic bead
M-DESI	Membrane - desorption electrospray ionization
mRNA	Messenger RNA
MS	Mass spectrometry
MS ²	Tandem mass spectrometry
MTEC	Multi-track electrospray chip
MudPIT	Multidimensional protein identification technique
<i>m/z</i>	mass-to-charge ratio
ND-EESI	Neutral desorption extractive electrospray ionization
NMR	Nuclear magnetic resonance
P	Peptide

PA	Polyamide	
PADI	Plasma - assisted desorption ionization	
PDMS	Polydimethylsiloxane	
PE	Polyethylene	
PET	Polyethylene terephthalate	
PDF	Pressure-driven flow	
PMMA	Poly(methyl methacrylate)	
PMF	Peptide mass fingerprinting	
PTFE	Polytetrafluoroethylene	
PTM	Post-translational modification	
PVDF	Polyvinylidene Fluoride	
QAT	Quaternary amine tag	
RNA	Ribonucleic acid	
RP	Reversed-phase	
SCX	Strong cation exchange	
SDS	Sodium dodecyl sulfate	
SPE	Solid phase extraction	
SSP	Surface sampling probe	
TFA	Trifluoroacetic acid	
TIC	Total ion current	[counts·s ⁻¹]
TLC	Thin-layer chromatography	
TM-DESI	Transmission mode – Desorption electrospray ionization	
TMT	Tandem mass tag	
ToF	Time-of-flight	
UV	Ultra-violet	
XPS	X-ray photoelectron spectroscopy	

LIST OF SYMBOLS

Roman alphabet

\mathbf{B}	magnetic flux density vector	[T]
c_i	concentration of the species i	[M or mol·l ⁻¹]
c_0	initial concentration	[M or mol·l ⁻¹]
d	distance	[m]
D_i	diffusion coefficient of the species i	[m ² ·s ⁻¹]
D	diffusion coefficient	[m ² ·s ⁻¹]
E	electric field strength	[V·m ⁻¹]
F	Faraday constant	96 485 C·mol ⁻¹
\mathbf{F}_{drag}	drag force vector	[N]
\mathbf{F}_{mag}	magnetic force	[N]
F_x	x -component of the force	[N]
F_y	y -component of the force	[N]
F_V	volumic flow rate	[m ³ ·s ⁻¹]
H	magnetic field strength	[A·m ⁻¹]
$2h$	microchannel width	[m]
i_{ES}	electrospray current	[A]
i_F	Faradaic current	[A]
\mathbf{J}_i	flux vector of the species i	[mol·m ⁻² ·s ⁻¹]
J	current density	[A·m ⁻²]
k	reaction rate constant (for a reaction of second order)	[M ⁻¹ ·s ⁻¹]
L	longitudinal length	[m]
L_m	magnet length	[m]
L_0	characteristic transversal length	[m]
m	magnetic moment	[A·m ²]
M	magnetization	[A·m ⁻¹]

pH	pH	[-]
pI	isoelectric point	[-]
p <i>K_a</i>	p <i>K_a</i>	[-]
<i>p</i>	pressure	[Pa]
<i>p</i> [*]	dimensionless pressure	[-]
<i>Q</i>	volumic flow rate	[m ³ ·s ⁻¹]
<i>r</i>	dimensionless interface width	[-]
<i>r_c</i>	capillary radius	[m]
<i>R</i>	radius	[m]
<i>R_i</i>	rate of consumption of the species <i>i</i>	[M·s ⁻¹]
<i>t</i>	time	[s]
<i>t</i> [*]	dimensionless time	[-]
<i>t_R</i>	residence time	[s]
<i>V</i>	linear velocity	[m·s ⁻¹]
<i>V</i>	bead volume	[m ³]
<i>V</i>	velocity vector	[m·s ⁻¹]
<i>V</i> [*]	dimensionless velocity vector	[-]
<i>v</i>	velocity	[m·s ⁻¹]
<i>v</i>	reaction rate	[m·s ⁻¹]
<i>W</i>	channel width	[m]
<i>x, X</i>	cartesian space coordinate	[m]
<i>y, Y</i>	cartesian space coordinate	[m]
<i>z, Z</i>	cartesian space coordinate	[m]
Re	Reynolds number	[-]
Pe	Péclet number	[-]
Da	Damköhler number	[-]

Greek alphabet

ξ	reaction extent	[%]
---	-----------------	-----

ε	permittivity of the solution	$[\text{J}^{-1} \cdot \text{C}^2 \cdot \text{m}^{-1}]$
ε_0	permittivity of the vacuum	$8.85419 \times 10^{-12} \text{ J}^{-1} \cdot \text{C}^2 \cdot \text{m}^{-1}$
κ	conductivity	$[\text{S} \cdot \text{m}^{-1}]$
γ	surface tension	$[\text{N} \cdot \text{m}^{-1}]$
δ_i	diffusion distance (transversal) of the species i	$[\text{m}]$
δ_h	thickness of a diffusion sub-layer	$[\text{m}]$
η	dynamic viscosity	$[\text{kg} \cdot \text{m}^{-1} \cdot \text{s}^{-1}]$
μ	dynamic viscosity	$[\text{kg} \cdot \text{m}^{-1} \cdot \text{s}^{-1}]$
μ	magnetic permeability	$[\text{H} \cdot \text{m}^{-1}]$
μ_0	magnetic permeability of vacuum	$4\pi \cdot 10^{-7} \text{ H} \cdot \text{m}^{-1}$
μ_r	relative permeability	$[-]$
χ	magnetic susceptibility	$[-]$
ν	kinematic viscosity ($\nu = \mu / \rho$)	$[\text{m}^2 \cdot \text{s}^{-1}]$
ρ	density	$[\text{kg} \cdot \text{m}^{-3}]$
Γ	surface concentration	$[\text{mol} \cdot \text{m}^{-2}]$

TABLE OF CONTENTS

CHAPTER I: Introduction.....	1
1. 2009, Darwin's anniversaries.....	1
2. From genomics to proteomics.....	2
3. Importance of analytical sciences in proteomics.....	4
3.1. The dynamic range problematic.....	4
3.2. Brief history of analytical developments in proteomics.....	5
3.3. Top-down and bottom-up approaches in proteomics.....	7
3.4. Tagging methods in proteomics.....	8
4. Towards miniaturization of analytical systems.....	10
4.1. Introduction and relevance of theoretical studies and numerical simulations.....	10
4.2. Miniaturization of ionization source in mass spectrometry.....	10
4.2.1. Demonstration of nano-spray efficiency.....	10
4.2.2. ESI – related microfluidic devices.....	12
4.2.3. MALDI – related microfluidic devices.....	15
OBJECTIVE OF THE WORK.....	17
REFERENCES.....	19

CHAPTER II: Numerical investigation of a sandwich mixer-reactor :

Influence of the diffusion coefficient and flow rate ratios.....	27
1. Introduction.....	27
2. Theory and numerical description.....	32
2.1. Theoretical description.....	32
2.2. Numerical model and validation.....	34
2.2.1. Numerical model and assumptions.....	34
2.2.2. Validation of the finite element model.....	35

2.2.2.1. Validation of the kinetic model.....	35
2.2.2.2. Validation of the convection-diffusion model.....	37
2.3. Numerical parameters, normalization, and calibration.....	39
2.3.1. Numerical parameters.....	39
2.3.2. Normalization of the results.....	40
2.3.3. Evaluation of the chemical / diffusional regime.....	40
2.3.4. Determination of the Péclet limit.....	42
2.3.5. Extent to well-known geometries.....	43
3. Results and Discussions	45
3.1. Gain due to the number of substreams ($D_B/D_A = 1$).....	45
3.2. Gain due to the diffusion coefficient ratio of the reactants in a sandwich mixer.....	45
3.2.1. Influence of the species diffusion coefficient ratio, for $k = 200 \text{ M}^{-1} \cdot \text{s}^{-1}$	45
3.2.2. Quantification of the parabolic flow profile contribution (PDF vs. EOF).....	49
3.2.3. Optimal vs. non-optimal sandwich design and extent to other kinetics ($k = 20, 200$, and $2000 \text{ M}^{-1} \cdot \text{s}^{-1}$).....	50
3.3. Gain due to the external flow rate Q_A decrease and local kinetics kc_A	53
3.3.1. Relation between the flow rate ratio and the external A layer thickness.....	53
3.3.2. Gain due to the external flow rate Q_A decrease and local kinetics kc_A	54
3.4. Application to a consecutive reaction.....	56
4. Conclusions.....	58
REFERENCES.....	60
APPENDIX II-1 : Finite-element formulation.....	63
APPENDIX II-2 : Complementary results.....	65
APPENDIX II-3 : Influence of the reactant concentration ratio.....	66

CHAPTER III: Hyphenation of a polymer electrospray emitter microchip to a LC-MS workflow.....	69
1. Introduction.....	69
2. Basics of electrospray ionization mass spectrometry.....	71
2.1. Overview of the electrospray process.....	71
2.2. From ions in solution to ions in gas-phase.....	72
2.2.1. Operating regimes.....	72
2.2.2. Steady cone-jet mode and charged droplet emission.....	73
2.2.3. ESI viewed as an electrochemical process.....	76
2.2.4. Two theories behind the gas-phase ion production from charged droplets.....	78
2.3. Practical considerations.....	80
3. Microfabrication of electrospray emitter microchips.....	81
3.1. UV laser ablation process.....	81
3.2. Excimer laser operation.....	83
3.3. ESI emitter microchip with integrated carbon electrode.....	84
3.4. Alternatives to the on-chip carbon electrode.....	85
4. Hyphenation of the electrospray emitter microchip to a LC-MS workflow : key features, issues and solutions.....	88
4.1. Material & Methods.....	88
4.2. Hyphenation of the electrospray emitter to a LC-MS analysis.....	92
4.2.1. Feasibility.....	92
4.2.2. Flow rate (F_v) considerations.....	94
4.2.3. Influence of the solvent composition on the analyte detection..	95
4.3. LC-MS analysis of a tryptic digest using an ESI microchip interface.....	96
4.3.1. Reproducibility of the tryptic digest analysis by LC-MS.....	96
4.3.2. LC-MS analysis with an ESI emitter microchip vs. a standard ESI source.....	98
4.4. Design and evaluation of the ESI emitter microchip with liquid junction.....	100
4.4.1. Microchip design and operation.....	100
4.4.2. Efficiency of the sheath liquid delivery.....	101

4.4.3. Effect of the on-chip sheath liquid on the ionization efficiency in LC-MS analyses.....	102
4.5. Towards the use of pre-column peptide modification to enhance peptide ionization efficiency	103
5. Conclusions.....	105
REFERENCES.....	106

CHAPTER IV: Electrospray micromixer chip for on-line derivatization

and kinetic studies.....	111
1. Introduction.....	111
2. Experimental section.....	115
3. Results and Discussions.....	118
3.1. Mixing efficiency with different groove geometries.....	119
3.2. MS evaluation of the electrospray micromixer for chemical modification of peptides.....	120
3.3. Comparative study of the reaction extent without and with mixing unit.....	122
3.4. Comparative study of the experimental reaction extent with a kinetic model.....	124
3.5. Evaluation of the reaction gain using the electrospray micromixer.....	127
3.6. On-line LC-MS derivatization of tryptic cysteinyl peptides of BSA.....	128
4. Conclusions.....	132
REFERENCES.....	134

CHAPTER V: Magnetic track array for efficient bead capture in

microchannels.....	137
1. Introduction.....	137

2. Theory and numerical description.....	138
2.1. Basics of magnetism.....	138
2.2. Magnetic beads in analytical sciences.....	140
2.3. Microfabrication and magnetic actuation.....	141
2.4. Magnetic bead transport in a microfluidic system.....	142
2.5. Numerical description.....	144
2.5.1. Numerical model and assumptions.....	144
2.5.2. Geometry and numerical parameters.....	145
3. Experimental section.....	146
4. Results and Discussions.....	150
4.1. Forces and magnet length.....	150
4.2. Magnetic track integration and field addressing.....	152
4.3. Magnetic force mapping and resulting magnetic bead capture.....	153
4.4. Design considerations.....	155
4.5. Relative quantification of the magnetic bead capture.....	157
5. Conclusions.....	159
REFERENCES.....	161
APPENDIX V-1 : Finite-element formulation.....	164

CHAPTER VI: Multi-track electrospray chip..... 165

1. Introduction.....	165
2. Experimental section.....	168
3. Results and Discussions.....	171
3.1. Proof-of-concept.....	171
3.1.1. Sample screening.....	171
3.1.1.1. Two-track microchip.....	171
3.1.1.2. Six-track microchip.....	172
3.1.2. Counting of cysteine residues in peptides.....	174
3.1.3. Relative quantification.....	176
3.2. Latest developments on the MTEC.....	177
4. Conclusions.....	181

REFERENCES.....	182
APPENDIX VI-1 : Switch box LavView interface.....	184
CHAPTER VII: Membrane desorption electrospray ionization (M-DESI)	
mass spectrometry.....	185
1. Introduction.....	185
2. Desorption electrospray ionization (DESI).....	187
3. Membrane – Desorption electrospray ionization (M-DESI).....	191
3.1. Experimental section.....	192
3.2. Results and Discussions.....	196
3.2.1. M-DESI of peptides and proteins.....	196
3.2.2. Mesh size and spray transmission.....	198
3.2.3. Gas flow considerations.....	199
3.2.4. Areas of the deposited sample and of the spray impact onto a membrane.....	200
3.2.5. Geometry considerations.....	202
3.2.6. Remarks on the membrane properties.....	203
5. Conclusions & Perspectives.....	203
REFERENCES.....	205
CHAPTER VIII: Conclusions & Perspectives.....	209
APPENDIX I : Amino acids.....	215
APPENDIX II : Basics of a mass spectrometer.....	217
<i>CURRICULUM VITAE.....</i>	223

CHAPTER I.

Introduction

1. 2009, Darwin's anniversaries

2009 marks the double anniversary of Charles Darwin's birth (1809) and the publication in 1859 of *On the Origin of Species by Means of Natural Selection*.¹ For the first time, the principles of evolution based on descent with *modification* and *natural selection* of favorable variants were evoked. At that time, Darwin's theory suffered of a lack of explanation on how the organisms pass traits on to their offspring. Like many of his contemporaries, he speculated that characteristics of the parents were blended as they passed on to the offspring. However, as evolution was due to random mutations, inheritance mechanisms would then result in quick disappearance of new traits. Ironically, a Darwin's contemporary, Gregor Mendel, "solved" the problem of heredity according to his study of the inheritance of certain traits in pea plants published in the short monograph, *Experiments with Plant Hybrids*.⁹ Mendel showed that the inheritance of these traits follows particular laws: hereditary factors do not combine but are passed intact; each member of parental generation transmits only half of its hereditary factors to each offspring (with certain factors "dominant" over others); and different offspring of the same parents receive different sets of hereditary factors. The significance of Mendel's work was not recognized until the turn of the 20th century with the advance of molecular biology. Its rediscovery prompted the foundation of the discipline of genetics.

Both theories from Darwin and Mendel were formulated from observations and hypotheses in the absence of fundamental principles that were yet to come to light. Thanks to their capacity of observation, curiosity, need of understanding, they established by means of suppositions (not always true) the foundations of the species evolution and genetics, developed later by

other scientists, but at his time highly debated. The evocation of these two pioneers seems a good starting point to this thesis, as they are good examples to follow mainly because of the scientific curiosity that animates their investigations.

Imagination [...] which is ever wandering beyond the bounds of truth, joined to self-love and that self-confidence we are so apt to indulge prompts us to draw conclusions which are not immediately derived from the facts; [...] Hence it is by no means surprising that, in the science of physics in general, men have so often formed suppositions, instead of drawing conclusions. These suppositions, handed down from one age to another acquire additional weight from the authorities by which they are supported, till at last they are received even by men of genius, as fundamental truths.” A.L. Lavoisier, *The Elements of Chemistry*, 1789.

Texte original adapté: *L'imagination [au contraire qui tend à nous porter continuellement au delà du vrai]; l'amour-propre & la confiance en nous-meme, qu'il sait si bien nous inspirer, nous sollicitent à tirer des conséquences qui ne dérivent pas immédiatement des faits [: en sorte que nous sommes en quelques façons intéressés à nous séduire nous-même]. Il n'est donc pas étonnant que dans les sciences physiques en général, on ait souvent supposé au lieu de conclure; que les suppositions transmises d'âge en âge, soient devenues de plus en plus imposantes par le poids des autorités qu'elles ont acquises, & qu'elles aient enfin été adoptées & regardées comme des vérités fondamentales, même par de très bons esprits.*”, A.L. Lavoisier, *Préface du Traité élémentaire de Chimie*, 1789.

2. From genomics to proteomics

Both Darwin and Mendel observed trait characteristics in species, now also known as phenotypes and established as resulting from the genome expression. The cellular machinery is relatively complex and nowadays the general mechanisms are well identified, as schematically illustrated in Figure I-1. Each individual is characterized by his own genetic code. The DNA located in the nucleus of cells is transcribed into RNA that after processing forms the mRNA, which carries a genetic message to the protein synthesizing machinery of the cell. Once in the cytoplasm of cells, the mRNA is then translated into a specific amino

acid sequence, known as protein. After synthesis, the proteins are submitted to maturation and modification steps, known as post-translational modifications (PTMs).¹⁴ PTMs are various and involve the addition of functional groups (alkylation, methylation, phosphorylation, glycosylation...) or structural changes (disulfide bridges, proteolytic cleavage...) that determine their tertiary and quaternary structures and, regulate their activity and function.

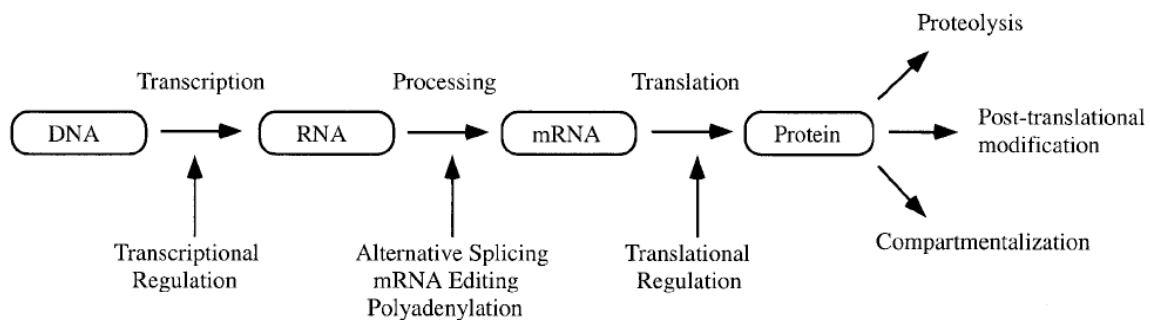


Figure I- 1 Mechanisms by which a single gene gives rise to multiple gene products. Multiple protein isoforms can be generated by RNA processing when RNA is alternatively spliced or edited to form mature mRNA. mRNA in turn, can be regulated by stability and efficiency of translation. Proteins can be regulated by additional mechanisms, including post-translational modification, proteolysis or compartmentalization. Reprinted from Ref.⁷

The sequence of the human genome encodes the genetic instructions for human physiology, as well as rich information about human evolution. The Human Genome Project (HGP) was launched in 1990 with the scope to entirely map the human genome, and was completed in 2003.¹⁵ Unexpectedly, the human genome seems to encode only 20'000 - 25'000 protein-coding genes. It has been estimated that each human genes through post-translational modifications and differential splicing can produce three or more proteins.^{16, 17} Consequently, the estimated number of proteins encoded by these genes is two to three orders of magnitude higher. It has become clear now that organism complexity is generated more by a complex proteome^a than a complex genome^b. In response to external factors, the proteome is indeed very dynamic with time and differs substantially between cell types.

^a The *proteome* is defined here as the proteins expressed in a cell at one time, including isoforms and protein modifications

^b The *genome* is defined as the complete set of DNA of an organism.

The “proteomics” field appeared in the middle of the 90’s and is dedicated to the analysis of the proteome.¹⁸ Proteomic researches can be either global or targeted, *i.e.* directed towards all proteins, or restricted to a well-defined group, such as glycoproteins, organelle proteins, or ribosomal proteins, for instance. It includes as well many areas of study as the protein-protein interactions, protein modifications, protein functions, protein localization, etc.

In a larger extent, the ability to identify a large number of proteins and characterize their differential expression and post-translational modifications, will contribute significantly to the understanding of biological systems in health, disease, and help for drug discovery.^{7, 18-20}

At the beginning of the 21st century a new paradigm came up, known as “Systems biology” that aims at system-level understanding of biological systems that in fact cannot be considered *only* at the molecule-level (*i.e.* as gene-, transcript-, protein-, metabolite-level, etc.) but as a dynamic system. More explicitly, systems biology focuses on all the components and the interactions among them, all as part of one system. These interactions are ultimately responsible for an organism’s form and functions.

3. Importance of analytical sciences in proteomics

3.1. The dynamic range problematic

The study of cellular extract is quite challenging mainly because of the dynamic range of protein expression.²¹ Figure I-2 illustrates the protein concentrations of plasma sample, which present a dynamic range of twelve orders of magnitude. Many proteins that are disease biomarkers generally exist in low abundance. The ability to identify and quantify such low abundant proteins depends strongly on the analytical workflow chosen and the sensitivity of the detection method. Sample preparation and intensive separation are therefore required to analyze complex cellular extracts.²²⁻²⁵ As proteins differ by their amino acid sequence, they present various physico-chemical properties in terms of molecular mass, charge, hydrophobicity, isoelectric point (pI) or conformation as well (Appendix I-1: Amino acids). Subsequently, many analytical separation systems can be applied to fractionate such complex protein samples.

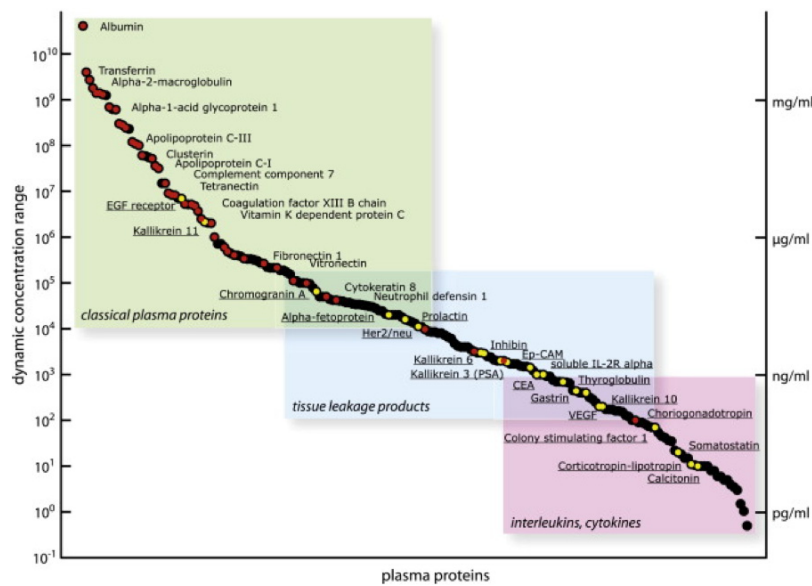


Figure I- 2 Plasma protein concentration as described by Anderson and Anderson². The proteins can be grouped in three main categories (classical plasma proteins, tissue leakage products, interleukins/cytokines). Red dots indicate proteins that were identified by the HUPO plasma proteome initiative⁵ and yellow dots represent currently utilized biomarkers. Reprinted from Ref.¹³

3.2. Brief history of analytical developments in proteomics

The first proteomic studies began in 1975 with the introduction of the two-dimensional (2D) gel electrophoresis by O'Farrel²⁶, Klose²⁷ and Scheele²⁸, respectively. Proteins are separated according to isoelectric focusing (IEF) in the first dimension, and according to molecular weight by sodium dodecyl sulfate (SDS) electrophoresis in the second dimension.²⁹ Although many proteins can be separated and visualized, the main limitations of this technique remain the amount of proteins that can be loaded, the difficulty to resolve low abundant proteins in complex samples as well as highly alkaline, extremely high and low molecular size protein groups, and finally, the need of parallel methods to sequence proteins. While Edman degradation was first used for protein post-sequencing after gel blotting, 2D gel electrophoresis has undeniably benefited by the progresses made in mass spectrometric (MS) techniques since they gave access to confident identification of proteins separated on the gels.

Since the demonstration in the late 80's of the analysis of biomolecules by electrospray ionization (ESI) and matrix-assisted laser desorption ionization (MALDI) mass spectrometry,

as well as the apparition of tandem mass spectrometry (MS/MS),^{30, 31} MS appears as the most sensitive and accurate technique for protein identification¹⁹ Driven by the need to identify, characterize, and quantify proteins at ever increasing sensitivity and in ever more complex samples, a wide range of new mass spectrometry-based analytical platforms and experimental strategies have emerged.^{19, 32-34} To provide good quality proteomic analysis, mass analyzers have to present several features, explicitly mass accuracy, sensitivity, resolution and capability to generate tandem mass spectra (Appendix II). In addition to instrumental developments, bioinformatic tools became essential as well, notably with the creation of databases and search engines.

Despite the development and widespread use of 2D gel electrophoresis coupled to MS detection, large-scale MS - based protein analysis started to be investigated more vigorously, mainly relying on gel-free separation techniques, such as liquid chromatography (LC) or capillary electrophoresis (CE).

Chromatographic techniques appeared in proteomics as a practical and reliable tool to analyze complex samples as the separation occurs in liquid phase with buffers compatible with MS. Chromatographic separations include a broad range of physical methods that separate components in complex mixtures in function of their distribution between two phases: a stationary-phase and a mobile phase that percolates through the stationary bed. The complex mixture enters the chromatographic column and the components migrate at different rates depending on their affinity for each of the phases. The higher the affinity a molecule has for the stationary phase, the longer the time needed to egress the column.^{35, 36} The most widely used liquid chromatographic methods in proteomics are the *reversed-phase chromatography* (RP, *e.g.* hydrophobic interaction chromatography), *ion exchange chromatography* (as strong cation exchange, SCX), *affinity chromatography* that is often used for the depletion of abundant proteins in samples, and *size-exclusion chromatography*.

An important feature in fractionation techniques concerns the peak capacity of the method. The larger is the peak capacity, the higher is the resolution. Orthogonal separations enhance significantly the separation efficiency of complex samples. 2D gel electrophoresis is typically an orthogonal separation technique as the molecular mass and *pI* of proteins are not physically related. Orthogonal separations were introduced in liquid chromatography by Yates with the so-called *Multidimensional Protein identification* technique (MudPit).^{37, 38} For the first time, the analysis of *S. Cerevisiae* proteome was performed by a combination of SCX-RP liquid chromatography tandem mass spectrometry workflow.

The development of LC-MS or LC-MS/MS workflows, eventually combined with multi-dimensional separations, was a real advance in the study of complex mixtures of proteins. The most commonly used MS-based proteomic workflows (top-down and bottom-up approaches) will be detailed in the section below.

Finally, capillary electrophoresis (CE) and its variants (capillary electrochromatography (CEC), capillary isoelectric focusing (cIEF), were also successfully coupled on-line to MS. Gel-free electrophoretic separation in combination with MS provide a powerful technique that opens the door for rapid, efficient and sensitive analysis with a limited sample consumption.³⁹

3.3. Top-down and bottom-up approaches in proteomics

Advances in MS-based proteomic workflows rely on multidimensional separation concepts, sensitive mass spectrometers, and powerful bioinformatics tools. The actual research focused on protein identification is oriented towards two main ways: the top-down and bottom-up strategies, as illustrated in Figure I-3.

In *top-down* strategies the protein identification and characterization is based on subjecting intact protein ions and large protein fragments directly to tandem mass spectrometry. Such approaches require high-resolution mass spectrometers.⁴⁰⁻⁴² In contrast, in the *bottom-up* strategy, the protein identification is based on mass spectrometric analysis of peptides derived from proteolytic digestion of a protein complex mixture, eventually after a 2D gel electrophoresis separation. Different methodologies were explored in the bottom-up approach. The first so-called *Peptide Mass Fingerprinting (PMF)* consists in enzymatically-digested proteins. The mass of the resulting tryptic peptides allows the identification of the parent proteins by mean of bioinformatics tools. This method relies on the accuracy of the mass spectrometer and is efficient only with relatively simple protein mixture, typically resulting from 2D gel electrophoresis.⁴³ It has been also demonstrated that adding information on the peptidic sequence (as the number of rare amino acids like cysteines) enhances the confidence in the protein identification by PMF.⁴⁴ The other identification methodology consists in *MS/MS sequencing* of the tryptic peptides and confronting the experimental to the theoretical mass fragments from databases. It is typically applied in the

shotgun approach, consisting in digesting of complex protein mixtures followed by analysis of the tryptic peptides by multi-dimensional liquid chromatography and MS/MS. The shotgun method permits the analysis of very complex samples. The challenge here is to deal with the high quantity of data generated by MS/MS analysis. Now, highly performing softwares are available to deal with MS/MS spectra and database searching.⁴⁵⁻⁴⁷

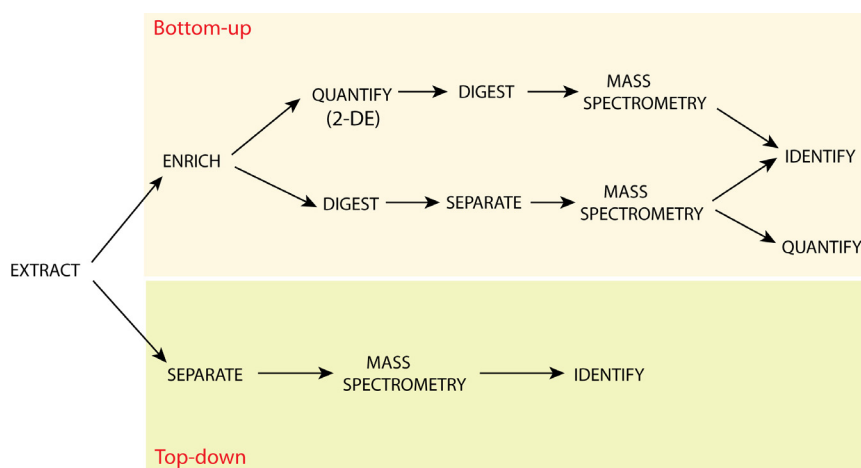


Figure I- 3 General scheme of the top-down and bottom-up approaches in MS-based proteomics.

3.4. Tagging methods in proteomics

Chemical tagging in MS – based protein studies are used for various purposes to help their identification and characterization.^{48, 49}

First, protein (or peptide) modification by the attachment of affinity tags can enable selecting a subset of proteins/peptides according to certain properties or presence of a specific amino acid. Typically, it is used to enrich the peptides carrying certain PTMs or to identify low abundant proteins. As example, in phosphoproteomic studies, chemical tagging reactions are predominantly based on the β -elimination of phosphate (p) groups in pSer and pThr residues under alkaline conditions, followed by a Michael-type addition of a thiol compound. Tags may be differentially isotope-coded or include a recognition site for affinity enrichment.^{50, 51} Secondly, labels in protein studies have proven to be useful tools for relative and absolute quantitation.^{52, 53} In 2D gel electrophoresis, the *difference gel electrophoresis* (DIGE) is used

as a quantitation tool. CyDye fluors that are spectrally resolvable (Cy2, Cy3, Cy5) and matched for mass and charge are used to covalently modify the ϵ -amino group of lysines in proteins via an amine linkage. The labeled samples are combined and run in a single gel to allow better spot matching and minimize gel-to-gel variations. In gel-free approach, *stable isotope labeling* was introduced for MS-based protein quantitation of different samples representative of different states. One widely used quantitation method is the isotope-coded affinity tags (ICAT) developed by Aebersold and co-workers.⁵⁴ Essentially, proteins from the two states to be compared are labeled at cysteine residues with respectively, light and heavy tags carrying a biotin moiety. The labeled proteins are then mixed and digested. After a cation exchange chromatography step to remove excess reagent, the mixed peptides are affinity purified using immobilized avidin. The peak intensities of the peptides, discriminated by the mass difference, correlate directly with the relative abundance of the proteins in the two states. An improved version of the tag, namely cleavable ICAT (cICAT) reagent employs ^{13}C isotopes and an acid-cleavable biotin group.^{55, 56} More recent quantitative methods are the isobaric tagging with isobaric tags for relative and absolute quantification (iTRAQ)⁵⁷ and tandem mass tags (TMT)⁵⁸. Both tag technologies employ an x -plex set of amine reactive isobaric tags to derivatize peptides at the N-terminus and the lysine side chains, thereby labeling all the peptides in a digest mixture. In MS, peptides labeled with any of the isotopic tags are indistinguishable (as isobaric). Upon fragmentation in MS/MS, signature ions are produced, which provide quantitative information upon integration of the peak area. This succinct list of quantitation-devoted labels, present the tags most commonly used in current proteomics studies. The three quantitation methods, DIGE, cICAT and iTRAQ, were recently compared yielding reasonably good results and highlighting their complementarities.⁵³ At last, the modification of functional groups in peptides can improve their sensitivity for MS detection. In some case, chemical tagging steps are employed to influence the fragmentation behavior of peptides, facilitating *de novo* sequencing.⁵⁹ As another example, Regnier's group notably worked on the derivatization of amino acids by hydrophobic quaternary amine tags to facilitate their ionization by reversed-phase LC-MS.⁶⁰

4. Towards miniaturization of analytical systems

4.1. Introduction, and relevance of theoretical studies and numerical simulations

It is foreseen that miniaturized systems will eventually provide improved performance in analytical chemistry, in fields as diverse as bioanalysis, drug analysis, on-site environmental and industrial monitoring, homeland security, clinical, and forensic studies. The driving force of miniaturization is the low reagent and time consumption, the portability, the lower cost and high-throughput.⁶¹⁻⁶³ Since the 90's, this field has grown up rapidly and a plethora of microfluidic devices appeared in the literature. In any case, the device must be designed and optimized in accordance to the requirements of a specific application.

Numerical simulation is a great tool that is useful in many fields including microfluidics. A recent review from Boy presents the advantages of using simulations, and also reports that only "25% of the microfluidic papers also contain simulations".⁶⁴ Indeed, numerical simulations enable going more in depth in the understanding and characterization of physico-chemical phenomena. In this thesis some investigations were supported by finite-element simulation in order to understand physical phenomena and optimize the design of the microsystems.

4.2. Miniaturization of ionization source in mass spectrometry

4.2.1. Demonstration of nano-spray efficiency

In parallel to the developments of MS-based proteomics workflows described above, microfluidic devices established themselves in the mass spectrometry's community, as illustrated by the raising number of publications observed these last 10 years. The first step towards miniaturization was the introduction of nanospray ionization by Wilm and Mann in 1994.⁶⁵ They demonstrated both by theoretical descriptions and experiments, the benefits of using nanoliters per minute flow rates, leading to an increase of sensitivity because of the emission of small droplets (< 200 nm) during the electrospray process. Subsequently, the sample required for the analysis is rather small (< 1 μ L), nebulizing gas can be avoided and a diminution of the ion suppression phenomenon is observed. However, nanosprays present some issues as the emitter tip clogging and the limited range of possible flow rates. It is notably circumvented by the design of multi-spray emitters.⁶⁶

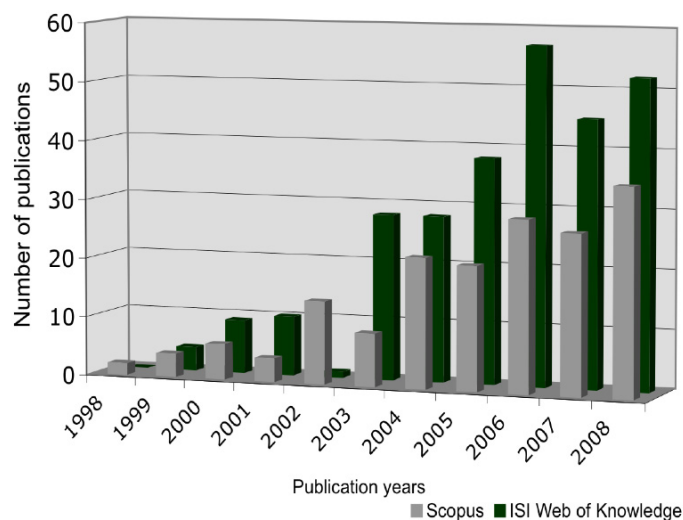


Figure I- 4 Evolution of the number of publication about miniaturized bio-analytical systems in the last ten years. (Search in Scopus and ISI Web of Knowledge: microfluidic, chip, mass spectrometry).

The terminology about nano- and micro-electrospray is not well defined. In the literature, it is often encountered that nano-electrospray concerns flow rate lower than $100 \text{ nL}\cdot\text{min}^{-1}$, and micro-electrospray from 100 to $1000 \text{ nL}\cdot\text{min}^{-1}$. However, the terminology could also refer to the dimensions of the electrospray emitter, or the “real” flow rate units, *i.e.* nanoliter or microliter per minute range. In the terminology used in the present thesis micro-electrospray are defined as being operated at flow rates higher than $1 \mu\text{L}\cdot\text{min}^{-1}$.

Since the demonstration of the benefits of using smaller ESI emitters, the field of microfluidic chips for mass spectrometry has grown rapidly. The groups of Karger, Ramsey and Aebersold were among the first to realize the advantages of microchips in protein sample preparation for ESI-MS, and have played a prominent role in the initial demonstration of the promise of chip-MS for protein analysis.^{6, 67-69} Till now, there has been a real fervour to develop novel miniaturized systems coupled to mass spectrometers. Some recent reviews covered this field presenting the various developments of electrospray emitter devices as well as the microfluidics developments in matrix-assisted laser desorption ionization mass spectrometry.⁷⁰⁻⁷⁷ In parallel, and driven by the desire of building a portable analytical platform, several researches were carried out to miniaturize the MS analyzers themselves. Although it presents a real interest, this last point will not be treated here.

4.2.2. ESI – related microfluidic devices

Microfabricated ESI emitters are most often made of silicon, glass or polymer substrates. Originally, the spray was achieved from the planar chip edge (Figure I-5.A), as developed by Ramsey⁶ and Xue⁷⁸ with glass chip. However, the limitation here is the hydrophilic nature of the material that leads to sample spillage on the chip edge with a large Taylor cone. Xue *et al.* made an attempt to overcome the problem of wettability of planar-edge emitters by applying a hydrophobic coating around the spraying orifice. Others use hydrophobic polymers, such as PDMS⁷⁹ or PET⁸⁰. The use of hydrophobic membranes⁸¹ or porous polymer monoliths integrated to the microchannel outlet⁸² were also reported. Nevertheless, such additional coatings and membranes increase the complexity of the fabrication and present a limited lifetime. Another limitation of the spray from planar chip edge is the electric field density that cannot be focused on a particular point leading to a larger Taylor cone.

The second approach consists in attaching an external emitter, such as a fused silica capillary, a nanospray needle, or a separate microsyringe to the microchannel outlet (Figure I-5.B). The objective was to overcome the limitations of the spray from planar chip edge. The chip can be coupled to external liquid junction or sheath liquid interfaces through transfer capillaries.⁸³⁻⁹⁰ Separately assembled external microsyringes can also be attached to the microchannel outlet.^{91, 92} On-chip liquid junction⁹³ or sheath flow channels⁹⁴ can be coupled to external spray emitter as well. Sheathless ionization through nanospray needles attached directly to the end of the microchannel was also reported.^{8, 95-99} However, the integration of such external emitters with a microchannel creates large dead volumes that can be an important issue in case of analyte separation. A drilling procedure was developed for low dead volume connections between a glass microfluidic chip and an ESI emitter.¹⁰⁰ However, this approach remains hardly practical because of the manual post-processing after microfabrication.

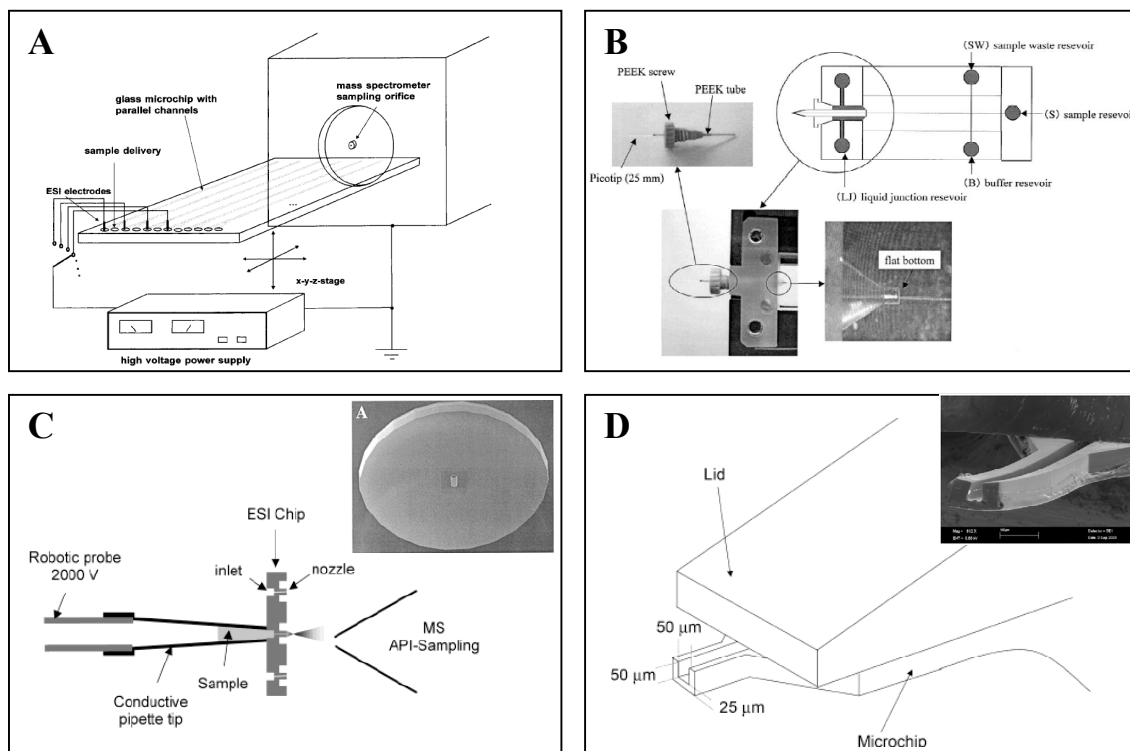


Figure I-5 Selection of electrospray emitter devices. A) Spray from the planar edge. Reprinted from Ref.⁶. B) Spray from an emitter attached to the chip. Reprinted from Ref.⁸. C) Spray from out-of-plane integrated emitter. Reprinted from Ref.^{10, 11}. D) Spray from in-plane integrated emitter. Reprinted from Ref.¹²

To the view of the two first approaches, microfabricated emitters with shaped-pointed tips are the best solutions even if it poses the challenge of the microfabrication process. Out-of-plane^{11, 101, 102} and in-plane¹⁰³⁻¹⁰⁶ silicon-based ESI emitters and have been investigated by several groups. A famous example of silicon out-of-plane emitter is the multi-nozzle array chip, now commercialized by Advion Biosciences (Figure I-5.C).^{10, 11, 107, 108} The device demonstrates a good reproducibility and a detection sensitivity at the nanomolar level for small drug compounds. In comparison with silicon-based device, the realization of pointed tip emitters in glass substrate is trickier. Emitter can be post-processed on a glass chip by milling a cone structure at the end of the microchannel, after which the cone is tapered to a tip.¹⁰⁹ As a simple alternative, the channel outlet can be directed towards a rectangular corner of the chip.^{110, 111} Finally, in contrast with silicon- or glass- based structures, the microfabrication process of polymer chip with integrated emitter is easier. PDMS ESI chip can be made by various casting methods (Figure I-5.D)^{12, 112-115} including for some, graphite - coated PDMS in order to apply the spray voltage directly to the chip^{112, 115}. Micromilling of PMMA¹¹⁶,

photo-ablation of polycarbonate (PC)¹¹⁷, polyimide¹¹⁸ or SU8 negative photoresist lithography^{119, 120} were also reported in the literature. In the examples mentioned above, the fabrication of the pointed emitter tip was a part of the chip fabrication process. Alternatively, the pointed emitter tip can be made as post-process by manually cut and polish the substrate, as done with PMMA^{121, 122}, polyimide,¹²³ or PET.¹²⁴ In this thesis work, ESI emitter chip were fabricated by laser photo-ablation of PET with a pointed emitter tip made by manual cutting.

The large panel of microfabrication processes and designs of ESI emitter chips enables a wide range of possible applications. The various applications of ESI- and MALDI- related microfluidic systems, have been reviewed several times.^{71, 125-130} Sample preparation, pre-concentration, enzymatic digestion or separation methods can be conveniently performed on a microchip, making sample preparation for MS faster and more efficient. The microsystems can be either *i*) an infusion-based microchip downstream a standard separation technique, *ii*) a microchip including analytical functions upstream the ionization source, *iii*) or an ESI emitter microchip including analytical functions. Only the major achievements about the hyphenation of analytical units directly onto the electrospray chip are presented thereafter (point *iii*).

Desalting and pre-concentration are a requisite in sample preparation in order to limit ion suppression effects in ESI-MS. On-chip sample desalting has been reported with the use of a hydrophobic PVDF membrane fixed into an inlet channel of an electrospray polyimide chip.¹³¹ Separation techniques can also be easily adapted in microfluidic formats. However, when implementing separation steps directly to an ESI chip, one should consider the possible dead volume of the structure and the electrical interferences between separation and spray voltages. Electrophoresis-based separation as on-chip capillary electrophoresis^{8, 73, 88, 90, 93, 95, 115, 132-134}, capillary electrochromatography¹³⁵, isoelectrophoretic focusing¹³⁶, combined digestion unit – CE separation^{86, 98, 137-141}, or 2D separation as SPE-CE¹¹² have been successfully implemented to electrospray devices. Regarding chromatography-based separation, on-chip reversed-phase chromatography^{118, 142-146}, or even multi-dimensional separation as SCX – RP (C18)¹⁴⁷ were reported. Several issues in affinity-based separations should be considered as the immobilization of the stationary phase in the microchannel (packed beads, monoliths, magnetic beads), but also the generation of solvent gradient. The HPLC Chip commercialized by Agilent is a great example of fully integrated electrospray

device including a pre-concentration and separation unit.¹⁴⁵ At last, on-chip electrochemical reaction was developed in ESI-chip for on-line modification of peptides and detection by MS.¹²⁴ On-chip reaction, as tryptic digestion combined or not with an additional separation step was also demonstrated as a useful tool for fast sample analysis.^{67, 98}

4.2.3. MALDI – related microfluidic devices

Few years ago microfluidics also appeared in MALDI mass spectrometry. On-line coupling of liquid flow to MALDI-TOF MS using a continuous vacuum interface was first reported by Karger's group (Figure I-6.A).¹³¹ On-line coupling of microfluidic devices may be done using a mechanical interface^{3, 148} as in this former example, or continuous flow^{149, 150}. In both cases, the sample is delivered on-line to the MALDI vacuum chamber. In contrast, off-line coupling of microfluidic devices remains more practical, as the sample is deposited onto the plate via a microfluidic interface and before incursion into the MS. The standard method to deposit samples to a MALDI plate relies on manual or robotized sample (and matrix) dropping. Sample dropping has been reported then with microfluidic devices as interface.^{151, 152} Another approach consists to electrospray the sample, and eventually the matrix, onto the MALDI plate (Figure I-6.B).^{4, 153} One of the later reported work, namely the spinning CD, uses the chip itself as a fully integrated microfluidic interface.¹⁵⁴

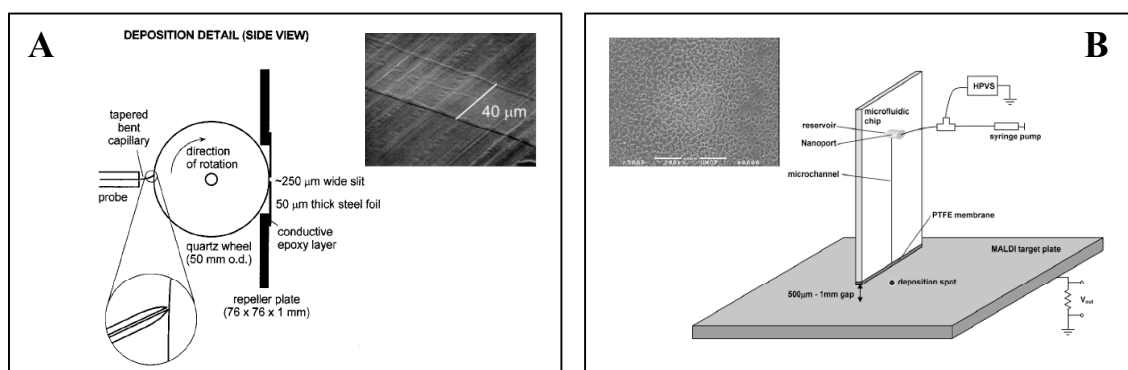


Figure I- 6 Selection of microfluidic interface for MALDI deposition. A) On-line microfluidic coupling with in-vacuum liquid deposition.³ Reprinted from Ref. B) Off-line electrospray microfluidic interface for MALDI deposition. Reprinted from Ref.⁴

The implementation of analytical units to microfluidic interfaces coupled to MALDI – MS is less investigated than the ones for ESI –MS. However, great achievements have been reported yet. The spinning CD mentioned above enables parallel preparation of 96 samples. The tryptic peptides are concentrated, desalted, and subsequently eluted from the columns directly into MALDI target areas on the CD. A microchip with parallel-immobilized enzyme reactor including piezo-actuated flow-through dispenser was also demonstrated for protein digestion and sample deposition on MALDI plate.^{155, 156} Electrowetting-on-dielectric (EWOD) based on manipulation of single droplets on a microfluidic plate was used for sample preparation before analysis.¹⁵⁷ Finally, microfluidic CE separation was interfaced to MALDI¹⁵⁸, as well as cIEF with PMMA chip including channels that are covered only during the separation.¹⁵⁹

OBJECTIVE OF THE WORK

In this general context combining protein studies, mass spectrometry and microfluidic devices, the objective of this thesis was to develop novel analytical systems dedicated to the study of proteins, mainly coupled to mass spectrometric detection. Experimentation and/or numerical simulations enabled to design and characterize the microsystems investigated in the various chapters.

CHAPTER II presents a numerical investigation of a sandwich mixer-reactor that consists of mixing two solutions providing the reactants in a channel, one central laminar flow being sandwiched between two outer incoming solutions. The simulations aimed to optimize a chemical tagging reaction, and show how the diffusion coefficient and flow rate ratios influence, via the transversal diffusion length and reaction kinetics, the reaction extent at the end of a sandwich mixer.

CHAPTER III refreshes first some basic concepts about electrospray ionization and describes the microfabrication of the electrospray emitter microchips used in this thesis, and based on polymer laser ablation. As infusion-based electrospray microchips are known to present great advantages in terms of sensitivity compared to standard ionization source, an ESI emitter microchip was designed. The hyphenation of the chip in a capillary LC-MS workflow is evaluated by comparison with a standard pneumatically-assisted ESI source.

CHAPTER IV concerns the development of an electrospray micromixer chip, as a substitute design to the sandwich mixer-reactor, to perform enhanced on-chip post-column derivatization of peptides and kinetic studies before ESI-MS analysis. After a characterization of the mixing efficiency both by fluorescence imaging and on-chip tagging reaction, the device was hyphenated to a capillary LC-MS workflow to perform post-column derivatization of tryptic cysteinyl peptides.

CHAPTER V is devoted to the development of a novel design of polymer microchip integrating a magnetic track array in order to distribute precisely the magnetic field generated by permanent magnets all along the microchannel. The resulting multi-plug bead capture is

presented, enhancing the overall amount of trapped beads and subsequently, the specific binding surface available for further affinity separation.

CHAPTER VI illustrates the multiplexing of ESI emitter devices. A multi-track polymer electrospray chip composed of parallel channels was designed to sequentially analyze up to six samples by mass spectrometry and perform relative quantification of peptides.

CHAPTER VII presents preliminary results of a novel method of ambient desorption ionization for rapid and efficient sample screening. The principle of the so-called membrane – desorption electrospray ionization (M-DESI) mass spectrometry technique is similar to the desorption electrospray ionization method (DESI). But in M-DESI the sample is desorbed from a mesh membrane positioned vertically and in-axis between the ESI emitter and the mass spectrometer inlet. The proof-of-concept is demonstrated with the desorption of proteins and peptides.

REFERENCES

1. C. Darwin, *On the Origin of Species by Means of Natural Selection, or the Preservation of Favoured Races in the Struggle for Life*, 1859.
2. N. L. Anderson and N. G. Anderson, The human plasma proteome: history, character, and diagnostic prospects, *Molecular & cellular proteomics*, 2002, 1, 845-867.
3. J. Preisler, F. Foret and B. L. Karger, On-line MALDI-TOF MS using a continuous vacuum deposition interface, *Analytical Chemistry*, 1998, 70, 5278-5287.
4. Y. X. Wang, Y. Zhou, B. M. Balgley, J. W. Cooper, C. S. Lee and D. L. DeVoe, Electrospray interfacing of polymer microfluids to MALDI-MS, *Electrophoresis*, 2005, 26, 3631-3640.
5. D. J. States, G. S. Omenn, T. W. Blackwell, D. Fermin, J. Eng, D. W. Speicher and S. M. Hanash, Challenges in deriving high-confidence protein identifications from data gathered by a HUPO plasma proteome collaborative study, *Nature Biotechnology*, 2006, 24, 333-338.
6. Q. Xue, F. Foret, Y. M. Dunayevskiy, P. M. Zavracky, N. E. McGruer and B. L. Karger, Multichannel microchip electrospray mass spectrometry, *Analytical Chemistry*, 1997, 69, 426-430.
7. P. R. Graves and T. A. J. Haystead, Molecular biologist's guide to proteomics, *Microbiology and Molecular Biology Reviews*, 2002, 66, 39-63.
8. Y. Tachibana, K. Otsuka, S. Terabe, A. Arai, K. Suzuki and S. Nakamura, Robust and simple interface for microchip electrophoresis-mass spectrometry, *Journal of Chromatography A*, 2003, 1011, 181-192.
9. G. Mendel, *Versuche über Pflanzen-Hybriden*, *Verhandlungen des naturforschenden Vereines in Brunn*, 1866, 4, 3-47.
10. J. M. Dethy, B. L. Ackermann, C. Delatour, J. D. Henion and G. A. Schultz, Demonstration of direct bioanalysis of drugs in plasma using nanoelectrospray infusion from a silicon chip coupled with tandem mass spectrometry, *Analytical Chemistry*, 2003, 75, 805-811.
11. G. A. Schultz, T. N. Corso, S. J. Prosser and S. Zhang, A fully integrated monolithic microchip electrospray device for mass spectrometry, *Analytical Chemistry*, 2000, 72, 4058-4063.
12. M. Svedberg, M. Veszelei, J. Axelsson, M. Vangbo and F. Nikolajeff, Poly(dimethylsiloxane) microchip: Microchannel with integrated open electrospray tip, *Lab on a Chip - Miniaturisation for Chemistry and Biology*, 2004, 4, 322-327.
13. R. Schiess, B. Wollscheid and R. Aebersold, Targeted proteomic strategy for clinical biomarker discovery, *Molecular Oncology*, 2009, 3, 33-44.
14. J. Seo and K. J. Lee, Post-translational modifications and their biological functions: Proteomic analysis and systematic approaches, *Journal of Biochemistry and Molecular Biology*, 2004, 37, 35-44.
15. http://www.ornl.gov/sci/techresources/Human_Genome/home.shtml.
16. F. S. Collins, E. S. Lander, J. Rogers and R. H. Waterson, Finishing the euchromatic sequence of the human genome, *Nature*, 2004, 431, 931-945.
17. T. Fröhlich and G. J. Arnold, Proteome research based on modern liquid chromatography - Tandem mass spectrometry: Separation, identification and quantification, *Journal of Neural Transmission*, 2006, 113, 973-994.
18. S. D. Patterson and R. H. Aebersold, Proteomics: The first decade and beyond, *Nature Genetics*, 2003, 33, 311-323.
19. R. Aebersold and M. Mann, Mass spectrometry-based proteomics, *Nature*, 2003, 422, 198-207.
20. D. F. Hochstrasser, J. C. Sanchez and R. D. Appel, Proteomics and its trends facing nature's complexity, *Proteomics*, 2002, 2, 807-812.
21. C. L. Corthals, V. C. Wasinger, D. F. Hochstrasser and J. C. Sanchez, The dynamic range of protein expression: A challenge for proteomic research, *Electrophoresis*, 2000, 21, 1104-1115.

22. W. S. Hancock, S. L. Wu and P. Shieh, The challenges of developing a sound proteomics strategy, *Proteomics*, 2002, 2, 352-359.
23. T. C. Hunter, N. L. Andon, A. Koller, J. R. Yates Iii and P. A. Haynes, The functional proteomics toolbox: Methods and applications, *Journal of Chromatography B: Analytical Technologies in the Biomedical and Life Sciences*, 2002, 782, 165-181.
24. P. G. Righetti, A. Castagna, P. Antonioli and E. Boschetti, Prefractionation techniques in proteome analysis: The mining tools of the third millennium, *Electrophoresis*, 2005, 26, 297-319.
25. H. J. Issaq, The role of separation science in proteomics research, *Electrophoresis*, 2001, 22, 3629-3638.
26. P. H. O'Farrell, High resolution two dimensional electrophoresis of proteins, *Journal of Biological Chemistry*, 1975, 250, 4007-4021.
27. J. Klose, Protein mapping by combined isoelectric focusing and electrophoresis of mouse tissues. A novel approach to testing for induced point mutations in mammals, *HUMANGENETIK*, 1975, 26, 231-243.
28. G. A. Scheele, Two dimensional gel analysis of soluble proteins. Characterization of guinea pig exocrine pancreatic proteins, *Journal of Biological Chemistry*, 1975, 250, 5375-5385.
29. R. Smith, Two-dimensional electrophoresis: an overview, *Methods in molecular biology* (Clifton, N.J.), 2009, 519, 1-16.
30. T. L. Kruger, Mixture analysis by mass-analyzed ion kinetic energy spectrometry, *Analytical Chemistry*, 1976, 48, 2113-2119.
31. F. W. McLafferty, Tandem mass spectrometric analysis of complex biological mixtures, *International Journal of Mass Spectrometry*, 2001, 212, 81-87.
32. B. Domon and R. Aebersold, Mass spectrometry and protein analysis, *Science*, 2006, 312, 212-217.
33. B. Domon and R. Aebersold, Review - Mass spectrometry and protein analysis, *Science*, 2006, 312, 212-217.
34. P. L. Ferguson and R. D. Smith, Proteome analysis by mass spectrometry, *Annual Review of Biophysics and Biomolecular Structure*, 2003, 32, 399-424.
35. P. Lescuyer, D. F. Hochstrasser and J. C. Sanchez, Comprehensive proteome analysis by chromatographic protein prefractionation, *Electrophoresis*, 2004, 25, 1125-1135.
36. Y. Jmeian and Z. El Rassi, Liquid-phase-based separation systems for depletion, prefractionation and enrichment of proteins in biological fluids for in-depth proteomics analysis, *Electrophoresis*, 2009, 30, 249-261.
37. A. J. Link, J. Eng, D. M. Schieltz, E. Carmack, G. J. Mize, D. R. Morris, B. M. Garvik and J. R. Yates Iii, Direct analysis of protein complexes using mass spectrometry, *Nature Biotechnology*, 1999, 17, 676-682.
38. M. P. Washburn, D. Wolters and J. R. Yates, Large-scale analysis of the yeast proteome by multidimensional protein identification technology, *Nature Biotechnology*, 2001, 19, 242-247.
39. A. Staub, J. Schappler, S. Rudaz and J.-L. Veuthey, CE-TOF/MS: Fundamental concepts, instrumental considerations and applications, *Electrophoresis*, 2009, 30, 1610-1623.
40. N. L. Kelleher, Top-down proteomics, *Analytical Chemistry*, 2004, 76, 196A-203A.
41. G. E. Reid and S. A. McLuckey, 'Top down' protein characterization via tandem mass spectrometry, *Journal of Mass Spectrometry*, 2002, 37, 663-675.
42. N. L. Kelleher, H. Y. Lin, G. A. Valaskovic, D. J. Aaserud, E. K. Fridriksson and F. W. McLafferty, Top down versus bottom up protein characterization by tandem high-resolution mass spectrometry, *Journal of the American Chemical Society*, 1999, 121, 806-812.
43. W. J. Henzel, C. Watanabe and J. T. Stults, Protein identification: The origins of peptide mass fingerprinting, *Journal of the American Society for Mass Spectrometry*, 2003, 14, 931-942.
44. P. James, M. Quadroni, E. Carafoli and G. Gonnet, Protein identification by mass profile fingerprinting, *Biochemical and Biophysical Research Communications*, 1993, 195, 58-64.
45. W. H. McDonald and J. R. Yates, Shotgun proteomics: Integrating technologies to answer biological questions, *Current Opinion in Molecular Therapeutics*, 2003, 5, 302-309.

46. S. K. Swanson and M. P. Washburn, The continuing evolution of shotgun proteomics, *Drug Discovery Today*, 2005, 10, 719-725.
47. A. I. Nesvizhskii and R. Aebersold, Interpretation of shotgun proteomic data - The protein inference problem, *Molecular & Cellular Proteomics*, 2005, 4, 1419-1440.
48. A. Leitner and W. Lindner, Chemistry meets proteomics: The use of chemical tagging reactions for MS-based proteomics, *Proteomics*, 2006, 6, 5418-5434.
49. A. Leitner and W. Lindner, Current chemical tagging strategies for proteome analysis by mass spectrometry, *Journal of Chromatography B: Analytical Technologies in the Biomedical and Life Sciences*, 2004, 813, 1-26.
50. M. B. Goshe, T. P. Conrads, E. A. Panisko, N. H. Angell, T. D. Veenstra and R. D. Smith, Phosphoprotein isotope-coded affinity tag approach for isolating and quantitating phosphopeptides in proteome-wide analyses, *Analytical Chemistry*, 2001, 73, 2578-2586.
51. Y. Oda, T. Nagasu and B. T. Chait, Enrichment analysis of phosphorylated proteins as a tool for probing the phosphoproteome, *Nature Biotechnology*, 2001, 19, 379-382.
52. M. Hamdan and P. G. Righetti, Modern strategies for protein quantification in proteome analysis: Advantages and limitations, *Mass Spectrometry Reviews*, 2002, 21, 287-302.
53. W. W. Wu, G. Wang, S. J. Baek and R. F. Shen, Comparative study of three proteomic quantitative methods, DIGE, cICAT, and iTRAQ, using 2D gel- or LC-MALDI TOF/TOF, *Journal of Proteome Research*, 2006, 5, 651-658.
54. S. P. Gygi, B. Rist, S. A. Gerber, F. Turecek, M. H. Gelb and R. Aebersold, Quantitative analysis of complex protein mixtures using isotope-coded affinity tags, *Nature Biotechnology*, 1999, 17, 994-999.
55. K. C. Hansen, G. Schmitt-Ulms, R. J. Chalkley, J. Hirsch, M. A. Baldwin and A. L. Burlingame, Mass spectrometric analysis of protein mixtures at low levels using cleavable ¹³C-isotope-coded affinity tag and multidimensional chromatography, *Molecular & cellular proteomics : MCP.*, 2003, 2, 299-314.
56. L. R. Yu, T. P. Conrads, T. Uo, H. J. Issaq, R. S. Morrison and T. D. Veenstra, Evaluation of the acid-cleavable isotope-coded affinity tag reagents: Application to camptothecin-treated cortical neurons, *Journal of Proteome Research*, 2004, 3, 469-477.
57. P. L. Ross, Y. N. Huang, J. N. Marchese, B. Williamson, K. Parker, S. Hattan, N. Khainovski, S. Pillai, S. Dey, S. Daniels, S. Purkayastha, P. Juhasz, S. Martin, M. Bartlett-Jones, F. He, A. Jacobson and D. J. Pappin, Multiplexed protein quantitation in *Saccharomyces cerevisiae* using amine-reactive isobaric tagging reagents, *Molecular and Cellular Proteomics*, 2004, 3, 1154-1169.
58. L. Dayon, A. Hainard, V. Licker, N. Turck, K. Kuhn, D. F. Hochstrasser, P. R. Burkhard and J. C. Sanchez, Relative quantification of proteins in human cerebrospinal fluids by MS/MS using 6-plex isobaric tags, *Analytical Chemistry*, 2008, 80, 2921-2931.
59. K. D. W. Roth, Z. H. Huang, N. Sadagopan and J. T. Watson, Charge derivatization of peptides for analysis by mass spectrometry, *Mass Spectrometry Reviews*, 1998, 17, 255-274.
60. W. C. Yang, H. Mirzaei, X. Liu and F. E. Regnier, Enhancement of amino acid detection and quantification by electrospray ionization mass spectrometry, *Analytical Chemistry*, 2006, 78, 4702-4708.
61. J. P. Brody, P. Yager, R. E. Goldstein and R. H. Austin, Biotechnology at low Reynolds numbers, *Biophysical Journal*, 1996, 71, 3430-3441.
62. P. S. Dittrich, K. Tachikawa and A. Manz, Micro total analysis systems. Latest advancements and trends, *Analytical Chemistry*, 2006, 78, 3887-3907.
63. D. Janasek, J. Franzke and A. Manz, Scaling and the design of miniaturized chemical-analysis systems, *Nature*, 2006, 442, 374-380.
64. D. A. Boy, F. Gibou and S. Pennathur, Simulation tools for lab on a chip research: Advantages, challenges, and thoughts for the future, *Lab on a Chip - Miniaturisation for Chemistry and Biology*, 2008, 8, 1424-1431.
65. M. S. Wilm and M. Mann, Electrospray and Taylor-Cone theory, Dole's beam of macromolecules at last?, *International Journal of Mass Spectrometry and Ion Processes*, 1994, 136, 167-180.

66. R. T. Kelly, J. S. Page, K. Tang and R. D. Smith, Array of chemically etched fused-silica emitters for improving the sensitivity and quantitation of electrospray ionization mass spectrometry, *Analytical Chemistry*, 2007, 79, 4192-4198.
67. Q. Xue, Y. M. Dunayevskiy, F. Foret and B. L. Karger, Integrated multichannel microchip electrospray ionization mass spectrometry: Analysis of peptides from on-chip tryptic digestion of melittin, *Rapid Communications in Mass Spectrometry*, 1997, 11, 1253-1256.
68. D. Figeys, Y. B. Ning and R. Aebersold, A microfabricated device for rapid protein identification by microelectrospray ion trap mass spectrometry, *Analytical Chemistry*, 1997, 69, 3153-3160.
69. R. S. Ramsey and J. M. Ramsey, Generating Electrospray from Microchip Devices Using Electroosmotic Pumping, *Analytical Chemistry*, 1997, 69, 1174-1178.
70. I. M. Lazar, J. Grym and F. Foret, Microfabricated devices: A new sample introduction approach to mass spectrometry, *Mass Spectrometry Reviews*, 2006, 25, 573-594.
71. R. D. Oleschuk and D. J. Harrison, Analytical microdevices for mass spectrometry, *TrAC - Trends in Analytical Chemistry*, 2000, 19, 379-388.
72. P. A. Limbach and Z. Meng, Integrating micromachined devices with modern mass spectrometry, *Analyst*, 2002, 127, 693-700.
73. W. C. Sung, H. Makamba and S. H. Chen, Chip-based microfluidic devices coupled with electrospray ionization-mass spectrometry, *Electrophoresis*, 2005, 26, 1783-1791.
74. F. Foret and P. Kusy, Microfluids for multiplexed MS analysis, *Electrophoresis*, 2006, 27, 4877-4887.
75. S. Koster and E. Verpoorte, A decade of microfluidic analysis coupled with electrospray mass spectrometry: An overview, *Lab on a Chip - Miniaturisation for Chemistry and Biology*, 2007, 7, 1394-1412.
76. T. Sikanen, S. Franssila, T. J. Kauppila, R. Kostianen, T. Kotiaho and R. A. Ketola, Microchip technology in mass spectrometry, *Mass Spectrometry Reviews*, 2009, DOI: 10.1002/mas.20238.
77. G. T. T. Gibson, S. M. Mugo and R. D. Oleschuk, Nanoelectrospray emitters: Trends and perspective, *Mass Spectrometry Reviews*, 2009, DOI: 10.1002/mas.20248.
78. R. S. Ramsay and J. M. Ramsey, Generating Electrospray from Microchip Devices Using Electroosmotic Pumping, *Analytical Chemistry*, 1997, 69, 1174-1178.
79. K. Huikko, P. Östman, K. Grigoras, S. Tuomikoski, V. M. Tiainen, A. Soininen, K. Puolanne, A. Manz, S. Franssila, R. Kostianen and T. Kotiaho, Poly(dimethylsiloxane) electrospray devices fabricated with diamond-like carbon-poly(dimethylsiloxane) coated SU-8 masters, *Lab on a Chip - Miniaturisation for Chemistry and Biology*, 2003, 3, 67-72.
80. T. C. Rohner, J. S. Rossier and H. H. Girault, Polymer microspray with an integrated thick-film microelectrode, *Analytical Chemistry*, 2001, 73, 5353-5357.
81. Y. X. Wang, J. W. Cooper, C. S. Lee and D. L. DeVoe, Efficient electrospray ionization from polymer microchannels using integrated hydrophobic membranes, *Lab on a Chip - Miniaturisation for Chemistry and Biology*, 2004, 4, 363-367.
82. M. F. Bedair and R. D. Oleschuk, Fabrication of porous polymer monoliths in polymeric microfluidic chips as an electrospray emitter for direct coupling to mass spectrometry, *Analytical Chemistry*, 2006, 78, 1130-1138.
83. S. Benetton, J. Kameoka, A. Tan, T. Wachs, H. Craighead and J. D. Henion, Chip-Based P450 Drug Metabolism Coupled to Electrospray Ionization-Mass Spectrometry Detection, *Analytical Chemistry*, 2003, 75, 6430-6436.
84. D. Figeys, S. P. Gygi, G. McKinnon and R. Aebersold, An Integrated Microfluidics-Tandem Mass Spectrometry System for Automated Protein Analysis, *Analytical Chemistry*, 1998, 70, 3728-3734.
85. J. Kameoka, R. Orth, B. Ilic, D. Czaplewski, T. Wachs and H. G. Craighead, An electrospray ionization source for integration with microfluidics, *Analytical Chemistry*, 2002, 74, 5897-5901.
86. J. Li, W. Can, J. F. Kelly, D. J. Harrison and P. Thibault, Rapid and sensitive separation of trace level protein digests using microfabricated devices coupled to a quadrupole - time-of-flight mass spectrometer, *Electrophoresis*, 2000, 21, 198-210.

87. J. Li, P. Thibault, N. H. Bings, C. D. Skinner, C. Wang, C. Colyer and J. Harrison, Integration of microfabricated devices to capillary electrophoresis- electrospray mass spectrometry using a low dead volume connection: Application to rapid analyses of proteolytic digests, *Analytical Chemistry*, 1999, 71, 3036-3045.
88. X. Mao, I. K. Chu and B. Lin, A sheath-flow nanoelectrospray interface of microchip electrophoresis MS for glycoprotein and glycopeptide analysis, *Electrophoresis*, 2006, 27, 5059-5067.
89. Z. Meng, S. Qi, S. A. Soper and P. A. Limbach, Interfacing a polymer-based micromachined device to a nanoelectrospray ionization fourier transform ion cyclotron resonance mass spectrometer, *Analytical Chemistry*, 2001, 73, 1286-1291.
90. B. Zhang, H. Liu, B. L. Karger and F. Foret, Microfabricated devices for capillary electrophoresis-electrospray mass spectrometry, *Analytical Chemistry*, 1999, 71, 3258-3264.
91. Y. Deng, J. Henion, J. Li, P. Thibault, C. Wang and D. J. Harrison, Chip-based capillary electrophoresis/mass spectrometry determination of carnitines in human urine, *Analytical Chemistry*, 2001, 73, 639-646.
92. Y. Deng, H. Zhang and J. Henion, Chip-based quantitative capillary electrophoresis/mass spectrometry determination of drugs in human plasma, *Analytical Chemistry*, 2001, 73, 1432-1439.
93. B. Zhang, F. Foret and B. L. Karger, A microdevice with integrated liquid junction for facile peptide and protein analysis by capillary electrophoresis/electrospray mass spectrometry, *Analytical Chemistry*, 2000, 72, 1015-1022.
94. T. T. Razunguzwa, J. Lenke and A. T. Timperman, An electrokinetic/hydrodynamic flow microfluidic CE-ESI-MS interface utilizing a hydrodynamic flow restrictor for delivery of samples under low EOF conditions, *Lab on a Chip - Miniaturisation for Chemistry and Biology*, 2005, 5, 851-855.
95. S. Akashi, K. Suzuki, A. Arai, N. Yamada, E. I. Suzuki, K. Hirayama, S. Nakamura and Y. Nishimura, Top-down analysis of basic proteins by microchip capillary electrophoresis mass spectrometry, *Rapid Communications in Mass Spectrometry*, 2006, 20, 1932-1938.
96. H. Liu, C. Felten, Q. Xue, B. Zhang, P. Jedrzejewski, B. L. Karger and F. Foret, Development of multichannel devices with an array of electrospray tips for high-throughput mass spectrometry, *Analytical Chemistry*, 2000, 72, 3303-3310.
97. W. C. Sung, S. Y. Huang, P. C. Liao, G. B. Lee, C. W. Li and S. H. Chen, Poly(dimethylsiloxane)- based microfluidic device with electrospray ionization-mass spectrometry interface for protein identification, *Electrophoresis*, 2003, 24, 3648-3654.
98. C. Wang, R. Oleschuk, F. Ouchen, J. Li, P. Thibault and D. J. Harrison, Integration of immobilized trypsin bead beds for protein digestion within a microfluidic chip incorporating capillary electrophoresis separations and an electrospray mass spectrometry interface, *Rapid Communications in Mass Spectrometry*, 2000, 14, 1377-1383.
99. Y. Yang, C. Li, J. Kameoka, K. H. Lee and H. G. Craighead, A polymeric microchip with integrated tips and in situ polymerized monolith for electrospray mass spectrometry, *Lab on a Chip - Miniaturisation for Chemistry and Biology*, 2005, 5, 869-876.
100. N. H. Bings, C. Wang, C. D. Skinner, C. L. Colyer, P. Thibault and D. J. Harrison, Microfluidic devices connected to fused-silica capillaries with minimal dead volume, *Analytical Chemistry*, 1999, 71, 3292-3296.
101. J. Sjödaahl, J. Melin, P. Griss, Ö. Emmer, G. Stemme and J. Roeraade, Characterization of micromachined hollow tips for two-dimensional nanoelectrospray mass spectrometry, *Rapid Communications in Mass Spectrometry*, 2003, 17, 337-341.
102. W. Deng, J. F. Klemic, X. Li, M. A. Reed and A. Gomez, Increase of electrospray throughput using multiplexed microfabricated sources for the scalable generation of monodisperse droplets, *Journal of Aerosol Science*, 2006, 37, 696-714.
103. S. Arscott, S. L. Gac and C. Rolando, A polysilicon nanoelectrospray-mass spectrometry source based on a microfluidic capillary slot, *Sensors and Actuators, B: Chemical*, 2005, 106, 741-749.
104. W. Kim, M. Guo, P. Yang and D. Wang, Microfabricated monolithic multinozzle emitters for nanoelectrospray mass spectrometry, *Analytical Chemistry*, 2007, 79, 3703-3707.

105. B. Legrand, A. E. Ashcroft, L. Buchaillot and S. Arscott, SOI-based nanoelectrospray emitter tips for mass spectrometry: A coupled MEMS and microfluidic design, *Journal of Micromechanics and Microengineering*, 2007, 17, 509-514.
106. T. Nissilä, L. Sainiemi, T. Sikanen, T. Kotiaho, S. Franssila, R. Kostainen and R. A. Ketola, Silicon micropillar array electrospray chip for drug and biomolecule analysis, *Rapid Communications in Mass Spectrometry*, 2007, 21, 3677-3682.
107. S. Zhang and C. K. Van Pelt, Chip-based nanoelectrospray mass spectrometry for protein characterization, *Expert Review of Proteomics*, 2004, 1, 449-468.
108. S. Zhang, C. K. Van Pelt and J. D. Henion, Automated chip-based nanoelectrospray-mass spectrometry for rapid identification of proteins separated by two-dimensional gel electrophoresis, *Electrophoresis*, 2003, 24, 3620-3632.
109. P. Hoffmann, U. Häusig, P. Schulze and D. Belder, Microfluidic glass chips with an integrated nanospray emitter for coupling to a mass spectrometer, *Angewandte Chemie - International Edition*, 2007, 46, 4913-4916.
110. S. L. S. Freire, H. Yang and A. R. Wheeler, A practical interface for microfluidics and nanoelectrospray mass spectrometry, *Electrophoresis*, 2008, 29, 1836-1843.
111. J. S. Mellors, V. Gorbounov, R. S. Ramsey and J. M. Ramsey, Fully integrated glass microfluidic device for performing high-efficiency capillary electrophoresis and electrospray ionization mass spectrometry, *Analytical Chemistry*, 2008, 80, 6881-6887.
112. A. P. Dahlin, S. K. Bergström, P. E. Andrén, K. E. Markides and J. Bergquist, Poly(dimethylsiloxane)-based microchip for two-dimensional solid-phase extraction-capillary electrophoresis with an integrated electrospray emitter tip, *Analytical Chemistry*, 2005, 77, 5356-5363.
113. J. M. Iannacone, J. A. Jakubowski, P. W. Bohn and J. V. Sweedler, A multilayer poly(dimethylsiloxane) electrospray ionization emitter for sample injection and online mass spectrometric detection, *Electrophoresis*, 2005, 26, 4684-4690.
114. J. S. Kim and D. R. Knapp, Microfabrication of polydimethylsiloxane electrospray ionization emitters, *Journal of Chromatography A*, 2001, 924, 137-145.
115. S. Thorslund, P. Lindberg, P. E. Andrén, F. Nikolajeff and J. Bergquist, Electrokinetic-driven microfluidic system in poly(dimethylsiloxane) for mass spectrometry detection integrating sample injection, capillary electrophoresis, and electrospray emitter on-chip, *Electrophoresis*, 2005, 26, 4674-4683.
116. M. Schilling, W. Nigge, A. Rudzinski, A. Neyer and R. Hergenröder, A new on-chip ESI nozzle for coupling of MS with microfluidic devices, *Lab on a Chip - Miniaturisation for Chemistry and Biology*, 2004, 4, 220-224.
117. K. Tang, Y. Lin, D. W. Matson, T. Kim and R. D. Smith, Generation of multiple electrosprays using microfabricated emitter arrays for improved mass spectrometric sensitivity, *Analytical Chemistry*, 2001, 73, 1658-1663.
118. H. Yin, K. Killeen, R. Brennen, D. Sobek, M. Werlich and T. Van De Goor, Microfluidic chip for peptide analysis with an integrated HPLC column, sample enrichment column, and nanoelectrospray tip, *Analytical Chemistry*, 2005, 77, 527-533.
119. S. Arscott, S. Le Gac, C. Druon, P. Tabourier and C. Rolando, Micromachined 2D nanoelectrospray emitter, *Electronics Letters*, 2003, 39, 1702-1703.
120. S. Le Gac, S. Arscott, C. Cren-Olive and C. Rolando, Two-dimensional microfabricated sources for nanoelectrospray, *Journal of Mass Spectrometry*, 2003, 38, 1259-1264.
121. A. Muck and A. Svatos, Atmospheric molded poly(methylmethacrylate) microchip emitters for sheathless electrospray, *Rapid Communications in Mass Spectrometry*, 2004, 18, 1459-1464.
122. C. H. Yuan and J. Shiea, Sequential electrospray analysis using sharp-tip channels fabricated on a plastic chip, *Analytical Chemistry*, 2001, 73, 1080-1083.
123. V. Gobry, J. Van Oostrum, M. Martinelli, T. C. Rohner, F. Reymond, J. S. Rossier and H. H. Girault, Microfabricated polymer injector for direct mass spectrometry coupling, *Proteomics*, 2002, 2, 405-412.

124. L. Dayon, C. Roussel and H. H. Girault, On-line electrochemical tagging of free cysteines in peptides during nanospray ionisation mass spectrometry: An overview, *Chimia*, 2004, 58, 204-207.
125. L. Bindila and P.-K. J., Chip-mass spectrometry for glycomic studies, *Mass Spectrometry Reviews*, 2009, 28, 223-253.
126. D. Figeys and D. Pinto, Proteomics on a chip: Promising developments, *Electrophoresis*, 2001, 22, 208-216.
127. N. Lion, T. C. Rohner, L. Dayon, I. L. Arnaud, E. Damoc, N. Youhnovski, Z. Y. Wu, C. Roussel, J. Josserand, H. Jensen, J. S. Rossier, M. Przybylski and H. H. Girault, Microfluidic systems in proteomics, *Electrophoresis*, 2003, 24, 3533-3562.
128. A. D. Zamfir, L. Bindila, N. Lion, M. Allen, H. H. Girault and J. Peter-Katalinifá, Chip electrospray mass spectrometry for carbohydrate analysis, *Electrophoresis*, 2005, 26, 3650-3673.
129. D. L. DeVoe and C. S. Lee, Microfluidic technologies for MALDI-MS in proteomics, *Electrophoresis*, 2006, 27, 3559-3568.
130. I. M. Lazar, Recent advances in capillary and microfluidic platforms with MS detection for the analysis of phosphoproteins, *Electrophoresis*, 2009, 30, 262-275.
131. N. Lion, J. O. Gellon, H. Jensen and H. H. Girault, On-chip protein sample desalting and preparation for direct coupling with electrospray ionization mass spectrometry, *Journal of Chromatography A*, 2003, 1003, 11-19.
132. I. M. Lazar, R. S. Ramsey, S. Sundberg and J. Michael Ramsey, Subattomole-sensitivity microchip nanoelectrospray source with time-of-flight mass spectrometry detection, *Analytical Chemistry*, 1999, 71, 3627-3631.
133. Y. Tachibana, K. Otsuka, S. Terabe, A. Arai, K. Suzuki and S. Nakamura, Effects of the length and modification of the separation channel on microchip electrophoresis-mass spectrometry for analysis of bioactive compounds, *Journal of Chromatography A*, 2004, 1025, 287-296.
134. B. Zhang, F. Foret and B. L. Karger, High-throughput microfabricated CE/ESI-MS: Automated sampling from a microwell plate, *Analytical Chemistry*, 2001, 73, 2675-2681.
135. I. M. Lazar, L. Li, Y. Yang and B. L. Karger, Microfluidic device for capillary electrochromatography-mass spectrometry, *Electrophoresis*, 2003, 24, 3655-3662.
136. J. Wen, Y. Lin, X. Fan, D. W. Matson, H. R. Udseth and R. D. Smith, Microfabricated isoelectric focusing device for direct electrospray ionization-mass spectrometry, *Electrophoresis*, 2000, 21, 191-197.
137. J. Gao, J. Xu, L. E. Locascio and C. S. Lee, Integrated microfluidic system enabling protein digestion, peptide separation, and protein identification, *Analytical Chemistry*, 2001, 73, 2648-2655.
138. J. Li, J. F. Kelly, I. Chemushevich, D. J. Harrison and P. Thibault, Separation and identification of peptides from gel-isolated membrane proteins using a microfabricated device for combined capillary electrophoresis/nanoelectrospray mass spectrometry, *Analytical Chemistry*, 2000, 72, 599-609.
139. J. Li, T. LeRiche, T. L. Tremblay, C. Wang, E. Bonneil, D. J. Harrison and P. Thibault, Application of microfluidic devices to proteomics research: identification of trace-level protein digests and affinity capture of target peptides, *Molecular & cellular proteomics : MCP*, 2002, 1, 157-168.
140. J. Li, T. L. Tremblay, P. Thibault, C. Wang, S. Attiya and D. J. Harrison, Integrated system for high-throughput protein identification using a microfabricated device coupled to capillary electrophoresis/nanoelectrospray mass spectrometry, *European Journal of Mass Spectrometry*, 2001, 7, 143-155.
141. W. Li, C. L. Hendrickson, M. R. Emmett and A. G. Marshall, Identification of intact proteins in mixtures by alternated capillary liquid chromatography electrospray ionization and LC ESI infrared multiphoton dissociation fourier transform ion cyclotron resonance mass spectrometry, *Analytical Chemistry*, 1999, 71, 4397-4402.
142. M. Ghitun, E. Bonneil, M. H. Fortier, H. Yin, K. Killeen and P. Thibault, Integrated microfluidic devices with enhanced separation performance: Application to phosphoproteome

- analyses of differentiated cell model systems, *Journal of Separation Science*, 2006, 29, 1539-1549.
143. J. Hardouin, M. Duchateau, R. Joubert-Caron and M. Caron, Usefulness of an integrated microfluidic device (HPLC-Chip-MS) to enhance confidence in protein identification by proteomics, *Rapid Communications in Mass Spectrometry*, 2006, 20, 3236-3244.
 144. S. Xie, F. Svec and J. M. J. Fréchet, Design of reactive porous polymer supports for high throughput bioreactors: Poly(2-vinyl-4;4 dimethylazlactone-co-acrylamide-co-ethylene dimethacrylate) monoliths, *Biotechnology and Bioengineering*, 1999, 62, 30-35.
 145. H. Yin and K. Killeen, The fundamental aspects and applications of Agilent HPLC-Chip, *Journal of Separation Science*, 2007, 30, 1427-1434.
 146. I. M. Lazar, P. Trisiripisal and H. A. Sarvaiya, Microfluidic liquid chromatography system for proteomic applications and biomarker screening, *Analytical Chemistry*, 2006, 78, 5513-5524.
 147. M. H. Fortier, E. Bonneil, P. Goodley and P. Thibault, Integrated microfluidic device for mass spectrometry-based proteomics and its application to biomarker discovery programs, *Analytical Chemistry*, 2005, 77, 1631-1640.
 148. H. K. Musyimi, J. Guy, D. A. Narcisse, S. A. Soper and K. K. Murray, Direct coupling of polymer-based microchip electrophoresis to online MALDI-MS using a rotating ball inlet, *Electrophoresis*, 2005, 26, 4703-4710.
 149. M. Brivio, R. H. Fokkens, W. Verboom, D. N. Reinhoudt, N. R. Tas, M. Goedbloed and A. Van den Berg, Integrated microfluidic system enabling (bio)chemical reactions with on-line MALDI-TOF mass spectrometry, *Analytical Chemistry*, 2002, 74, 3972-3976.
 150. M. Brivio, N. R. Tas, M. H. Goedbloed, H. J. G. E. Gardeniers, W. Verboom, A. Van Den Berg and D. N. Reinhoudt, A MALDI-chip integrated system with a monitoring window, *Lab on a Chip - Miniaturisation for Chemistry and Biology*, 2005, 5, 378-381.
 151. J. Lee, H. K. Musyimi, S. A. Soper and K. K. Murray, Development of an Automated Digestion and Droplet Deposition Microfluidic Chip for MALDI-TOF MS, *Journal of the American Society for Mass Spectrometry*, 2008, 19, 964-972.
 152. S. Ekström, L. Wallman, J. Malm, C. Becker, H. Lilja, T. Laurell and G. Marko-Varga, Integrated selective enrichment target - A microtechnology platform for matrix-assisted laser desorption/ionization-mass spectrometry applied on protein biomarkers in prostate diseases, *Electrophoresis*, 2004, 25, 3769-3777.
 153. X. Lou and J. L. J. Van Dongen, Direct sample fraction deposition using electrospray in narrow-bore size-exclusion chromatography/matrix-assisted laser desorption/ionization time-of-flight mass spectrometry for polymer characterization, *Journal of Mass Spectrometry*, 2000, 35, 1308-1312.
 154. M. Gustafsson, D. Hirschberg, C. Palmberg, H. Jörnvall and T. Bergman, Integrated Sample Preparation and MALDI Mass Spectrometry on a Microfluidic Compact Disk, *Analytical Chemistry*, 2004, 76, 345-350.
 155. M. Bengtsson, S. Ekström, G. Marko-Varga and T. Laurell, Improved performance in silicon enzyme microreactors obtained by homogeneous porous silicon carrier matrix, *Talanta*, 2002, 56, 341-353.
 156. S. Ekström, P. Önnérffjord, J. Nilsson, M. Bengtsson, T. Laurell and G. Marko-Varga, Integrated microanalytical technology enabling rapid and automated protein identification, *Analytical Chemistry*, 2000, 72, 286-293.
 157. A. R. Wheeler, H. Moon, C. A. Bird, R. R. O. Loo, C. J. Kim, J. A. Loo and R. L. Garrell, Digital microfluidics with in-line sample purification for proteomics analyses with MALDI-MS, *Analytical Chemistry*, 2005, 77, 534-540.
 158. J. Liu, K. Tseng, B. Garcia, C. B. Lebrilla, E. Mukerjee, S. Collins and R. Smith, Electrophoresis separation in open microchannels. A method for coupling electrophoresis with MALDI-MS, *Analytical Chemistry*, 2001, 73, 2147-2151.
 159. M. L. S. Mok, L. Hua, J. B. C. Phua, M. K. T. Wee and N. S. K. Sze, Capillary isoelectric focusing in pseudo-closed channel coupled to matrix assisted laser desorption/ionization mass spectrometry for protein analysis, *Analyst*, 2004, 129, 109-110.

CHAPTER II.

Numerical investigation of a sandwich mixer-reactor: Influence of the diffusion coefficient and flow rate ratios

Based on M. Abonnenc, J. Josserand, H.H. Girault, Lab Chip, 2009, 9, 440 – 448.

1. Introduction

Microfluidics is now established in the field of (bio)chemistry and life science as a good alternative to all conventional laboratory-scale equipment, because it allows low reagent and time consumption, lower costs and high-throughput.¹⁻³ Because of the small dimensions of the microchannels and the limited range of obtainable linear flow rates, flow in microchannels is generally confined to the laminar regime and mixing is dominated by molecular diffusion. Micromixing may be accomplished using different approaches.^{4, 5} Active mixing may involve external energy sources such as electroosmotic flow,^{6, 7} external pressure gradient⁸, electrokinetic instability^{9, 10} or shaken droplets¹¹ to perturb fluid streamlines to induce a macroscopic mixing. Another approach may consist in passive micromixing¹² that relies mainly on geometrical or surface effect such as the multi-lamellae mixer,¹³ chaotic flow configuration,¹⁴ flow recirculation,¹⁵ or moving droplets.¹⁶

Parallel lamination micromixers are based on the decrease of the diffusion distance of molecules by splitting the streams to mix into n substreams, and then joining them into

one stream as alternated laminae of the species to mix.¹⁷ In small structures, because the time a molecule needs to travel a distance δ/n by diffusion decreases as $1/n^2$, the mixing is quite enhanced. The simplest design is a long microchannel with two inlets ($n = 2$), often called T-mixer or Y-mixer according to its geometry, as illustrated in Figure II-1. The T-mixer has been demonstrated as a tool for the measurements of diffusion coefficients, and as a platform for chemical assays,¹⁸⁻²⁰ as a diffusion based immunoassay.²¹⁻²³

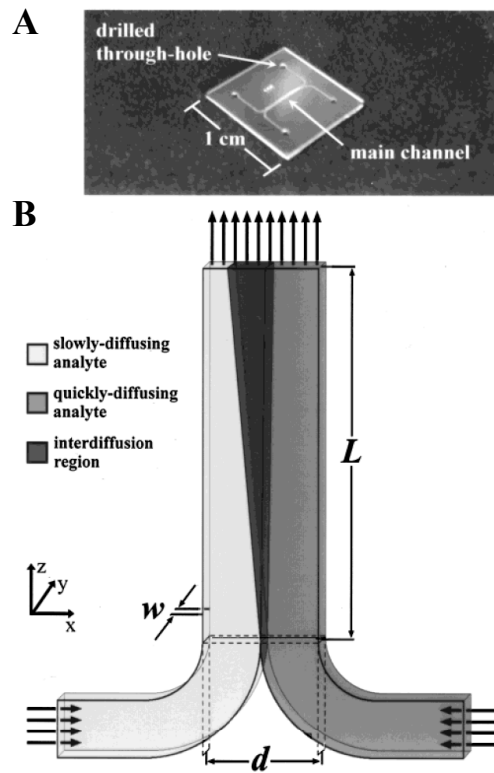


Figure II- 1 A) Photograph of a silicon microfabricated device. For operation as a T-sensor, two-inputs and one output are used. Both outputs are active when the device is used as a H-filter. B) Schematic representation of flow in the T-sensor with two input fluids, each containing one diffusing species. The flow is steady state, projecting the interdiffusion along the length of the channel. The asymmetric development of the interdiffusion region (relative to the center of the channel at $\frac{1}{2}d$) is due to the difference in diffusion coefficients between the two diffusing species. Reprinted from Ref¹³.

Knight *et al.* introduced a similar laminar flow mixer with three inlets ($n = 3$) known as “hydrodynamic focusing mixing” (Figure II-2).²⁴ The buffer solutions from two symmetric orthogonal side channels focus the sample solution entering from the centre channel into a thin stream. In such a design the sample flow is focused only in the horizontal dimension.

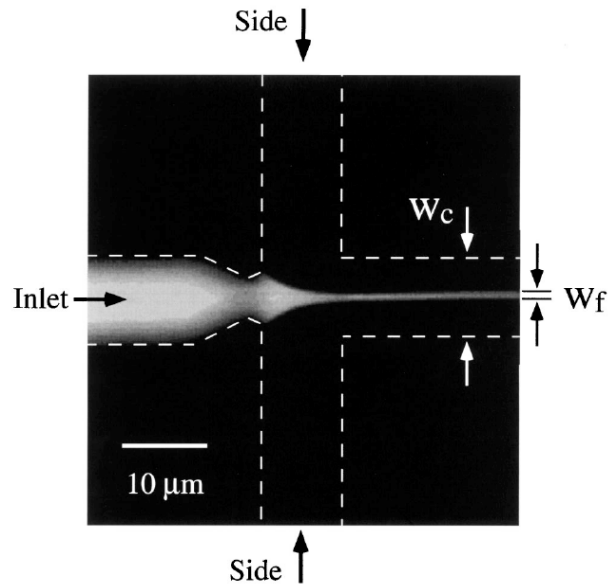


Figure II- 2 Picture of 2D - hydrodynamic focusing. The edges of the channel are outlined with a dashed line for reference. W_c and W_f are the width of the channel and the focused inlet stream, respectively. Reprinted from Ref ²⁴.

Sundararajan *et al.* presented a generalisation of this conventional two-dimensional (2D) hydrodynamic focusing to a three-dimensional (3D) one that offers the advantage to focus the sample flow in both horizontal and vertical direction to get the sample at the centre of the channel.²⁵ More recently, a novel fluid manipulation technique so-called “Microfluidic drifting”²⁶ was presented with two focusing steps combined with a channel curvature resulting in a 3D hydrodynamically focused flow in the centre of the microfluidic channel (Figure II-3).

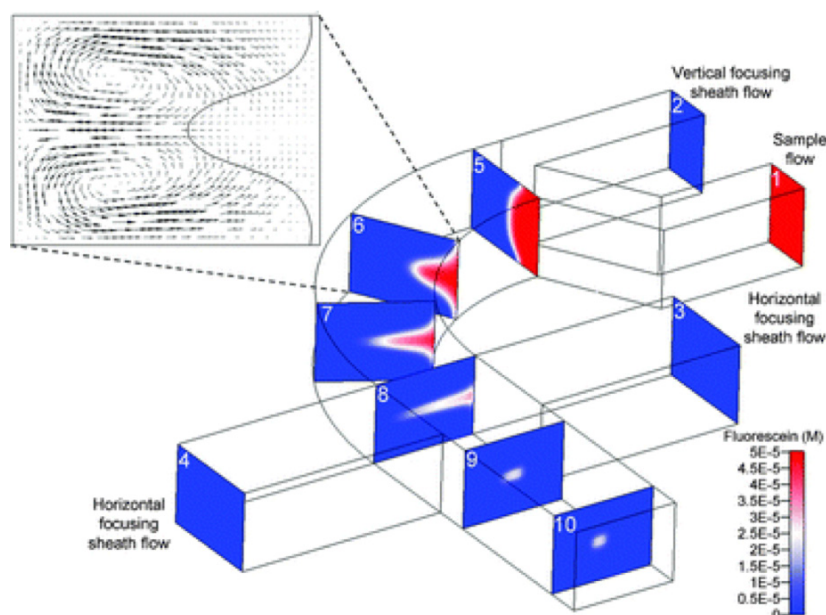


Figure II- 3 Scheme of the 3D hydrodynamic focusing process by employing the “microfluidic drifting” technique. Slices 1-10 are the cross-sectional profiles of the fluorescein dye concentration in the focusing device. Inset: the simulation of the secondary flow velocity field shows the formation of vortices in the 90-degree curve. An iso-curve of fluorescein concentration = $25 \mu\text{M}$ is arbitrary chosen as the boundary of the sample flow. Reprinted from Ref²⁶.

While the 2D and 3D hydrodynamic focusing are based on the focusing of the sample to mix in a thin layer at the microchannel centre, we propose here to study a sandwich mixer design with three flows of equal width. When high throughput is not the main constraint, this sandwich mixer-reactor presents the advantage of a simple fabrication process compared to multi-lamellae mixers, and well suited for polymer microchip fabrication technology. In particular, our laboratory is interested in the design of combined post-column reactors and microsyringes for the specific tagging of target molecules after a chromatographic or electrophoretic separation for electrospray mass spectrometry analysis.^{27, 28}

In the field of microfluidics and microreactors, computational methods have proven to be efficient tools to understand physical mechanisms, validate analytical models, design and optimise microsystems.²⁹ In the particular case of lamination based mixing, the influence of aspect ratio (height/width), asymmetrical vs. symmetrical microstructures or inlet angle

has been widely investigated.³⁰⁻³² More particularly, finite element (FE) simulations have been used in our laboratory to study mixing as in zig-zag structure,¹⁵ as well as convection-diffusion-reaction phenomena in adsorption immuno-assay,³³ or multi-tagging of cysteinyl peptides in microchannel during the electrospray ionization process.²⁸

In the present study, a sandwich mixer, under pressure-driven flow (PDF) conditions, is investigated to optimise a one-stage chemical reaction $A + B \xrightarrow{k} C$. In comparison to electroosmotic driven flow (EOF),³⁴ pressure-driven flow present some advantages such as the relative ease and flexibility of implementation, insensitivity to surface contamination, ionic strength and pH. However, such PDF flows in microfluidic rectangular-shaped channel generate additional complexity in the distribution of analytes because of the velocity profile across one or both cross-sectional dimensions, referred to as Taylor dispersion.^{18, 35-37} Herein, we propose two approaches to optimise a chemical reaction in a sandwich mixer.

(i) The first one concerns the positioning of the reactants according to their diffusive properties in order to benefit of the parabolic flow profile. The gain of reaction extent obtained by using three flows instead of two, due to the decrease of the diffusion length, was first quantified. Then, the study was mainly focused on the sandwich design and the optimised positioning of the reactants across the velocity profile, according to their own diffusion coefficient. A comparison with a bulk reaction, where the species are ideally mixed, was done to highlight the influence of the local residence time value, directly linked to the transversal location of the reactants across the parabolic flow profile. To estimate the contribution of this flow profile, the same simulations were performed with a typical electroosmotic flat flow profile.

(ii) The second approach relies on the decrease of the lateral flow rates as another way to confine the reaction close to the walls while acting on the local kinetics.

(iii) To extend the conclusions to other chemical reactions, both methods were applied to a first order consecutive reaction ($A + B \xrightarrow{k_1} AB_1 + B \xrightarrow{k_2} AB_2 + B \xrightarrow{k_3} AB_3$).

In supplement, the influence of the species concentration ratio was evaluated as well. However, as the effect is limited and it is not the centre of this chapter, the results are kept in Appendix II-3.

2. Theory and Numerical description

2.1. Theoretical description

In lamellae mixing, the mixing efficiency depends on the maximal transversal dimension (thickness), $\delta_h = 2h/n$, of the n substreams to mix (with $2h$ the microchannel height). Splitting the flow into n substreams (or layers) decreases the mixing time. The mean residence time, \bar{t}_R , that governs the reaction extent, is fixed by the value of the main channel length L downstream the fluid junction, and the mean linear velocity, \bar{V} . At a given time t , the species transversal diffusion distance is estimated by $\delta_i(t) = \sqrt{D_i t}$, where D_i is the diffusion coefficient of the species i .

Figure II-4.A-B depicts the two geometries investigated: an asymmetrical two-flow geometry (Dual mixer) and a symmetrical three-flow design (Sandwich mixer). Both geometries present the same channel dimensions ($2h, L$) and an inlet angle of $\pm 45^\circ$ compared to the main microchannel position. The chemical reactants A and B are introduced from separated inlets, with the reaction $A + B \xrightarrow{k} C$ occurring downstream the fluid junction. To insure the comparison of reaction extent between the designs, the incoming flux of the A and B reactants are maintained equal (as well as the mean residence time, \bar{t}_R) by changing the species concentration. Figure II-4.C is the local flow velocity across the microchannel under pressure-driven flow condition with a mean velocity \bar{V} of $1.5 \text{ mm}\cdot\text{s}^{-1}$. Near the microchannel walls the local residence time is higher than the mean residence time ($t_R > \bar{t}_R$) while it is the contrary at the centre of the microchannel ($t_R < \bar{t}_R$). The scope of the present study is therefore to take benefit of this local velocity distribution to enhance the reaction extent in a sandwich mixer.

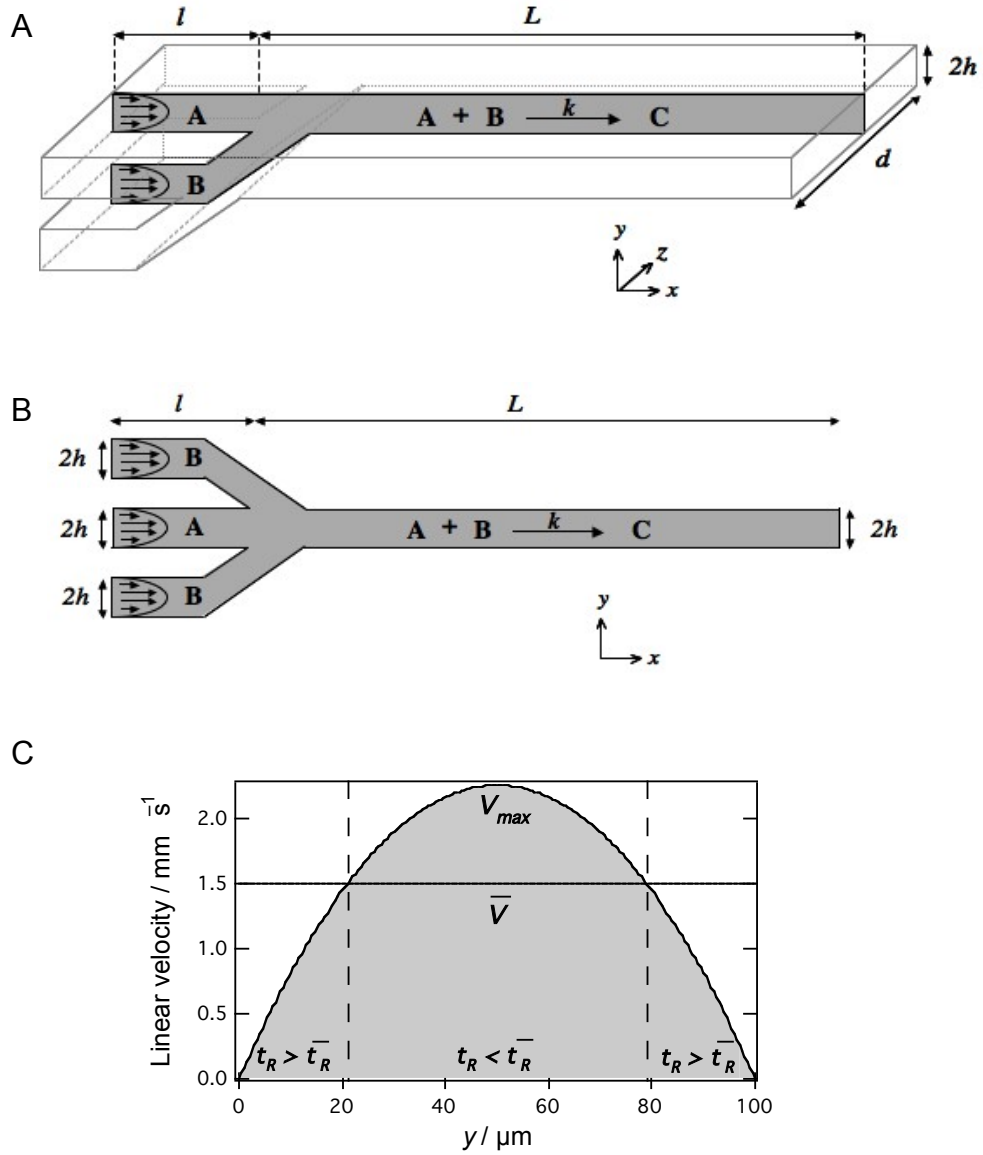


Figure II- 4 Geometries with A) two inlets (Dual AB) and B) three inlets (Sandwich mixer BAB). The A and B reactants are introduced at the inlets. The three-inlet geometry was also tested with the reactants inverted (Sandwich ABA or BAB). A geometry with $L = 2$ mm was used for the study of the diffusion coefficient ratio while a longer one with $L = 20$ mm was used for the study of the residence time and reaction extent effects. C) Local flow velocity across the microchannel under pressure-driven flow (PDF) condition, with a mean flow velocity \bar{V} of 1.5 mm·s⁻¹.

2.2. Numerical Model and validation

2.2.1. Numerical model and assumptions

The present model considers the laminar mixing of species along a 2D microchannel section, resulting from the contact between at least two incoming fluids featuring the same dynamic viscosity, μ , and the same density, ρ . The following assumptions are proposed:

(i) The solution is assumed to be sufficiently dilute and isothermal so that the viscosity and the density of the fluid can be considered as unmodified by temperature and concentration variations. All the simulations consider the injection of two identical fluids (same viscosity and density) as many reactions are performed by mixing the reactants into a same solution. The diffusion coefficient of each species is also treated as uniform in the entire study domain. (ii) The channel walls are considered to be smooth. (iii) The depth d of the channel is assumed to be much larger than its height $2h$ ($2h$ can be considered as “width” in a design fabrication point of view) so that the velocity gradient in the third dimension can be neglected (2D Cartesian assumption to overcome numerical limitations, valid for $d/2h > 10$). (iv) The fluid is assumed to be Newtonian and its velocity is described according to a parabolic flow profile (or PDF) in laminar conditions. (v) The modification of diffusion laws near the walls is not taken into account.^{35, 36}

In this model, the mixing process occurring at microscale is studied by solving the momentum and mass transport equations in two steps. First, the Navier-Stokes equation (eqn. 1) and the continuity equation (eqn. 2) are solved in the case of an incompressible fluid in an horizontal channel:

$$\frac{\partial \mathbf{V}^*}{\partial t^*} + \mathbf{V}^* \cdot \nabla \mathbf{V}^* = -\nabla p^* + \frac{1}{\text{Re}} \nabla^2 \mathbf{V}^* \quad (1)$$

$$\nabla \cdot \mathbf{V}^* = 0 \quad (2)$$

where \mathbf{V}^* , p^* , t^* are the dimensionless velocity vector, pressure and time with $\mathbf{V}^* = \mathbf{V}/V_0$, $p^* = p/\rho V_0^2$, $t^* = tV_0/L_0$, $x^*, y^* = x, y/L_0$ using the characteristic variables V_0 ,

L_0 , t_0 . For Reynolds numbers (eqn. 4) ranging from 10^{-3} to 1 in this study, the Navier-Stokes equation is solved in laminar conditions without taking into account chaotic instabilities. In addition, we assume that the parabolic flow profile is established at the inlets.

In a second step, the distribution of the species concentration within the geometry is addressed through the convection-diffusion-reaction equation (eqn. 3):

$$\frac{\partial c_i^*}{\partial t} + \mathbf{V}^* \cdot \nabla c_i^* - \frac{1}{\text{Pe}} \nabla^2 c_i^* = R_i \quad (3)$$

where $c_i^* = c_i/c_0$ is the concentration normalised by a characteristic concentration c_0 and R_i the rate of consumption of the species i .

The transversal Reynolds (Re) and Péclet (Pe) are defined as following:

$$\text{Re} = \frac{\bar{V}l_0}{\nu} \quad (4)$$

$$\text{Pe}_i = \frac{\bar{V}l_0}{D_i} \quad (5)$$

where \bar{V} is the average linear velocity, l_0 a characteristic transversal length, ν the kinematic viscosity ($\nu = \mu/\rho$), and D_i the diffusion coefficient of the species i .

2.2.2. Validation of the finite element model

The FE model was validated by comparison with analytical models regarding first the kinetic and then, the convection-diffusion model.

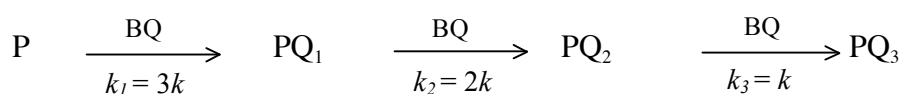
2.2.2.1. Validation of the kinetic model

Analytical model. The FE model, which describes the kinetics of single (and consecutive) reactions was validated with an analytical model originally used to predict cysteine-targeted tagging extents at the end of an electrospray emitter microchip.^{27, 38, 39} Considering a reaction between benzoquinone (BQ) tags and a peptide (P) containing one cysteine ($\text{P} + \text{BQ} \xrightarrow{k} \text{PQ}_1$), the rate law follows a first order kinetics for each reactant:

$$\nu = -\frac{d[\text{BQ}]}{dt} = -\frac{d[\text{P}]}{dt} = \frac{d[\text{PQ}_1]}{dt} = k[\text{P}][\text{BQ}] \quad (6)$$

where v is the rate of the reaction, k is the rate constant and $[BQ]$, $[P]$ and $[PQ_1]$ represent respectively the concentration of BQ tags, of a peptide P containing one cysteine residue and of the tagged product PQ_1 at the time t .

This kinetic model can be applied to consecutive reactions when the peptide possesses several cysteine units. In the case of a three-cysteine-containing peptide, the first step has an apparent rate constant that can be considered as $k_1 = 3k$, since the rate law can be here formulated as illustrated below. This model has been implemented in Maple 10.0 and was previously validated experimentally.^{27, 28}



Numerical model. The FE model was validated for the same consecutive reaction in a 1-D conditions (Figure II-5), with the following assumptions: *i*) the reactants (*i.e.* P and BQ) are ideally mixed at the microchannel inlet. *ii*) a flat flow profile (EOF) is applied in order to get a uniform flow velocity along the microchannel cross-section, and *iii*) the reaction time is controlled by the residence time inside the microchannel.

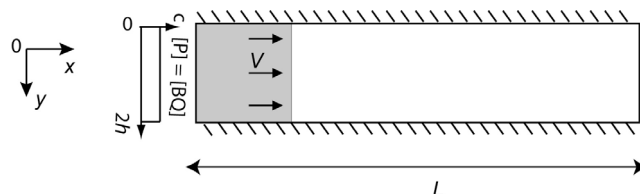


Figure II- 5 Geometry with a single microchannel (one inlet, one outlet) used for the FE model validation. The reactants (P, BQ) are provided from the inlet. The velocity is uniform across the microchannel. The reaction time (or residence time) is controlled according to the flow velocity and the channel length.

Validation. Figure II-6 compares the reaction extents obtained from both models in the case of the consecutive reaction described above. Considering the relative abundance of the reactants and products for an initial $[BQ]_0 = 20$ mM, the relative error is 1.60 %, 0.09 % and 1.45 % for PQ_1 , PQ_2 and PQ_3 , respectively. Consequently, the mean relative error between the analytical and the FE model is 1.04 % for $[BQ]_0 = 20$ mM, which is acceptable to validate

the kinetic model. This validation concerns the consecutive reaction but is also valuable for a single reaction as the one presented in this chapter. Indeed, the same equations were used in the present study with the PQ_2 , PQ_3 , k_2 , k_3 variables not defined.

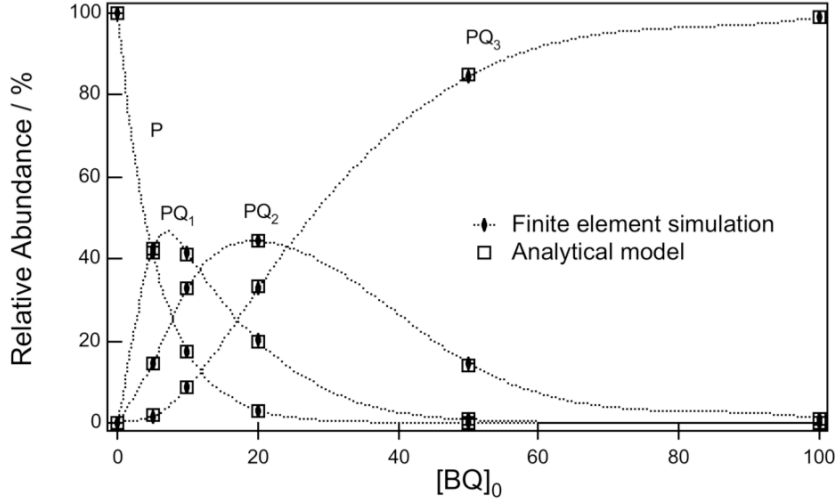


Figure II- 6 Relative abundance of the species involved in the consecutive reaction as a function of the initial concentration of the BQ reactant.

2.2.2.2. Validation of the convection-diffusion model

Analytical model. The FE convection-diffusion model in a two-lamellae mixer was validated with the analytical model described by Z. Wu *et al.*³⁸ The simplified 2-D analytical model of convective-diffusive transport in parallel lamination micromixers is depicted in Figure II-7. The geometry is a long channel of width W , two inlets and one outlet. One inlet stream is the solute with a concentration $c = c_0$ and a diffusion coefficient D . The other inlet stream is the solvent with a concentration $c = 0$. The two streams present the same viscosity and fluid density. As in the present work the calculations were performed for two-inlet streams of equal width, the dimensionless interface width r is set equal to 0.5.

Neglecting the diffusion in the flow direction ($Pe > 100$), the analytical solution is as follows:

$$c^*(x^*, y^*) = \frac{2}{\pi} \sum_{n=1}^{\infty} \frac{\sin n\alpha\pi}{n} \cos(n\pi y^*) \exp\left(-\frac{n^2 \pi^2}{Pe} x^*\right) + \alpha \quad (7)$$

$n = 1, 2, 3, \dots$

with W the channel width ($L_0 = W$), $c^* = c/c_0$, $y^* = y / W$ and $x^* = x / W$.

The calculations were performed with Maple 10.0 software.

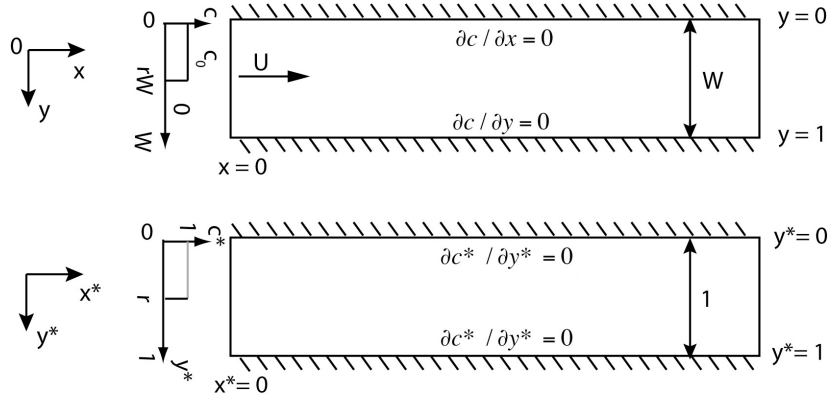


Figure II- 7 Models for convective-diffusive mixing ratio in the channels. (Top) The physical model. (Bottom) The dimensionless model. Adapted from Ref.⁴³.

Numerical model. The analytical results were compared with the 2-D finite element model with the following settings: *i*) the solute was injected in one half of the microchannel inlet ($c = 1$), *ii*) no chemical reaction ($k = 0$), *iii*) a uniform flow velocity across the channel (*i.e.* flat flow profile), and *iv*) the reaction time is controlled by the residence time in the microchannel.

Figure II-8 illustrates the isovalues of the solute concentration presenting a diffusion coefficient $D = 10^{-10} \text{ m}^2 \cdot \text{s}^{-1}$ ($\text{Pe} = 1500$) or $D = 10^{-9} \text{ m}^2 \cdot \text{s}^{-1}$ ($\text{Pe} = 150$). As expected, when the solute presents a higher diffusion coefficient, it diffuses more rapidly in the microchannel.

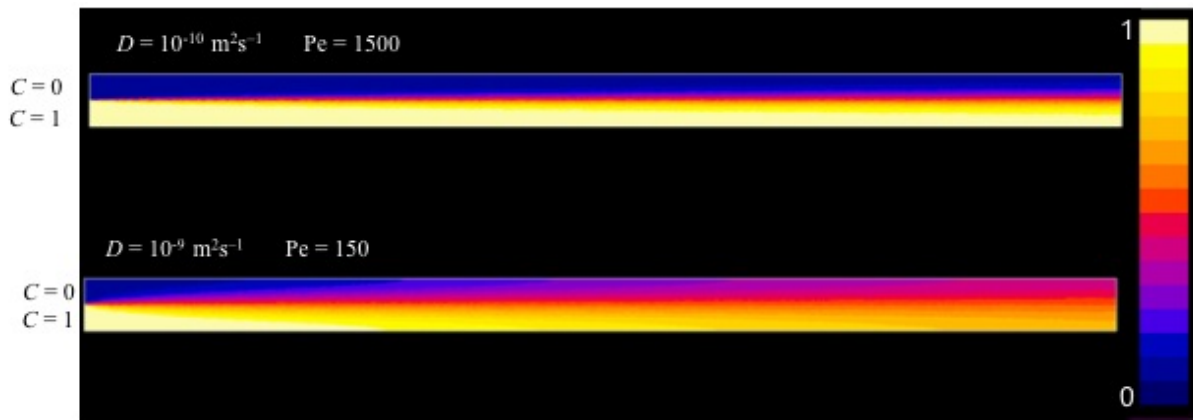


Figure II- 8 Isovalues of the solute distribution along the microchannel for $D = 1 \cdot 10^{-10} \text{ m}^2 \cdot \text{s}^{-1}$ and $D = 1 \cdot 10^{-9} \text{ m}^2 \cdot \text{s}^{-1}$.

Validation. Figure II-9 is the comparison of the analytical and numerical models in the same conditions, for $D = 1 \cdot 10^{-10} \text{ m}^2 \cdot \text{s}^{-1}$ and $D = 1 \cdot 10^{-9} \text{ m}^2 \cdot \text{s}^{-1}$. The two models follow the same trend for the positions $x^* = 10, 20$ and 40 along the microchannel, with a difference of 1.3% (averaged error value) that validates the numerical convection-diffusion model used in this study.

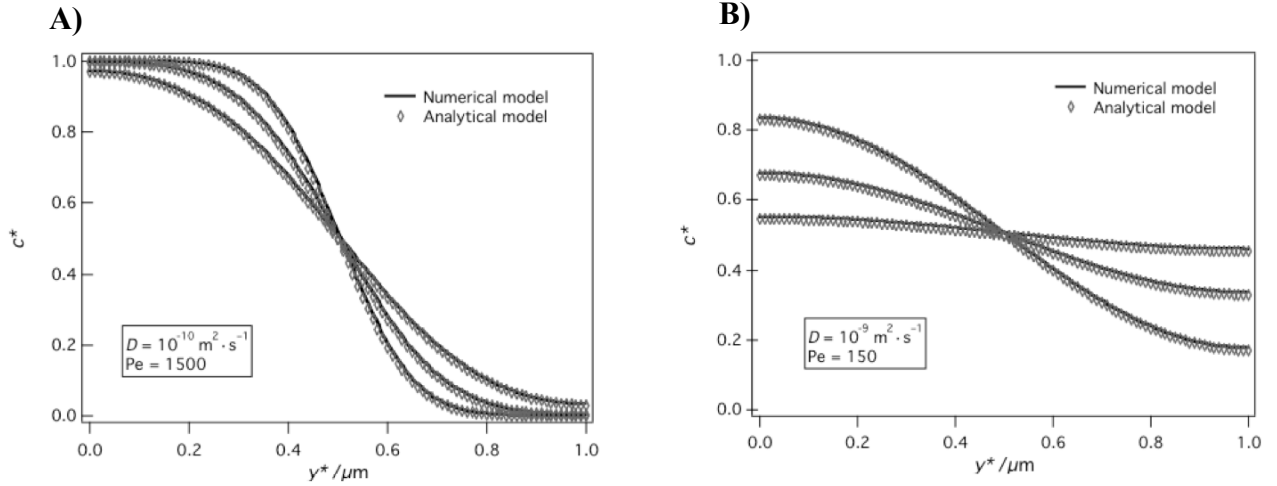


Figure II- 9 Dimensionless concentration distribution for two stream mixing in a channel for $x^*=10, 20$ and 40 . A) $D = 1 \cdot 10^{-10} \text{ m}^2 \cdot \text{s}^{-1}$ and B) $D = 1 \cdot 10^{-9} \text{ m}^2 \cdot \text{s}^{-1}$.

2.3. Numerical Parameters, normalization and calibration

2.3.1. Numerical parameters

The finite element formulation (Appendix II-1) was implemented in the commercial software Flux-Expert™ (Astek, Rhône-Alpes, France) on a Mac Pro with Ubuntu Linux 7.10 operating system. The numerical parameters used in this study are given in Table II-1. d is not simulated ($d / 2h > 10$ assumption).

Parameters	Numerical value	Parameters	Numerical value
$2h / \mu\text{m}$	100	$D_{A, Ref} / \text{m}^2 \cdot \text{s}^{-1}$	$1 \cdot 10^{-10}$
$L / \mu\text{m}$	2000 / 20000	$D_{B, Ref} / \text{m}^2 \cdot \text{s}^{-1}$	from $1 \cdot 10^{-10}$ to $1 \cdot 10^{-8}$
$l / \mu\text{m}$	200	$k / \text{M}^{-1} \cdot \text{s}^{-1}$	20 / 200 / 2000
$\bar{V} / \text{m} \cdot \text{s}^{-1}$	$1.5 \cdot 10^{-3}$	$v / \text{m}^2 \cdot \text{s}^{-1}$	10^{-6}

Table II- 1 Numerical reference parameters

2.3.2. Normalization of the results

The reaction extent ξ (%) is calculated by normalizing the integrated flux J_i of the produced species ($i = \text{C}$) by the flux of the initial reactant ($i = \text{A}$) at the inlet(s) (eqn. 8, 9).

$$J_i = \int_0^{2h} V_i \cdot c_i \cdot dh \quad (8)$$

$$\xi = \frac{J_C}{J_A} \times 100 \quad (9)$$

As the flux is depending on the local flow velocity V_i , the benefit of the near wall region is counterbalanced by its low contribution to the flux (low V_i value).

2.3.3. Evaluation of the chemical/diffusional regime

The second Damköhler number (Da)⁴⁰⁻⁴⁴ establishes the relationship between the reaction rate and the mixing rate. For an homogeneous phase reaction, this number is defined as:

$$\text{Da}_i = \frac{kc_i \delta_h^2}{D_i} \quad (10)$$

where k is the reaction rate constant, δ_h the thickness of a diffusion sub-layer as described previously, and c_i and D_i the volumic concentration and diffusion coefficient of the species i ,

respectively.^a It allows defining whether diffusion, kinetics or both of them control the reaction rate. Therefore, systems dealing with diffusion-based mixing and chemical reactions can be classified in three groups:

$Da \ll 1$: The reaction is limited by the kinetics.

$0.1 < Da < 10$: The regime is mixed and therefore the reaction is governed both by the kinetics and the diffusion.

$Da \gg 1$: The reaction is limited by the diffusion.

Figure II-10 represents the reaction extent as a function of the kinetics and calculated Da number, for three mean residence time of 0.23, 0.67 and 1.33 s, and with the two sandwich designs. When the reaction rate constant is increasing, which implies a higher Da number value, the reaction extent is higher and reaches a plateau. The simulations could not have been run for higher values of k due to a non-convergence of the calculations. To overcome this limitation, another way to increase the extent with reasonable value of k would have been to increase both c and D (same Da number) or to increase the residence time.

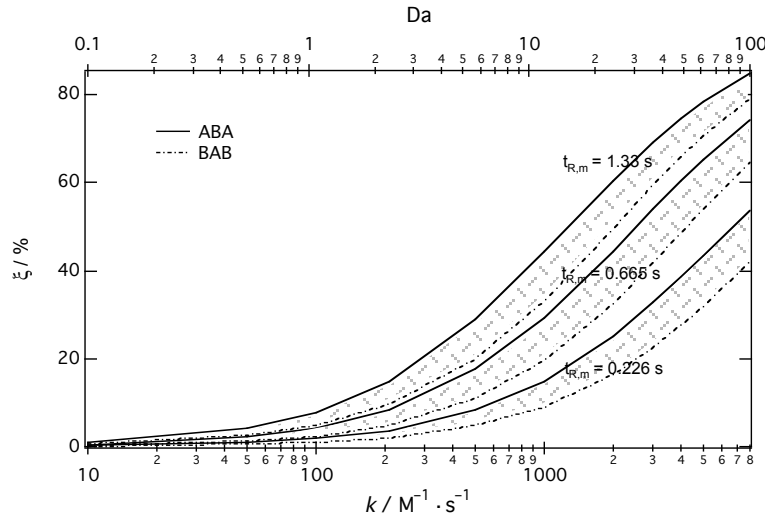


Figure II- 10 Influence of the reaction kinetics (and Damköhler number) on the reaction extent. Full line corresponds to the *ABA* design and the dashed line to the *BAB* design, for $D_B/D_A = 10$.

^a For a reaction at a surface, the Damköhler number is defined as: $Da = \frac{k_{on} \Gamma L_c}{D_i}$, where Γ is the surface concentration and L_c a characteristic length.

The major part of this study is performed at moderate reaction extents ($\xi_{Ref} < 10\%$ for $k = 200 \text{ M}^{-1}\cdot\text{s}^{-1}$, $c_A = c_B = 1 \text{ mM}$, $L = 2000 \text{ }\mu\text{m}$) for two main reasons.

(i) Because our objective was to compare the reaction enhancement between several designs, it appeared more interesting to compare the reaction extent when both designs can still gain in performance (*i.e.* the reaction does not reach completion). According to the Da number, a mixed regime ($0.1 < \text{Da} < 10$) is required. Indeed, the resulting Da number for $k = 200 \text{ M}^{-1}\cdot\text{s}^{-1}$ is 2.

(ii) The reaction rate constant of $210 \text{ M}^{-1}\cdot\text{s}^{-1}$ corresponds to the value of the 1,4-benzoquinone, a reactant used for the derivatization of cysteinyl peptides,⁴⁵ as the goal of this numerical work is to optimise a sandwich reactor for the post-column tagging of cysteines. Moreover, the simulated flow velocities are adjusted to conserve the same mean residence time than in experimental conditions: $(L, \bar{V})_{\text{exp}} = (1 \text{ cm}, 1.5 \text{ cm}\cdot\text{s}^{-1})$ and $(L, \bar{V})_{\text{sim}} = (1 \text{ mm}, 1.5 \text{ mm}\cdot\text{s}^{-1})$.

Nevertheless, the study is extended to slower ($k = 20 \text{ M}^{-1}\cdot\text{s}^{-1}$, $\text{Da} = 0.2$) and faster reaction rates ($k = 2000 \text{ M}^{-1}\cdot\text{s}^{-1}$, $\text{Da} = 20$) to determine the applicability of this study to other reaction kinetics.

2.3.4. Determination of the Péclet limit

The reaction extent normalized by the reaction rate and mean residence time ($\xi/k\bar{t}_R$) was calculated for different values of diffusion coefficient D . Indeed, as the reaction extent is depending on both the mixing and the kinetics, this normalization allows evaluating only the mixing contribution. For each value of D , the residence time is adapted in order to keep constant the term $D\bar{t}_R$ (constancy of the diffusion length $\sqrt{D\bar{t}_R}$). The adaptation of the residence time is done by extracting the reaction extent at different microchannel lengths. As $D\bar{t}_R/\delta^2 = \bar{t}_R/t_D$, this ratio is also constant in all the points in Figure II-11 ($\bar{t}_R/t_D \cong 0.05$). Consequently, when the normalized reaction extent ($\xi/k\bar{t}_R$) is independent of Pe values, the effect of the axial diffusion is negligible. According to the plateau, the results of Figures II-16.B, II -19.B, II-20 can be extrapolated for another value of (D, \bar{t}_R, δ_h) giving for the same values of \bar{t}_R/t_D , and with the condition that respectively: $\text{Pe} > 50$ for $k = 20 \text{ M}^{-1}\cdot\text{s}^{-1}$, $\text{Pe} > 300$ for $k = 200 \text{ M}^{-1}\cdot\text{s}^{-1}$, $\text{Pe} > 10000$ for $k = 2000 \text{ M}^{-1}\cdot\text{s}^{-1}$ (values determined for a maximal deviation fixed at 1%). Consequently, the results presented in Figures II-16.B, II -19.B, II-20

for $k = 2000 \text{ M}^{-1}\cdot\text{s}^{-1}$ cannot be extrapolated as the Pe number in this study is 1500 (not included in the plateau in Figure II-11).

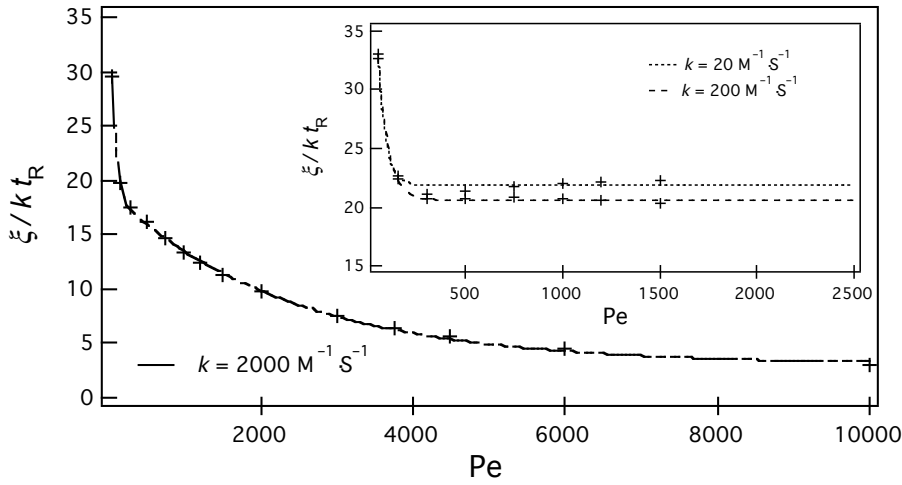


Figure II- 11 Reaction extent normalized by the reaction rate and residence time as a function of the Peclet value. The simulations were performed with $D_A = D_B$ and for $k = 20, 200$ and $2000 \text{ M}^{-1}\cdot\text{s}^{-1}$.

2.3.5. Extent to well-known geometries

Because geometries with orthogonal inlets are often used in the litterature,^{3,12, 46} the performance of the Dual and Sandwich designs presented here was compared to an equivalent Y-mixer and cross-mixer. The reaction extent is simulated for identical residence time, reaction rate, reactant concentration and diffusion coefficients.

The results are presented in the following Table II-2. The geometries were compared for an advanced reaction extent ξ ($k = 5000 \text{ M}^{-1}\cdot\text{s}^{-1}$) and a low reaction extent ξ_{Ref} ($k = 200 \text{ M}^{-1}\cdot\text{s}^{-1}$). The relative error between the two double-inlet designs and the two triple-inlet designs is slightly higher at low reaction extents. Nevertheless, in all the conditions the relative error is inferior or equal to 0.6% meaning that the conclusions from this study are also valuable for more “commonly” used designs such as the Y-mixer, T-mixer or the cross-mixer.





	Advanced reaction extent		Low reaction extent (Reference case)	
Geometries	ξ (%)	Relative error	ξ_{ref} (%)	Relative error
	45.21	0.03%	2.6236	0.24%
	45.2		2.629	
	53.61	0.13%	5.707	0.60%
	53.67		5.741	

Table II- 2 Comparison of the inlet design influence for a side-branch mixer, a Y-mixer, a sandwich mixer and a cross mixer.

3. Results and Discussions

According to the parabolic flow profile occurring in a microchannel, the reaction extent can be enhanced by several ways. The following sections aim to study the influence of the diffusion coefficient ratio D_B/D_A , the reaction extent $\xi(k, c, t)$, and the ratio between the diffusion length and the layer thickness \sqrt{Dt}/δ_n on the final reaction extent at the end of a microchannel.

3.1. Gain due to the number of substreams ($D_B/D_A = 1$)

The geometrical advantage of using a three- instead of a two-flow design was first quantified. Figure II-12 represents the reaction extent ξ as a function of the diffusion coefficient ratio of the A and B reactants within the Dual and Sandwich geometries, for a given reaction rate constant $k = 200 \text{ M}^{-1} \cdot \text{s}^{-1}$. The reference case for which the reactant diffusion coefficient ($D_A/D_B = 1$) and incoming flux are equals is first considered (with equal incoming flux $J_A = J_B$ for all the simulations). The reaction extents, ξ_{Ref} , for the Dual and Sandwich designs are 2.6% and 5.7%, respectively. In addition, two sets of simulations for the sandwich design were performed by inverting the position of the A and B reactants at the inlets (ABA or BAB). As $D_A = D_B$ in the reference case, the two sandwich configurations are symmetrical and present an equal reaction extent, as expected. The gain of the three-flow design compared to the two-flow design (*i.e.* the ratio $\xi_{\text{Sandwich}} / \xi_{\text{Dual}}$) is therefore of 2.2 (*i.e.* 120 % reaction extent improvement) and is due to the decrease of δ_h as it will be illustrated later.

3.2. Gain due to the diffusion coefficient ratio of the reactants in a sandwich mixer

3.2.1. Influence of the species diffusion coefficient ratio, for $k = 200 \text{ M}^{-1} \cdot \text{s}^{-1}$.

The curves Sandwich ABA & BAB and Dual in Figure II-12 illustrate the influence of the A and B reactant position within the inlets, according to the values of their diffusion coefficient for a reaction rate of $200 \text{ M}^{-1} \cdot \text{s}^{-1}$. By increasing the value of the diffusion

coefficient of B from 10^{-10} to $10^{-8} \text{ m}^2 \cdot \text{s}^{-1}$ (D_B/D_A ranging from 1 to 100), a higher reaction extent is observed when the reactant with the lowest diffusion coefficient (reactant A) is injected from the outer flows, near the microchannel walls where the species get a longer residence time inside the microchannel compared to the mean residence time ($t_R > \bar{t}_R$, as shown in Figure II-4.C).

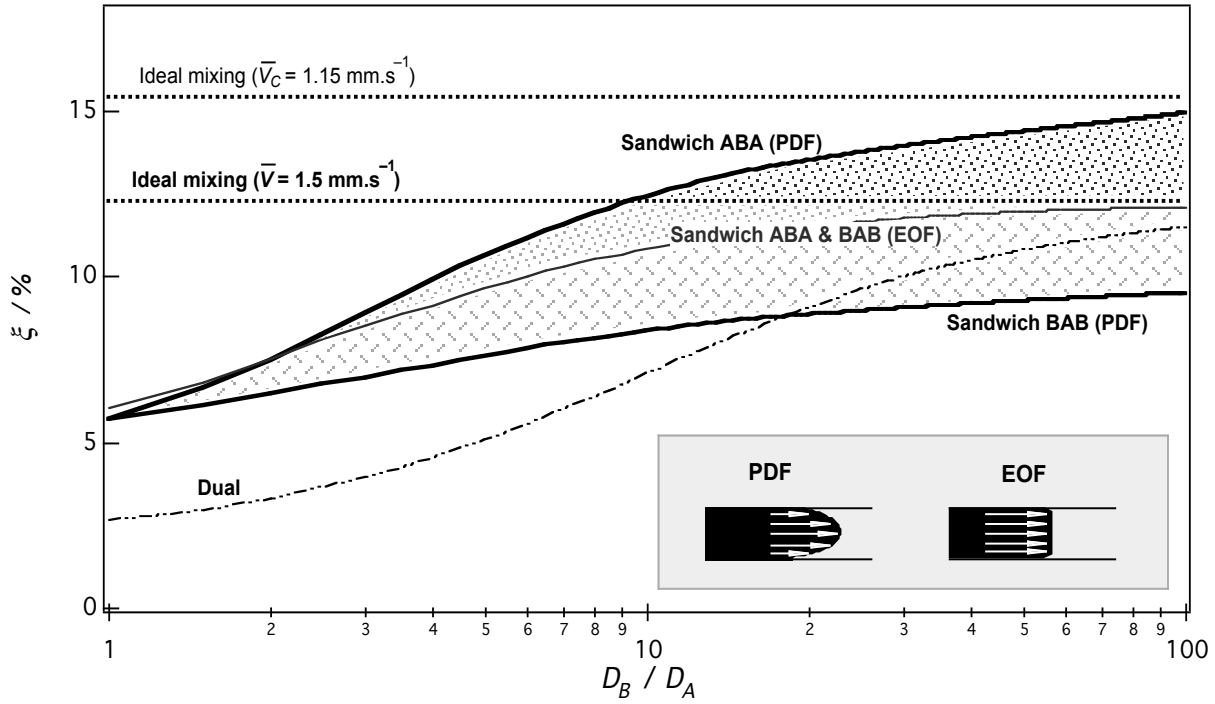


Figure II- 12 Effect of the diffusion coefficient ratio of the A and B reactants on the reaction extent within the three geometries (sandwich *ABA* & *BAB*, Dual) and comparison with a reaction in bulk condition and with a flat flow profile (EOF). Parameters: $k = 200 \text{ M}^{-1} \cdot \text{s}^{-1}$, $L = 2000 \text{ } \mu\text{m}$, $\bar{t}_R = 1.33 \text{ s}$ for $\bar{V} = 1.5 \text{ mm} \cdot \text{s}^{-1}$.

Figure II-13 shows the isovalues and the concentration distribution of the species involved in the reaction, along a cross-section at a distance $L/2 = 1000 \text{ } \mu\text{m}$ downstream the fluid junction ($D_B/D_A = 10$). Within the sandwich *BAB* geometry (Figure II-13.A), the B reactant presenting a higher diffusion coefficient, diffuses along all the microchannel cross-section, while the A reactant is mainly located at the microchannel centre. The reaction is therefore mainly located at the centre of the microchannel where C is produced, as illustrated on the corresponding isovalues. On the contrary, within the optimal sandwich *ABA* geometry (Figure II-13.B), the A reactant is close to the walls allowing the reaction to occur where $t_R > \bar{t}_R$. In the case of the Dual geometry (Figure II-

13.C), as the species are initially present in two symmetrical flows, the reaction mainly takes place in one half side of the microchannel. It explains why, for $D_B/D_A > 20$, the Dual design can provide better results than the non-optimal sandwich BAB .

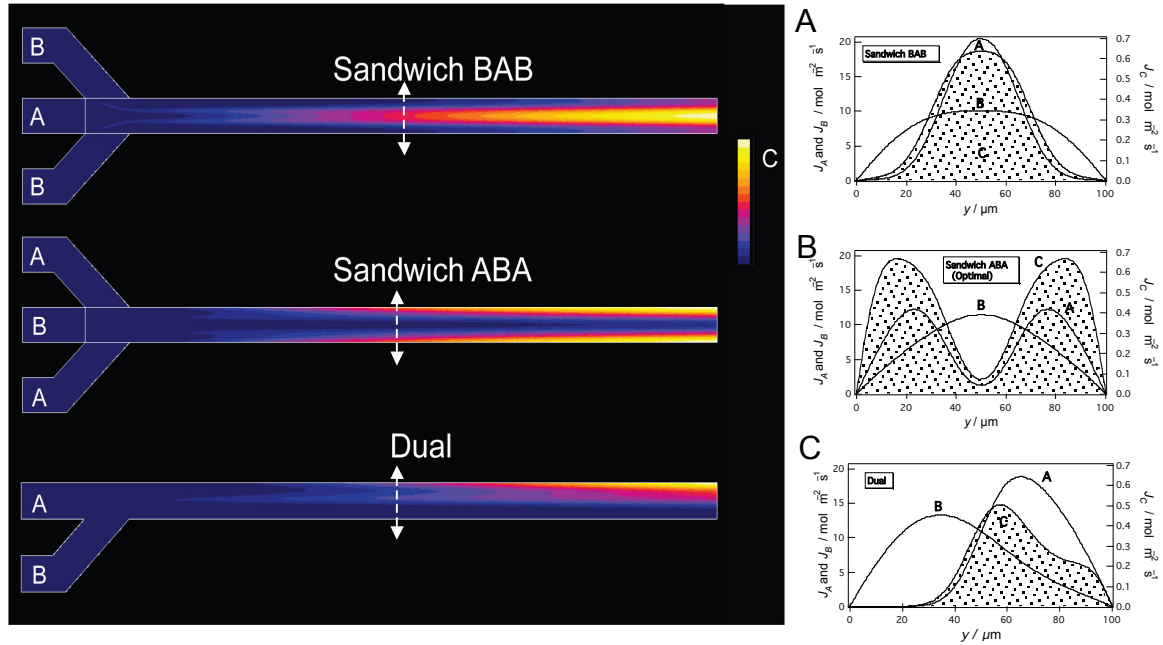


Figure II- 13 (Left) Isovalues of the reaction product C along the microchannel length within the three geometries, for $D_B/D_A = 10$ and $L = 2000 \mu\text{m}$. (Right) Species concentration distribution along the microchannel cross-section, at the position $L/2$ downstream of the fluid junction. A-B-C) Species concentration distribution of the A and B reactants and C product with the non-optimal (Sandwich BAB), optimal (Sandwich ABA) triple inlet or double inlet (Dual) geometries, respectively, and for $D_B/D_A = 10$. The concentration distribution of C is represented by the grey surface.

The reaction extent within the three geometries of mixer-reactors (sandwich ABA & BAB , Dual) was compared to a reaction in bulk conditions where the species are ideally mixed. The simulations were performed in a 1-D microchannel presenting the same dimensions and mean residence time $\bar{t}_R = 1.33 \text{ s}$ ($\bar{V} = 1.5 \text{ mm}\cdot\text{s}^{-1}$). In bulk conditions, the reaction extent is independent of the reactant diffusion coefficients, as illustrated by the constant value of ξ in Figure II-12 (dotted line). By increasing the D_B/D_A ratio, the Dual geometry is approaching the reaction extent of an ideal mixing. For $D_B/D_A > 10$, as the reaction is mainly occurring next to the walls where the local value $t_R > \bar{t}_R$, the optimal sandwich mixer (ABA) overpasses the bulk reaction extent for a same \bar{t}_R . Our hypothesis was that this overpassing of the bulk

reaction extent is due to the location of C (and so the location of the reaction) close to the walls where $t_R > \bar{t}_R$. The mean velocity of the product \bar{V}_C is therefore lower than the mean flow velocity \bar{V} . Figure II-14 represents the flux density of the C product along a cross-section of the microchannel at L , $L/2$ and $L/4$. The flat flow profile corresponding to the mean flow velocity ($\bar{V} = 1.5 \text{ mm}\cdot\text{s}^{-1}$) is represented by the horizontal dotted line. The intersection between this line and the parabolic flow velocity profile delimitate three areas: the two zones next to the walls where $t_R > \bar{t}_R$, and the one at the centre of the microchannel where $t_R < \bar{t}_R$. Figure II-12 shows that for high D_B/D_A , the reaction extent is higher than a bulk reaction for the same mean residence time \bar{t}_R . To validate our hypothesis, the mean flow velocity \bar{V}_C of the C species was determined according to the position of the maximal production of C across the microchannel. This position was then reported on the parabolic flow profile curve in order to define the corresponding velocity $\bar{V}_C = 1.15 \text{ mm}\cdot\text{s}^{-1}$. The simulation in bulk was run a second time with this corrected value as presented in Figure II-12. With this corrected mean residence time corresponding to \bar{V}_C , the reaction extent in PDF condition tends asymptotically to the bulk reaction extent that validates our hypothesis.

Therefore, by taking care of the reactant position, for $D_B/D_A > 10$ the optimised sandwich mixer can provide similar or even better results than a corresponding bulk reaction.

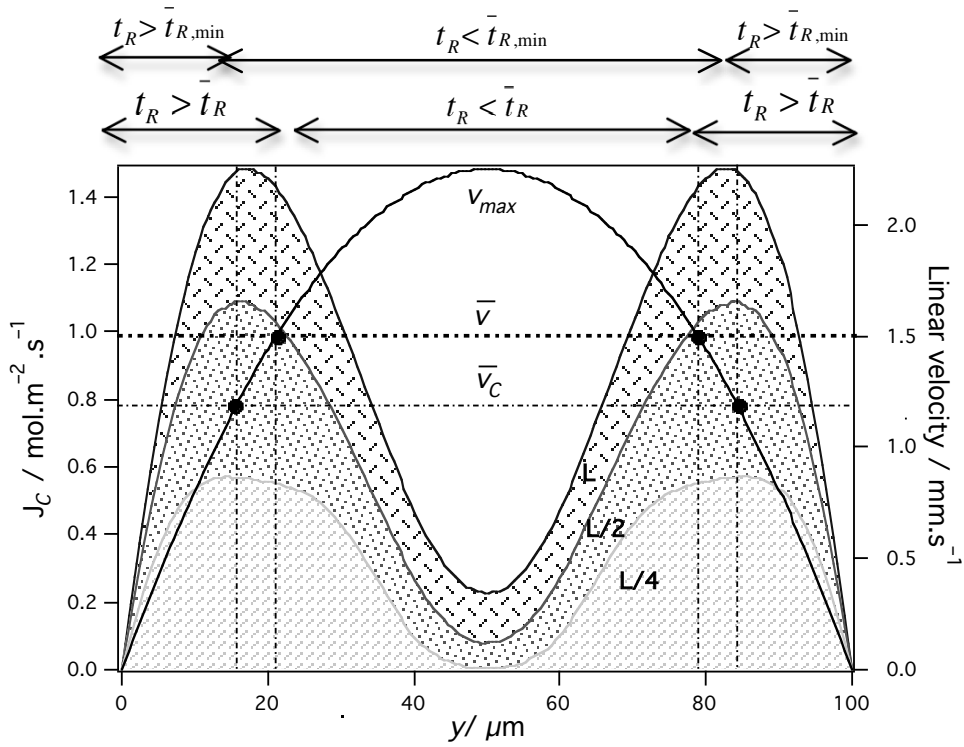


Figure II- 14 Flux density distribution of the C product (filled areas) along the microchannel cross-section at a distance L (i.e. microchannel outlet), $L/2$ and $L/4$. The pressure-driven flow profile in the microchannel is represented by the dark line and the corresponding mean flat flow profile (in the case of a EOF profile or ideal mixing) by the dotted line. $L = 2000 \mu\text{m}$.

3.2.2. Quantification of the parabolic flow profile contribution (PDF vs. EOF)

To quantify the contribution of the parabolic flow profile in the reaction extent observed, the results in PDF conditions were compared to the ones obtained with a flat EOF flow profile within the Sandwich geometries. Figure II-15 quantifies the contribution of the flow velocity profile to the reaction extent as a function of D_B/D_A ratio. In optimal conditions, the parabolic profile allows an increase of the reaction extent from 0 to 22% for high D_B/D_A . For $D_B/D_A < 2$, the simulation in EOF conditions gives better results than the one with a parabolic profile. On the contrary, when the position of the reactants is not optimised according to their diffusion coefficients, the loss induced by the parabolic flow profile compared to a flat flow profile reaches 20% for high D_B/D_A ratio.

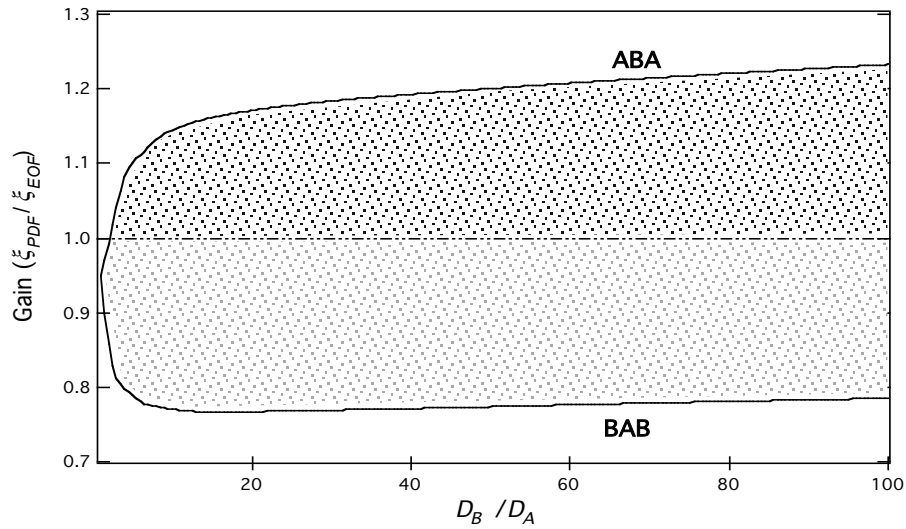


Figure II- 15 Evaluation of the gain due to the flow profile in the optimal (*ABA*) and non-optimal (*BAB*) sandwich mixer.

3.2.3. Optimal vs. non-optimal sandwich design and extent to other kinetics ($k = 20, 200$ and $2000 \text{ M}^{-1}\cdot\text{s}^{-1}$)

To extend the study to other conditions, three different rate constants ($k = 20, 200$ and $2000 \text{ M}^{-1}\cdot\text{s}^{-1}$) were simulated. Figure II-16.A summarizes the evolution of the gain calculated between the optimal *ABA* and non-optimal *BAB* designs as a function of the diffusion coefficient ratio between A and B. These values were integrated vertically at a fixed position at the end of a microchannel ($L = 2000 \mu\text{m}$). With a correct position of the reactant, a gain of 70%, 55% or 20% reaction enhancement can be reached for $D_B/D_A = 100$, and $k = 20, 200$ and $2000 \text{ M}^{-1}\cdot\text{s}^{-1}$, respectively. As expected, a higher gain is obtained for low reaction rates, as the initial reaction extent is smaller.

Figure II-16.B considers the case where $D_B/D_A = 10$ with the gain represented as a function of the dimensionless time \bar{t}_R/t_D . It is interesting to note that $\bar{t}_R/t_D = D\bar{t}_R/\delta_n^2$ also corresponds to the square of the diffusion length normalised by the multilayer thickness δ_n . A longer microchannel ($L = 20000 \mu\text{m}$) was used to enable a sufficient residence time to tend to reaction completion. For low time values, the evolution of the gain follows the same trend for different kinetics with a maximum shifted to higher \bar{t}_R/t_D for lower reaction kinetics. The increase of the gain up to this maximum is due to the diffusion of

the B reactant (with the highest diffusion coefficient) that determines, in a first stage, the transversal location of the reaction across the flow velocity profile.

For the optimal *ABA* geometry, the increase of gain is the consequence of the diffusion of B from the microchannel centre to the walls, confining the reaction in a longer t_R area. When B is homogeneous along the microchannel cross-section, the slow diffusion of the A reactant towards the centre displaces progressively the position of reaction from the walls to the centre, inducing a loss of the gain. If we consider that the optimisation is of interest for a minimal gain of 20% reaction enhancement, the position of the reactants in a sandwich mixer is valuable for $\bar{t}_R/t_D < 0.7, 0.4$ and 0.1 for $k = 20, 200$ and $2000 \text{ M}^{-1}\cdot\text{s}^{-1}$, respectively. Complementary results for other D_B/D_A ratios are in Appendix II-2.

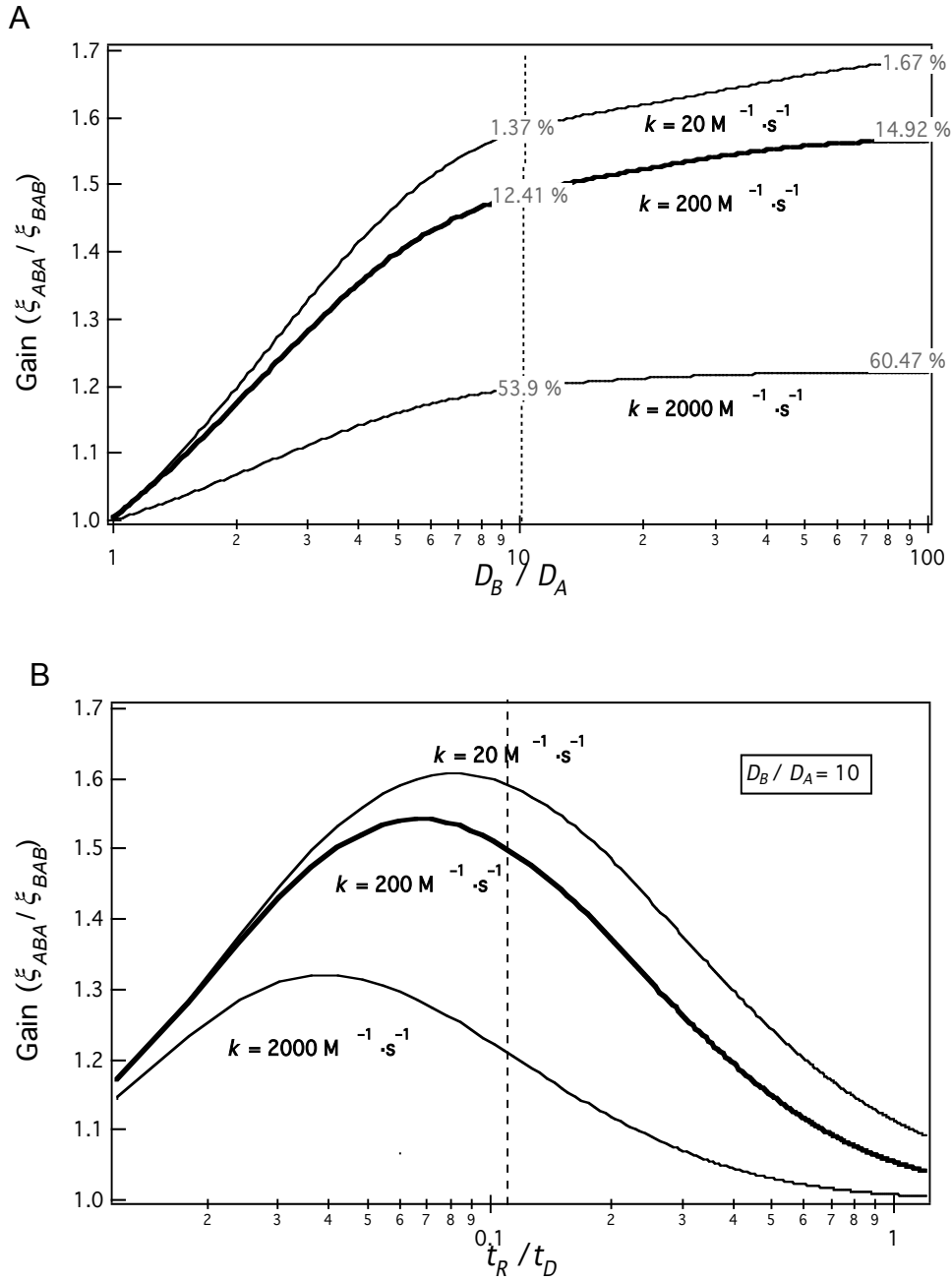


Figure II-16 Gain due to the optimal positioning of the reactants in a sandwich mixer. A) Gain of the optimal (*ABA*) vs. the non-optimal (*BAB*) sandwich mixer as a function of the reactant diffusion coefficient ratio for $k = 20$ ($Da = 0.2$), 200 ($Da = 2$) and $2000 \text{ M}^{-1} \cdot \text{s}^{-1}$ ($Da = 20$), with $L = 2000 \text{ }\mu\text{m}$. The vertical dashed line corresponds to the D_B/D_A of 10 used as reference in this study. B) Gain *ABA* vs. *BAB* as a function of dimensionless time (\bar{t}_R / t_D) for $D_B/D_A = 10$ and $L = 20000 \text{ }\mu\text{m}$. The vertical dashed line is the \bar{t}_R / t_D value of 0.12 that corresponds to $\bar{t}_R = 1.33 \text{ s}$ at the end of a microchannel of $L = 2000 \text{ }\mu\text{m}$.

Figure II-17 represents the evolution of this geometrical gain as a function of the reaction extent calculated in the non-optimal *BAB* geometry. The envelop of the gain grouping the three kinetics at a given D_B/D_A clearly shows a decrease of the gain for high reaction extent. For a value above 70%, this optimisation is not useful as the reaction tends to completion, also for the *BAB* geometry.

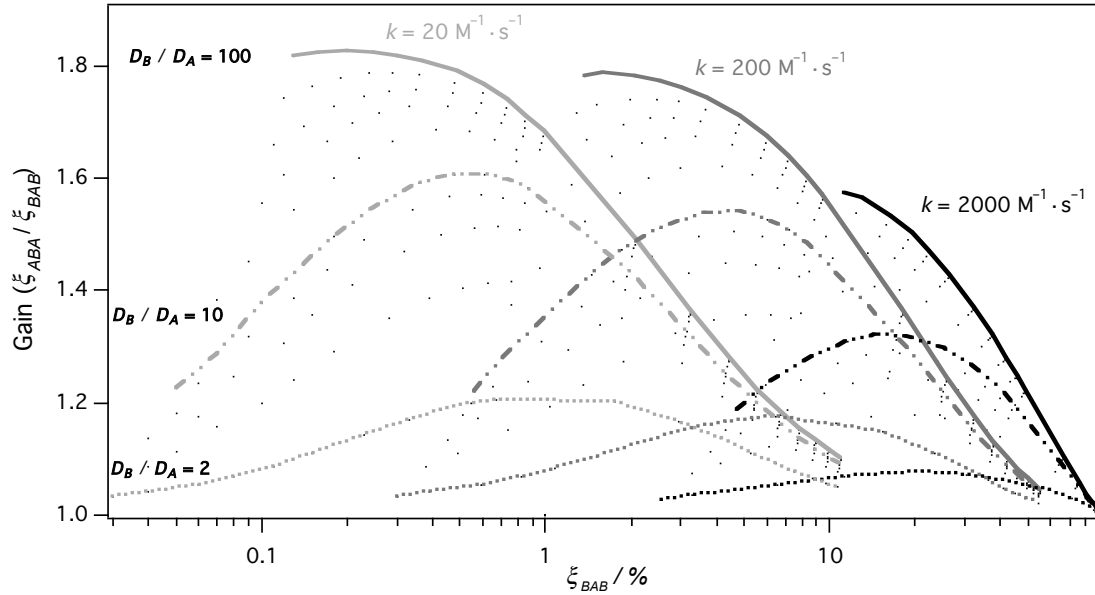


Figure II- 17 Gain of the optimal (*ABA*) vs. non-optimal (*BAB*) geometry as a function of the reaction extent of the *BAB* design ($L = 2000 \mu\text{m}$), for $k = 20, 200$ and $2000 \text{ M}^{-1}\cdot\text{s}^{-1}$ and $D_B/D_A = 2$ (dotted line), 10 (dashed line) and 100 (full line). Dots are the intermediate values for the other D_B/D_A ratios.

3.3. Gain due to the external flow rate Q_A decrease and local kinetics kc_A

Another way to confine the reaction close to the walls in a sandwich design is to decrease the volumic flow rate Q_A of the outer flows ($D_A = D_B$).

3.3.1. Relation between the flow rate ratio and the external A layer thickness

The A layer thickness was determined for different flow rate ratios in a *ABA* sandwich mixer ($D_A = D_B$ and $J_A = J_B$). Along the transversal A and B concentration profile, the thickness of the A layer is defined by the intersection between two consecutive streams where $c_A > c_B$ for

the first one and $c_B > c_A$ for the other one. As illustrated in Figure II-18, the decrease of the A layer thickness is linear for $0.5 < Q_A/Q_{A,Ref} < 1$ and amplified after ($Q_A/Q_{A,Ref} < 0.5$).

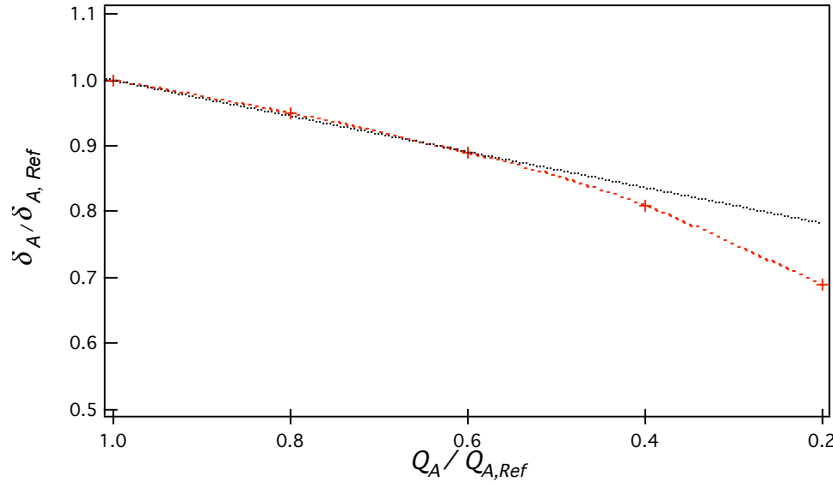


Figure II- 18 Relation between the lateral stream flow rate and the transversal diffusion length. Simulated data are in red. The black line is the extrapolated linear correlation for the first points.

3.3.2. Gain due to the external flow rate Q_A decrease and local kinetics kc_A

The Figure II-19.A illustrates the gain due to the decrease of Q_A by comparison to the reference case (*i.e.* the *ABA* design with $Q_{A,Ref} = Q_A = Q_B$ and $D_A = D_B$). To be in a comparable situation of reactant consumption, the following simulations were performed with an equal flux of A and B reactants ($J_A = J_B$). It results in a larger value of the local concentration of A that strongly amplifies the reaction kinetics ($kc_A c_B$ in the R_i term of eqn 3) and acts as a “booster” of the reaction starting from the small residence time values. Therefore, the gain observed is due to the kinetic increase, the location of the reaction close to the walls, and the decrease of the external flow layer thickness.

The results were extracted at corrected positions along the microchannel to maintain the same \bar{t}_R (without this correction, the gain is even stronger). By decreasing $Q_A/Q_{A,Ref}$, the gain exponentially increases to reach 2.4 for $Q_A/Q_{A,Ref} = 0.2$ and $k = 200 \text{ M}^{-1} \cdot \text{s}^{-1}$ (3.2 and 1.4 for $k = 20$ and $2000 \text{ M}^{-1} \cdot \text{s}^{-1}$, respectively). It can be explained by the decrease of the A layer thickness as the $Q_A/Q_{A,Ref}$ ratio is reduced. As shown in Figure II-18, this decrease is linear for $0.5 < Q_A/Q_{A,Ref} < 1$ and amplified after ($Q_A/Q_{A,Ref} < 0.5$) which

results in the strong gain increase observed in Figure II-19.A.

Figure II-19.B is the evolution of the gain for $Q_A/Q_{A,Ref} = 0.2$ as a function of dimensionless time \bar{t}_R/t_D . The maximal gain is reached for small \bar{t}_R/t_D that corresponds to small residence time and then it decreases progressively. After the fluid junction, the reaction is rapidly located next to the walls, as δ_A is decreased by the low lateral flow rate. As for the previous method, the gain decrease is then due to the reaction that is progressively displaced from the walls to the centre with the diffusion of A. The contribution of the parabolic flow profile in the gain value was evaluated by comparison with an EOF profile, and it reaches 11.3% for the lowest value of the outer flow velocities. It confirms that the kinetic effect is the main source of the present gain increase.

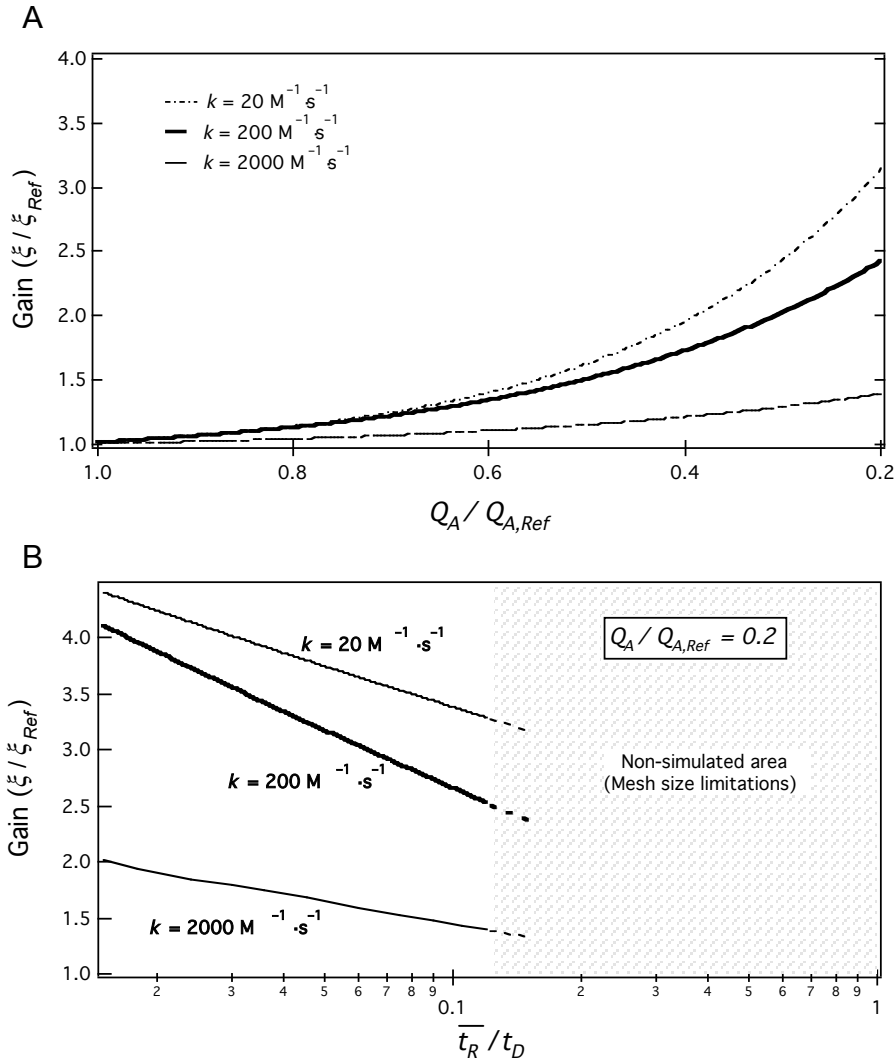
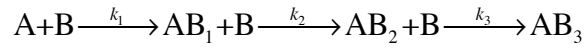


Figure II- 19 Effect of the external flow rate decrease on the reaction extent. A) Reaction extent gain due to the decrease of the lateral flow rate. The gain is evaluated by comparison with the reference case ($Q_{A,Ref} = Q_{B,Ref}$) at the end of a microchannel length of $L = 2000 \mu\text{m}$. The simulations are run with $D_A = D_B$. B) Evaluation of the reaction extent gain as a function of dimensionless time \bar{t}_R / t_D , with $L = 20000 \mu\text{m}$.

3.4. Application to a consecutive reaction

The previous simulations concern the optimisation of a one-stage chemical reaction in a sandwich mixer. In order to extend this study to other chemical reactions, the two methods presented herein were applied to consecutive first order reactions, described as:



where A and B are the reactants and AB_1 , AB_2 and AB_3 the intermediate and final products of the reaction, with $k_1 = 3k$, $k_2 = 2k$, $k_3 = k$.

Figure II-20.A is an illustration of the first method that consists in placing the reactant in the sandwich mixer-reactor according to their diffusion coefficient ratio ($D_B/D_A = 10$ and $D_B/D_A = 100$). For $D_B/D_A = 10$, the one-stage and consecutive reaction are presented. For a consecutive reaction, the gain is 1.5, 2.1 and 3.2 for AB_1 , AB_2 , and AB_3 , respectively, while the reaction extent for a one-stage reaction is around 1.5. For $D_B/D_A = 100$, the gain is still higher and is occurring at lower \bar{t}_R/t_D as the diffusion of the B reactant is faster.

Figure II-20.B is the comparison of the gain of a one-stage versus a consecutive reaction when the reaction is located close to the walls and the kinetics is increased by the higher concentration of A (conservation of the flux), for $Q_A/Q_{A,Ref} = 0.2$. In this second method and for the same method as before, the maximal gain is obtained at low \bar{t}_R/t_D , and is 3.5, 6.8 and 13 for AB_1 , AB_2 , and AB_3 . The maximal gain of the one-stage reaction is 4.

The present study of chemical reaction optimisation in a sandwich mixer-reactor is even more interesting for consecutive reactions as the reaction is increased for all the intermediate products that finally yield a higher global reaction extent.

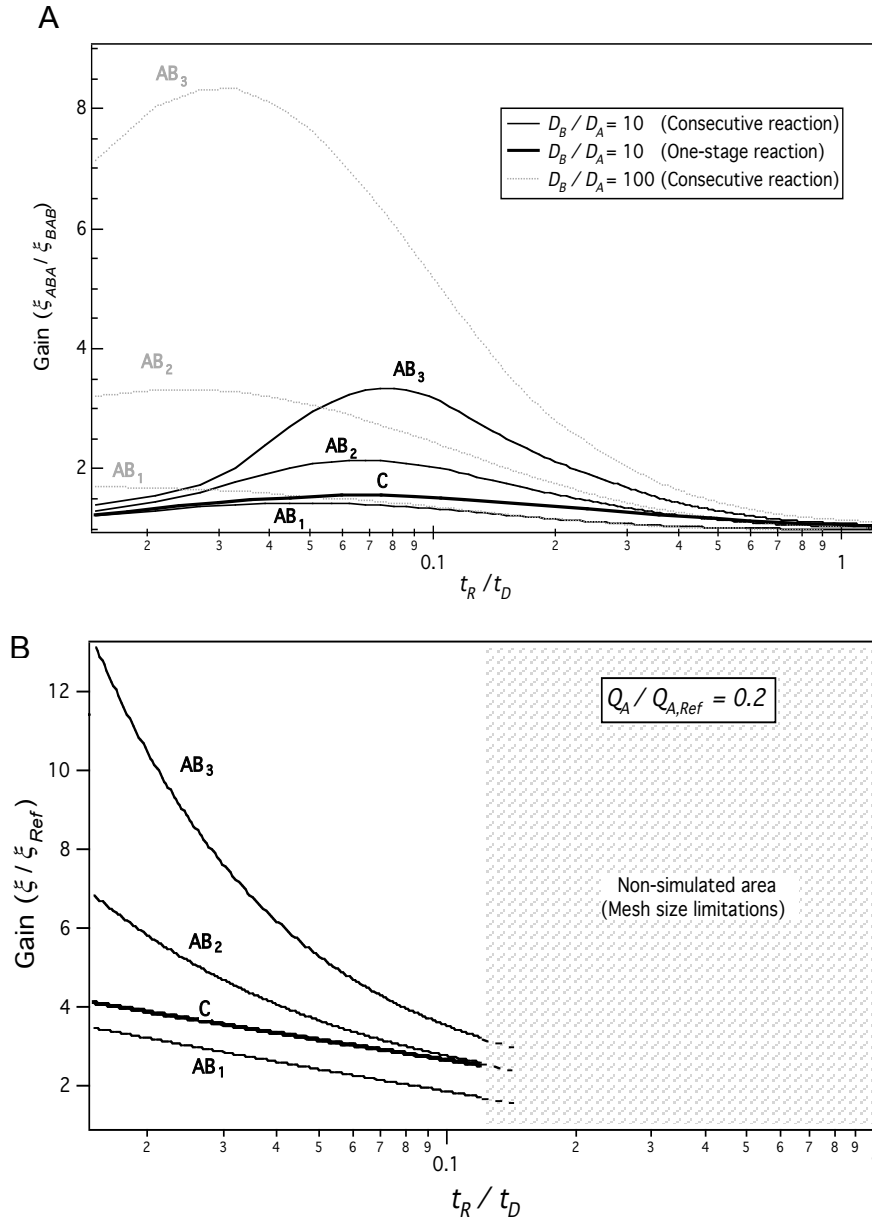


Figure II- 20 Consecutive reaction gain in function of the dimensionless time $\overline{t_R} / t_D$. A) Reaction extent gain by placing the reactants according to their diffusion coefficient ratio and comparison with a one-stage reaction, for $D_B / D_A = 10$ and 100 ($L = 2000 \mu m$). B) Reaction extent gain by decreasing the lateral flow rates (conservation of the flux, $L = 20000 \mu m$).

4. Conclusions

Simulation of chemical reaction extent relying on microfluidic properties and diffusive characteristics of molecules has been investigated in a *sandwich* mixer by a finite element method.

The diffusion coefficient ratio of the molecules to react was demonstrated to be an important factor to take into account in such a mixer-reactor. Within this geometry, the reactive species that present the lowest diffusion coefficient have to be introduced from the outer inlets. Thus, the reaction mainly occurs next to the walls where the local residence time is higher than the mean residence time in the microchannel. This optimisation becomes even more relevant as the difference of diffusion coefficient increases, allowing reaching 60% of reaction enhancement, and is of interest for moderate reaction extent lower than 70%. Another way to improve the reaction extent in a *sandwich* mixer is to confine the reaction as close as possible to the walls by the decrease of the outer flow rate. This is a way of increasing the kinetics (high local value of A concentration to keep the flux ratio of A and B) while maintaining a reasonable global flow rate typically required as example for mass spectrometry analysis (V_B unchanged). With such a technique, the reaction can be improved by 300%, provided that the over concentration applied from the low velocity outer inlets does not induce a precipitation or adsorption of the molecules. As expected, improvement is no more valuable for advanced residence time (typically $\bar{t}_R/t_D > 0.5$) for which the non-optimal case approaches reaction completion. These two methods of optimisation of a sandwich mixer were even more interesting for consecutive reactions as each intermediate species is increased.

For further investigations, it would be interesting to evaluate other kind of reactions as parallel or reversible reactions, as well as second order reactions. In a more general view, the conclusions about the influence of the diffusion coefficient ratio can be applied to different kind of species as, for example, on-line deuterium exchange experiments (as diffusion coefficient of heavy water is $10^{-9} \text{ m}^2\cdot\text{s}^{-1}$ compared to proteins at $10^{-10} \text{ m}^2\cdot\text{s}^{-1}$), on-line chemical modification of peptides/proteins, or antibody-antigen reactions. The study of the influence of the flow rate ratio considers a reaction between species of similar diffusion coefficient that typically can be applied to protein-protein interactions, as example.

In practice, such simulations are very useful to optimise on-line chemical reactions such as, for example, on-line chemical derivatization of biomolecules after a chromatographic or

electrophoretic separation where the flow rate of the target molecules is imposed by the separation process. The sandwich mixer-reactor, with an optimal positioning of the reactants, is a simple design for this kind of application. As based on classical microscopic diffusion, such mixing however requires that the residence time is not too low. An alternative will be presented in Chapter IV. Post-column modification of cysteinyl peptides from a tryptic protein digest will be assessed directly on an electrospray microchip for mass spectrometry including a mixing unit in order to mix the reactants.²⁷

REFERENCES

1. J. P. Brody, P. Yager, R. E. Goldstein and R. H. Austin, *Biotechnology at low Reynolds numbers*, *Biophys. J.*, 1996, 71, 3430-3441.
2. P. S. Dittrich, K. Tachikawa and A. Manz, *Micro total analysis systems. Latest advancements and trends*, *Analytical Chemistry*, 2006, 78, 3887-3907.
3. D. Janasek, J. Franzke and A. Manz, *Scaling and the design of miniaturized chemical-analysis systems*, *Nature*, 2006, 442, 374-380.
4. V. Hessel, H. Löwe and F. Schönfeld, *Micromixers - A review on passive and active mixing principles*, *Chem. Eng. Sci.*, 2005, 60, 2479-2501.
5. N.-T. Nguyen and Z. Wu, *Micromixers - A review*, *J. Micromech. Microengineering*, 2005, 15.
6. T. J. Johnson, D. Ross and L. E. Locascio, *Rapid microfluidic mixing*, *Analytical Chemistry*, 2002, 74, 45-51.
7. J. L. Lin, K. H. Lee and G. B. Lee, *Active mixing inside microchannels utilizing dynamic variation of gradient zeta potentials*, *Electrophoresis*, 2005, 26, 4605-4615.
8. A. Dodge, M. C. Jullien, Y. K. Lee, X. Niu, F. Okkels and P. Tabeling, *An example of a chaotic micromixer: The cross-channel micromixer*, *Comptes Rendus Physique*, 2004, 5, 557-563.
9. M. H. Oddy, J. G. Santiago and J. C. Mikkelsen, *Electrokinetic instability micromixing*, *Analytical Chemistry*, 2001, 73, 5822-5832.
10. N. Sundaram and D. K. Tafti, *Evaluation of microchamber geometries and surface conditions for electrokinetic driven mixing*, *Analytical Chemistry*, 2004, 76, 3785-3793.
11. P. Paik, V. K. Pamula and R. B. Fair, *Rapid droplet mixers for digital microfluidic systems, Lab on a Chip - Miniaturisation for Chemistry and Biology*, 2003, 3, 253-259.
12. S. Hardt, K. S. Drese, V. Hessel and F. Schönfeld, *Passive micromixers for applications in the microreactor and μ TAS fields*, *Microfluidics and Nanofluidics*, 2005, 1, 108-118.
13. A. E. Kamholz, B. H. Weigl, B. A. Finlayson and P. Yager, *Quantitative analysis of molecular interaction in a microfluidic channel: The T-sensor*, *Anal. Chem.*, 1999, 71, 5340-5347.
14. A. D. Stroock, S. K. W. Dertinger, A. Ajdari, I. Mezic, H. A. Stone and G. M. Whitesides, *Chaotic mixer for microchannels*, *Science*, 2002, 295, 647-651.
15. V. Mengeaud, J. Josserand and H. H. Girault, *Mixing processes in a zigzag microchannel: Finite element simulations and optical study*, *Anal. Chem.*, 2002, 74, 4279-4286.
16. M. Joanicot and A. Ajdari, *Droplet control for microfluidics*, *Science*, 2005, 309, 887-888.
17. S. Hardt, H. Pennemann and F. Schönfeld, *Theoretical and experimental characterization of a low-Reynolds number split-and-recombine mixer*, *Microfluidics and Nanofluidics*, 2006, 2, 237-248.
18. A. E. Kamholz, E. A. Schilling and P. Yager, *Optical measurement of transverse molecular diffusion in a microchannel*, *Biophys. J.*, 2001, 80, 1967-1972.
19. C. D. Costin, R. K. Olund, B. A. Staggemeier, A. K. Torgerson and R. E. Synovec, *Diffusion coefficient measurement in a microfluidic analyzer using dual-beam microscale-refractive index gradient detection: Application to on-chip molecular size determination*, *Journal of Chromatography A*, 2003, 1013, 77-91.
20. C. D. Costin and R. E. Synovec, *Measuring the transverse concentration gradient between adjacent laminar flows in a microfluidic device by a laser-based refractive index gradient detector*, *Talanta*, 2002, 58, 551-560.
21. A. Hatch, A. E. Kamholz, K. R. Hawkins, M. S. Munson, E. A. Schilling, B. H. Weigl and P. Yager, *A rapid diffusion immunoassay in a T-sensor*, *Nat. Biotechnol.*, 2001, 19, 461-465.
22. K. E. Nelson, J. O. Foley and P. Yager, *Concentration gradient immunoassay. 1. An immunoassay based on interdiffusion and surface binding in a microchannel*, *Anal. Chem.*, 2007, 79, 3542-3548.

23. J. O. Foley, K. E. Nelson, A. Mashadi-Hossein, B. A. Finlayson and P. Yager, Concentration gradient immunoassay. 2. Computational modeling for analysis and optimization, *Anal. Chem.*, 2007, 79, 3549-3553.
24. J. B. Knight, A. Vishwanath, J. P. Brody and R. H. Austin, Hydrodynamic focusing on a silicon chip: Mixing nanoliters in microseconds, *Physical Review Letters*, 1998, 80, 3863-3866.
25. N. Sundararajan, M. S. Pio, L. P. Lee and A. A. Berlin, Three-dimensional hydrodynamic focusing in polydimethylsiloxane (PDMS) microchannels, *Journal of Microelectromechanical Systems*, 2004, 13, 559-567.
26. X. Mao, J. R. Waldeisen and T. J. Huang, "Microfluidic drifting" - Implementing three-dimensional hydrodynamic focusing with a single-layer planar microfluidic device, *Lab Chip Miniaturisation Chem. Biol.*, 2007, 7, 1260-1262.
27. M. Abonnenc, L. Dayon, B. Perruche, N. Lion and H. H. Girault, Electrospray Micromixer Chip for On-Line Derivatization and Kinetic Studies, *Analytical Chemistry*, 2008.
28. L. Dayon, J. Josserand and H. H. Girault, Electrochemical multi-tagging of cysteinyl peptides during microspray mass spectrometry: Numerical simulation of consecutive reactions in a microchannel, *Physical Chemistry Chemical Physics*, 2005, 7, 4054-4060.
29. D. A. Boy, F. Gibou and S. Pennathur, Simulation tools for lab on a chip research: advantages, challenges, and thought for the future, *Lab on a Chip - Miniaturisation for Chemistry and Biology*, 2008.
30. N. Aoki, S. Hasebe and K. Mae, Geometric design of fluid segments in microreactors using dimensionless numbers, *AIChE Journal*, 2006, 52, 1502-1515.
31. A. Soleymani, E. Kolehmainen and I. Turunen, Numerical and experimental investigations of liquid mixing in T-type micromixers, *Chemical Engineering Journal*, 2007, 135.
32. J. Yang, X. Pi, L. Zhang, X. Liu, Y. Cao, W. Zhang and X. Zheng, Diffusion characteristics of a T-type microchannel with different configurations and inlet angles, *Analytical sciences : the international journal of the Japan Society for Analytical Chemistry*, 2007, 23, 697-703.
33. A. Lionello, J. Josserand, H. Jensen and H. H. Girault, Dynamic protein adsorption in microchannels by "stop-flow" and continuous flow, *Lab on a Chip - Miniaturisation for Chemistry and Biology*, 2005, 5, 1096-1103.
34. U. Tallarek, E. Rapp, T. Scheenen, E. Bayer and H. Van As, Electroosmotic and pressure-driven flow in open and packed capillaries: Velocity distributions and fluid dispersion, *Analytical Chemistry*, 2000, 72, 2292-2301.
35. R. F. Ismagilov, A. D. Stroock, P. J. A. Kenis, G. Whitesides and H. A. Stone, Experimental and theoretical scaling laws for transverse diffusive broadening in two-phase laminar flows in microchannels, *Appl. Phys. Lett.*, 2000, 76, 2376-2378.
36. A. E. Kamholz and P. Yager, Theoretical analysis of molecular diffusion in pressure-driven laminar flow in microfluidic channels, *Biophys. J.*, 2001, 80, 155-160.
37. A. E. Kamholz and P. Yager, Molecular diffusive scaling laws in pressure-driven microfluidic channels: Deviation from one-dimensional Einstein approximations, *Sens Actuators, B Chem.*, 2002, 82, 117-121.
38. Z. Wu and N.-T. Nguyen, Convective-diffusive transport in parallel lamination micromixers, *Microfluid. Nanofluid.*, 2005, 1, 208-217.
39. L. Dayon, C. Roussel and H. H. Girault, Probing cysteine reactivity in proteins by mass spectrometric EC-tagging, *Journal of Proteome Research*, 2006, 5, 793-800.
40. J. M. Ottino, Mixing and chemical reactions a tutorial, *Chemical Engineering Science*, 1994, 49, 4005-4027.
41. F. J. Muzzio and J. M. Ottino, Diffusion and reaction in a lamellar system: Self-similarity with finite rates of reaction, *Physical Review A*, 1990, 42, 5873-5884.
42. M. J. Clifford, S. M. Cox and E. P. L. Roberts, Lamellar modelling of reaction, diffusion and mixing in a two-dimensional flow, *Chemical Engineering Journal*, 1998, 71, 49-56.
43. T. John and I. Mezic, Maximizing mixing and alignment of orientable particles for reaction enhancement, *Physics of Fluids*, 2007, 19.
44. T. M. Squires, R. J. Messinger and S. R. Manalis, Making it stick: Convection, reaction and diffusion in surface-based biosensors, *Nature Biotechnology*, 2008, 26, 417-426.

45. L. Dayon, C. Roussel, M. Prudent, N. Lion and H. H. Girault, On-line counting of cysteine residues in peptides during electrospray ionization by electrogenerated tags and their application to protein identification, *Electrophoresis*, 2005, 26, 238-247.
46. N. T. Nguyen and Z. Wu, Micromixers - A review, *Journal of Micromechanics and Microengineering*, 2005, 15.

APPENDIX II-1: FINITE-ELEMENT FORMULATION

The general equation (eqn 3 in the manuscript) is treated by taking into account the diffusion-convection-reaction equations for the 3 considered species (A, B and C).

$$\frac{\partial c_A}{\partial t} + \nabla \bullet (-D_A \nabla c_A + V c_A) = -k c_A c_B \quad (\text{A.1})$$

$$\frac{\partial c_B}{\partial t} + \nabla \bullet (-D_B \nabla c_B + V c_B) = -k c_A c_B \quad (\text{A.2})$$

$$\frac{\partial c_C}{\partial t} + \nabla \bullet (-D_C \nabla c_C + V c_C) = k c_A c_B \quad (\text{A.3})$$

The local expressions of the flux conservation (A.1-3) are derived in the global form (A.7-9) by using the Galerkin's formulation (multiplication by a projective function α and integration on the domain of study, Ω):

$$\iint_{\Omega} \alpha \left[\frac{\partial c_i}{\partial t} + \nabla \bullet (-D_i \nabla c_i + V c_i) \pm k_i c_i \right] d\Omega = 0 \quad (\text{A.4})$$

The convection term of (A.4) is derived by taking into account the continuity equation $\nabla \bullet V = 0$. The diffusion term is derived by decomposing the product between α and the divergence to reduce the second order derivative of c_i (divergence of the gradient) as following:

$$\alpha \nabla \bullet (-D_i \nabla c_i) = \nabla \bullet (-\alpha D_i \nabla c_i) + D_i \nabla \alpha \bullet \nabla c_i \quad (\text{A.5})$$

$$\iint_{\Omega} \alpha \nabla \bullet (-D_i \nabla c_i) d\Omega = \int_{\partial\Omega} -\alpha D_i \frac{\partial c_i}{\partial n} dl + \iint_{\Omega} D_i \nabla \alpha \bullet \nabla c_i d\Omega \quad (\text{A.6})$$

Integrating (A.5) on the domain Ω and using the Ostrogradsky theorem, the divergence term is rejected at the boundary (A.6), where it expresses the flux boundary condition of each species. This boundary condition is here equal to zero: no flux at the boundaries of the domain, excepted the inlet and outlet of the channel where the equation is not solved due to the Dirichlet conditions (imposed value of the unknowns). This leads to the final formulation (A.7-9) that is introduced in the equation generator of the Flux-ExpertTM software.

$$\left\{ \iint_{\Omega} \left[\alpha \frac{\partial c_A}{\partial t} + D_A \nabla \alpha \bullet \nabla c_A + \alpha V \bullet \nabla c_A + \alpha k c_A c_B \right] d\Omega = 0 \right. \quad (\text{A.7})$$

$$\left\{ \iint_{\Omega} \left[\alpha \frac{\partial c_B}{\partial t} + D_B \nabla \alpha \bullet \nabla c_B + \alpha V \bullet \nabla c_B + \alpha k c_A c_B \right] d\Omega = 0 \right. \quad (\text{A.8})$$

$$\left\{ \iint_{\Omega} \left[\alpha \frac{\partial c_C}{\partial t} + D_c \nabla \alpha \bullet \nabla c_c + \alpha V \bullet \nabla c_c - \alpha k c_A c_B \right] d\Omega = 0 \right. \quad (\text{A.9})$$

A non-linear algorithm based on the Gauss inversion method was used for all the calculations. To prevent numerical errors, the mesh size was refined in the zones of maximum concentration gradient (junction between the incoming fluids) in order to maintain a local mesh Péclet number inferior to 100.^{S15} The error in calculations was evaluated to be 0.1% when comparing a mesh size of 5 μm with a 3 μm one. Consequently, for all the geometries tested, the mesh size was kept to 10 μm at the microchannel extremities (inlets and outlet) and was decreased to 3 μm at the fluid junction.

The transient model is there applied in a steady-state regime to a 2D cross-section of the geometry. A design with orthogonal inlets was needed for simulation with electroosmotic flow profile due to the velocity boundary conditions applied to the walls, as well as for the calculations with lower lateral flow velocities. For these two particular situations, a transient algorithm was preferred to improve the convergence of the calculations (the convergence criteria was fixed to 0.1%).

APPENDIX II-2: COMPLEMENTARY RESULTS

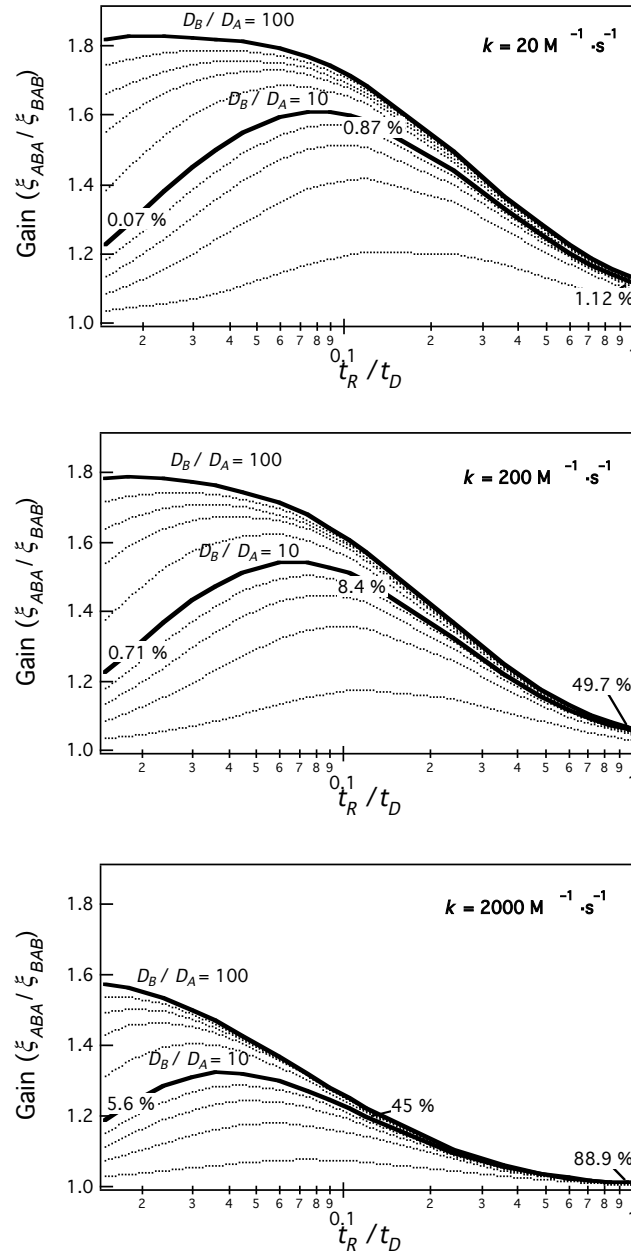


Figure II- 21 Gain of the optimised sandwich *ABA* vs. non-optimised *BAB* as a function of the non-dimensional time for D_B/D_A from 1 to 100, for $k = 20, 200$, and $2000 \text{ M}^{-1} \cdot \text{s}^{-1}$, $L = 20000 \text{ }\mu\text{m}$.

APPENDIX II-3: INFLUENCE OF THE REACTANT CONCENTRATION RATIO

The study deals with convection-diffusion-reaction between two species along a microchannel defined as sandwich mixer-reactor. As illustrated by the Damköhler number, kinetic and diffusion are related and this number determines whether a reaction is governed by the diffusion and/or the kinetics.

This section evaluates the effect of the position of the reactants according to their concentration ratio ($c_B \geq c_A$) on the reaction extent in a microchannel. Figure II-22 is the gain between *ABA* and *BAB* geometries that is determined for concentration ratios ranging from 1 to 1000, for $k = 20$ and $200 \text{ M}^{-1}\cdot\text{s}^{-1}$, at the end of a microchannel of $L = 2000 \text{ }\mu\text{m}$. The maximal gain obtained is 12% and 11% for $k = 20$ (with $c_B/c_A = 200$) and $200 \text{ M}^{-1}\cdot\text{s}^{-1}$ (with $c_B/c_A = 20$), respectively. The reaction extent for the two sandwich configurations shows a decrease of the gain when ξ is higher than 60%. Afterwards, the reaction is tending to completion that limits the gain.

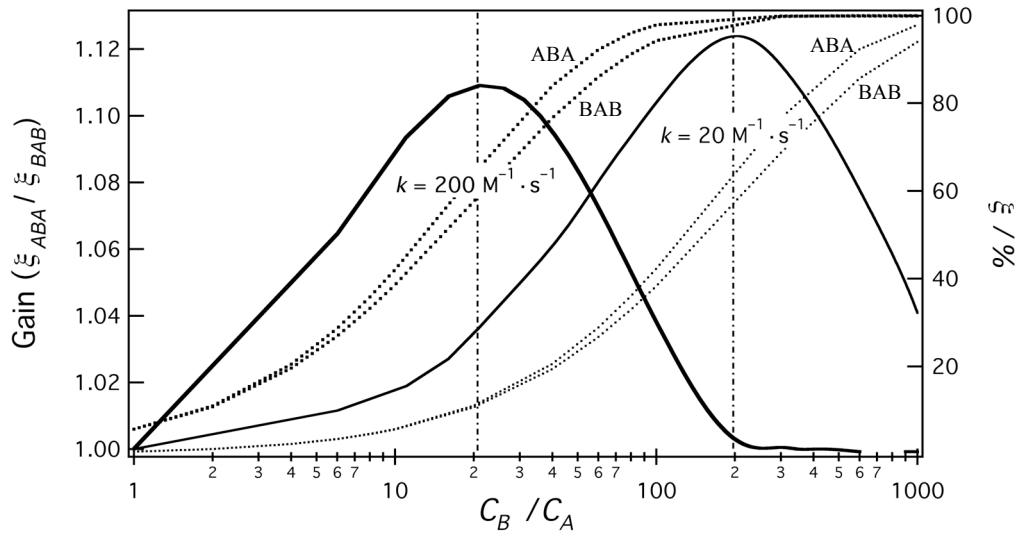


Figure II- 22 Gain between the sandwich ABA and BAB as a function of the concentration ratio of the reactants A and B, for $k = 20$ and $200 \text{ M}^{-1}\cdot\text{s}^{-1}$ and $L = 2000 \text{ }\mu\text{m}$. Full line: gain. Dashed line: ξ .

Figure II-23 represents the evolution of the gain as a function of the non-dimensional time t_R/t_D . As t_D is not changed, it allows visualizing the fluctuation of the gain along the microchannel. The change of species concentration modifies the reaction kinetics as the reaction rate in a first order reaction is correlated to kc_{AcB} . By increasing the concentration of B, the reaction kinetics is then increased to reach more rapidly reaction completion.

The small gain between *ABA* and *BAB* is probably due to the positioning of the concentration gradient across the parabolic velocity profile. We determined the contribution of the concentration gradient on the diffusion (for the *ABA* design). In one case the simulations were performed with $c_A = c_B$ and $k = 200 \text{ M}^{-1}\cdot\text{s}^{-1}$ ($\xi = 5.71\%$). In the other case we fixed $c_B = 10\cdot c_A$ and $k = 20 \text{ M}^{-1}\cdot\text{s}^{-1}$ ($\xi = 6.01\%$). So, in both case, kc_{AcB} is the same. According to the simulations, the concentration gradient increases by 5% the reaction extent by modifying slightly the diffusion. This effect explained the difference observed between the two geometries.

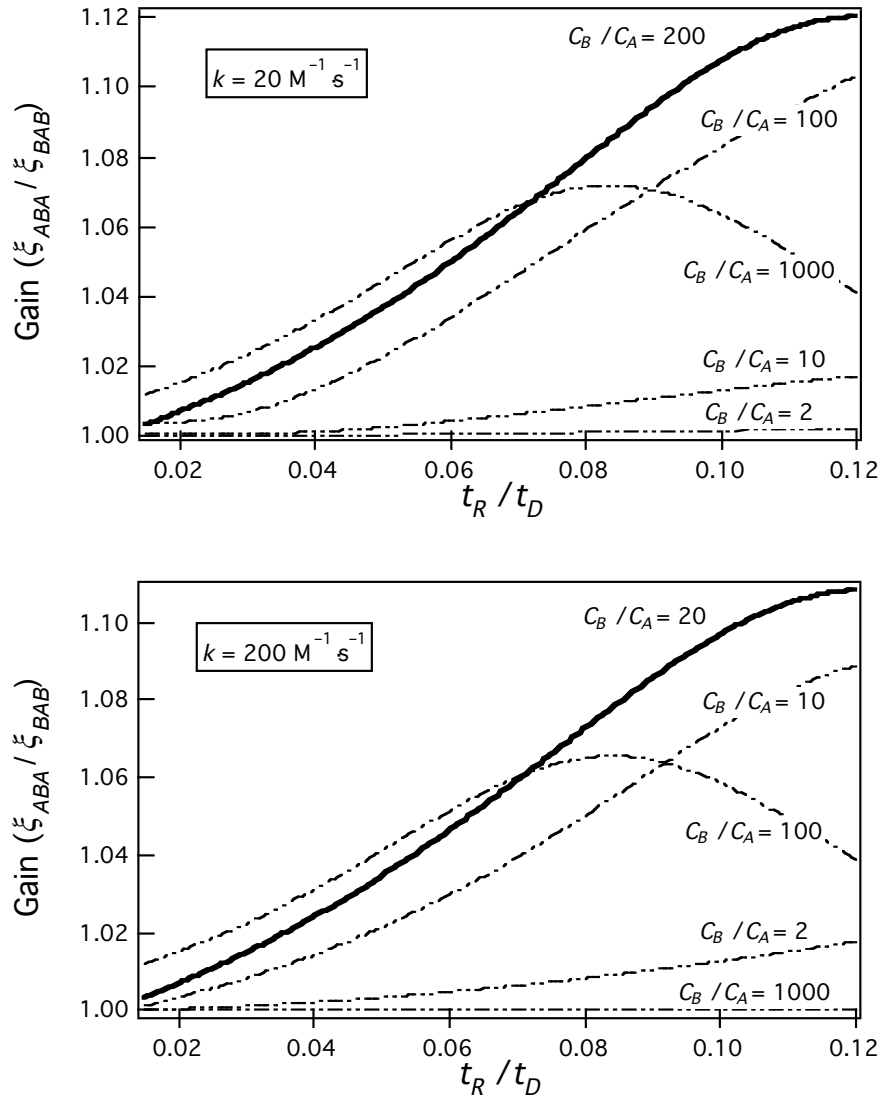


Figure II- 23 Gain between the sandwich ABA and BAB as a function of the non-dimensional time, for $k = 20$ (Top) and $200 \text{ M}^{-1} \cdot \text{s}^{-1}$ (Bottom) and $L = 2000 \text{ } \mu\text{m}$. The c_B/c_A ratios of 2, 10, 20, 100, 200 and 1000 are presented.

CHAPTER III.

Hyphenation of a polymer electrospray emitter microchip to a LC-MS workflow

1. Introduction

Liquid chromatography – mass spectrometry (LC-MS) is a well-established technique in analytical science to fractionate and analyze compounds.⁵ Reversed-phase (RP) LC is most commonly used, but also many other LC techniques can be applied such as ion exchange, ion-pair, affinity or size exclusion chromatography.⁶⁻⁹ In the present study, capillary RP-LC for which the separation flow rates are in the order of the microliter per minute was used to fractionate protein digests. The LC column is generally connected to a standard capillary electrospray (ESI) source with the possibility to use a sheath gas (so-called “pneumatically-assisted ESI” or “ion spray” introduced by Bruins et al.¹⁰) and in some case, a sheath liquid to aid the ESI process. In most cases, working with micro-flows requires a sheath gas, typically nitrogen.^{11, 122} Although capillary LC-MS is a well-established technique in protein studies, it presents few issues that are the cost of the analysis mainly due to the high consumption of gas, and the limited flexibility of the ESI source (only one emitter of fixed diameter).

Since the nineties, microtechnologies have offered numerous options to fabricate devices for applications in the field of analytical sciences and especially in MS. Micro- and nano-spray have been widely investigated and were demonstrated to provide a better sensitivity than standard ESI sources.¹³⁻¹⁵ Microfluidic devices can be used in a LC-MS analysis in two ways.¹⁶ Whether the LC column can be directly integrated to the ESI chip or, an infusion – based ESI chip can be connected downstream a LC system. Several groups worked on the development of devices including analytical functions such as pre-concentration or separation

units.¹⁷ A famous example is the HPLC-Chip commercialized by Agilent¹⁸ that integrates both pre-concentration and LC separation units as well as a nanoelectrospray emitter at the microchannel outlet. In contrast, the TriVersa™ NanoMate™ ESI-Chip from Advion Biosciences¹⁹ is an infusion-based out-of-plane chip with an array of 400 nozzles with different inner diameters to manage flow rates ranging from 20 to 300 nL·min⁻¹. A robotic probe delivers the sample through a conductive pipette tip, which interfaces directly to the back plane of the ESI chip. This microsystem can be operated as an infusion-based device, as interface after a LC separation and enables collecting fractions after splitting flows from LC setup. Compared to the Agilent HPLC-Chip, the TriVersa™ NanoMate™ can deal with micro and nano flow rate separation, due to the flow splitter and fraction collector. Despite the fact that the NanoMate™ chip is experiencing a good success, the use of post-column infusion – based electrospray chip has not been so investigated yet. There are few reports in the literature in which an ESI chip is directly connected to a LC system and indeed no study considers micro flow rate separations.

The present chapter aims firstly to overview some basics of electrospray ionization and then, describes the microfabrication of polymer ESI emitter based on laser photoablation. Secondly, the hyphenation of the ESI emitter microchip to a capillary LC-MS workflow is characterized and the potential issues are discussed.

2. Basics of electrospray ionization mass spectrometry

2.1. Overview of the electrospray process

The electrospray of gas-phase ions and their detection by MS was first reported by Dole in 1968 but at that time the results on polymeric species were not convincing yet.²⁰ Later in 1984 and thanks to the works done by Yamashita and Fenn, ESI-MS was recognized as a valuable analytical technique for the study of large compounds.^{21, 22} Contemporary, Aleksandrov and co-workers reported similar developments on ESI-MS.²³ In 2002, Fenn received the nobel prize of chemistry for his contribution to the development of soft ionisation methods for mass spectrometric analysis of biological compounds.²⁴

The ESI process is equivalent to an electrical circuit, as illustrated in Figure III-1.² By applying a high electric field between a capillary tip and the mass spectrometer, a spray of highly charged droplets is generated at the extremity of the tip. The ESI process can be operated either in positive or negative ionization mode. For clarity, the next discussions will focus on the positive ionization mode, *i.e.* when a positive voltage is applied to the solution. The charged droplets reduce in size by solvent evaporation and/or by Coulomb explosion to form gas phase ions representative of the species in solution. These ions are then analyzed and detected by the mass spectrometer. To insure the charge balance in the capillary, it is now well established that electrochemical reactions occur at the metal/solution interface. All the charges that are separated at the tip are neutralized at the counter-electrode or inside the mass spectrometer and returned to the power supply ($i_{ES} = i_{NE} + i_{MS}$).

The overall process²⁵⁻²⁸ can be subdivided in two major parts that are briefly described below: *i)* the emission of charged droplets from the capillary tip accompanied by the charge balance process and, *ii)* the formation of gas-phase ions from the emitted droplets, and their transmission from the atmospheric region towards the mass spectrometer detector. The scope of this brief overview is to provide some necessary concepts to interpret the experimental part of the present chapter, as well as the following ones.

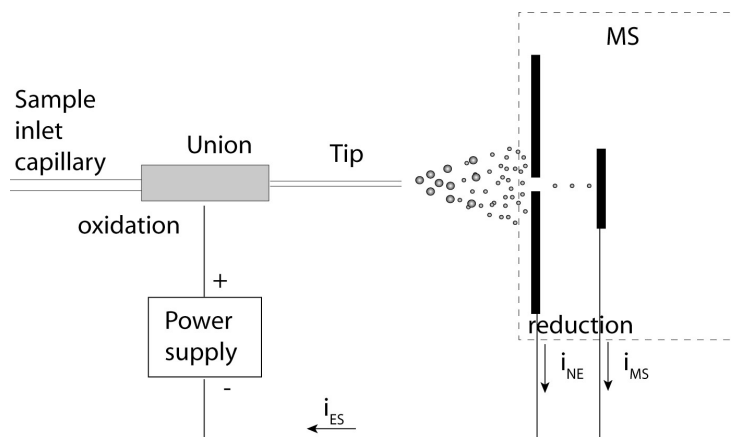


Figure III-1 Schematic view of the electrospray ionization process. Adapted from Ref².

2.2. From ions in solution to ions in gas-phase

2.2.1. Operating regimes

In 1914, Zeleny studied the effect of an electric field on a liquid meniscus. He observed that « *at higher potentials the discharge current is intermittent and this is followed by a steady current at still higher potential* ». ²⁹ He described several functioning modes leading to the production of aerosols with very different characteristics. Since this pioneered work, considerable theoretical and experimental studies have been accomplished and other transition modes have been described. Cloupeau *et al.* reviewed and classified the different modes based on droplet shape and emission rate. ³⁰⁻³⁵ It is now well known that changing the applied voltage or flow rate influences the ESI regime. More recently, Marginean and co-workers established a direct link between the electrohydrodynamic pulsation of the liquid meniscus (defining the ESI regime) and the measured electrospray current oscillations. ³⁶ In this work, they explored the formation, size, velocity, and chemical composition of droplets in the three main modes presented in Figure III-2: the *dripping* regime, the *pulsating* regime and the steady *cone-jet*. Among all of them, the steady (or stable) cone-jet regime is often preferred because of the small radius of parent droplets, and regular emission. This mode is indeed the most described in the literature. ³⁷⁻⁴¹ For clarity, the next considerations will focus on the steady cone-jet mode.

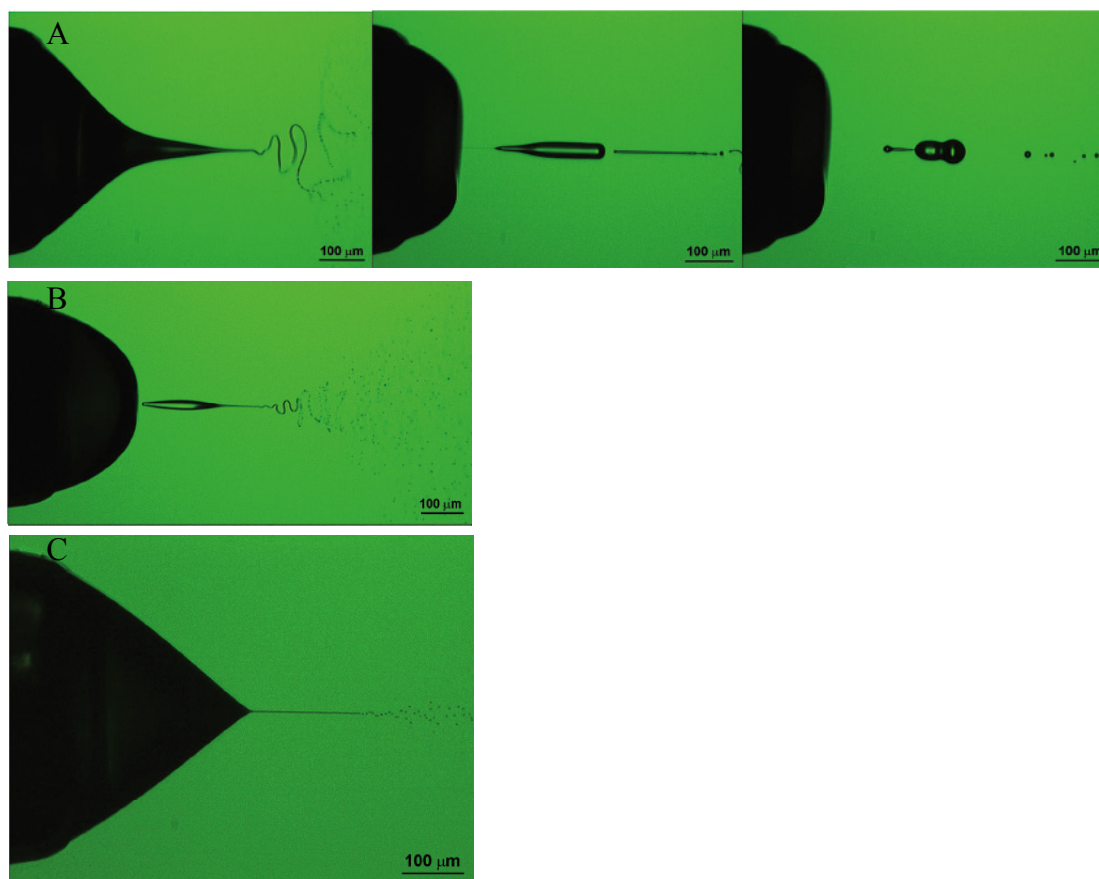


Figure III-2 Comparison of typical meniscus shapes in A) dripping mode (a liquid filament exhibits kink instabilities and produces relatively small droplets. The majority of the liquid is ejected from a few very large droplets of varying shape), B) pulsating Taylor cone mode (a spindle like large droplet is accompanied by a significant amount of smaller ones produced by lateral kink instabilities at the end of the jet), and C) the steady cone-jet mode (continuous emission of small droplets). The flow rate was fixed at $1 \mu\text{L}\cdot\text{min}^{-1}$. The applied voltage was set at 2.75 kV, 2.95 kV and 4.05 kV for the A), B) and C), respectively. Reprinted from Ref⁴.

2.2.2. Steady cone-jet mode and charged droplet emission

In the positive ionization mode, positive ions are enriched at the surface of the liquid at the capillary tip whereas negative ions are depleted thereby forming a diffuse double layer. The accumulation of charges results in a lowering of surface tension, a phenomenon known as electrocapillarity, and under the presence of an electric field the meniscus tends to form a cone, called the *Taylor cone*.⁴² The thin liquid filament at the tip of the *Taylor cone*, expands until it breaks up into individual charged droplets, as illustrated in Figure III-2.C. The process has been subjected to theoretical and

experimental studies by a number of authors, including Smith,³⁸ De la Mora and Locertales.⁴³ When the counter-electrode is large and planar, the field can be approximate by the following relationship^{44, 45}:

$$E_c = \frac{2V_c}{r_c \ln(4d/r_c)} \quad (1)$$

where V_c is the applied potential, r_c the capillary outer radius, and d the distance between the capillary tip and the counter-electrode. Smith derived equations to evaluate the electrospray onset that requires an electrical field E_{on} and its corresponding V_{on} , defined as³⁸:

$$E_{on} = \left(\frac{2\gamma \cos \theta}{\epsilon_0 r_c} \right)^{0.5} \quad (2)$$

$$V_{on} \approx \left(\frac{r_c \gamma \cos \theta}{2\epsilon_0} \right)^{0.5} \ln(4d/r_c) \quad (3)$$

where γ is the surface tension of the solvent, ϵ_0 the permittivity of the vacuum, and $\cos \theta$ is the half-angle Taylor cone with $\theta = 49.3^\circ$.⁴²

The electric field required for the onset of the ESI increases with the surface tension of the solution. This is illustrated by the calculation made from eqn. 3 where $V_{on} = f(\gamma, d, r_c)$ and represented in Figure III-3. The influence on the onset voltage of the ESI emitter – MS inlet distance and the ESI emitter radius was evaluated for pure water and acetonitrile solvents as these solvents are commonly used in LC separations. The grey area corresponds to water : acetonitrile mixtures. Solutions with a high surface tension, as water, require high onset fields, that can lead to electrical discharges which partially suppress the ESI process. Increasing the ESI emitter – MS inlet distance or increasing the emitter outer radius requires a higher voltage to onset the ESI as the electric field decreases. These calculations are in adequation with experimental observations. However, one can already mention that the experimental onset voltages are generally slightly higher than those predicted by the calculations. This was also noted by Cole and co-workers.²⁵ The effect of the outlet capillary radius was typically highlighted in various studies about nanosprays.^{13, 15}

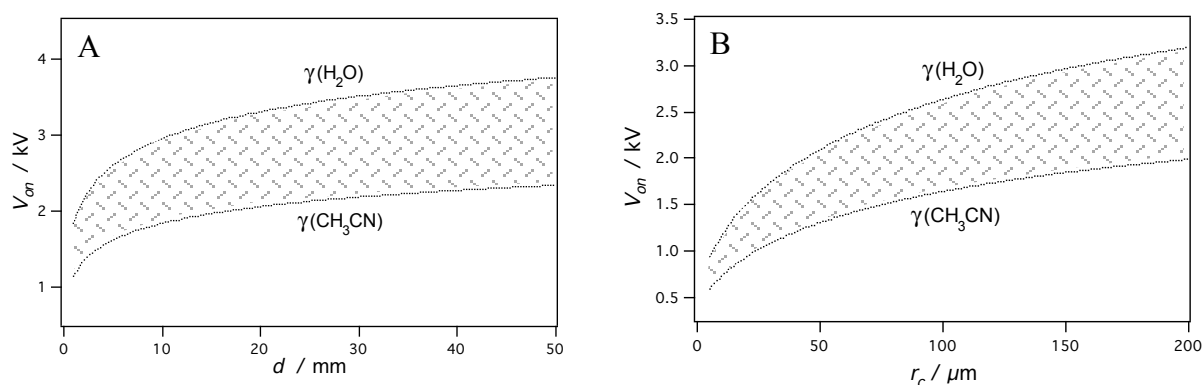


Figure III- 3 Influence of the A) ESI emitter – MS inlet distance (for fixed $r_c = 100 \mu\text{m}$) and B) capillary tip radius (for fixed $d = 5 \text{ mm}$) on the electro spray onset voltage, V_{on} , calculated according to eqn. 3. In both cases, the calculations were obtained for pure aqueous and acetonitrile solution. For mixtures of $\text{H}_2\text{O}:\text{CH}_3\text{CN}$, V_{on} values are thus included in the grey zone.

The emission rate of charged droplets at the Taylor cone is defined as the electro spray current, i_{ES} . Several studies have been performed to determine the parameters influencing this current. Pfeiffer and Hendricks proposed an empirical relationship for the ESI current that depends on the physico-chemical properties and flow rate of the electrosprayed solution, as well as the applied electric field:

$$i_{ES} = \left[\left(\frac{4\pi}{\epsilon} \right)^3 (9\gamma)^2 \epsilon_0^5 \right]^{1/7} (\kappa E_c)^{3/7} F_v^{4/7} \quad (5)$$

where ϵ is the permittivity of the solvent, κ the conductivity of the infused solution and F_v the volumic flow rate.⁴⁵

De la Mora ended with a simplified relationship based on experimental observations⁴³, where :

$$i_{ES} = f(\epsilon_r)(\gamma \kappa F_v \epsilon_r)^{1/2} \quad (6)$$

with ϵ_r is the relative permittivity.

It is worth noting that no dependance on the electric field was considered in the last equation. It was verified for sufficiently conducting solutions, for which the effect of the electric field can be neglected.

The surface tension required to hold the droplets together at the Taylor cone, is defined by the Rayleight equation,⁴⁶ which gives the condition in which the excess charge Q_R becomes just sufficient to overcome the surface tension:

$$Q_R = 8\pi(\epsilon_0 \gamma R^3)^{0.5} \quad (7)$$

where R is the radius of the droplet.

Gomez and Tang were the first to study ESI droplets with phase Doppler anemometry and flash shadowgraph techniques.⁴⁷ From their conclusions, De la Mora and Locortales proposed relationships for the radius R and charge q of the parent droplets formed at the capillary tip, and defined as⁴³:

$$R \approx (F_v \epsilon / \kappa)^{1/3} \quad (8)$$

$$q \approx 0.7[8\pi(\epsilon_0 \gamma R^3)^{1/2}] \quad (9)$$

From these equations, it is relevant to underline the dependance of the parent droplet size emitted from the Taylor cone with the flow rate, permittivity and conductivity of the solution.⁴⁸

In a LC-MS analysis, as the solution is evolving according to the elution gradient, the fluctuation of all these parameters (permittivity, conductivity, flow rate, surface tension...) significantly impact on the electrospray process.

2.2.3. ESI viewed as an electrochemical process

Kebarle and co-workers suggested the electrospray process as an electrolysis cell *« considering the requirements for charge balance in such a continuous electric current device and the fact that only electrons can flow through the metal wire supplying the electric potential to the electrodes, one comes to the conclusion that the electrophoretic charge separation mechanism [...] should involve an electrochemical conversion of ions*

to electrons ».⁴⁹ Observation of molecular radical cation by Van Berkel *et al.* in mass spectra suggested that either chemical oxidation or oxidation at the electrode had occurred during the process.⁵⁰ Van Berkel and Zhou further characterized the ESI process as a controlled-current electrolytic flow cell.⁵¹⁻⁵³ Consequently, the ESI current i_{ES} due to the positive charges leaving the capillary is equal to the faradaic current i_F resulting from the electrolysis reaction occurring at the metal/solution interface:⁵⁴

$$i_{ES} = i_F = \sum_j n_j A_j F F_v \quad (10)$$

$$[Q] = \frac{i_{ES}}{F F_v} \quad (11)$$

where n_j is the number of electrons involved in the oxidation of one molecule of species j , A_j the concentration of oxidized species j , and F the Faraday constant ($9.648 \cdot 10^4 \text{ C} \cdot \text{mol}^{-1}$). $[Q]$ is the excess charge concentration that corresponds to the number of charges leaving the capillary.

Solvent and electrode reactions occur during the electrochemical reaction process and influence the final composition of the flowing solution. Oxidation at the metallic contact may also induce changes in the solution pH.⁵⁵ As example, when water oxidation first occurs ($2\text{H}_2\text{O} \rightarrow \text{O}_2 + 4\text{H}^+ + 4\text{e}^-$, $E_0 = 1,299 \text{ V vs SHE}$), a pH decrease down to 4 units from a neutral initial solution was reported at low flow rate. It is crucial to note that such pH variations may modify the conformation of proteins, typically reflected by a change of protein charge state distribution in MS.⁵⁶

Mass transport at the electrode is primordial in such a process and depends on the diffusion coefficient of the species in solution. At high capillary flow rates, and with the standard capillary ESI source (i.d. $\geq 100 \text{ } \mu\text{m}$), the mass transport is relatively low and almost does not affect the analytes. Obviously, when the electrochemical reactions are within the scope of the study,⁵⁷⁻⁶⁵ the emitter geometry and fluidic parameters have to be well defined to follow the products by mass spectrometry.

According to the characteristics of the analytes in solution, different types of ion formation within the spray can be distinguished: (i) electrochemical ionization when analyte oxidation is one of the charge balancing processes. It can lead to the formation of radical cations from neutral compounds as metallocenes, porphyrins, oxidation of hydroquinone into benzoquinone, cysteine oxidation, etc. ($\text{M} \rightarrow \text{M}^+ + \text{e}^-$), (ii) protonation

that leads to the generation of $[M + nH]^{n+}$ ions (depends on the analyte proton affinity) is very common for peptides, proteins and all other analytes that possess basic site, (iii) electrode dissolution, or (iv) analyte ion pair formation as example by sodium ($A + Na^+ \rightarrow ANa^+$) and results in extra peak mass spectra ($[M + Na]^+$).

2.2.4. Two theories behind the gas-phase ion production from charged droplets

In the sections above, we defined the electrospray current, i_{ES} , as the total charged droplets leaving the capillary tip. However, the current monitored at the MS that represents the ions produced in the gas-phase and reaching the detector, i_{MS} , is much lower. Indeed, sensitivity in ESI-MS is mainly depending on two factors, the gas-phase ion production (*i.e.* the fraction of the droplet charge converted into gas-phase ions) and the ion transmission efficiency.

The emitted parent droplets when travelling towards the detector, are subjected to evaporation processes leading to a droplet size diminution and a concentration of the charged species. At this stage, two different mechanisms have been proposed for the formation of gas-phase ions from the small and highly charged droplets (Figure III-4).^{47,}

66-68

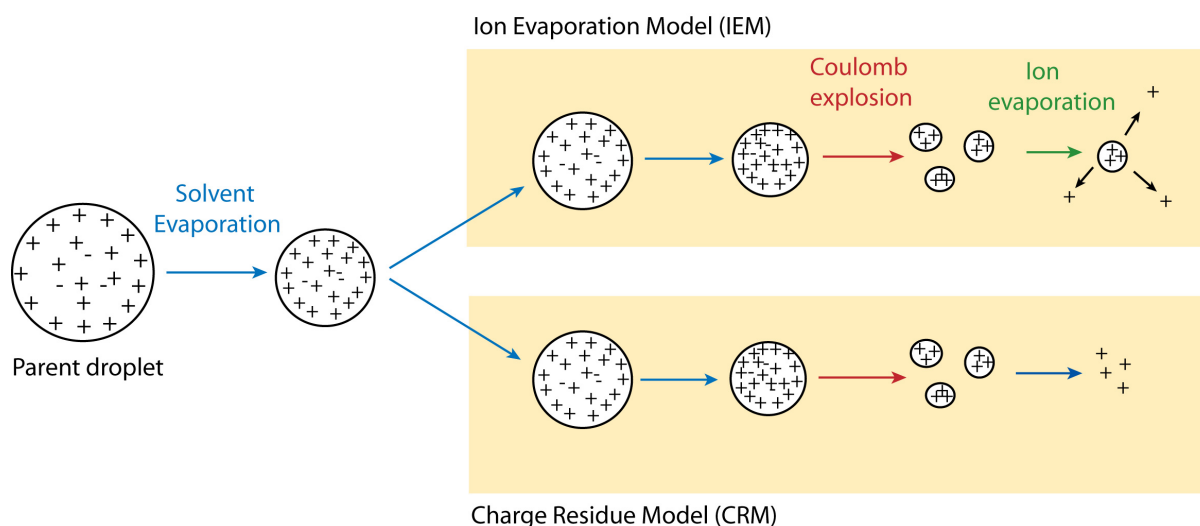


Figure III- 4 Schematic view of the two mechanisms proposed for the generation of gas-phase ions (IEM: Ion Evaporation Model, CRM: Charge Residue Model).

The first mechanism was proposed by Dole and is called the Charged Residue Model (CRM). It relies on the final formation of extremely small droplets ($R \approx 1\text{ nm}$), which contain only one analyte ion²⁰. Therefore, solvent evaporation from such a droplet leads to the formation of a gas-phase ion. This theory was supported by Röllgen who studied the desolvation of ions by thermospray and concluded that at low solute concentrations ($C \leq 10^{-3}\text{ M}$) single ions and molecules are predominantly desolvated from small droplets.⁶⁹ This early work did not provide any details on how such droplets should be formed or whether the process should selectively favor the formation of gas phase ions A^+ relative to B^+ as a result of specific physicochemical differences between these two species.

The second mechanism was proposed by Iribarne and Thomson and assumes ion evaporation (or ion emission, IE) from very small and highly charged droplets^{70, 71}. This IEM theory predicts that, after the radii of the droplets decrease to a given size, direct ion emission from the droplets becomes possible. This process, which is called ion evaporation, becomes dominant over coulomb fission for droplets with radii $r \leq 10\text{ nm}$.

Although there are some exceptions,⁷² most investigators seem finally to believe that the IEM of Iribarne and Thomson is more applicable than the CRM of Dole.^{73, 74}

An important consideration in electrospray ionization is that, in equimolar solutions, analytes often have ESI response that differ due to their physico-chemical properties. In addition, matrix effects can be dramatic, such that the presence of co-analytes and salts can cause signal suppression of the species of interest. It is now commonly accepted that analytes with high affinity for the surface of the ESI droplets (surface-active analytes) have higher ESI response.^{66, 73} This phenomenon was first evoked by Iribarne and Thomson who observed an increased response with atmospheric-pressure ion-evaporation mass spectrometry (AP-MS) for nonpolar analytes.⁷⁵ They suggested that such ions would prefer the droplet air interface, and thus reside at the droplet surface. Kebarle and Tang expanded on the ion-evaporation theory, and developed a comprehensive theory that describes ESI response in terms the evaporation rate from ESI droplets. They observed a higher response for less solvated cations explained by the fact that they present higher evaporation rates.⁷⁶ For more complex molecules, the evaporation rate is not sufficient to explain the ESI response and one should consider other factors such as the surface activity. Enke proposed an equilibrium partitioning model that rationalizes the effect of

nonpolar character on ESI response without evoking evaporation rates.⁷⁷ This model postulates that two separate phases exist in an ESI droplet. Excess charge produced in the ESI process (eqn. 11) resides on the surface of the droplet while its interior is electrically neutral and consists of solvent molecules, electrolytes, and charged analyte molecules matched by an equal number of counterions. An equilibrium partitioning coefficient exists for each analyte corresponding to the ratio of its concentration on the surface and at the interior of the droplet. Factors such as polarity, charge density, and basicity are important and determine the magnitude of this partition coefficient for a given ion. Cech and Enke put forward the linear relationship between the ESI response and the nonpolar surface area of the peptides, based on the equilibrium partitioning model.⁷⁸ As ESI response can be also correlated to Gibbs free energy of transfer from nonpolar to polar solution, analytes with higher Gibbs free energy of transfer (more nonpolar analytes) tend to have a higher ESI response. The authors also correlated the RP-LC retention time with the ESI response for small peptides.⁷⁹ However, it has not been yet determined for large and multiply charged molecules.

Finally, once the ions are in the gas-phase they need to travel towards the detector. The ion transmission efficiency at this stage depends on the ion transfer optics and on the type of mass analyzer.

2.3. Practical considerations

The most commonly described ESI-MS equivalent circuit is illustrated in Figure III-5.A and schematizes in Figure III-1⁸⁰. The ESI resistance between the emitter electrode and the MS detector, R_{ES} , is global and is mainly due to the air gap resistance. It is often recommended by manufacturers to ground the upstream fluidic connection before the metallic junction where the spray voltage is applied (Figure III-5.B). Nonetheless, the presence of a grounded loop and its consequences are poorly considered in the literature. Konermann studied its implication on the oxidation rate and thus, signal intensities during ESI-MS.⁸¹ An enhancement of ESI response for protonated analyte such as reserpine was shown. In presence of an upstream separation, as a liquid chromatography or capillary electrophoresis system, it is not always well identified if the instrument is grounded or not and where it is.

In this thesis work, ESI emitter chips were connected to a LC instrument. In our experiments, the upstream flow was not voluntarily grounded. However, if the contrary were true (*i.e.* the LC setup was grounded), R_{LOOP} would have been too large compared to R_{ES} (because of the longer LC - emitter electrode distance) to observe any significant effects on the ESI current.

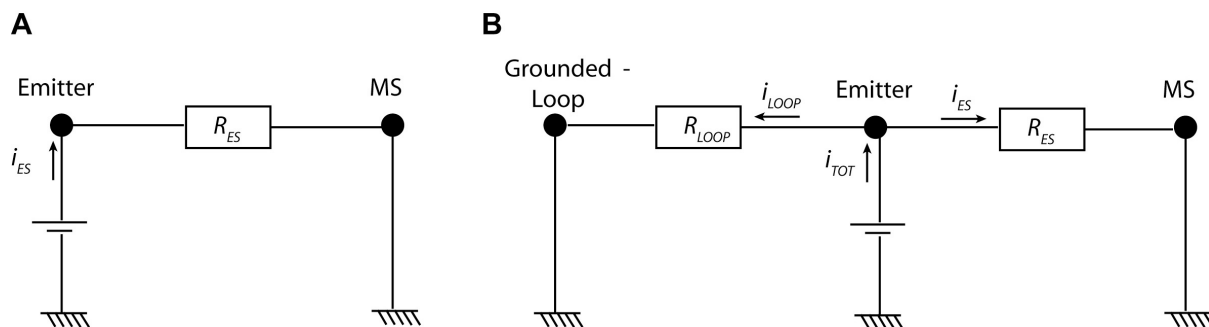


Figure III- 5 Simplified ESI equivalent circuit. A) Standard ESI circuit with the high voltage applied to the emitter electrode. B) ESI circuit with a grounded loop upstream the emitter where $i_{TOT} = i_{LOOP} + i_{ES}$ (as example, a grounded LC system upstream the ESI source).

3. Microfabrication of electrospray emitter microchips

The ESI emitter microchips used in this thesis were fabricated by laser photoablation of poly(ethylene terephthalate) (PET) substrates.⁸² The fabrication process is detailed in this section.

3.1. UV laser ablation process

Excimer lasers typically use a combination of an inert gas (argon, krypton, xenon) and a reactive gas (fluorine or chlorine) and can emit at wavelengths between 157 and 351 nm such as Fluorine (157 nm), Argon fluoride or ArF (193 nm), Krypton fluoride or KrF (248 nm), Xenon bromide or XeBr (282 nm), Xenon chloride or XeCl (308 nm), Xenon fluoride or XeF (351nm).

Photoetching of organic polymer using UV laser radiation was first reported in 1982 with PET substrates by Srinivasan⁸³ and with polymethyl methacrylate (PMMA) by Kawamura.⁸⁴ When pulsed UV laser radiation falls on the surface of an organic polymer, the material at the surface is spontaneously etched away to a depth of 0.1 μm to several microns, as depicted in Figure III-6.⁸⁵ Polymer photoablation mechanisms have been debated for more than two decades. It is generally accepted that the energy of laser pulses is initially transformed into electronic excitations. However, subsequent energy transfer can take various forms. The *photo-chemical model* assumes that the excited electronic state can undergo decomposition resulting in direct bond breaking, while the *photo-thermal model* states that the excited molecules undergo internal conversion to a vibrationally excited ground state, any subsequent decomposition can be considered to be the equivalent of a thermal process (*i.e.* the photons merely act as a source of thermal energy). In the *photophysical model*, both thermal and non-thermal processes are considered.⁸⁶

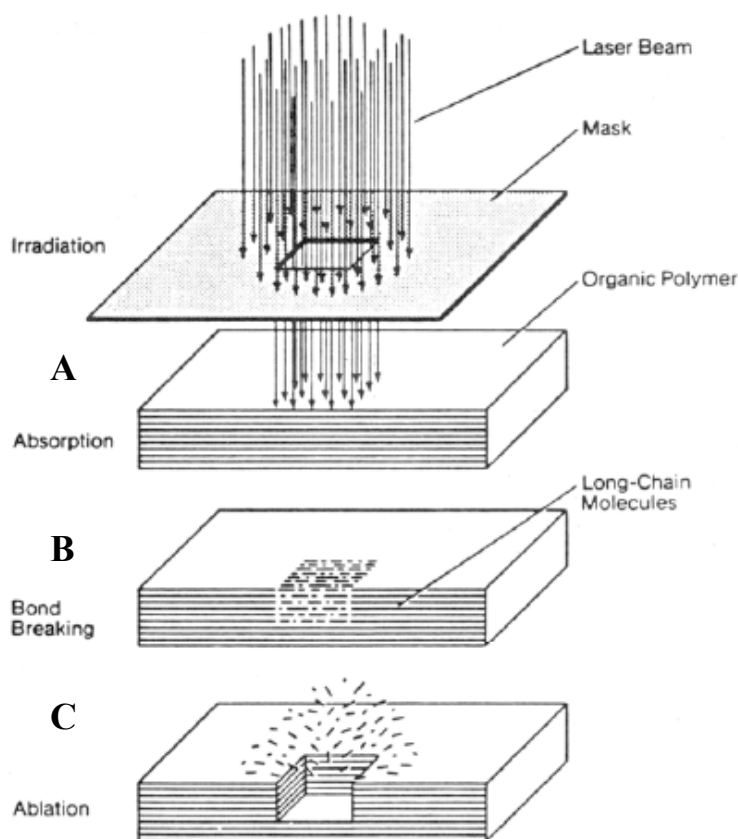


Figure III- 6 Schematic representation of the interaction of a laser pulse with a polymer surface. A) The stream of photons from a single laser pulse falls on the polymer and is absorbed to a defined depth. B) Within the absorption depth, there are numerous bond breaks. C) The revealed fragments are ejected from the surface, leaving an etched cavity behind. Reprinted from Ref³.

Most of organic polymers absorb UV radiation, and their ablation rate, as well as their ablation properties, depends on the laser fluence (*i.e.* Joules/pulse/unit surface area of sample), wavelength, pulse duration, and surrounding atmosphere. In this work, the photoablation process was performed at atmospheric condition. The obtained ablated surfaces are characterized by an increased roughness depending on polymers and laser beam fluence. In addition, a lower O/C ratio has been observed by X-Ray photoelectron spectroscopy (XPS) on the cavity surface of ablated PET substrates, accompanied with the formation of aldehyde and alcohol groups.^{87, 88} This modification results in enhanced hydrophobic behaviors of the etched surface.⁸⁹

3.2. Excimer laser operation

The excimer laser ArF 193 nm (Lambda Physik, Gröttingen, Germany) setup used for the fabrication of the ESI emitter microchip is depicted in Figure III-7. The substrate is placed on an X,Y translation stage perpendicularly with respect to the laser beam. A mask positioned upstream on the laser beam defines the shape of the structure. The polymer ablation can be performed either in static or dynamic mode. In dynamic condition, the X,Y stage is translated during ablation allowing microchannel drilling. Keeping the laser energy and frequency constant, the depth of the structure is controlled by the translation speed of the X,Y table. In static mode, the depth of the structure is then controlled by the number of pulses and laser energy.

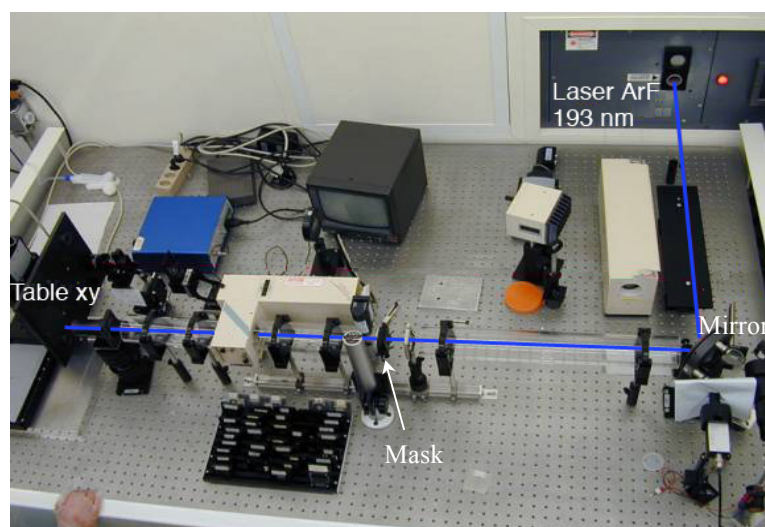


Figure III- 7 Picture of the excimer laser (ArF 193 nm) setup, in a clean-room environment.

3.3. ESI emitter microchip with integrated carbon electrode

Figure III-8 illustrates the microfabrication steps of an ESI emitter microchip with an integrated carbon electrode. A) First, the microelectrode is made by drilling a L-shape microchannel on the PET substrate (100 μm -thickness Melinex[®] sheet from Dupont, Wilmington, DE, USA). B) The L-microchannel is filled with carbon ink (Electrador, Electra Polymer & Chemicals Ltd. UK), C) laminated with a 25/10 μm PE/PET composite sheets (Morane, Oxone, UK), where PE acts as the sealing agent when rolled at 130 °C at 3 bars for 3 s. To insure good lamination, the entire structure is additionally cured 1 h at 80 °C. D) In a second time, the microchannel is drilled on the backside of the chip to cross the carbon electrode and reveal it at the microchannel bottom (Figure III-9). E) During the microchannel photoablation, reservoirs are drilled at its extremities by static laser shoots. The microchannel is then closed by lamination. F) The last step consists in cutting the microchannel outlet with scissors in order to give a V-shape to the outlet.

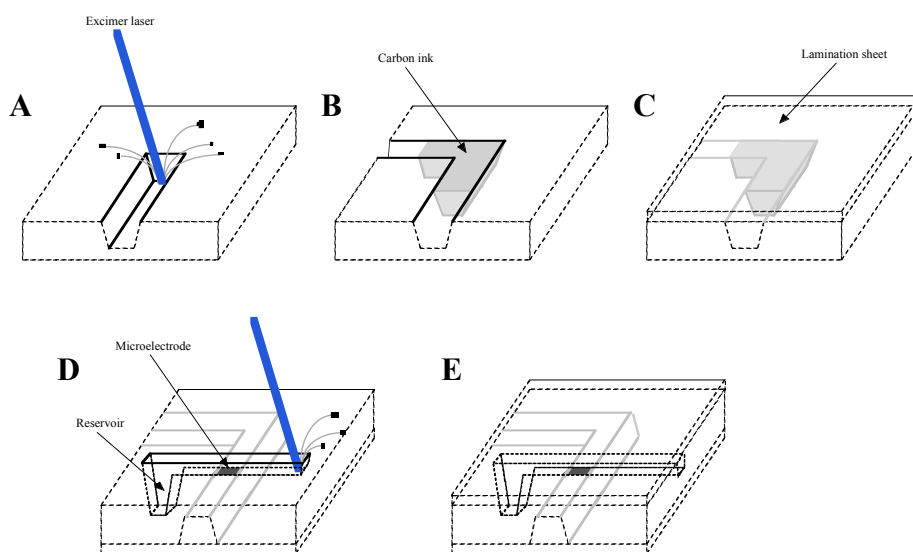


Figure III- 8 Main steps of the fabrication of the microspray emitter. A) The PET substrate is photoablated. B) The channel is filled with carbon ink. C) The track is sealed with a lamination sheet. D) On the other side of the substrate, the infusion microchannel is drilled, revealing the microelectrode. E) The infusion microchannel is closed by lamination. Reprinted from ¹.

The resulting microchip is illustrated in Figure III-9. In use, the microchip can either be placed in a holder with capillary connections for sample delivery or a reservoir can be fixed

at the inlet. In the former setup, a syringe pump controls the flow while in the later case the flow is controlled by gravity, and consequently is not constant during the analysis.

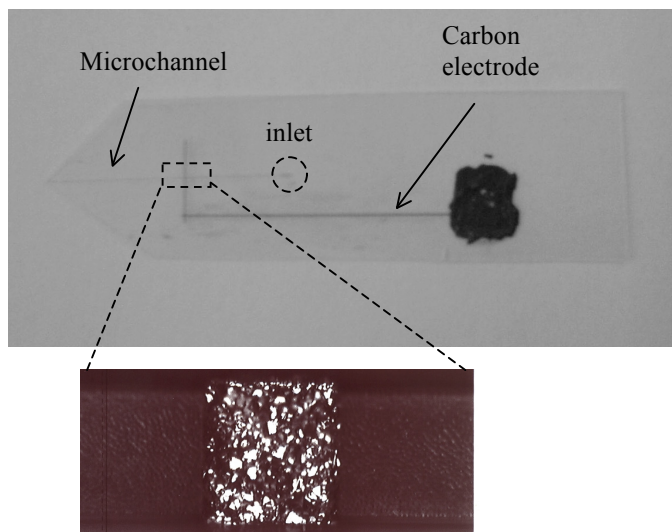


Figure III- 9 Picture of the ESI emitter microchip with a microscope view of the revealed carbon electrode at the bottom of the microchannel.

3.4. Alternatives to the on-chip carbon electrode

Most of the studies presented in this work were performed with ESI microchips embedding a carbon electrode (Figure III-9 and Figure III-10.B).

An alternative, when working under controlled flow, is to apply the voltage directly to the metallic needle of the syringe (Figure III-10.A). However, a higher oxidation of the analytes is observed in this configuration (as example, when the KCTCCA peptide is electrosprayed only the oxidized form at $m/z = 626.3$ Th is detected). It might be due to the larger surface of the metallic needle.

Another option is to cover the external layer of the capillary with a conductive coating at its end (Figure III-10.C). The coated capillary can be then connected to the microchip inlet inside a holder where there is a direct contact with the flowing solution. In preliminary experiments, the capillary was covered with a silver ink. Obviously, electrode reactions might occur ($\text{Ag} \rightleftharpoons \text{Ag}^+ + e^-$, $E^0 = 0.80 \text{ V vs SHE}$), however we neglected the effect of such reactions. In further work, the use of an inert conductive coating would be more appropriated.

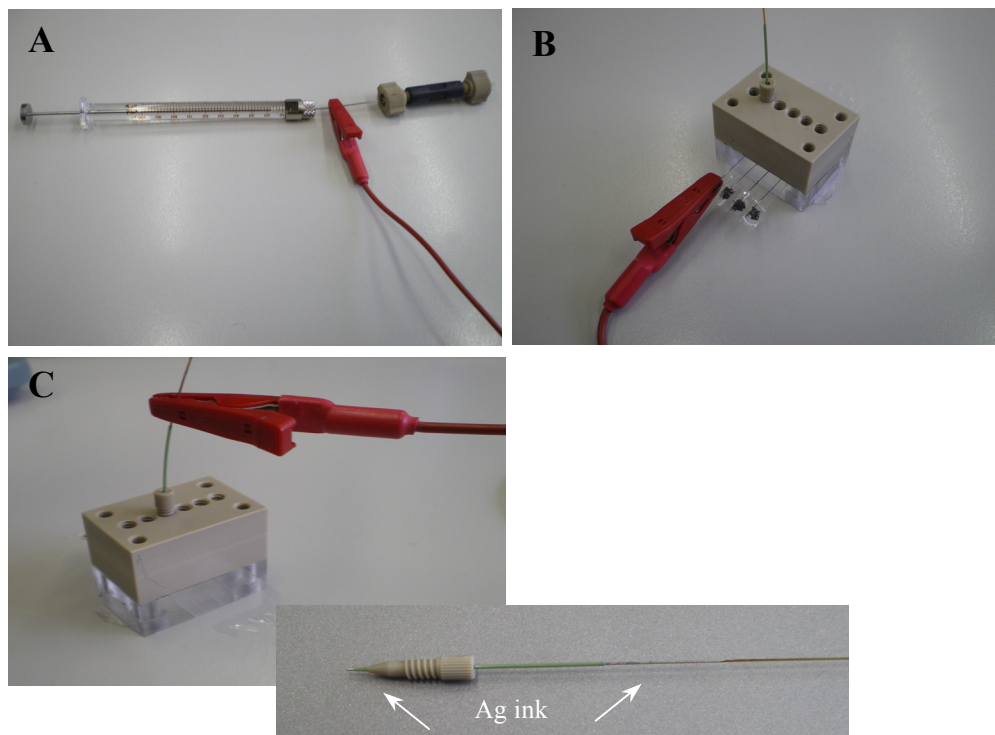


Figure III- 10 Illustration of the different ways to apply the spray voltage to the solution with the present setup. A) Metallic needle of the syringe, B) on-chip carbon electrode, C) capillary end-side covered with silver ink.

Figure III-11.A is a comparison of the total ion current (TIC) recorded by MS when the voltage is successively applied to the silver ink electrode and then, to the on-chip carbon electrode. A solution of myoglobin (10 μM in $\text{H}_2\text{O}:\text{MeOH}$ 50:49 with 1% AcOH) was electrosprayed at a flow rate of 4 $\mu\text{L}/\text{min}$, with an applied voltage of 3.5 kV. The TIC was monitored continuously during 6 min. At $t = 3$ min, the electric connection was quickly moved from the silver to the carbon electrode. The resulting TIC is comparable in both conditions with a relative standard deviation (RSD) of 3.53% and 4.53% for the silver and carbon ink, respectively. The average mass spectra of the myoglobin obtained from this experiment is shown in Figure III-11.B. The main advantage of the capillary coating is the simplicity of fabrication. Indeed, only few minutes are needed compared to the embedded carbon electrode that requires an additional fabrication step in cleanroom environment.

Finally, the ESI emitter microchips can be used with reservoirs, under gravity-controlled flow. In that case, the voltage is applied to an external platinum electrode fixed in the reservoir. This method was used in Chapter VI.

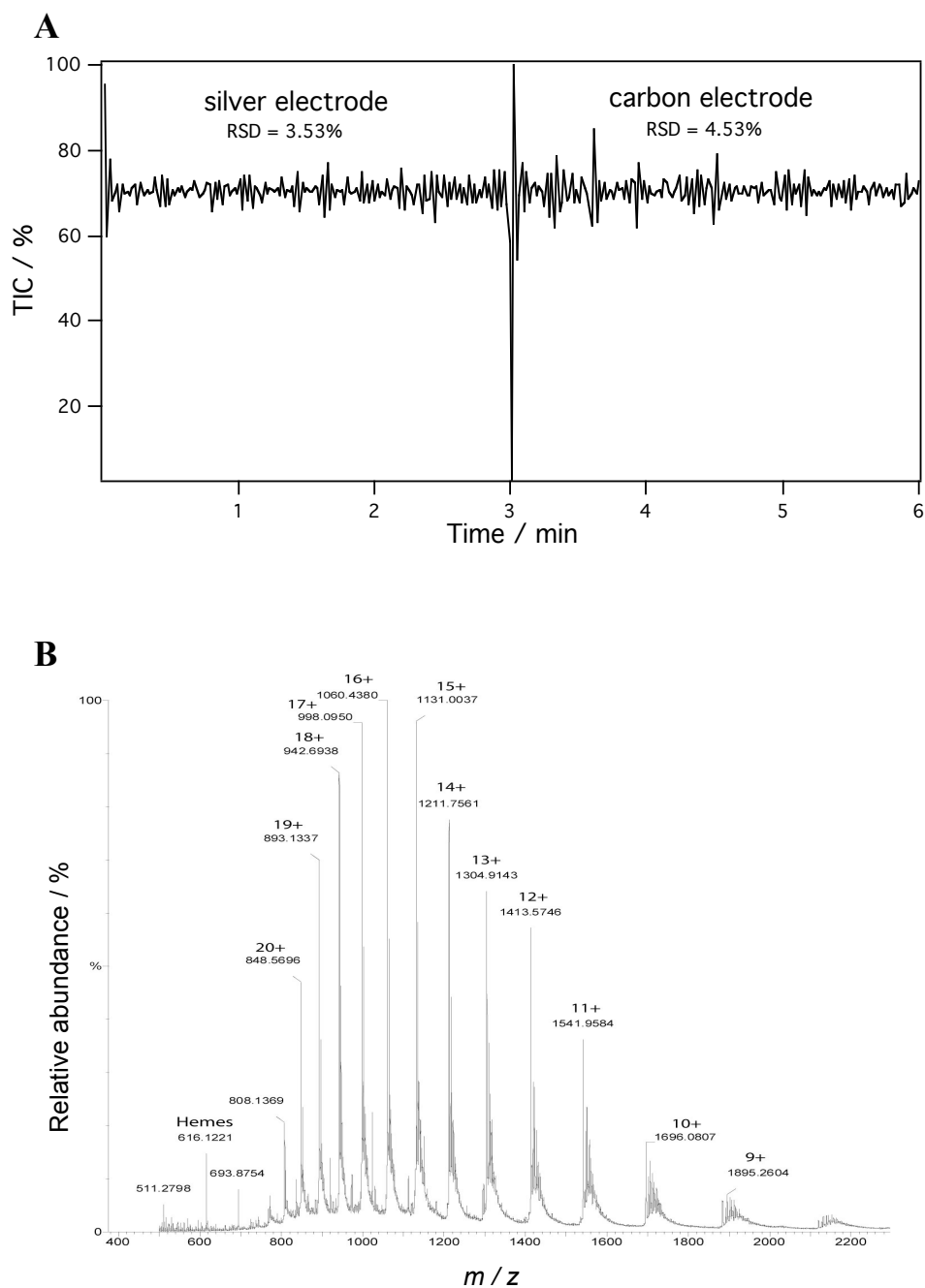


Figure III- 11 A) Stability of the total ion current (TIC) when the voltage is applied from a silver electrode covering the capillary or from the on-chip carbon electrode. B) Mass spectrum of myoglobin. Spray voltage: 3.5 kV, Infusion flow rate: $4\mu\text{L}\cdot\text{min}^{-1}$.

4. Hyphenation of the electrospray emitter microchip to a LC-MS workflow : key features, issues and solutions

4.1. Material & Methods

Chemicals.

KCTCCA (70%, $M = 627.8 \text{ g}\cdot\text{mol}^{-1}$) peptide was bought from Bachem (Bubendorf, Switzerland). Bovine serum albumin (BSA, $\geq 98\%$) and β -lactoglobulin A (BLA, $> 90\%$) were purchased from Sigma (St. Louis, MO, USA), formic acid from Merck (FA, $> 98\%$, Darmstadt, Germany). Water (UV-HPLC) and acetonitrile (HPLC-gradient grade) were from Panreac Quimica S.A. (Barcelona, Spain). 4-Iodobutyric acid (98%, MW: 214 g/mol), *N*-hydroxysuccinimide (NHS, 98%, $M = 115.09 \text{ g}\cdot\text{mol}^{-1}$), dicyclohexylcarbodiimide (DCC, 99%, $M = 206.33 \text{ g}\cdot\text{mol}^{-1}$), *N,N*-dimethyl-*N*-octylamine (technical grade, $M = 157.30 \text{ g}\cdot\text{mol}^{-1}$), silver trifluoromethanesulfonate ($\geq 99\%$, $M = 256.94 \text{ g/mol}$) were bought from Sigma-Aldrich. Anhydrous acetone (max. 0.01% H_2O) from Merck. Hydroxylamine (purum. 50% RT in H_2O , $M = 33.03 \text{ g}\cdot\text{mol}^{-1}$), HEPES (99.5%, $M = 238.30 \text{ g}\cdot\text{mol}^{-1}$), ethanol were from Fluka (Buchs, Switzerland).

Protocol for protein digestion and LC-MS setup.

One mg of protein (BLA or BSA) was dissolved in 1 mL of ammonium bicarbonate buffer (5 mM, pH = 8). Then, 0.62 mg of DTT (to get a final concentration of 4 mM) and 20 μg of trypsin (protein ratio 1:50 w:w) were added. The digestion was run at 37 °C for 5 h. One μg of the protein digest was separated on a LC Packings Ultimate™ (Dionex, Olten, Switzerland) capillary RP-HPLC system equipped with a UV detector (multi-monitoring at 214, 250 and 280 nm). An LC Packings C18 PepMap 100 column (15 cm, 3 μm , 100 Å) was used. The eluents were mixtures of $\text{H}_2\text{O}:\text{CH}_3\text{CN}$ 98:2 + 0.1% FA (solvent A) and $\text{H}_2\text{O}:\text{CH}_3\text{CN}$ 20:80 + 0.085% FA (solvent B). The separation flow rate was fixed at $F_V = 4 \mu\text{L}\cdot\text{min}^{-1}$.

The ESI emitter microchip was processed according to the protocol described above and present a typical cross-section of $100 \times 35 \mu\text{m}^2$. The HPLC capillary outlet was directly connected to the ESI emitter microchip using a custom-made holder. The ESI microchip was then positioned in front of the mass spectrometer inlet. The general setup is shown in Figure III-12. Whether the ESI emitter was infused directly with the flow eluted from the LC

column (referred as *on-line* analysis) or with a flow controlled by the syringe pump (referred as *off-line* analysis). The ESI voltage was applied *via* the embedded carbon electrode using the mass spectrometer power supply. An ammeter was placed on the electric circuit in order to measure the ESI current.

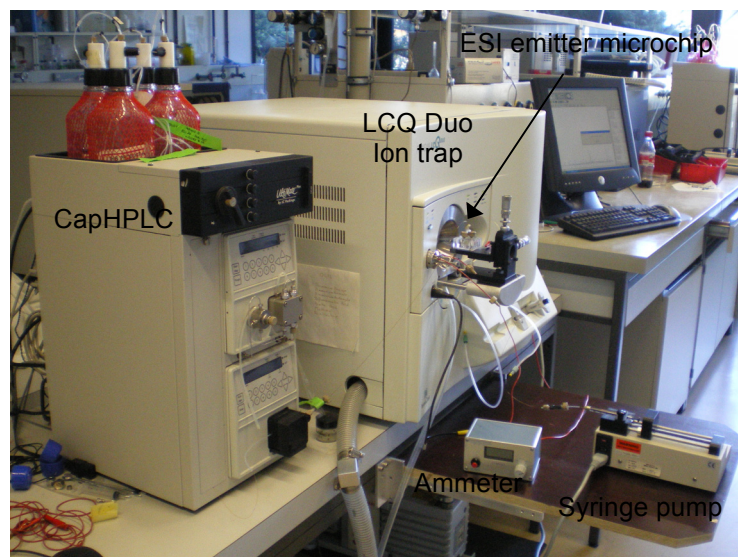


Figure III- 12 LC-MS setup using an ESI emitter microchip as interface. An ammeter was added to the electric circuit to measure the electrospray current, i_{ES} . In off-line analysis a syringe pump was used to control the flow rate.

Conductivity of the different eluents measured by capillary electrophoresis.

The conductivity of the A:B solvent mixtures was determined by capillary electrophoresis (PACE MDQ system from Beckman-Coulter, Nyon, Switzerland) and is presented in Figure III-13. For the conductivity measurements, the capillary was filled with the solution to test and the current was measured for applied voltages of 10, 15, 20 and 25 kV. The conductivity was calculated from the Ohm's law:

$$J = \sigma E \quad (12)$$

where J is the current density and E the electric field.

In parallel, the conductivity of the solutions was confirmed with a conductimeter (Metrohm, Herisau, Switzerland).

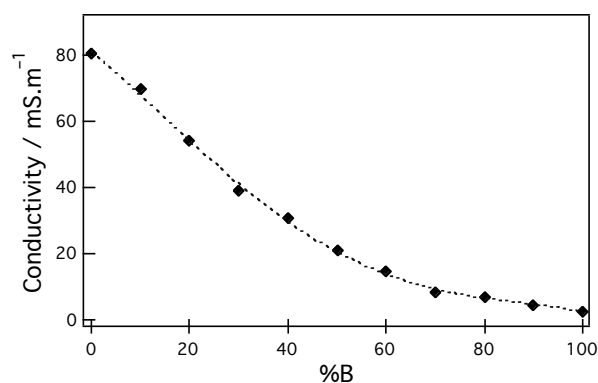


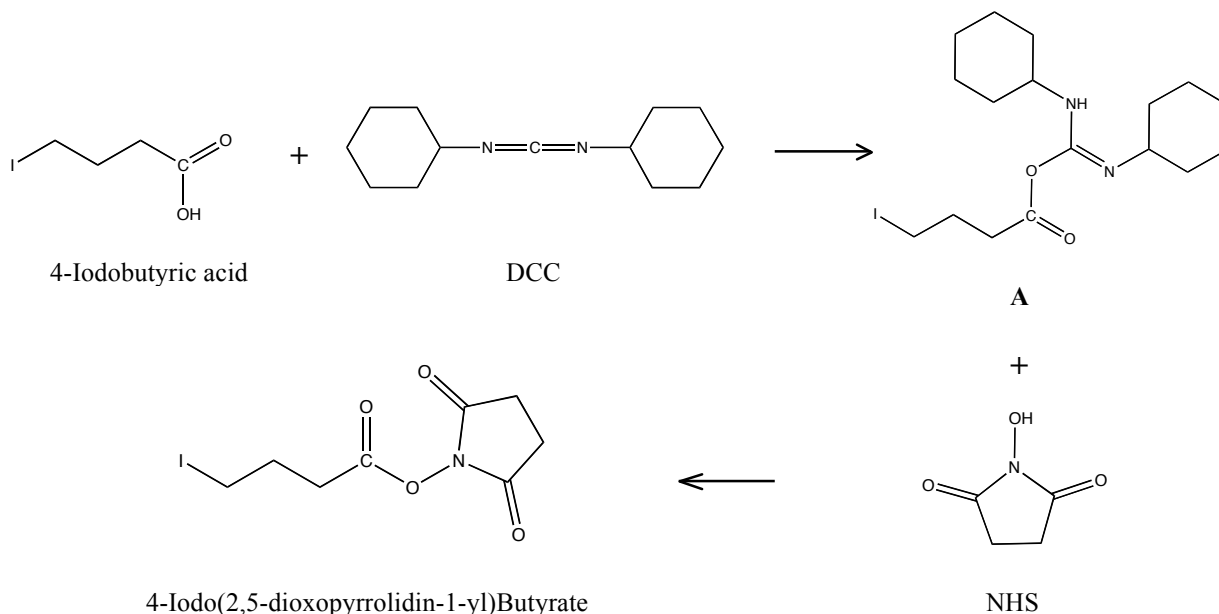
Figure III- 13 Conductivity of typical LC eluents, measured by capillary electrophoresis. Solvent A: H₂O:CH₃CN 98:2 + 0.085% FA. Solvent B: H₂O:CH₃CN 20:80 + 0.1% FA.

Synthesis of the C₈QAT tag.

Synthesis of 4-iodo(2,5-dioxopyrrolidin-1-yl)butyrate

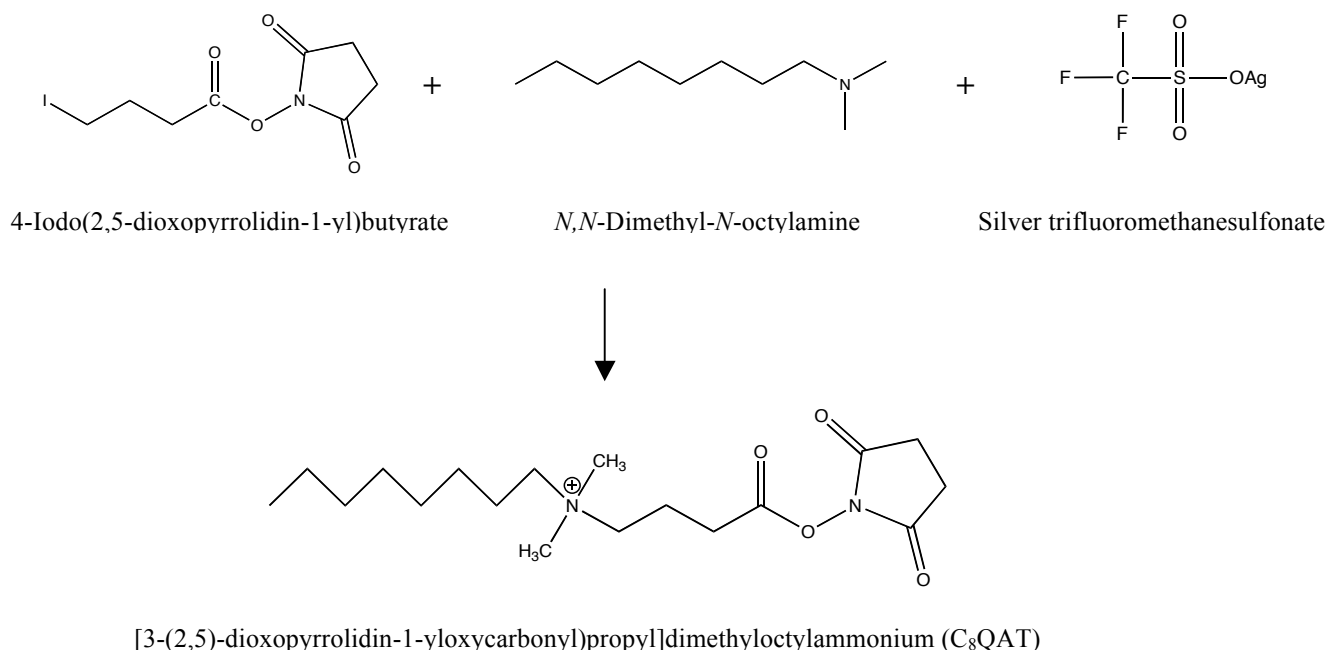
4-Iodobutyric acid (1 g, 4.67 mmol), NHS (0.54 g, 4.69 mmol), and DCC (0.96 g, 4.66 mmol) were dissolved in 10 mL of AcOEt. The reaction mixture was stirred at room temperature for 16 h. The dicyclohexyl urea formed was discarded by filtration over celite, and the crude material was concentrated and chromatographed on silical gel (petroleum ether/AcOEt, 1/1). The resultant yellow powder was recrystallized from petroleum ether/EtOH (9/1) yielding activated ester 4-iodo(2,5-dioxopyrrolidin-1-yl) butyrate. The product obtained was checked by NMR.

The quantity of 4-iodo(2,5-dioxopyrrolidin-1-yl)butyrate obtained was 420.86 mg (yield ≈ 29%).



Synthesis of [3-(2,5-dioxopyrrolidin-1-yloxy)carbonyl]propyl]dimethyloctylammonium (C₈QAT)

N,N-Dimethyl-*N*-octylamine (263 μ L, 1.28 mmol), activated ester 4-iodo(2,5-dioxopyrrolidin-1-yl)butyrate (395 mg, 1.28 mmol), and silver trifluoromethanesulfonate (330.4 mg, 1.28 mmol) were dissolved in 2 mL of anhydrous acetone. The solution was stirred for 16 h at room temperature. The silver iodide was discarded over celite, and the solvent was evaporated. The resultant orange oil was dissolved in 1 mL of CH₃CN, and the final product was precipitated by addition of 10 mL of diethyl ether. Filtration, evaporation and crystallization were repeated again because of visible silver residues in the product. The quantity of C₈QAT obtained was 182 mg (yield \approx 42%). The final product (m/z = 341 Th) was checked by NMR, MS and MS².

**Protocol for the modification of a peptide mixture with the C₈QAT tag.**

The protein digestion was performed in HEPES 50 mM pH 8.0 according to the protocol described above. The C₈QAT tag was mixed in excess with the digest following the excess ratio 50:1. The reaction was run at room temperature for 2 h. Then, hydroxylamine solution was added to quench the excess of tag and reverse reaction with tyrosine. The pH was adjusted to 11.4 with NaOH. The reaction was run for 10 min. Finally, glacial acetic acid was added to adjust the pH to 7-8.

4.2. Hyphenation of the electrospray microchip to a LC-MS workflow

The overall ESI process is relatively complex, as illustrated earlier in this chapter, and several characteristics of the solvents and additives, such as the volatility, surface tension, viscosity, conductivity, ionic strength, dielectric constant, electrolyte concentration, pH have to be considered. In the following experimental part, some of these parameters will be discussed.

MS detection is indeed not compatible with all the solvents and eluent additives that are commonly used in LC separation. For example, some additives as strong acids like trifluoroacetic acid (TFA) may significantly suppress the ESI signal, as it is a too strong ion-pairing agent.⁹⁰ While the eluents and additives can be appropriately chosen according to the ESI-MS detection requirements, the time-dependent eluent composition when operating under gradient elution is a constraint that cannot be avoided (except if an isocratic elution is preferred but it is not the case in our study and for general peptide separation).

4.2.1. Feasibility

First of all, the feasibility to get a continuous ESI current, i_{ES} , at capillary flow rate when the ESI microchip is used as MS interface was evaluated and is shown in Figure III-14. A LC gradient from 0 to 100% of B solvent was programmed over 30 minutes at a flow rate $F_v = 4 \mu\text{L}\cdot\text{min}^{-1}$. A voltage of 4.5 kV was applied to the on-chip carbon electrode and kept constant during the entire analysis. The total ion current (TIC) was monitored over 50 min showing a continuous spray without any interruptions. This result is quite relevant as it illustrates the feasibility to replace a standard ESI source, which requires a pneumatically-assisted ESI to maintain a spray at such flow rates and with highly aqueous solvents (as it is the case at the beginning of the LC gradient), by the ESI microchip. The ability to maintain a continuous spray with the ESI microchip is likely due to the hydrophobic properties of the photoablated PET substrate, the V shape and smaller cross-section of the emitter tip.

At this stage, it is important to point out again that the evolution of the ESI current i_{ES} cannot be directly correlated to the TIC recorded at the MS detector, as explained earlier in this chapter. The i_{ES} was measured with an ammeter placed in the circuit between the power supply and the on-chip carbon electrode. As illustrated in the inset of Figure III-14, i_{ES} decreases with time, *i.e.* when the proportion of the B solvent content increases in the eluent.

Indeed, according to the eqn. 6, the ESI current scales with the square root of the surface tension, conductivity, and flow rate. Here, the flow rate was kept constant at $F_V = 4 \mu\text{L}\cdot\text{min}^{-1}$ during the analysis. The conductivity of the different solvent mixtures was determined experimentally (Figure III-13), and supports the observations from De la Mora regarding the evolution of i_{ES} as a function of the solution conductivity. The eluent conductivity is indubitably one important factor that explains the higher i_{ES} monitored at the beginning of the LC gradient. Here only the conductivity is discussed but it is evident that other parameters such as the solution permittivity, surface tension or ionic strength for example also influence the spray current.

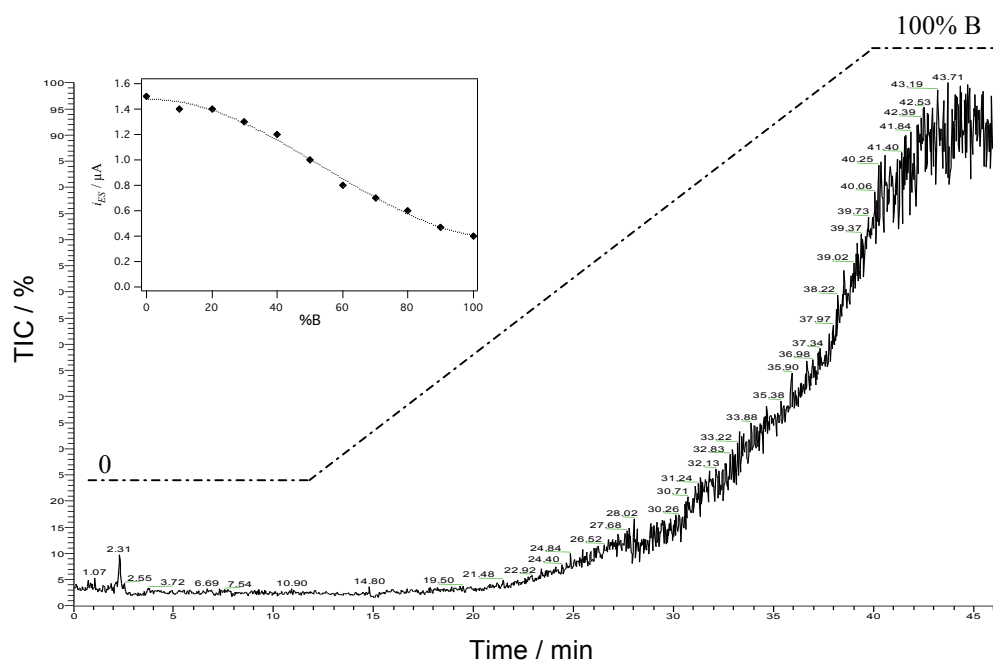


Figure III- 14 Chromatogram of the total ion current (TIC) in a LC-MS setup. The dashed line illustrates the LC elution gradient programmed over 30 min. The beginning of the gradient on the time scale was corrected adding the time from the eluent to be detected at the MS. Solvent A ($\text{H}_2\text{O}:\text{CH}_3\text{CN}$ 98:2 with 0.1% FA), and solvent B ($\text{H}_2\text{O}:\text{CH}_3\text{CN}$ 20:80 with 0.085% FA). The inset figure shows the evolution of the ESI current as a function of the percentage of B solvent.

In contrast to i_{ES} , the corresponding TIC recorded at the mass spectrometer detector increases with time. At the beginning of the LC gradient, the eluent is highly aqueous as the proportion of A solvent is higher. The eluent presents a higher surface tension that acts first on the emission rate of charged droplets at the Taylor cone. The second consequence, once the droplets are emitted, is the slower evaporation rate of the charged droplets that might not be

completed before reaching the MS inlet. When the less polar solvent content, which is more volatile, increases (higher %B), the TIC goes up due to the more efficient droplet desolvation and gas-phase ion production.

4.2.2. Flow rate (F_V) considerations

The effect of the flow rate on the peptide detection with the chip was evaluated off-line, with F_V controlled by a syringe pump (Figure III-15). KCTCCA peptide 10 μM in 50% B solvent was infused at different flow rates. The ESI microchip, presenting a cross section of $100 \times 35 \mu\text{m}^2$, was positioned at a fixed distance $d = 5 \text{ mm}$ from the MS inlet. With flow rates lower than $1 \mu\text{L} \cdot \text{min}^{-1}$, the ESI was not stable because not enough solution insured the ESI process. Inversely, too high flow rates could first delaminate the microchip and create solvent drops at the emitter tip. Thus, the ESI microchip could be safely operated with flow rates ranging from 1 to $7 \mu\text{L} \cdot \text{min}^{-1}$, which is valuable without the assistance of a sheath gas.

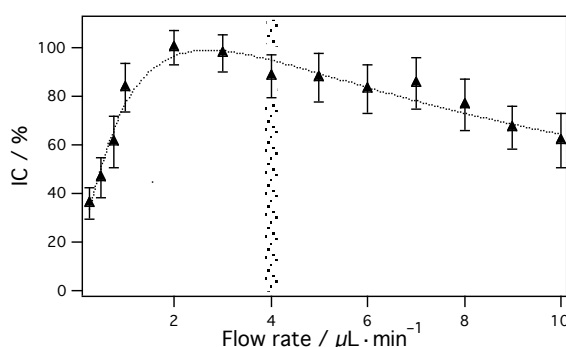


Figure III. 15 Evolution of the ion counts relative to KCTCCA peptide as a function of the flow rate F_V . KCTCCA 10 μM in 50% B was sprayed at 4.5 kV.

According to Figure III-15, the peptide ion counts detected by MS increase with the flow rate up to $3\text{--}4 \mu\text{L} \cdot \text{min}^{-1}$ as more peptides are provided. For higher flow rates ($> 5 \mu\text{L} \cdot \text{min}^{-1}$), the additional peptides are lost due to inefficient ionization. Because small droplet radius is desirable, increasing the volumic flow rate is counterproductive (eqn. 8). When larger droplets are produced, the time required for the droplet evaporation process is longer and, in some cases, the delay is not sufficient to allow a good production of gas-phase ions. The flow

rate increase and its influence on peptide ionization should be also considered when a liquid junction is used in a LC-MS workflow. At high flow rates, a longer emitter – MS inlet distance might be used enabling the desolvation of charged droplets and more droplet fission events.

4.2.3. Influence of the solvent composition on the analyte detection

Sensitivity in MS depends both on chemical and physical properties of the analyte itself, including pK_a , hydrophobicity, surface activity, ion solvation energy, and proton affinity. In a reversed-phase LC separation, the peptides are eluted according to their hydrophobic properties. The most hydrophilic peptides therefore egress at the beginning of the gradient when the content of polar solvent is high.

The influence of the eluent composition on the analyte detection was evaluated using a model peptide that allows determining the efficiency of the ion production. KCTCCA was chosen as a model, as it is a relatively hydrophilic peptide and consequently more difficult to ionize. In C18 reversed-phase LC-MS analysis, KCTCCA peptide elutes at the beginning of the LC gradient, *i.e.* at 20% of B solvent.

The ion counts (IC) relative to the peptide as a function of the solvent composition are presented in Figure III-16. From 0 to 50 % of B solvent, the IC is rather low (< 20%). When the percentage of B is higher than 50% the IC increases rapidly to reach 100% for B = 80%. When the spray solution is composed of 100% B, the IC decreases down to 80%. When the organic content of the sprayed solution is higher, the droplet desolvation is easier, enabling a higher ion production. The signal decrease for B > 80% is probably due to a lower solubility of the peptides in such a solvent. In some cases, a decrease of the ESI response was observed for organic content higher than 80%, as reported by Zhou & Hamburger, and is likely due to a liquid surface tension which is below the ideal to maintain spray stability.^{26, 91}

This experiment suggests the possible requirements of an appropriate sheath liquid at the beginning of a LC gradient that can aid hydrophilic peptide ionization. This option is described below.

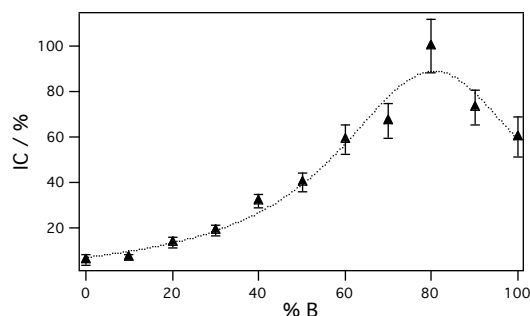


Figure III- 16 Evolution of the the ion counts relative to KCTCCA peptide as a function of the solvent composition. KCTCCA is prepared at a concentration of 10 μM in the different eluent compositions.

4.3. LC-MS analysis of a tryptic digest using an ESI microchip interface

4.3.1. Reproducibility of the tryptic digest analysis by LC-MS

The β -lactoglobulin A (BLA) digest was injected on a C18 column at a flow rate of 4 $\mu\text{L}\cdot\text{min}^{-1}$. The TIC chromatogram from the mass spectrometer (Figure III-17.B) presents almost the same profile and elution time window than the UV chromatogram monitored at 214 nm (Figure III-17.A). As shown by the overlaid TIC chromatogram corresponding to a second LC-MS analysis of the same sample, very good reproducibility of the LC-MS coupling using the infusion – based ESI microchip is achieved.

The position of the microchip in front of the mass spectrometer is of importance for the quality of the detection as demonstrated earlier in this chapter. Moreover, in order to maximize reproducibility between analysis, the distance between the ESI microchip and the MS entrance should be precisely controlled. Several positions were tested with distance ranging from 2 to 10 mm. When the distance increased, the electrospray current decreased and it required a higher onset voltage (Figure III-3). In this first study, we preferred to maintain a constant distance and voltage. The adjustment of the spray mode during the LC gradient, indeed requires to have a precise feedback on it. The best signal stability was observed for a distance $d = 5$ mm and an applied voltage of 4.5 kV. These two parameters were kept constant during the whole LC-MS analysis.

The m/z peak values detected by MS were then analyzed with Mascot search engine (Matrix science, London, UK) to match peptides and identify the protein. Twenty peptides were matched by peptide mass fingerprinting (PMF) to the BLA peptides. It corresponded to the peptides identified in a previous control experiment of the same digest by using the standard ESI source (data not shown). A very slight peak tailing was noted but did not affect the peptide ionization and detection by MS.

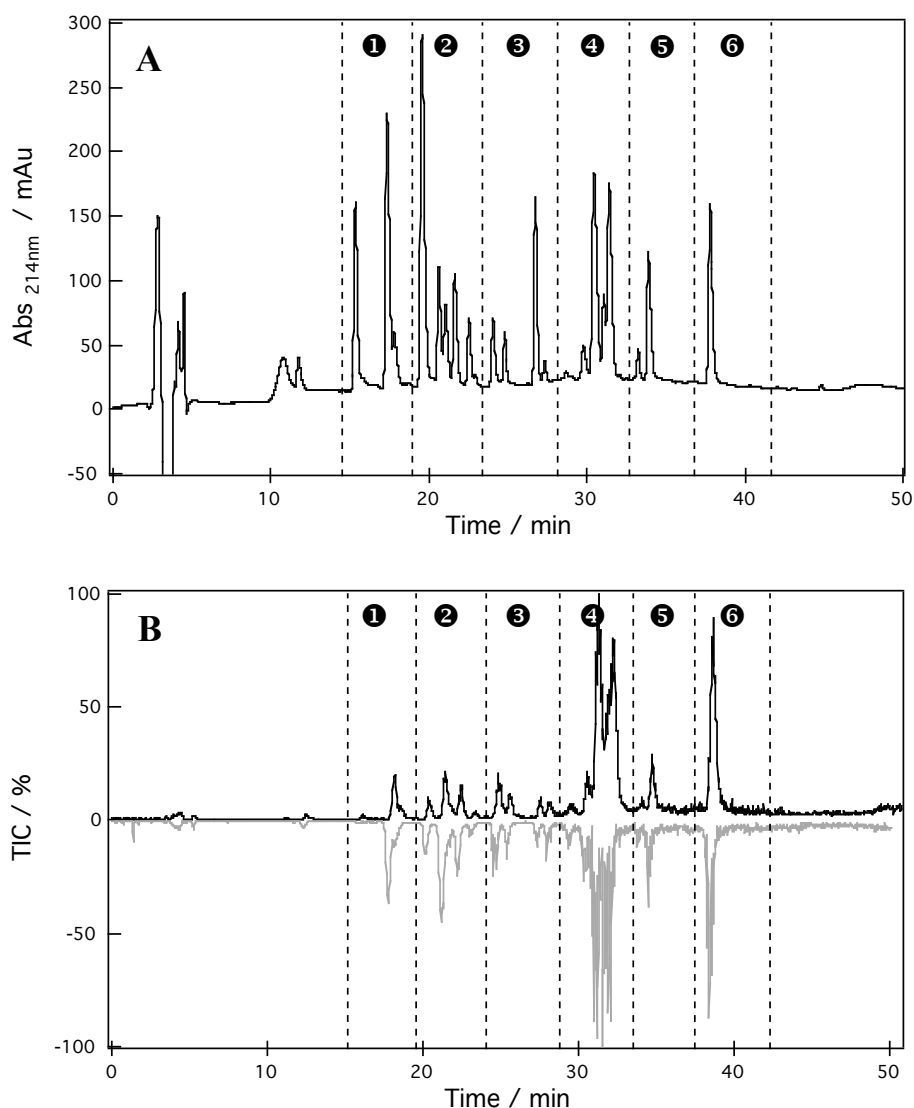


Figure III- 17 LC-MS analysis of a β -lactoglobulin A (BLA) tryptic digest using an ESI emitter microchip. A) UV chromatogram. B) TIC chromatograms of two successive LC-MS analysis of the BLA digest (displayed as mirror).

4.3.2. LC-MS analysis with an ESI emitter microchip vs. a standard ESI source

The performances of the ESI emitter microchip and the standard capillary ESI source were qualitatively compared in Figure III-18. With the standard ESI source, a sheath gas (40 a.u.) and a sheath liquid (50% of B solution) at $1 \mu\text{L}\cdot\text{min}^{-1}$ were applied to aid the ESI process. In both experiments, the separation flow rate was set at $4 \mu\text{L}\cdot\text{min}^{-1}$. The same elution profile was observed with both ESI sources. However, with the ESI microchip, the intensity of the first eluted peaks was lower than when recorded with the standard ESI source (dashed rectangular region). It indicated a better ionization with the standard source at the beginning of the gradient thanks to the use of sheath gas and sheath liquid.

Several possible solutions can be put forward:

- 1) A post-column liquid junction can be added to the microchip in order to deliver an appropriate sheath liquid to aid the peptide ionization at the beginning of the LC gradient, as illustrated by the experiment with KCTCCA presented in Figure III-16. However, one should consider that a continuous sheath liquid may induce negative effects as a sample dilution and a higher total flow rate.
- 2) The variations of the eluent surface tension can be balanced by the applied voltage in order to maintain a stable cone-jet regime. This voltage adaptation in function of the electrospray current feedback has been proposed recently by Marginean for gradient nanoflow LC-MS measurements.⁹² Valskovic et al. developed an automated feedback-controlled electrospray source controlled by a computer and relying on an image-processing algorithm for the spray regime. The changes in mobile phase composition and flow rates are compensated in real-time allowing the source to be maintained in the cone-jet or pulsed cone-jet regime.⁹³
- 3) Pre- or post-column peptide derivatization can be applied to enhance peptide ionization efficiency, as example by adding a hydrophobic tag to the peptides.

Points 1) and 3) are assessed in the following parts.

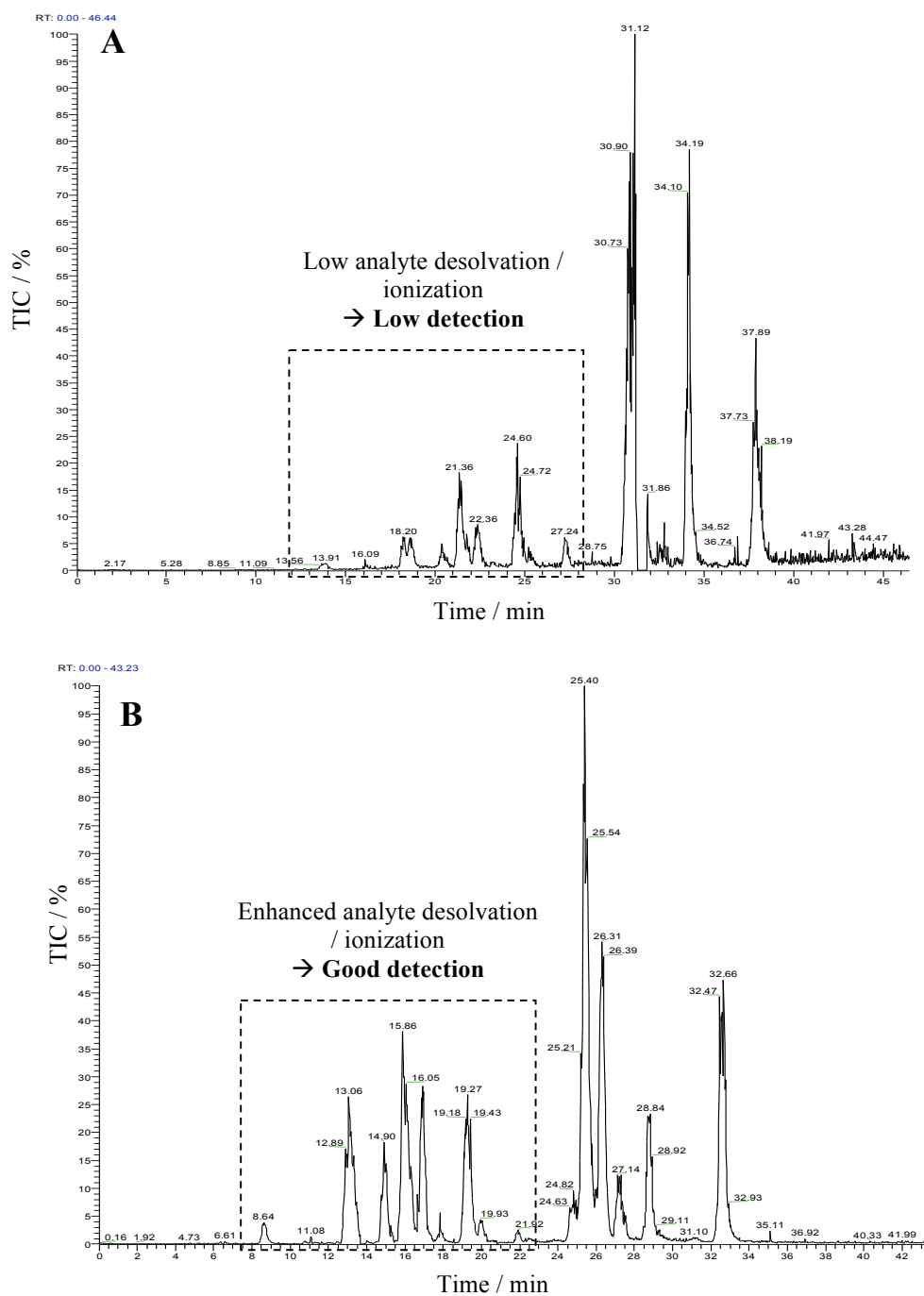


Figure III- 18 TIC chromatogram of a LC-MS analysis of a BLA digest using A) the ESI emitter microchip and B) the standard ESI source. Spray voltage: 4.5 kV, $d = 5$ mm.

4.4. Design and evaluation of the ESI emitter microchip with liquid junction

4.4.1. Microchip design and operation

The fabrication process of a microchip including a liquid junction is similar to the one of a single-channel microchip. The second channel (presenting a cross-section of $100 \times 35 \mu\text{m}^2$) was photoablated at a given angle (30°) with respect to the main microchannel. A carbon electrode was incorporated to the microchip in order to apply the ESI voltage. The microchannel **1** was fed with the highest flow rate (the flow coming from the capillary LC), and the microchannel **2** with the lowest flow rate called “sheath liquid”. The microchip was then placed in a holder with two capillary connections, as illustrated in Figure III-19, and aligned in front of the mass spectrometer inlet.

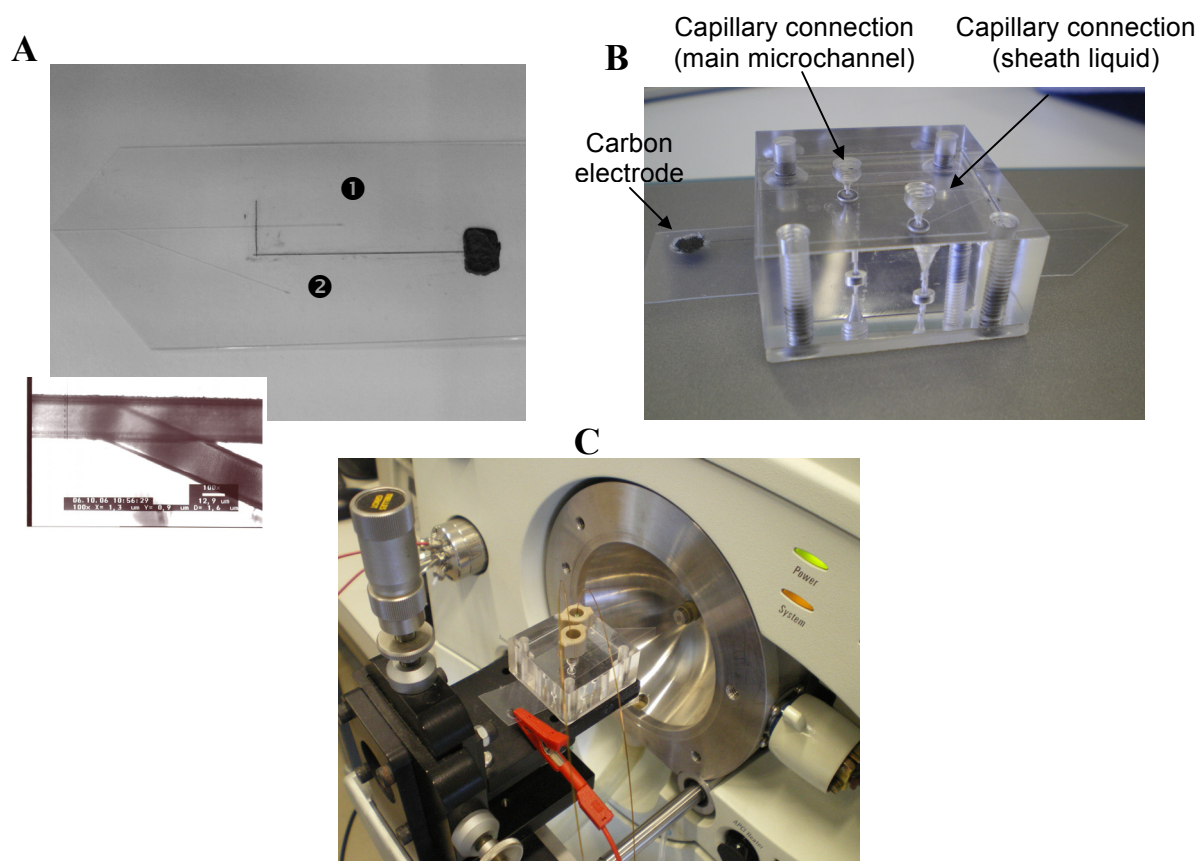


Figure III- 19 A) Picture and microscope view of the ESI emitter microchip with liquid junction. B) The chip is then fixed in a custom-made holder, and C) aligned in front of the MS entrance.

4.4.2. Efficiency of the sheath liquid delivery

The microchannel ❶ was infused with a solution of KCTCCA 50 μM (in 50% B solvent) and the microchannel ❷ with a solution of Leu-Enkephalin 50 μM suspended in the same solvent. Two syringe pumps were used to control the flow rates. The flow in the microchannel ❶ was maintained at 4 $\mu\text{L}\cdot\text{min}^{-1}$ during the entire experiment while the flow rate of the sheath liquid was progressively increased from 0 to 2 $\mu\text{L}\cdot\text{min}^{-1}$.

The TIC was monitored continuously during the experiment while changing the sheath liquid flow rate. Few minutes were necessary for the syringe pump to stabilize at the applied flow rate. The ion counts (ICs) for each peptide are represented in Figure III-20. At the beginning, only the syringe pump of the main microchannel was activated. Thus, only the KCTCCA ions were detected by MS. At 8 min, the junction delivered a flow at 0.5 $\mu\text{L}\cdot\text{min}^{-1}$ and the ions counts were monitored during 8 minutes. The sheath liquid was increased up to 2 $\mu\text{L}\cdot\text{min}^{-1}$ by step increment. As illustrated on the chromatogram, the microchip with sheath liquid responded well. The response for the Leu-Enkephalin increases with the sheath liquid flow rate. In parallel, a diminution of the KCTCCA ions was observed due to a dilution of the KCTCCA peptides and an increase of the total flow rate. The reproducibility of the sheath liquid delivery was confirmed by proceeding to the same experiment but inverting the two samples (data not shown).

The phenomenon of ion suppression inherent of the ESI process, which was previously evoked in this chapter, is evidenced in this experiment. The two samples, of KCTCCA and Leu-Enkephalin, were prepared at the same concentration and in the same solution (50% B). Even if the KCTCCA flow is higher than that of the Leu-Enkephalin, the respective ESI response is quite different and is higher for the Leu-Enkephalin. This fact illustrates the phenomenon of *ion suppression/competition* that can occur during the ion production in the gas-phase when at least two analytes presenting different surface activities are in competition in the ESI droplets. According to the partitioning model proposed by Cech and Enke the less polar peptides are located at the surface of the ESI droplets.⁷⁸ It is confirmed in the present experiment as the more hydrophobic Leu-Enkephalin (YGGFL) peptide is more detected than KCTCCA.

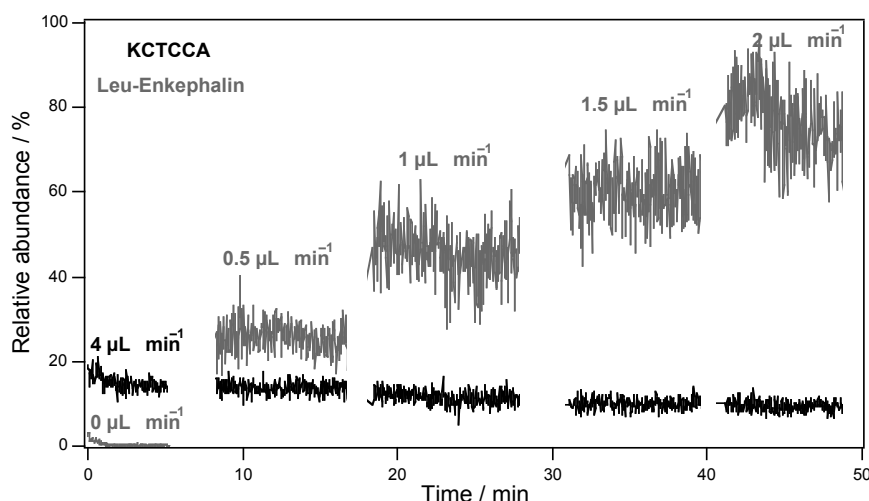


Figure III- 20 Integration of a sheath liquid to the ESI emitter microchip. The signal corresponding to the KCTCCA peptide infused from the main microchannel is displayed in red color while the Leu-Enkephalin signal from the sheath liquid is in blue. The chromatogram shows the evolution of the ion counts when changing the sheath liquid flow rate. KCTCCA 50 μ M and Leu-Enkephalin 50 μ M in 50 %B, $d = 5$ mm, $V_{on} = 4.5$ kV.

4.4.3. Effect of the on-chip sheath liquid on the ionization efficiency in LC-MS analyses

The microchip with liquid junction was then hyphenated to the LC-MS setup. A digest of BLA was injected with a LC gradient programmed over 30 min, as for the experiment presented in Figure III-18. A solution containing 50% of B solvent was infused continuously at

1 μ L \cdot min $^{-1}$ from the liquid junction. The TIC was recorded over 45 min and is presented in Figure III-21. The detection sensitivity of the peptides at the beginning of the gradient was quite enhanced, as it was illustrated previously for the ionization of the KCTCCA peptide in different solutions with increasing percentage of B solvent (Figure III-16). However, the drawback was the noise level that was higher than without sheath liquid. Here, the sheath liquid was applied during the entire LC separation. In some recent studies, the change of eluent composition was counter-balanced by post-column combination with an inverted solvent. It led to a steady solvent composition at the cost of a possible decreased sensitivity because of analyte dilution and increased flow rate. It requires as well two systems of gradient pumps.⁹⁴

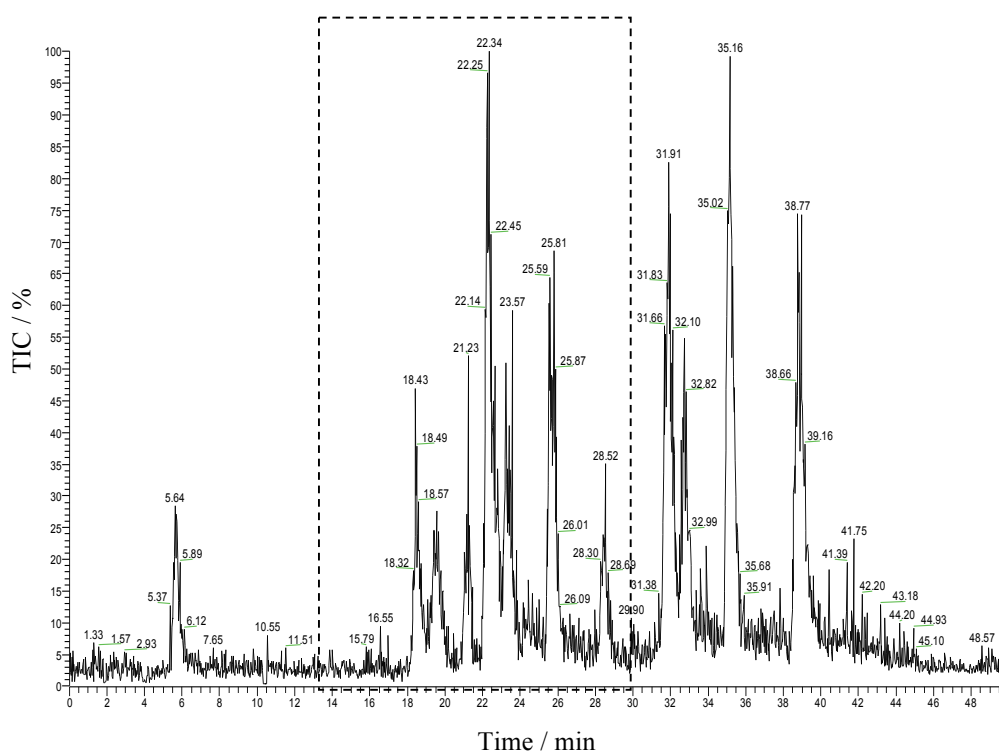


Figure III- 21 TIC chromatogram of a LC-MS analysis of a BLA digest using the ESI emitter microchip with liquid junction. The main microchannel was connected to the LC flow. The liquid junction was fed at $1 \mu\text{L}\cdot\text{min}^{-1}$ with a solution with 50% B in A solvent. Spray voltage: 4.5 kV.

4.5. Towards the use of pre-column peptide modification to enhance peptide ionization efficiency

Regnier and co-workers investigated the use of chemical tags for peptide and protein analysis.^{95, 96} One paper describes the use of a new labeling reagent that simultaneously adds a permanent positive charge to the peptides and increases their hydrophobicity. This so-called C₈QAT tag contains a quaternary amine with an adjacent *N*-octyl chain, and reacts with the N-terminal group and the lysine residues of peptides. It was demonstrated that the retention time of the tagged peptides is shifted significantly and that their ionization is quite enhanced.⁹⁷ Moreover, the C₈QAT tag is already included as modification in Mascot software. The mass shifts can thus be automatically taken into consideration during the data base interrogation.

As the C₈QAT is not commercially available, the tag was synthesized according to the procedure by Mirzaei et al.⁹⁷ and Taran et al.⁹⁸ with slight modifications. The detailed protocol is indicated in the experimental section.

The modified bovine serum albumin (BSA) digest was separated on a C18 column and with a multi-steps gradient (0 - 3 min: 0% B, 3 - 40 min: 0 - 50% B, 40 - 50 min 50 - 100% B, 50 - 60 min: 100% B). The C₈QAT and the non-modified digest were analyzed in the same conditions. The UV chromatograms are presented in Figure III-22. The comparison between the non-modified and modified digest clearly indicates that the modification was efficient, with all the peptides eluted later. This pre-column modification could be an elegant solution to circumvent the low peptide ionization at the beginning of the LC-MS when the ESI microchip is used as MS interface.

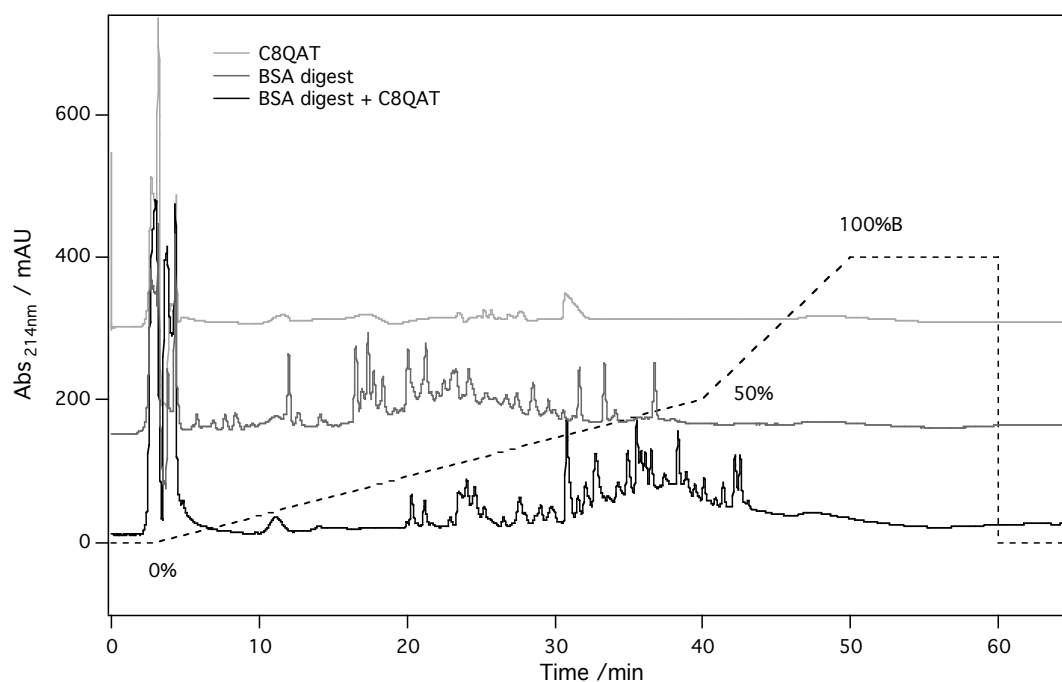


Figure III- 22 Comparison of the LC elution profiles of non-modified and C₈QAT modified BSA digests. Gradient: 0 - 3 min: 0% B, 3 - 40 min: 0 - 50% B, 40 - 50 min 50 - 100% B, 50 - 60 min: 100% B. Solvent A (H₂O:CH₃CN 98:2 with 0.1% FA), and solvent B (H₂O:CH₃CN 20:80 with 0.085% FA). Flow rate: 4 $\mu\text{L}\cdot\text{min}^{-1}$.

5. Conclusions

The hyphenation of an ESI emitter microchip as MS interface to a LC-MS workflow has been investigated. The main issues encountered when coupling a liquid chromatography separation with MS detection have been reviewed. The major concern remains the evolution of the eluent composition that highly influences the ESI current.

In contrast with a standard ESI source, the ESI emitter microchip enables to spray continuously at capillary flow rates and during the entire LC gradient, without the need of a sheath gas to help the desolvation/ionization process. This is an important consideration, as the use of gas is onerous. Moreover, the reproducibility of the LC-MS coupling using the ESI emitter microchip was demonstrated.

As expected, the peptide ionization was shown to be more difficult at the beginning of the LC gradient due to the polar surrounding eluent and the physico-chemical properties of these peptides that are relatively hydrophilic. Two options were investigated to circumvent this problem. The first was the integration of a liquid junction to the microchip in order to provide a sheath liquid. It showed an improvement of the peptide ionization at the beginning of the gradient but an increase of the noise was observed during the entire analysis. The alternative was to fully modify the protein digest with a permanently charged and hydrophobic tag (C₈QAT). With such a derivatization, the elution of the entire pool of peptides was delayed and the peptides presented a permanent positive charge that enhanced their detection by MS. Thus, hyphenation of the microchip coupled to C₈QAT derivatization should provide an elegant, low-cost solution for analysis of protein digests in such a LC-MS coupling. By incorporation of isotopes into the tags, quantitative capabilities could be obtained.

This chapter described the design of a novel ESI emitter microchip including a liquid junction, which was at the origin of the electrospray micromixer chip presented in the next chapter (Chapter IV).

REFERENCES

1. L. Dayon, Thiol-targeted microspray mass spectrometry of peptides and proteins through on-line EC-tagging, EPFL PhD thesis, 2006.
2. G. Jackson and C. Enke, Electrical equivalence of electrospray ionization with conducting and nonconducting needles, *Anal Chem*, 1999, 71, 3777-3784.
3. R. Srinivasan and B. Braren, Ultraviolet laser ablation of organic polymers, *Chemical Reviews*, 1989, 89, 1303-1316.
4. P. Nemes, I. Marginean and A. Vertes, Spraying mode effect on droplet formation and ion chemistry in electrosprays, *Anal Chem*, 2007, 79, 3105-3116.
5. R. Aebersold and M. Mann, Mass spectrometry-based proteomics, *Nature*, 2003, 422, 198-207.
6. H. J. Issaq, The role of separation science in proteomics research, *Electrophoresis*, 2001, 22, 3629-3638.
7. H. J. Issaq, K. C. Chan, J. Blonder, X. Ye and T. D. Veenstra, Separation, detection and quantitation of peptides by liquid chromatography and capillary electrochromatography, *Journal of Chromatography A*, 2009, 1216, 1825-1837.
8. H. J. Issaq, T. P. Conrads, G. M. Janini and T. D. Veenstra, Methods for fractionation, separation and profiling of proteins and peptides, *Electrophoresis*, 2002, 23, 3048-3061.
9. A. Bodzon-Kulakowska, A. Bierczynska-Krzysik, T. Dylag, A. Drabik, P. Suder, M. Noga, J. Jarzebinska and J. Silberring, Methods for samples preparation in proteomic research, *Journal of Chromatography B: Analytical Technologies in the Biomedical and Life Sciences*, 2007, 849, 1-31.
10. A. P. Bruins, Ion spray interface for combined liquid chromatography/atmospheric pressure ionization mass spectrometry, *Analytical Chemistry*, 1987, 59, 2642-2646.
11. M. G. Ikonomou, A. T. Blades and P. Kebarle, Electrospray-ion spray: A comparison of mechanisms and performance, *Analytical Chemistry*, 1991, 63, 1989-1998.
12. R. Kostianen and A. P. Bruins, Effect of solvent on dynamic range and sensitivity in pneumatically- assisted electrospray (ion spray) mass spectrometry, *Rapid Communications in Mass Spectrometry*, 1996, 10, 1393-1399.
13. G. T. T. Gibson, S. M. Mugo and R. D. Oleschuk, Nanoelectrospray emitters: Trends and perspective, *Mass Spectrometry Reviews*, 2009, DOI 10.1002/mas.20248.
14. T. Sikanen, S. Franssila, T. J. Kauppila, R. Kostianen, T. Kotiaho and R. A. Ketola, Microchip technology in mass spectrometry, *Mass Spectrometry Reviews*, 2009, DOI 10.1002/mas.20238.
15. M. Wilm and M. Mann, Analytical properties of the nanoelectrospray ion source, *Analytical Chemistry*, 1996, 68, 1-8.
16. S. Koster and E. Verpoorte, A decade of microfluidic analysis coupled with electrospray mass spectrometry: An overview, *Lab on a Chip - Miniaturisation for Chemistry and Biology*, 2007, 7, 1394-1412.
17. N. Lion, T. C. Rohner, L. Dayon, I. L. Arnaud, E. Damoc, N. Youhnovski, Z. Y. Wu, C. Roussel, J. Josserand, H. Jensen, J. S. Rossier, M. Przybylski and H. H. Girault, Microfluidic systems in proteomics, *Electrophoresis*, 2003, 24, 3533-3562.
18. <http://www.home.agilent.com>.
19. <http://www.advion.com/biosystems/chip-based-nanoelectrospray.php>.
20. M. Dole, L. L. Mack, R. L. Hines, D. O. Chemistry, R. C. Mobley, L. D. Ferguson and M. B. Alice, Molecular beams of macroions, *The Journal of Chemical Physics*, 1968, 49, 2240-2249.
21. M. Yamashita and J. B. Fenn, Negative ion production with the electrospray ion source, *Journal of Physical Chemistry*, 1984, 88, 4671-4675.
22. M. Yamashita and J. B. Fenn, Electrospray ion source. Another variation on the free-jet theme, *Journal of Physical Chemistry*, 1984, 88, 4451-4459.

23. M. L. Alexandrov, L. N. Gall, N. V. Krasnov, V. I. Nikolaev, V. A. Pavlenko and V. A. Shkurov, Short communication, *International Journal of Mass Spectrometry and Ion Processes*, 1983, 54, 231-235.
24. J. B. Fenn, http://nobelprize.org/nobel_prizes/chemistry/laureates/2002/index.html, 2002.
25. R. B. Cole, *Electrospray ionization mass spectrometry: Fundamentals, instrumentation & applications*, New York: ISBN 0-471-14564-5, 1997.
26. G. A. Arteca, C. T. Reimann and O. Tapia, Practical implications of some recent studies in electrospray ionization fundamentals, *Mass Spectrometry Reviews*, 2001, 20, 362-387.
27. P. Kebarle and Y. Ho, On the mechanism of electrospray mass spectrometry, *Electrospray Ionization Mass Spectrometry*, 1997, 3-63.
28. P. Kebarle, A brief overview of the present status of the mechanisms involved in electrospray mass spectrometry, *Journal of Mass Spectrometry*, 2000, 35, 804-817.
29. J. Zeleny, The electrical discharge from liquid points, and a hydrostatic method of measuring the electric intensity at their surfaces, *Physical Review*, 1914, 3, 69-91.
30. M. Cloupeau and B. Prunet-Foch, Electrohydrodynamic spraying functioning modes: a critical review, *Journal of Aerosol Science*, 1994, 25, 1021-1036.
31. M. Cloupeau and B. Prunet-Foch, Electrostatic spraying of liquids: Main functioning modes, *Journal of Electrostatics*, 1990, 25, 165-184.
32. M. Cloupeau and B. Prunet-Foch, Electrostatic spraying of liquids in cone-jet mode, *Journal of Electrostatics*, 1989, 22, 135-159.
33. G. H. Joffre and M. Cloupeau, Characteristic forms of electrified menisci emitting charges, *Journal of Electrostatics*, 1986, 18, 147-161.
34. G. Joffre, B. Prunet-Foch and M. Cloupeau, EVAPORATION OF CHARGED DROPLETS IN AN ELECTRIC FIELD, *Heat transfer. Soviet research*, 1980, 13, 81-87.
35. G. Joffre, B. Prunet-Foch and M. Cloupeau, Charged droplets evaporation and motion in an electric field, *International Journal of Multiphase Flow*, 1978, 4, 41-51.
36. I. Marginean, L. Parvin, L. Heffernan and A. Vertes, Flexing the electrified meniscus: The birth of a jet in electrosprays, *Analytical Chemistry*, 2004, 76, 4202-4207.
37. I. Hayati, A. I. Bailey and T. F. Tadros, Mechanism of stable jet formation in electrohydrodynamic atomization, *Nature*, 1986, 319, 41-43.
38. D. P. H. Smith, ELECTROHYDRODYNAMIC ATOMIZATION OF LIQUIDS, *IEEE Transactions on Industry Applications*, 1986, IA-22, 527-535.
39. I. Hayati, A. I. Bailey and T. F. Tadros, Investigations into the mechanisms of electrohydrodynamic spraying of liquids. I. Effect of electric field and the environment on pendant drops and factors affecting the formation of stable jets and atomization, *Journal of Colloid And Interface Science*, 1987, 117, 205-221.
40. D. C. Taflin, T. L. Ward and E. J. Davis, Electrified droplet fission and the Rayleigh limit, *Langmuir*, 1989, 5, 376-384.
41. J. Fernandez De La Mora, J. Navascues, F. Fernandez and J. Rosell-Llompart, *J. Aerosol. Sci.*, 1990, 21, 5673.
42. G. I. Taylor, Disintegration of water drops in an electric field, *Proc. R. Soc. London, Ser. A*, 1964, 280, 383-397.
43. J. F. De La Mora and I. G. Loscertales, Current emitted by highly conducting Taylor cones, *Journal of Fluid Mechanics*, 1994, 260, 155-184.
44. L. B. Loeb, A. F. Kip, G. G. Hudson and W. H. Bennett, Pulses in negative point-to-plane corona, *Physical Review*, 1941, 60, 714-722.
45. R. J. Pfeifer and C. D. Hendricks, Parametric studies of electrohydrodynamic spraying, *AIAA J.*, 1968, 6, 496-502.
46. L. Rayleigh, On the equilibrium of liquid conducting masses charged with electricity, *Philos. Mag.*, 1882, 14, 184-186.
47. A. Gomez and K. Tang, Charge and fission of droplets in electrostatic sprays, *Physics of Fluids*, 1994, 6, 404-414.
48. N. Lion, J. O. Gellon and H. H. Girault, Flow-rate characterization of microfabricated polymer microspray emitters, *Rapid Communications in Mass Spectrometry*, 2004, 18, 1614-1620.

49. A. T. Blades, M. G. Ikonou and P. Kebarle, Mechanism of electrospray mass spectrometry. Electrospray as an electrolysis cell, *Analytical Chemistry*, 1991, 63, 2109-2114.
50. G. J. Van Berkel, S. A. McLuckey and G. L. Glush, Electrochemical origin of radical cations observed in electrospray ionization mass spectra, *Analytical Chemistry*, 1992, 64, 1586-1593.
51. G. J. Van Berkel and F. Zhou, Characterization of an electrospray ion source as a controlled-current electrolytic cell, *Analytical Chemistry*, 1995, 67, 2916-2923.
52. G. J. Van Berkel, The electrolytic nature of electrospray, *Electrospray Ionization Mass Spectrometry*, 1997, 65-105.
53. G. J. Van Berkel and F. Zhou, Electrospray as a controlled-current electrolytic cell: Electrochemical ionization of neutral analytes for detection by electrospray mass spectrometry, *Analytical Chemistry*, 1995, 67, 3958-3964.
54. J. Fernandez De La Mora, G. J. Van Berkel, C. G. Enke, R. B. Cole, M. Martinez-Sanchez and J. B. Fenn, Electrochemical processes in electrospray ionization mass spectrometry, *Journal of Mass Spectrometry*, 2000, 35, 939-952.
55. G. J. Van Berkel, F. Zhou and J. T. Aronson, Changes in bulk solution pH caused by the inherent controlled-current electrolytic process of an electrospray ion source, *International Journal of Mass Spectrometry and Ion Processes*, 1997, 162, 55-67.
56. L. Konermann, E. A. Silva and O. F. Sogbein, Electrochemically induced pH changes resulting in protein unfolding in the ion source of an electrospray mass spectrometer, *Analytical Chemistry*, 2001, 73, 4836-4844.
57. L. Dayon, J. Josserand and H. H. Girault, Electrochemical multi-tagging of cysteinyl peptides during microspray mass spectrometry: Numerical simulation of consecutive reactions in a microchannel, *Physical Chemistry Chemical Physics*, 2005, 7, 4054-4060.
58. L. Dayon, C. Roussel and H. H. Girault, Probing cysteine reactivity in proteins by mass spectrometric EC-tagging, *Journal of Proteome Research*, 2006, 5, 793-800.
59. H. P. Permentier, A. P. Bruins and R. Bischoff, Electrochemistry-mass spectrometry in drug metabolism and protein research, *Mini-Reviews in Medicinal Chemistry*, 2008, 8, 46-56.
60. T. C. Rohner, J. Josserand, H. Jensen and H. H. Girault, Numerical investigation of an electrochemically induced tagging in a nanospray for protein analysis, *Analytical Chemistry*, 2003, 75, 2065-2074.
61. G. J. Van Berkel, K. G. Asano and V. Kertesz, Enhanced study and control of analyte oxidation in electrospray using a thin-channel, planar electrode emitter, *Analytical Chemistry*, 2002, 74, 5047-5056.
62. G. J. Van Berkel and V. Kertesz, Expanded electrochemical capabilities of the electrospray ion source using porous flow-through electrodes as the upstream ground and emitter high-voltage contact, *Analytical Chemistry*, 2005, 77, 8041-8049.
63. G. J. Van Berkel, V. Kertesz, M. J. Ford and M. C. Granger, Efficient analyte oxidation in an electrospray ion source using a porous flow-through electrode emitter, *Journal of the American Society for Mass Spectrometry*, 2004, 15, 1755-1766.
64. M. Prudent and H. H. Girault, On-line Electrogeneration of Copper-Peptide Complexes in Microspray Mass Spectrometry, *Journal of the American Society for Mass Spectrometry*, 2008, 19, 560-568.
65. M. Prudent, J. S. Rossier, N. Lion and H. H. Girault, Microfabricated dual sprayer for on-line mass tagging of phosphopeptides, *Analytical Chemistry*, 2008, 80, 2531-2538.
66. P. Kebarle and M. Peschke, On the mechanisms by which the charged droplets produced by electrospray lead to gas phase ions, *Analytica Chimica Acta*, 2000, 406, 11-35.
67. D. B. Hager, N. J. Dovichi, J. Klassen and P. Kebarle, Droplet Electrospray Mass Spectrometry, *Analytical Chemistry*, 1994, 66, 3944-3949.
68. G. Wang and R. B. Cole, Charged residue versus ion evaporation for formation of alkali metal halide cluster ions in ESI, *Analytica Chimica Acta*, 2000, 406, 53-65.
69. G. Schmelzeisen-Redeker, L. Böhmer and F. W. Röllgen, Desolvation of ions and molecules in thermospray mass spectrometry, *International Journal of Mass Spectrometry and Ion Processes*, 1989, 90, 139-150.
70. J. V. Iribarne and B. A. Thomson, On the evaporation of small ions from charged droplets, *The Journal of Chemical Physics*, 1976, 64, 2287-2294.

71. B. A. Thomson and J. V. Iribarne, Field induced ion evaporation from liquid surfaces at atmospheric pressure, *The Journal of Chemical Physics*, 1979, 71, 4451-4463.
72. T. Nohmi and J. B. Fenn, Electrospray mass spectrometry of poly(ethylene glycols) with molecular weights up to five million, *Journal of the American Chemical Society*, 1992, 114, 3241-3246.
73. J. B. Fenn, Ion formation from charged droplets: roles of geometry, energy, and time, *Journal of the American Society for Mass Spectrometry*, 1993, 4, 524-535.
74. S. Nguyen and J. B. Fenn, Gas-phase ions of solute species from charged droplets of solutions, *Proceedings of the National Academy of Sciences of the United States of America*, 2007, 104, 1111-1117.
75. J. V. Iribarne, P. J. Dziedzic and B. A. Thomson, Atmospheric pressure ion evaporation-mass spectrometry, *International Journal of Mass Spectrometry and Ion Physics*, 1983, 50, 331-347.
76. L. Tang and P. Kebarle, Dependence of ion intensity in electrospray mass spectrometry on the concentration of the analytes in the electrosprayed solution, *Analytical Chemistry*, 1993, 65, 3654-3667.
77. C. G. Enke, A Predictive Model for Matrix and Analyte Effects in Electrospray Ionization of Singly-Charged Ionic Analytes, *Analytical Chemistry*, 1997, 69, 4885-4893.
78. N. B. Cech and C. G. Enke, Relating electrospray ionization response to nonpolar character of small peptides, *Analytical Chemistry*, 2000, 72, 2717-2723.
79. N. B. Cech, J. R. Krone and C. G. Enke, Predicting electrospray response from chromatographic retention time, *Analytical Chemistry*, 2001, 73, 208-213.
80. G. S. Jackson and C. G. Enke, Electrical equivalence of electrospray ionization with conducting and nonconducting needles, *Analytical Chemistry*, 1999, 71, 3777-3784.
81. R. A. Ochran and L. Konermann, Effects of ground loop currents on signal intensities in electrospray mass spectrometry, *Journal of the American Society for Mass Spectrometry*, 2004, 15, 1748-1754.
82. T. C. Rohner, J. S. Rossier and H. H. Girault, Polymer microspray with an integrated thick-film microelectrode, *Analytical Chemistry*, 2001, 73, 5353-5357.
83. R. Srinivasan and V. Mayne-Banton, Self-developing photoetching of poly(ethylene terephthalate) films by far-ultraviolet excimer laser radiation, *Applied Physics Letters*, 1982, 41, 576-578.
84. Y. Kawamura, K. Toyoda and S. Namba, Effective deep ultraviolet photoetching of polymethyl methacrylate by an excimer laser, *Applied Physics Letters*, 1982, 40, 374-375.
85. P. E. Dyer, Excimer laser polymer ablation: Twenty years on, *Applied Physics A: Materials Science and Processing*, 2003, 77, 167-173.
86. T. Lippert and J. T. Dickinson, Chemical and spectroscopic aspects of polymer ablation: Special features and novel directions, *Chemical Reviews*, 2003, 103, 453-485.
87. S. Lazare, J. Lopez and F. Weisbuch, High-aspect-ratio microdrilling in polymeric materials with intense KrF laser radiation, *Applied Physics A: Materials Science and Processing*, 1999, 69, S1-S6.
88. H. Watanabe and M. Yamamoto, Chemical Structure Change of a KrF-Laser Irradiated PET Fiber Surface, *Journal of Applied Polymer Science*, 1999, 71, 2027-2031.
89. J. S. Rossier, P. Bercier, A. Schwarz, S. Lorient and H. H. Girault, Topography, crystallinity and wettability of photoablated PET surfaces, *Langmuir*, 1999, 15, 5173-5178.
90. M. C. Garcia, A. C. Hogenboom, H. Zappey and H. Irth, Effect of the mobile phase composition on the separation and detection of intact proteins by reversed-phase liquid chromatography-electrospray mass spectrometry, *Journal of Chromatography A*, 2002, 957, 187-199.
91. S. Zhou and M. Hamburger, Effects of solvent composition on molecular ion response in electrospray mass spectrometry: Investigation of the ionization processes, *Rapid Commun. Mass Spectrom.*, 1995, 9, 1516-1521.
92. I. Marginean, R. T. Kelly, R. J. Moore, D. C. Prior, B. L. LaMarche, K. Tang and R. D. Smith, Selection of the Optimum Electrospray Voltage for Gradient Elution LC-MS Measurements, *Journal of the American Society for Mass Spectrometry*, 2009, 20, 682-688.

93. G. A. Valaskovic, J. P. Murphy Iii and M. S. Lee, Automated orthogonal control system for electrospray ionization, *Journal of the American Society for Mass Spectrometry*, 2004, 15, 1201-1215.
94. R. Ramanathan, R. Zhong, N. Blumenkrantz, S. K. Chowdhury and K. B. Alton, Response Normalized Liquid Chromatography Nanospray Ionization Mass Spectrometry, *Journal of the American Society for Mass Spectrometry*, 2007, 18, 1891-1899.
95. F. E. Regnier, L. Riggs, R. J. Zhang, L. Xiong, P. R. Liu, A. Chakraborty, E. Seeley, C. Sioma and R. A. Thompson, Comparative proteomics based on stable isotope labeling and affinity selection, *Journal of Mass Spectrometry*, 2002, 37, 133-145.
96. F. E. Regnier and S. Julka, Primary amine coding as a path to comparative proteomics, *Proteomics*, 2006, 6, 3968-3979.
97. H. Mirzaei and F. Regnier, Enhancing electrospray ionization efficiency of peptides by derivatization, *Analytical Chemistry*, 2006, 78, 4175-4183.
98. F. Taran, P. Y. Renard, H. Bernard, C. Mioskowski, Y. Frobert, P. Pradelles and J. Grassi, Antibody-catalyzed decarboxylative oxidation of vanillylmandelic acid, *Journal of the American Chemical Society*, 1998, 120, 3332-3339.

CHAPTER IV.

Electrospray micromixer chip for on-line derivatization and kinetic studies

Based on M. Abonnenc, L. Dayon, B. Perruche, N. Lion, H.H. Girault, 2008, Anal. Chem., 80 (9), 3372-3378.

1. Introduction

Mass spectrometry based workflows play a major role in proteomics,^{1, 2} to identify, characterize and quantify proteins at an ever increasing throughput, and in ever more complex mixtures. A number of approaches have been investigated to complement the mass spectrometric analysis of tryptic peptides based on chemical tagging, in order to isolate specific subclasses of proteins by affinity baits, or for quantitation purposes. Furthermore, the use of non-quantitative addition of chemical probes to increase the information content of MS analysis is a promising approach. For example, Sechi and Chait proposed the differential alkylation of cysteine residues as a way to increase the identification score in peptide mass fingerprinting.³ Over the last years, our lab has been involved in the study of benzoquinone reagents as specific tags for cysteine residues in acidic solution. More particularly, a novel methodology based on the on-chip electrochemical tagging of cysteines, by oxidation of hydroquinone into benzoquinone at the microchip electrode, during ESI-MS of peptides has been introduced.⁴ The potential of this on-line electrochemical tagging was demonstrated with microfabricated electrospray emitters, where instrumental parameters (current density at the electrospray electrode, residence time of analytes and chemical probes) can be properly

tailored and controlled. However, this methodology was so far limited to off-line analysis of peptide fractions. In order to bring the potential of tagging methodologies to on-line analysis (*e.g.* in HPLC-ESI-MS analysis of tryptic peptides), we have developed here a combined derivatization/electrospray device where we physically mix the samples with a solution of benzoquinone.

A number of studies have been performed to study chemical reaction kinetics by ESI-MS, pioneered by Lee et al.⁵ In their setup shown in Figure IV-1, reactants were mixed manually in a vessel that was directly coupled to the ESI source. The time scale of these experiments was of the order of several seconds.

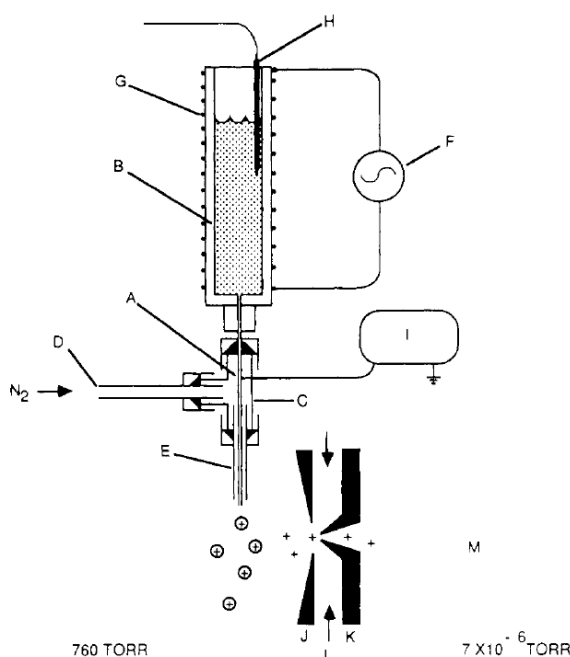


Figure IV- 1 Schematic illustration of the continuous-introduction ion-spray interface: (A) electro-spray electrode, (B) reaction chamber, (C) 1/16-in tee, (D) nebulizing gas inlet, (E) co-axial tube around electrode, (F) powerstat, (G) coiled nichrome wire, (H) thermocouple, (I) high-voltage power supply, (J) interface plate of mass spectrometer, (K) conical skimmer orifice of mass spectrometer, (L) nitrogen curtain gas, (M) mass analyzer. Reprinted from Ref³.

Continuous-flow mixing setup and ESI-MS detection were used for various purposes such as for the method of “time-resolved” ESI-MS⁶ to study protein folding⁷ and enzymatic reactions.^{8, 9} Microreactors offer a good alternative to all these conventional laboratory-scale equipments, because they allow low reagent consumption and fast mixing as well as a

continuous flow operative mode and real-time analysis.¹⁰ Reinhoudt's group introduced a nanoflow ESI interface (nESI) where a reactor chip, based on diffusion along a microchannel, was mounted on an ESI-MS nanoflow interface.¹¹ Whereas there have been numerous reports about chip MS interfaces such as direct emitters¹²⁻¹⁴, arrayed emitters¹⁵ or HPLC-chip MS^{16, 17}, there are few reports of microreactors directly coupled to the ESI-MS and even more directly integrated to the electrospray emitter microchip.

Because of the small dimensions of microchannels as well as the limited range of obtainable linear flow rates, flow in microchannels is confined to the laminar regime and mixing is dominated by molecular diffusion.¹⁸ Micromixing may be accomplished using different approaches. Active mixing may involve either external energy sources such as electro-osmotic flow,^{19, 20} external pressure gradient²¹ and electrokinetic instability^{22, 23} to perturb fluid streamlines into a mixing state. Another approach may consist in passive micromixing based on the use of geometries within the microchannels to mix the fluids,²⁴ such as the zigzag micromixer.²⁵ One of the best-known designs of passive microfluidic mixing is the herringbone mixer, depicted in Figure IV-2.^{26, 27} The system uses a series of herringbone ridges placed on the bottom of the channel to create two counter-rotating vortices. To date, there have been a number of theoretical, experimental, and numerical studies aimed at the optimization of such micromixers.^{28, 29} More particularly, in the case of the staggered herringbone micromixer, oblique grooves serve to transport fluid from the apex of the groove structure to the downstream edges of the microchannel. As a result, fluid near the top of the microchannels re-circulates in the opposite direction, and an overall helical flow pattern is created.

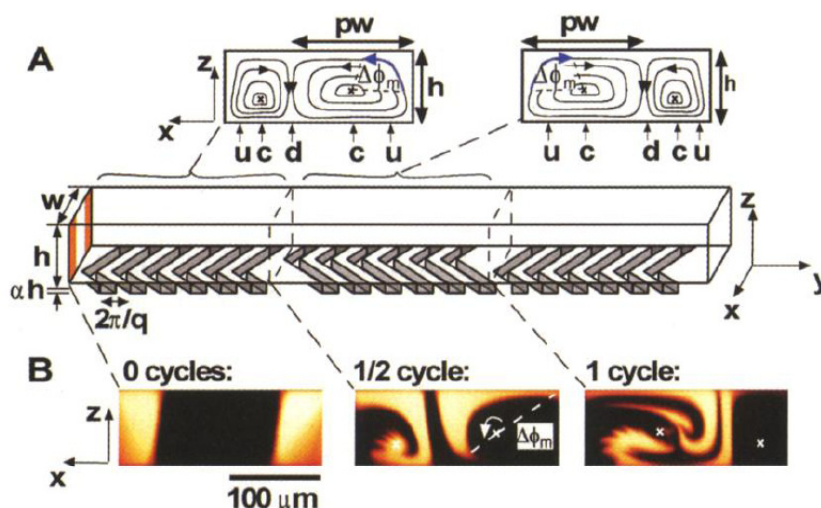


Figure IV- 2 Staggered herringbone mixer (SHM). A) Schematic diagram of one-and-a-half cycles of the SHM. B) Confocal micrographs of vertical cross-sections of a channel as in A). Reprinted from Ref ²⁶.

The present study explores the application of a new design of electrospray emitter microchip with integrated oblique grooves constituting a passive mixing unit for on-line chemical modification of peptides and direct ESI-MS analysis. The polymer microchip is composed of a main feed microchannel supplying the analyte, linked by a liquid junction to a secondary microchannel for providing the tagging reagents. Downstream of the liquid junction, a mixing unit constituted of a series of photo-ablated oblique grooves allows the mixing of the two incoming flows. A carbon micro-electrode in contact with the feed channel solution is also integrated to the microchip to apply the voltage to the solution and consequently induce the ESI process. First, the microfluidic device with mixing unit was characterized by fluorescence imaging and compare to a similar device without mixing unit in order to evaluate the efficiency of the mixing. In a second step, on-chip chemical tagging of cysteines with benzoquinone was performed on a model peptide containing three cysteines to illustrate the feasibility of on-line tagging reaction directly on the electrospray microchip and to assess the performance of such micromixers. Subsequently, the consecutive tagging on-chip of the three cysteines in the KCTCCA peptide was compared to an analytical kinetic model, showing a tagging kinetics close to that of bulk reactions in an ideally mixed reactor. Finally, on-line RP-HPLC-tagging-ESI-MS of tryptic cysteinyl peptides of bovine serum albumin (BSA) was achieved with the electrospray micromixer chip.

2. Experimental section

Chemicals.

KCTCCA (70%, $M = 627.8 \text{ g}\cdot\text{mol}^{-1}$) and Leu-Enkephalin (98.1%, $M = 555.6 \text{ g}\cdot\text{mol}^{-1}$) were bought from Bachem (Bubendorf, Switzerland). 1,4-benzoquinone (BQ) ($\geq 98\%$, $M = 108.1 \text{ g}\cdot\text{mol}^{-1}$), Fluorescein sodium ($M = 376.3 \text{ g}\cdot\text{mol}^{-1}$), and acetic acid ($> 99.5\%$) were supplied by Fluka (Buchs, Switzerland). Bovine serum albumin (BSA, $\geq 98\%$) was purchased from Sigma (St. Louis, MO, USA). Sequencing grade modified trypsin was from Promega (Madison, WI, USA). Methanol ($\geq 99.9\%$) and Formic acid ($> 98\%$) were from Merck (Darmstadt, Germany). Water (UV-HPLC) and acetonitrile (HPLC-gradient grade) were from Panreac Quimica S.A. (Barcelona, Spain). All chemicals were used without any further purification.

Device microfabrication.

The general ESI emitter microchip fabrication process has been previously described in details in Chapter III.¹² The process for the device composed of two microchannels linked by a liquid junction is as follows (Figure IV-3). First, a L-shape microchannel was drilled on the backside of a polyethylene-terephthate (PET) sheet of $100 \mu\text{m}$ thickness (Melinex sheet from Dupont, Wilmington, DE, USA) by photoablation with an ArF excimer laser (193nm, Lambda Physik, Göttingen, Germany). After laser ablation, the chip was cleaned with MeOH and dried under nitrogen. Then, the L-shape microchannel was filled twice with carbon ink to make the electrode. The chip was cured 1 hour at 80°C and then laminated. In a second step, the main microchannel ($100 \mu\text{m}$ wide, 6 cm long and $35 \mu\text{m}$ deep) was photo-ablated on the topside of the microchip in such a way that the microchannel crossed the carbon electrode and revealed it.

To introduce the mixing unit, a smaller mask rotated by 45° was used. Grooves ($40 \mu\text{m} \times 100 \mu\text{m}$) were made by regular static shots along a 1.5 cm long portion of the main microchannel and at 3.5 cm from the main microchannel inlet, the number of static shoots defining the groove depth (typically 100 static shoots for a $35 \mu\text{m}$ deep groove). Then, the microchip was rotated to drill the secondary microchannel ($100 \mu\text{m}$ wide, 2 cm long and $35 \mu\text{m}$ deep). The microchannels were cleaned with MeOH and dried under nitrogen. Reservoirs were drilled at the channel extremities by static laser shoots. The structure was closed by lamination.

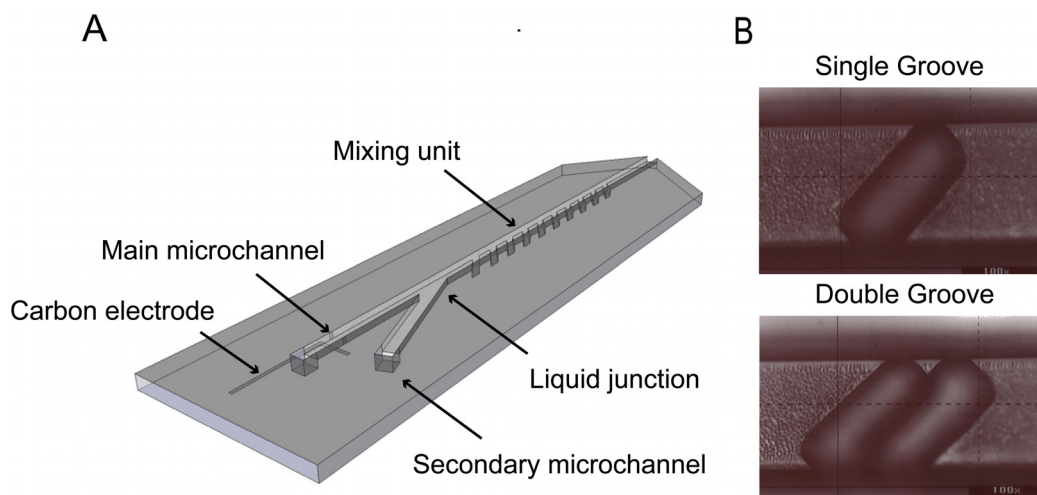


Figure IV-3. Electrospray microchip with a mixing unit. A) Schematic representation of the device. B) Microscope view of the single and double grooves composing the mixing unit (top-view). Typical dimensions of a single groove: $40 \times 100 \times 35 \mu\text{m}^3$; double groove: $70 \times 100 \times 35 \mu\text{m}^3$. The main and secondary microchannels are 6 and 2 cm long, respectively. The mixing unit is positioned at 3.5 cm from the main microchannel inlet. Grooves are photoablated on a 1.5 cm distance and are spaced by either 250 or 500 μm .

Mass spectrometry.

All experiments were performed on a LCQ DUO ion trap mass spectrometer (Thermo Electron, San José, USA). The heated capillary was kept at 200°C. The microchip was positioned inside a custom-made holder with two micro-holes for fluidic connections. The MS standard ESI interface was removed and the holder was placed on a plate positioned on the probe slide adapter of the mass spectrometer.

The tagging experiments with KCTCCA were achieved with an ESI voltage of 3.5 kV (positive ionization mode, m/z of 500 – 1000 Th). The HPLC-MS experiments were run with an ESI voltage of 3.7 kV (m/z of 150 – 2000 Th).

Fluorescence Imaging.

The microchips were observed in working conditions with a microscope Axiovert 200 and a CCD-IRIS camera (Sony). Water was infused in the main microchannel at flow rate $F_V = 4 \mu\text{L} \cdot \text{min}^{-1}$. A solution of fluorescein was provided from the secondary microchannel at F_V ranging from 0 to $2 \mu\text{L} \cdot \text{min}^{-1}$. The fluorescein distribution along the microchannel was observed under fluorescence. Pictures were taken before the mixing region and between each

mixer groove (*i.e.* each 500 μm) on a total distance of 25 mm. Imaging data were obtained both with microchips without and with mixing area.

Image analysis.

The fluorescence intensity profile along the microchannel cross-section was extracted from the images using Igor software (Wavemetrics, Portland, USA). For a same microchip all the fluorescence profile data were assembled using an in-house program written in C language, then interpolated and plotted with Gnuplot 4.2 under Ubuntu Linux 7.04.

On-chip chemical tagging of cysteinyl peptides.

KCTCCA and BQ were diluted in MeOH:H₂O:AcOH (50:49:1) at a concentration of 10 μM and from 5 to 100 mM, respectively. KCTCCA was provided by the main microchannel at $F_V = 4 \mu\text{L}\cdot\text{min}^{-1}$. The BQ solution was infused in the chip from the liquid junction at various F_V from 1 to 2 $\mu\text{L}\cdot\text{min}^{-1}$.

Simulations of the multi-tagging of cysteines in peptides.

The kinetic model was based on a set of differential equations that can be solved analytically. Calculations for each experimental condition were run on Maple 9.5 software (Waterloo Maple Inc.).

BSA digestion and on-line HPLC-tagging-MS of cysteinyl peptides.

One mg of BSA was dissolved in 1 mL of ammonium bicarbonate buffer (5 mM, pH = 8). Then, 0.62 mg of DTT (to get a final concentration of 4 mM) and 20 μg of trypsin (protein ratio 1:50 w:w) were added. The digestion was run at 37 °C for 5 h. One μg of the BSA digest was separated on a LC Packings Ultimate™ (Dionex, Olten, Switzerland) capillary RP-HPLC system equipped with a UV detector (multi-monitoring at 214, 250 and 280 nm). An LC Packings C18 PepMap 100 column (15 cm, 3 μm , 100 Å) was used. The separation was run for 60 minutes using a gradient of H₂O:CH₃CN 98:2 +0.1% FA (solvent A) and H₂O:CH₃CN 20:80 + 0.085% FA (solvent B). The gradient was run as follows: 0-3 min 100% A, then to 50% B at 40 min and 100% B at 50 min for 10 min, at $F_V = 4 \mu\text{L}\cdot\text{min}^{-1}$.

The HPLC capillary outlet was directly connected to the microchip inlet using the holder system described above. The secondary microchip inlet was fed either by a sheath liquid

solution ($\text{H}_2\text{O}:\text{CH}_3\text{CN}$ 50:50 + 0.1% FA) or the tagging reagent solution (*i.e.* BQ at concentration from 5 to 100 mM in $\text{H}_2\text{O}:\text{CH}_3\text{CN}$ 50:50 + 0.1% FA) at $F_V = 1 \mu\text{L}\cdot\text{min}^{-1}$.

Protein identification.

Mascot (<http://www.matrixscience.com>) was used to perform the database interrogation. Mascot enables, in its module “Sequence query”, the content specification of amino acids such as cysteine residues. The search was performed in the Swissprot database and restrained to the Chordata taxonomy. Trypsin was specified as enzyme with up to one missed cleavage allowed. No modification was entered. The peptide mass tolerance was fixed to ± 0.5 Da and the peptide charges to 1+, 2+ and 3+.

3. Results and Discussions

The ESI microchips studied here are typically made of a main microchannel with an embedded carbon band microelectrode and linked by a liquid junction to a secondary microchannel. The fabrication process is quite simple and based on UV-photoablation of PET. Downstream the liquid junction, a mixing unit made of photo-ablated parallel oblique grooves is integrated to create a flow perturbation along the microchannel as illustrated in Figure IV-3. The microchips were placed in a holder with capillary connections to fill in the two microchannels under flow-controlled conditions. The microchip was then positioned in front of the mass spectrometer and the spray voltage was directly applied to the embedded carbon electrode.

The two-inlet electrospray device was first characterized with two different peptide solutions showing a good correlation between the flow rates applied in both microchannels and the respective MS ion count intensities (see Chapter III).³⁰ The microchip geometry was shown to manage flow rates ranging from 1 to $7 \mu\text{L}\cdot\text{min}^{-1}$. In the present study, total flow rates from 4 to $6 \mu\text{L}\cdot\text{min}^{-1}$ were applied, at which good spray stability was demonstrated (mean RSD of 4.95 %).

3.1. Mixing efficiency with different groove geometries

Figure IV-4 illustrates the fluorescence repartition in a smooth microchannel in the absence of a mixing unit (Figure IV-4.A) and in a microchannel with photoablated oblique grooves (Figure IV-4.B) along a 15 mm portion. In all cases, the main microchannel was infused with water at flow rate $F_V = 4 \mu\text{L}\cdot\text{min}^{-1}$. A fluorescein solution was provided from the secondary microchannel at F_V ranging from 0 to $2 \mu\text{L}\cdot\text{min}^{-1}$. Under laminar flow conditions, diffusion and linear convection are the two parameters acting on fluids. However, with flow rates in the microliter per minute range, diffusion alone is not sufficient to mix the species in a few centimeter long microchannel. Typically, in the present experimental conditions, a microchannel of tens of centimeters length would be required to accomplish the mixing of both solutions by diffusion only. Comparatively, with the devices including a mixing unit, the fluorescence inside the microchannel becomes homogeneous after only few millimeters from the beginning of the mixer that clearly demonstrates the advantages of the mixer for fast chemical reaction at such flow rates.

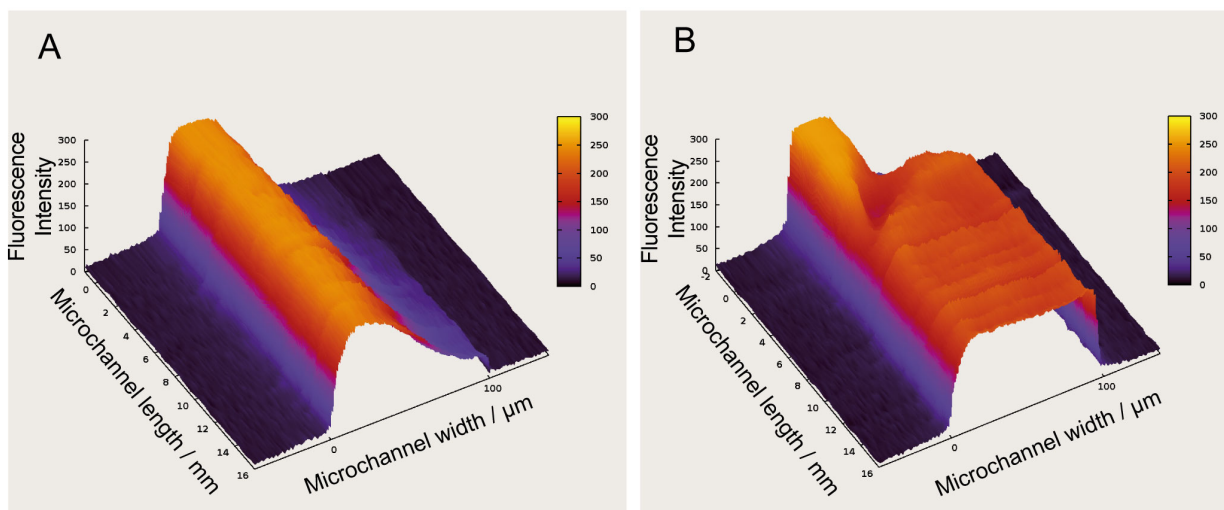


Figure IV- 4 Fluorescence distribution along the microchannel A) without or B) with a mixing unit integrated to the microchip. The single grooves of the mixing unit are spaced by $250 \mu\text{m}$. Flow rate F_V is $4 \mu\text{L}\cdot\text{min}^{-1}$ for the main microchannel and $1 \mu\text{L}\cdot\text{min}^{-1}$ for the liquid junction that provides the fluorescein.

The effects of the groove width, the inter-groove distance and the liquid flow rate were optimized by comparing the fluorescence distribution of four configurations of mixers, with

single or double grooves spaced either by 250 or 500 μm (Figure IV-5). Single grooves are more efficient than double grooves probably due to a sharper flow perturbation. Moreover, when comparing the efficient mixing distance between mixers with grooves spaced by 250 and 500 μm , it clearly appears that closer grooves increase the flow spiraling, speeding up the mixing. In the literature, optimized groove geometries have been simulated, showing that large grooves and smaller inter-groove distance results in a higher magnitude of helical flow.²⁹ Because of fabrication constraints, the polymer ESI microchip cannot present such design. The alternative proposed here allows a sufficient mixing in the microchip geometry used. The flow rates applied do not seem to affect the mixing efficiency. As a conclusion, the design with single grooves spaced by 250 μm was the most efficient for this electrospray micromixer chip.

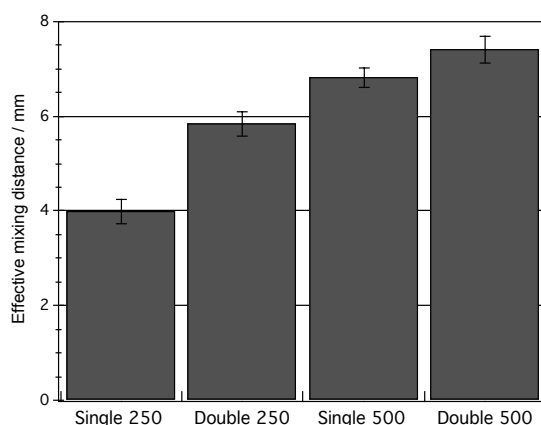


Figure IV- 5 Mixing efficiency depending on groove design constituting the mixing unit. Single or double grooves were drilled and spaced by 250 or 500 μm . The effective mixing distance, *i.e.* the distance for which the fluorescence becomes homogeneous ($\pm 10\%$) along the microchannel cross-section, was averaged for fluorescein solution flow rates of 0.5, 1, 1.5 and 2 $\mu\text{L}\cdot\text{min}^{-1}$. The flow rate of the main microchannel was fixed at 4 $\mu\text{L}\cdot\text{min}^{-1}$.

3.2. MS evaluation of the electrospray micromixer for chemical modification of peptides

The cysteine tagging in peptides with 1,4-benzoquinone (BQ) was compared when using microchips with and without integrated mixing units. With the typical flow rates and

microchip dimensions used, the species residence time once mixed, from the liquid junction to the outlet, is around 1 s. The reaction between the thiol group of cysteine and the BQ presents a reaction rate fast enough to be achieved on-line in the microchip.³¹ Here, the KCTCCA peptide was infused from the main microchannel at a concentration of 10 μM and $F_V = 4 \mu\text{L}\cdot\text{min}^{-1}$. The BQ was provided by the secondary microchannel at F_V from 1 to 2 $\mu\text{L}\cdot\text{min}^{-1}$. Different initial concentrations of BQ ($[\text{BQ}]_0$) were tested from 5 to 100 mM. Varying the flow rates modifies simultaneously the ratio of incoming concentrations between the peptide ($[\text{P}]_{\text{in}}$) and BQ ($[\text{BQ}]_{\text{in}}$), as well as the reaction time (*i.e.* residence time) inside the microchannel. Figure IV-6 is a comparison of the distribution of tagged peptides in both microchips for $[\text{BQ}]_0 = 10 \text{ mM}$. For such a concentration of tagging reagent, the reaction is not going to completion in 1 s, thus allowing the detection and comparison of the reaction intermediates. In the absence of mixing unit, the two most abundant species detected are the native peptide ($m/z = 628.2 \text{ Th}$) and the singly-tagged peptide ($m/z = 736.2 \text{ Th}$). Comparatively, with the micromixer, the two most abundant peaks correspond to the singly-tagged and doubly-tagged peptides ($m/z = 844.2 \text{ Th}$). Therefore, by increasing the encounter between the peptides and the tagging reagent, the passive mixing of flows improves significantly the tagging extent.

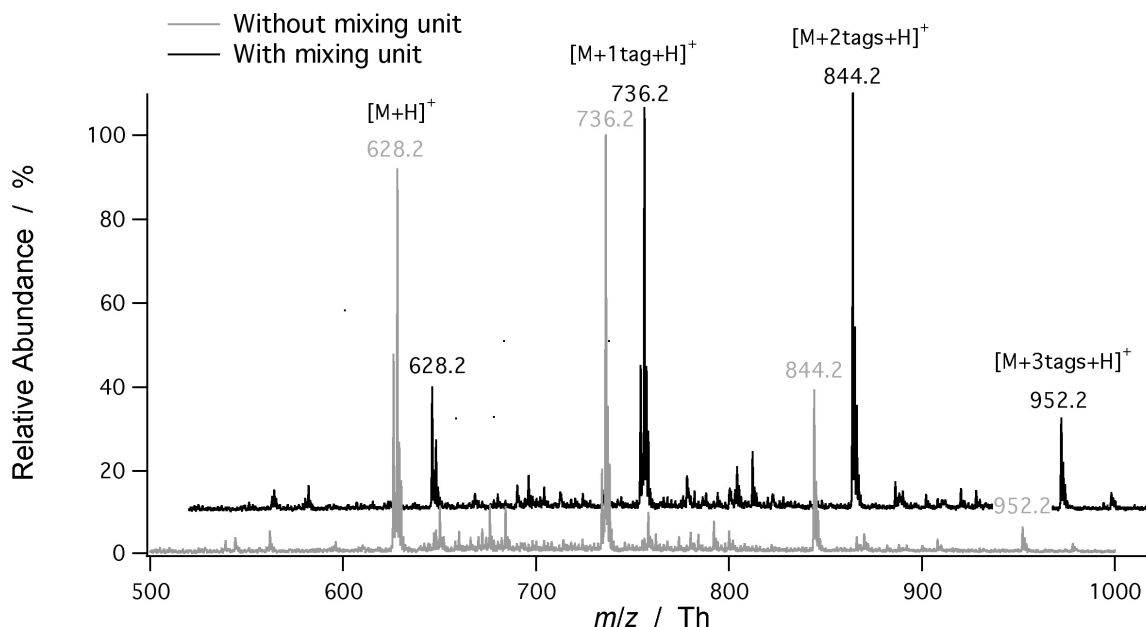


Figure IV- 6 Mass spectra corresponding to the multi-tagging of KCTCCA with BQ in an electrospray microchip with or without mixing unit. KCTCCA 10 μM was infused from the main microchannel at 4 $\mu\text{L}\cdot\text{min}^{-1}$ and BQ 10 mM from the liquid junction at 1 $\mu\text{L}\cdot\text{min}^{-1}$. The mass spectra were integrated over 4 minutes of monitoring.

3.3. Comparative study of the reaction extent without and with mixing unit

Figure IV-7.A-B represents the evolution of the tags on KCTCCA as a function of $[BQ]_{in}$ for a fixed BQ flow rate of $2 \mu L \cdot min^{-1}$. The relative abundance percentage of each species was calculated according to the following relationship:

$$\text{Relative Abundance \%} = \frac{IC_{S,i}}{\sum IC_{S,i}} \times 100 \quad (1)$$

where IC_s is the ion count for the peptide and i the number of tags attached to the peptide ($i = 0, 1, 2$ or 3).

As previously, the experiments were run with microchips without and with mixer. The total flow rate in the microchannel was kept at $6 \mu L \cdot min^{-1}$ that corresponds to a reaction time of 0.82 s from the beginning of the mixing unit to the microchannel outlet. When increasing $[BQ]_{in}$, the reaction rate increases as illustrated on Figures IV-7.A-B and the tagged species are formed more rapidly. When the mixing unit is present, the reaction efficiency is higher compared to the one obtained without. And, when increasing $[BQ]_{in}$ to 33.3 mM, the fully tagged peptide abundance finally reaches a plateau meaning that the reaction is close to completion. On a few millimeter long microchannel, the reaction extent is then exploitable at different stages varying the microchannel length, the flow rates, the concentration of each species and the presence or performance of the mixer.

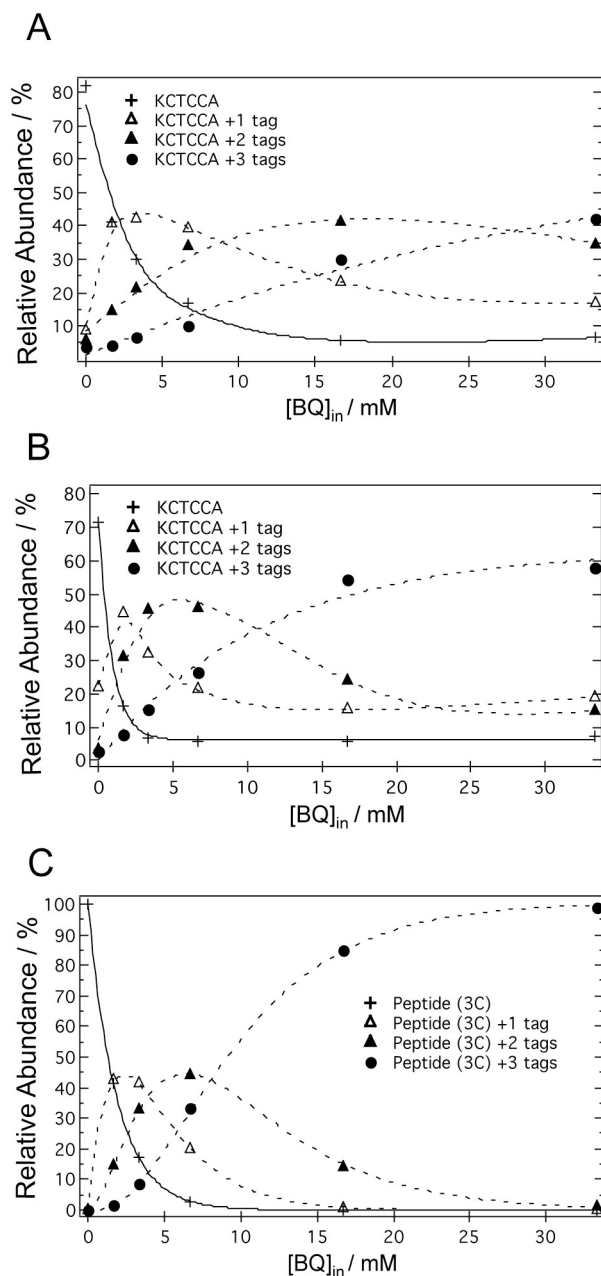


Figure IV- 7 Relative abundance percentage of the intermediary multi-tagged KCTCCA products as a function of the BQ concentration when using a microchip without A) or with B) mixing unit. In C) are represented the multi-tagged peptide distributions calculated from an analytical kinetic model for a bulk reaction. Dotted lines are interpolation of data points to aid visualization. KCTCCA 10 μM was infused from the main microchannel at 4 $\mu\text{L}\cdot\text{min}^{-1}$ and BQ from the liquid junction at different concentrations and $F_V = 2 \mu\text{L}\cdot\text{min}^{-1}$. The mass spectra were averaged over 4 min to determine the relative abundance of the tagged peptides.

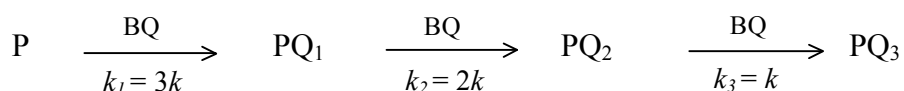
3.4. Comparative study of the experimental reaction extent with a kinetic model

An analytical kinetic model has been previously proposed to predict tagging extents at the end of a microchannel in an electrospray microchip where the tagging reagent is electrochemically generated at the embedded electrode during the ESI process, by oxidation of hydroquinone added to the sample solution.³² Here, when considering the addition between BQ tags and a peptide containing one cysteine, the rate law follows a first order kinetics for each reactant:

$$v = -\frac{d[BQ]}{dt} = -\frac{d[P]}{dt} = \frac{d[PQ_1]}{dt} = k[P][BQ] \quad (2)$$

where v is the rate of the reaction, k is the rate constant and $[BQ]$, $[P]$ and $[PQ_1]$ represent respectively the concentration of BQ tags, of a peptide P containing one cysteine residue and of the tagged product PQ_1 at the time t .

The kinetic model can be applied to consecutive reactions when the peptide possesses several cysteine units. In the case of a three-cysteine-containing peptide, the first step has an apparent rate constant that can be considered given as $k_1 = 3k$, since the rate law can be here formulated as illustrated below.



To simplify, this model assumes that *i*) the reactivity for a cysteine in any peptide is the same than that of L-cysteine ($k = 210 \text{ M}^{-1} \cdot \text{s}^{-1}$), and *ii*) all the cysteines have the same reactivity. Moreover, the concentration of BQ ($[BQ]_{in}$) used here is in excess compared to that of the cysteines. Typically, $[BQ]_{in}$ is at least 20 times higher than that of total cysteines. Therefore, the concentration of BQ can be assigned to be constant, simplifying the resolution of the kinetic equations.

Figure IV-7.C summarizes the theoretical calculation of the tagging extent on a three cysteine-containing peptide as a function of $[BQ]_{in}$. The goal of these calculations was to evaluate the efficiency of the mixer compared to an analytical model where the species are

assumed to be ideally mixed in solution. The comparison of the three graphs in Figure IV-7 clearly indicates that the kinetic behavior when species are flowing through a mixing unit approaches that of a bulk reaction. The small differences compared to the model have several explanations. A key feature to take into consideration is that, the reactivity of the cysteines in a peptide differs according to their position in the peptidic chain and their interaction with their neighboring amino acids. Moreover, after the addition of the first tag, the reactivity of the two other cysteines may even be modified by the presence of the tag. It is the same for the remaining free cysteines after the addition of the second tag. Finally, the ionization in ESI is different according to the tagged species and therefore the MS signal is not quantitative. (Distributions for BQ flow rates of 1 and 1.5 $\mu\text{L}\cdot\text{min}^{-1}$ are presented in Figure IV-8).

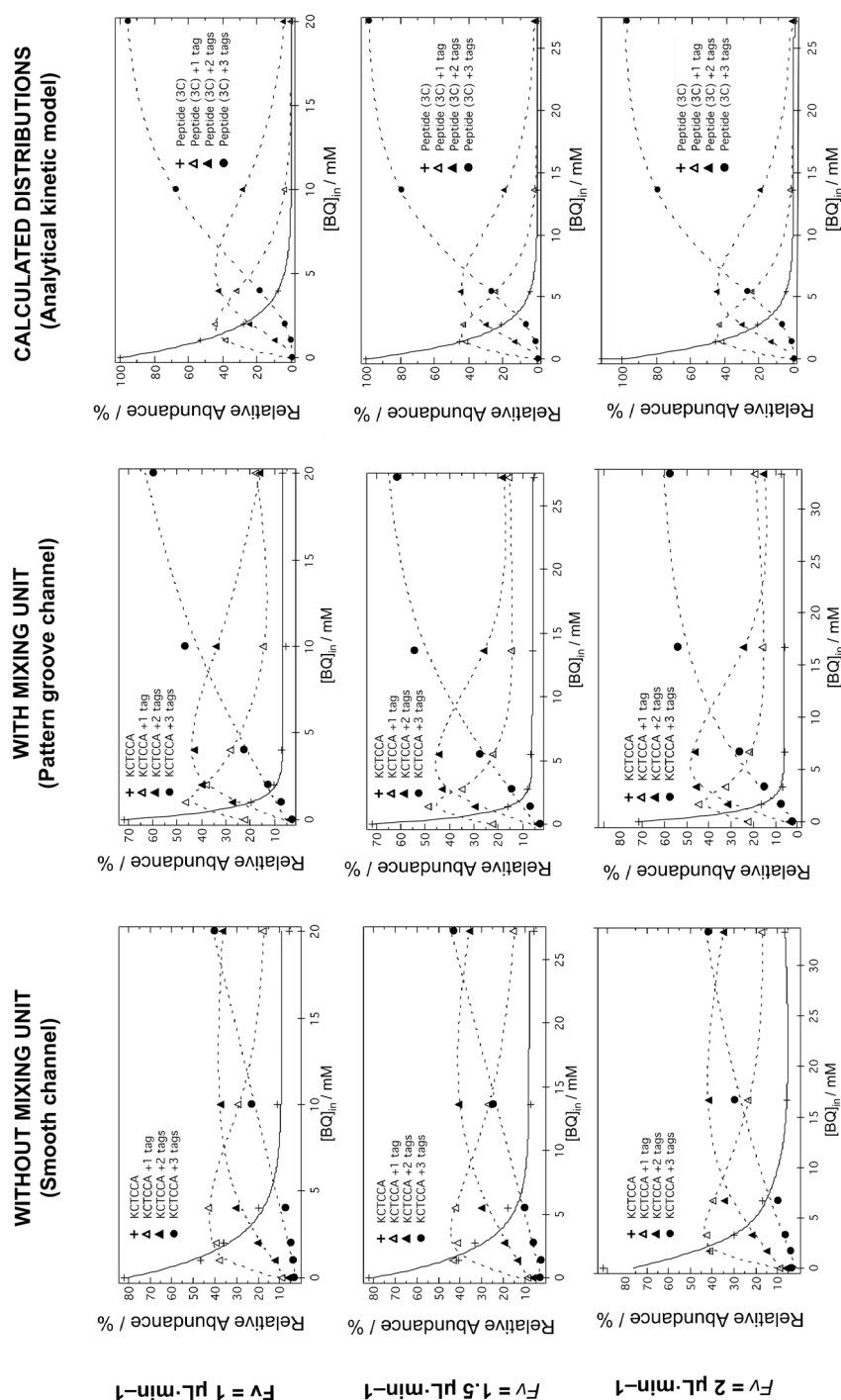


Figure IV-8 Relative abundance percentage of the intermediary multi-tagged KCTCCA products as a function of the BQ concentration when using a microchip without (left) or with (middle) mixing unit. (right) Multi-tagged peptide distributions calculated for a bulk reaction with an analytical kinetic model. Dotted lines are interpolation of data points to aid visualization. KCTCCA $10 \mu\text{M}$ was infused from the main microchannel at $4 \mu\text{L}\cdot\text{min}^{-1}$ and BQ from the liquid junction with different concentrations at $F_v = 1, 1.5$ and $2 \mu\text{L}\cdot\text{min}^{-1}$. The mass spectra were averaged over 4 min to determine the relative abundance of the tagged peptides.

3.5. Evaluation of the reaction gain using the electrospray micromixer

The gain was evaluated by comparing the relative abundance of fully-tagged species in both microchips assuming that the objective is to get reaction completion. The gain is then expressed according to the following relation:

$$\text{Gain} = \frac{\%PQ_3 \text{ Mixing}}{\%PQ_3 \text{ No Mixing}} \quad (3)$$

where %PQ₃ is the relative abundance of the fully-tagged peptide containing 3 cysteines.

The gain was calculated for different concentrations and flow rates of BQ (Figure IV-9). The gain with a mixer is at least of 50 % reaction enhancement for all the tested conditions, and reaches 275 % for [BQ]₀ = 20 mM, that quasi triples the tagging reaction extent.

The suitability of the electrospray micromixer to perform on-line chemical derivatization was therefore indubitably demonstrated.

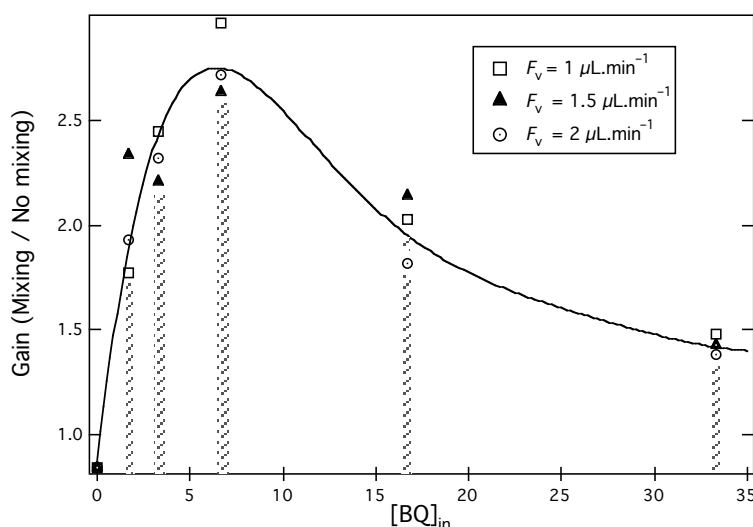


Figure IV- 9 Representation of the gain of reaction extent when using a microchip with a mixer compared to without. The gain is calculated as the ratio of the fully tagged KCCTCA relative abundances, obtained with both microchips. KCTCCA 10 μM was infused from the main microchannel at 4 μL·min⁻¹ and BQ from the liquid junction at different flow rates from 1 to 2 μL·min⁻¹ and concentrations.

As the gain follows similar fluctuations for all the flow rates tested, a mean curve of the gain as a function of [BQ]_{in} was determined in order to clearly point out the relevance of using the electrospray micromixer.

3.6. On-line LC-MS derivatization of tryptic cysteinyl peptides of BSA

The electrospray micromixer was then hyphenated to a LC-MS workflow by directly connecting the LC capillary outlet to the main microchannel (Chapter III). The secondary microchannel was infused either by a sheath liquid or a BQ solution at different concentrations of 10 mM, 20 mM, 50 mM and 100 mM. The BQ infusion flow rate was kept at $1 \mu\text{L}\cdot\text{min}^{-1}$ in the following study because it presents the best compromise between spray stability and reasonable sample dilution. Figure IV-10 compares two LC-MS analyses of the BSA digest using the same microchip infused with a sheath liquid providing or not the BQ reagent. A single microchip was infused during several hours without apparent diminution of the spray quality and showed good reproducibility for successive analyses as demonstrated by the monitored base peak chromatograms of Figures IV-10.A and IV-10.B. The memory effect, as well as the peak broadening effect, was evaluated with microchips with smooth microchannels or photo-ablated grooves. No memory effect was observed in both cases. A very slight peak tailing was noticed, mainly due to the dilution induced by the liquid junction, but without affecting the peak intensities. Figures IV-10.B and IV-10.D provide averaged mass spectra at the same elution time obtained from both experimental conditions (without and with BQ). During this time window, two cysteinyl peptides were eluted: a one cysteine-containing peptide present as singly and doubly charged ($m/z = 912.9$ Th and 1823.5 Th), and a singly-charged two-cysteine-containing peptide ($m/z = 1388.3$ Th). When $[\text{BQ}]_0 = 50$ mM was infused in the microchip, the cysteinyl peptides present adducts of BQ (+ 108 Da) with all the intermediary tagged species represented.

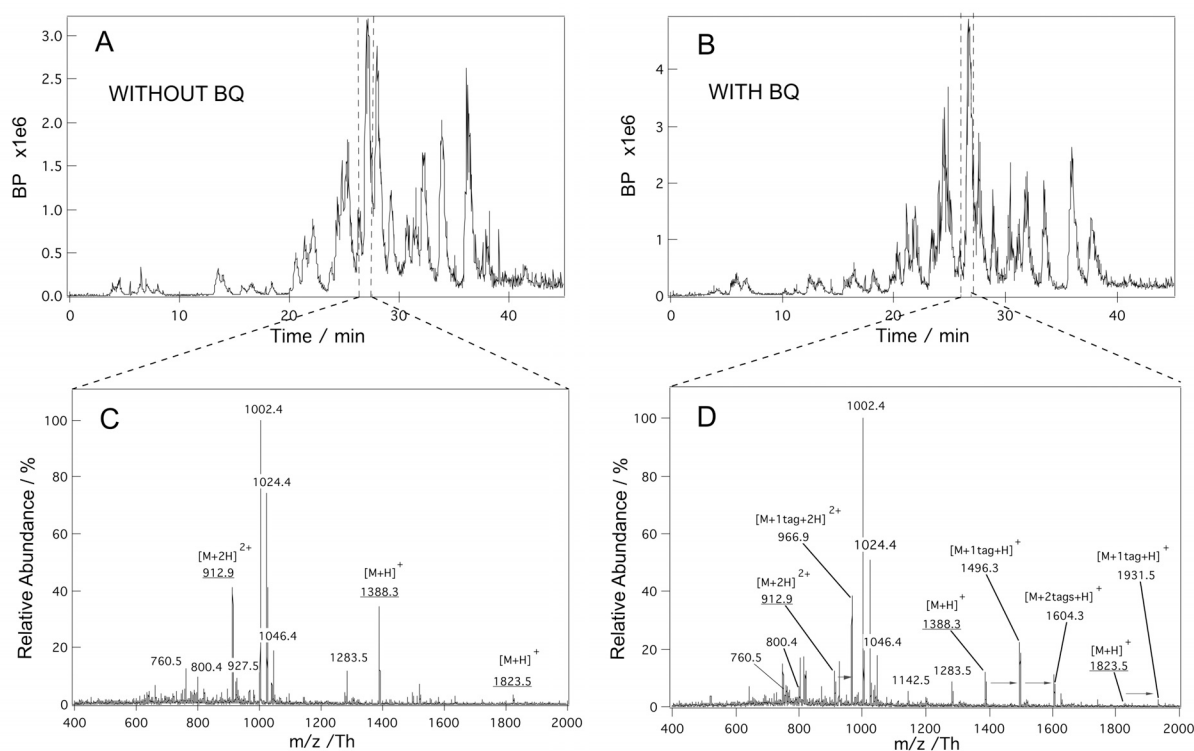


Figure IV- 10 On-line chemical derivatization of cysteinyl peptide of a BSA digest. A) and B) represent the base peak chromatograms of the LC-MS analysis of the BSA digest with a microchip infused by a solution containing or not the BQ reagent, respectively. The mass spectra were integrated over 1 min on both chromatograms at the same elution time. C) and D) present the integrated mass spectra in the absence or presence of BQ, respectively. Sequences of the cysteinyl identified peptides: $[M+H]^+ = 1388.3$ Th “EYEATLEECCA^K”; $[M+H]^+ = 1823.5$ Th RPCFSALTPDETYVPK. The main microchannel was connected to the HPLC flow outlet ($4 \mu\text{L}\cdot\text{min}^{-1}$). The solution provided by the liquid junction (without or with BQ) was kept at $1 \mu\text{L}\cdot\text{min}^{-1}$.

For protein identification by peptide mass fingerprinting including cysteine content, two ways of analysis are possible. i) to carry out a single run with a BQ concentration at which both the untagged peptides and the tagged species are present. It necessitates to carefully control the right concentration of BQ according to those of the eluted peptides. ii) to perform two successive runs, one without and one with BQ in large excess to fully tag the peptides, and then compare the two peak lists to determine the mass shifts and deduce the cysteine content. As the hydrophobicity properties of the peptides are modified by the BQ tags,³³ a post-column derivatization has the advantage not to modify the native peptide retention time that helps for easy and unmissaken peak list comparison and protein identification³⁴. The main inconvenience remains the need to perform two analyses that are sample and time

consuming. In the present study, both techniques have been assessed using the electrospray mixer for post-column cysteine tagging and showed comparable counting efficiency.

The cysteinyl peptides identified in a single tagging LC-MS run, at $[BQ]_0 = 50$ mM enabling on-line cysteine counting as all the species are present, are recapitulated in Table IV-1.

Start - End	Sequence ^a	Cysteine content	Theoretical $(m/z)^b$ / Th	Observed untagged $(m/z)^c$ /Th	Observed tagged $(m/z)^d$ /Th
89-100	SLHTLFGDELCK	1	1362.6722	1362.47	1470.4
89-109	SLHTLFGDELCKVASLR	1	1888.9949	1888.6 945.53	999 1052.47
106-117	ETYGDMADCCCK	2	1364.4803	1364.27	1472.2;1580.2
106-122	ETYGDMADCCCKQEPER	2	2003.7706	1002.33	-
123-130	NECFLSHK	1	977.4509	977.33	-
139-151	LKPDPNTLCDEFK	1	1519.7461	1519.47	1627.47
139-155	LKPDPNTLCDEFKADEK	1	1962.9477	1963.33	980.3; 1034.3
184-197	YNGVFQECCQAEDK	2	1633.6621	1633.33	1741.13;1849.33
198-204	GACLLPK	1	701.4015	701.4	809.4
223-228	CASIQK	1	649.3338	649.33	757.3
262-273	YICDNQDTISSK	1	1386.6206	1386.4	1494.4
298-309	LKECCDKPLLEK	2	1418.7382	1418.47	1526.47; 1634.4
300-309	ECCDKPLLEK	2	1177.5592	1177.33	1185.33;1293.33
310-318	SHCIAVEVK	1	1015.4877	1015.07 508.3	1123.2 562.9
375-386	EYEATLEECCA	2	1388.5708	1388.4	1496.4;1604.5
387-399	DDPHACYSTVFDK	1	1497.6315	1497.2 749.5	1605.02 803.4
413-420	QNCDQFEK	1	1011.42	1011.27	1119.33
456-468	VGTRCCTKPESER	2	1465.6886	- 733.4	- 841.3; 949.3
460-468	CCTKPESER	2	1052.4499	1052.47	1160.3;1268.3
469-482	MPCTEDYLSLILNR	1	1667.8131	1667.53 834.53	1775.5 888.47
483-489	LCVLHEK	1	841.46	841.33	949.33
499-507	CCTESLVNR	2	1024.455	1024.33	1132.27;1240.33
508-523	RPCFSALTPDETYVPK	1	1823.8996	1823.4 912.53	1931.4 966.53
588-597	EACFAVEGPK	1	1050.4925	1050.53	1158.53
588-607	EACFAVEGPKLVVSTQTALA	1	2034.0503	-	-
				1017.53	1125.5

Table IV-1 Identification of BSA cysteinyl peptides by on-line derivatization on an electrospray micromixer chip. ^a Sequence of cysteinyl identified peptides. ^b m/z of predicted cysteinyl peptides. ^c m/z of the experimentally observed untagged peptides. ^d m/z of the experimentally observed cysteinyl peptides tagged with BQ.

The database search with Mascot was done with the peptide mass alone (control score) or adding the information about the cysteine content (Figure IV-11). In both cases, the BSA was identified in first position. Without the information about the cysteine content, the BSA was identified with a score of 50 and a protein sequence coverage of 78%. Even with a good protein sequence coverage the score does not reach the confidence score. As expected,³ when the number of cysteines was indicated, the protein score reaches the value of 258 that definitively insures the confidence in its identification.

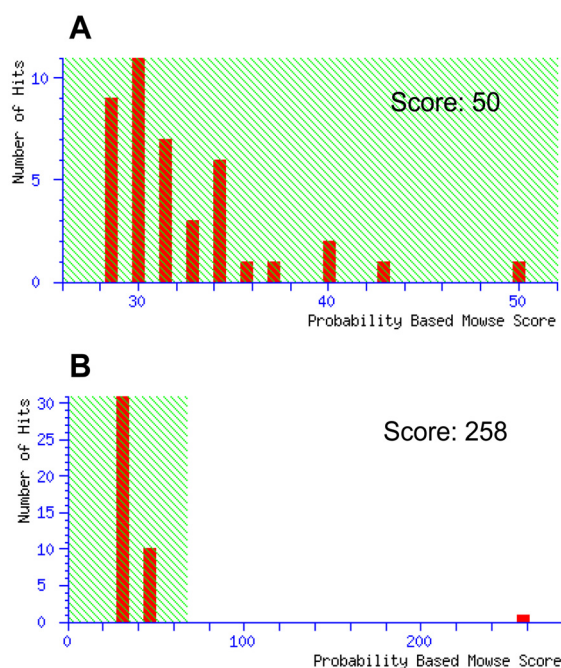


Figure IV- 11 Mascot identification scores of BSA after RP-LC-MS analysis A) without and B) with on-chip derivatization of tryptic cysteinyl peptides. Mascot score is $-10 \cdot \log(P)$ where P is the probability that the observed match is a random event. Protein scores greater than 72 are significant ($P < 0.05$).

4. Conclusions

A polymer electrospray microchip with a mixing unit has been designed based on polymer UV-photoablation. The mixing unit composed of a series of parallel oblique grooves along a portion of a channel is easily processed. By optical characterization of the mixing, single grooves 40 μm wide and 35 μm deep, spaced 250 μm apart were determined to provide the best mixing.

As a demonstration of efficiency, on-chip derivatization of cysteines in peptides was studied. KCTCCA peptide and benzoquinone reagent were provided by the main and secondary microchannels, respectively. The mixing unit clearly improves the reaction yield, approaching results obtained from reactions in bulk condition. Furthermore, this on-chip chemical tagging reaction was implemented as post-column derivatization in an LC-MS analysis of BSA tryptic peptides to determine their cysteine content. Other on-chip derivatization of (bio)molecules can also be envisaged, the only requirement being that the reaction rates should be fast enough to allow the reactions to reach completion within the short residence times in the electrospray micromixer. As a further development, this on-line tagging reaction could be implemented on a multi-electrospray device as the one already designed in our lab (Chapter VI).³⁵ The flow from the LC system can be divided on-chip into two sub-flows, one part of the analytes could be subjected to on-line quantitative tagging while the other part serves as blank. The analysis time will then be reduced to a single run for routine cysteine counting in peptides when successively electrospraying both samples in parallel.³⁶

Recently, the microchip design was improved thanks to the fabrication of a new mask for the laser ablation process. It allows drilling grooves similar to the ones of the staggered herringbone mixer, as illustrated in Figure IV-12. The performance of the mixer is still under evaluation but it seems to provide at least equal results than the mixer used in the present study.

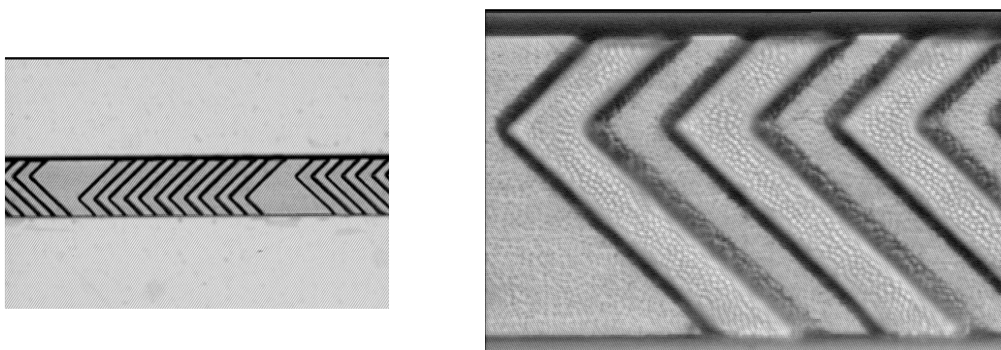


Figure IV- 12 New design of the photo-ablated mixing unit.

MS-based techniques have shown great promise in the area of chemical and biochemical kinetics. ESI-MS, in particular, has enormous potential as an alternative to the traditional methods for monitoring enzyme kinetics, because the reaction mixture can be infused directly into the ion source for on-line analysis, while the reaction occurs in solution. Up to now, the major part of the kinetics studies by ESI-MS reported in the literature was achieved by mixing the reactants prior the ionization source. Such a microchip with a mixing unit presents a great potential for chemical kinetic studies as the reaction occurs on-chip just before MS. By controlling the microchannel length and/or flow rate, the reaction time can be easily adjusted to investigate the reaction intermediates and products.

REFERENCES

1. R. Aebersold and M. Mann, Mass spectrometry-based proteomics, *Nature*, 2003, 422, 198-207.
2. B. Domon and R. Aebersold, Mass spectrometry and protein analysis, *Science*, 2006, 312, 212-217.
3. S. Sechi and B. T. Chait, Modification of cysteine residues by alkylation. A tool in peptide mapping and protein identification, *Analytical Chemistry*, 1998, 70, 5150-5158.
4. L. Dayon, C. Roussel, M. Prudent, N. Lion and H. H. Girault, On-line counting of cysteine residues in peptides during electrospray ionization by electrogenerated tags and their application to protein identification, *Electrophoresis*, 2005, 26, 238-247.
5. E. D. Lee, W. Muck, J. D. Henion and T. R. Covey, Real-time reaction monitoring by continuous-introduction ion-spray tandem mass spectrometry, *Journal of the American Chemical Society*, 1989, 111, 4600-4604.
6. L. Konermann, B. A. Collings and D. J. Douglas, Cytochrome c folding kinetics studied by time-resolved electrospray ionization mass spectrometry, *Biochemistry*, 1997, 36, 5554-5559.
7. L. Konermann, J. Pan and D. J. Wilson, Protein folding mechanisms studied by time-resolved electrospray mass spectrometry, *BioTechniques*, 2006, 40, 135-141.
8. D. J. Wilson and L. Konermann, Mechanistic Studies on Enzymatic Reactions by Electrospray Ionization MS Using a Capillary Mixer with Adjustable Reaction Chamber Volume for Time-Resolved Measurements, *Analytical Chemistry*, 2004, 76, 2537-2543.
9. A. Liesener and U. Karst, Monitoring enzymatic conversions by mass spectrometry: A critical review, *Analytical and Bioanalytical Chemistry*, 2005, 382, 1451-1464.
10. M. Brivio, W. Verboom and D. N. Reinhoudt, Miniaturized continuous flow reaction vessels: Influence on chemical reactions, *Lab on a Chip - Miniaturisation for Chemistry and Biology*, 2006, 6, 329-344.
11. M. Brivio, A. Liesener, R. E. Oosterbroek, W. Verboom, U. Karst, A. Van Den Berg and D. N. Reinhoudt, Chip-based on-line nanospray MS method enabling study of the kinetics of isocyanate derivatization reactions, *Analytical Chemistry*, 2005, 77, 6852-6856.
12. T. C. Rohner, J. S. Rossier and H. H. Girault, Polymer microspray with an integrated thick-film microelectrode, *Analytical Chemistry*, 2001, 73, 5353-5357.
13. I. M. Lazar, R. S. Ramsey, S. C. Jacobson, R. S. Foote and J. M. Ramsey, Novel microfabricated device for electrokinetically induced pressure flow and electrospray ionization mass spectrometry, *Journal of Chromatography A*, 2000, 892, 195-201.
14. D. Figeys, C. Lock, L. Taylor and R. Aebersold, Microfabricated device coupled with an electrospray ionization quadrupole time-of-flight mass spectrometer: Protein identifications based on enhanced-resolution mass spectrometry and tandem mass spectrometry data, *Rapid Communications in Mass Spectrometry*, 1998, 12, 1435-1444.
15. J. M. Dethy, B. L. Ackermann, C. Delatour, J. D. Henion and G. A. Schultz, Demonstration of direct bioanalysis of drugs in plasma using nanoelectrospray infusion from a silicon chip coupled with tandem mass spectrometry, *Analytical Chemistry*, 2003, 75, 805-811.
16. H. Yin and K. Killeen, The fundamental aspects and applications of Agilent HPLC-Chip, *Journal of Separation Science*, 2007, 30, 1427-1434.
17. H. Yin, K. Killeen, R. Brennen, D. Sobek, M. Werlich and T. Van De Goor, Microfluidic chip for peptide analysis with an integrated HPLC column, sample enrichment column, and nanoelectrospray tip, *Analytical Chemistry*, 2005, 77, 527-533.
18. T. M. Squires and S. R. Quake, Microfluidics: Fluid physics at the nanoliter scale, *Reviews of Modern Physics*, 2005, 77, 977-1026.
19. T. J. Johnson, D. Ross and L. E. Locascio, Rapid microfluidic mixing, *Analytical Chemistry*, 2002, 74, 45-51.
20. J. L. Lin, K. H. Lee and G. B. Lee, Active mixing inside microchannels utilizing dynamic variation of gradient zeta potentials, *Electrophoresis*, 2005, 26, 4605-4615.

21. A. Dodge, M. C. Jullien, Y. K. Lee, X. Niu, F. Okkels and P. Tabeling, An example of a chaotic micromixer: The cross-channel micromixer, *Comptes Rendus Physique*, 2004, 5, 557-563.
22. M. H. Oddy, J. G. Santiago and J. C. Mikkelsen, Electrokinetic instability micromixing, *Analytical Chemistry*, 2001, 73, 5822-5832.
23. N. Sundaram and D. K. Tafti, Evaluation of microchamber geometries and surface conditions for electrokinetic driven mixing, *Analytical Chemistry*, 2004, 76, 3785-3793.
24. S. Hardt, K. S. Drese, V. Hessel and F. Schönfeld, Passive micromixers for applications in the microreactor and μ TAS fields, *Microfluidics and Nanofluidics*, 2005, 1, 108-118.
25. V. Mengeaud, J. Jossierand and H. H. Girault, Mixing processes in a zigzag microchannel: Finite element simulations and optical study, *Analytical Chemistry*, 2002, 74, 4279-4286.
26. A. D. Stroock, S. K. W. Dertinger, A. Ajdari, I. Mezic, H. A. Stone and G. M. Whitesides, Chaotic mixer for microchannels, *Science*, 2002, 295, 647-651.
27. A. D. Stroock, S. K. Dertinger, G. M. Whitesides and A. Ajdari, Patterning flows using grooved surfaces, *Analytical Chemistry*, 2002, 74, 5306-5312.
28. H. Y. Lee and J. Voldman, Optimizing micromixer design for enhancing dielectrophoretic microconcentrator performance, *Analytical Chemistry*, 2007, 79, 1833-1839.
29. N. S. Lynn and D. S. Dandy, Geometrical optimization of helical flow in grooved micromixers, *Lab on a Chip - Miniaturisation for Chemistry and Biology*, 2007, 7, 580-587.
30. N. Lion, J. O. Gellon and H. H. Girault, Flow-rate characterization of microfabricated polymer microspray emitters, *Rapid Communications in Mass Spectrometry*, 2004, 18, 1614-1620.
31. C. Roussel, T. C. Rohner, H. Jensen and H. H. Girault, Mechanistic aspects of on-line electrochemical tagging of free L-cysteine residues during electrospray ionisation for mass spectrometry in protein analysis, *ChemPhysChem*, 2003, 4, 200-206.
32. L. Dayon, C. Roussel and H. H. Girault, Probing cysteine reactivity in proteins by mass spectrometric EC-tagging, *Journal of Proteome Research*, 2006, 5, 793-800.
33. L. Dayon and H. H. Girault, Diagonal chromatographic selection of cysteinyl peptides modified with benzoquinones, *Analytical and Bioanalytical Chemistry*, 2007, 389, 841-849.
34. E. F. Strittmatter, L. J. Kangas, K. Petritis, H. M. Mottaz, G. A. Anderson, Y. Shen, J. M. Jacobs, D. G. Camp II and R. D. Smith, Application of peptide LC retention time information in a discriminant function for peptide identification by tandem mass spectrometry, *Journal of Proteome Research*, 2004, 3, 760-769.
35. L. Dayon, M. Abonnenc, M. Prudent, N. Lion and H. H. Girault, Multitrack electrospray chips, *Journal of Mass Spectrometry*, 2006, 41, 1484-1490.
36. E. Bonneil, S. Tessier, A. Carrier and P. Thibault, Multiplex multidimensional nanoLC-MS system for targeted proteomic analyses, *Electrophoresis*, 2005, 26, 4575-4589.

CHAPTER V.

Magnetic track array for efficient bead capture in microchannels

Based on

M. Abonnenc, A-L. Gassner, J. Morandini, J. Josserand, H.H. Girault, Anal. Bioanal. Chem, 2009, DOI: 10.1007/s00216-009-3006-3.

A-L. Gassner, M. Abonnenc, H-X. Chen, J. Morandini, J. Josserand, J.S. Rossier, J-M. Busnel, H.H. Girault, Lab Chip, 2009, 9, 2356-2363.

1. Introduction

Target analytes in biological samples are often present in low concentrations relative to the surrounding matrix components, necessitating effective separation techniques. Nowadays, immuno-affinity separation is a widespread tool in clinical testing, diagnostic and biochemical sample analysis. Whereas ELISA (Enzyme Linked ImmunoSorbent Assay) tests require at best few minutes for easy-to-use formats and hours for classical microtiter well tests, immunoassays in microfluidic format present the advantages of reduced reagent consumption and fast time of analysis.¹ Proteins may be either attached directly to the walls of a capillary column or microchip channel, or to solid phase supports and packed into columns or channels. Solid support may consist of particles or beads made from plastic, silica, glass, or magnetic materials. Protein adsorption in polymer microchannels² and its dynamic under stopped-flow and continuous flow have been previously investigated in our lab.^{3, 4} Alternatively, magnetic beads were also used as solid phase support to develop

magnetic bead-based immunoassay both in microchip for biosensing and in capillary for immuno-affinity capillary electrophoresis (IA-CE).⁵⁻⁷ As the sensitivity of the analysis is highly depending on the magnetic bead trapping efficiency, we propose here a novel design of photo-ablated polymer microchip integrating a magnetic track array to enhance the magnetic bead capture in a microchannel.⁸⁻¹⁰ The actuation is made by two face-to-face permanent magnets placed in attraction and fixed on both microchannel sides to magnetize the tracks filled with a home-prepared magnetic ink. The magnetic field is therefore addressed through these tracks, symmetrically located as an array perpendicular to the microchannel, resulting in a multi-plug bead capture. The study includes microscope imaging showing the multi-plug bead organization in microchips with a magnetic track array. By comparison with a microchip without array, the gain of using multi-plugs vs. a single plug of beads is evaluated, when magnets of 2, 5 and 10 mm - long are used. Numerical simulations of the effect of the inter-track gap, channel-track gap and ink permeability provide an orientation to improve this gain.

2. Theory and numerical description

2.1. Basics of magnetism

When a material experiences a magnetic field, the individual atomic moments align themselves progressively and contribute to the overall response of the material to the field. The response is called magnetic induction \mathbf{B} and is an inherent property of the material; it is also known as magnetic flux density, measured in Tesla (T) and corresponds to the number of field lines per unit area. The relationship between the applied magnetic field \mathbf{H} and the induction response of the material is the absolute permeability of the material, μ :

$$\mathbf{B} = \mu \mathbf{H} \quad (1)$$

In any other medium, the permeability μ may not be a linear function of \mathbf{H} due to the saturation of the considered material; although, μ may vary with the applied magnetic field, particularly in ferromagnetic materials.

The magnetic flux density in free space is defined as:

$$\mathbf{B} = \mu_0 \mathbf{H} \quad (2)$$

with the permeability of the free space $\mu_0 = 4\pi \cdot 10^{-7} \text{ Wb} \cdot \text{A}^{-1} \cdot \text{m}^{-1}$.

In a material submitted to a magnetic field \mathbf{H} , by comparison with the free space conditions, the local induction \mathbf{B} is the sum of the induction $\mu_0 \mathbf{H}$ given by the source in the vacuum and of the local induction $\mu_0 \mathbf{M}$ due to the magnetization \mathbf{M} of the studied medium ($\mathbf{M} = \chi \mathbf{H}$ in the linear magnetization zone of the material):

$$\mathbf{B} = \mu_0 (\mathbf{H} + \mathbf{M}) = \mu_0 (1 + \chi) \mathbf{H} = \mu_0 \mu_r \mathbf{H} = \mu \mathbf{H} \quad (3)$$

where μ_r and χ are the relative permeability and the magnetic susceptibility of the material, respectively.

According to their magnetic susceptibility, χ , materials are classified in three categories. *Diamagnetic materials* ($\chi < 0$) are repelled from magnetic field and consequently, are forced towards the minima of magnetic fields. Water, proteins, DNA, cells, polymers and glass are few examples of this group. *Paramagnetic materials* ($\chi > 0$), such as oxygen, platinum or manganese(II) salts align in a magnetic field and are slightly attracted towards magnetic field maxima. The third category concerns *ferromagnetic materials* ($\chi > 1$), typically iron, cobalt or nickel, and presents the characteristic to be strongly attracted in to magnetic fields. *Superparamagnetic* particles are a combination of para- and ferro-magnetic material as they are composed of a core of small iron oxide crystals encapsulated in a polymer shell

We will consider the superparamagnetic beads as material in the following discussions. Then, for a bead of volume V immersed in a solution, the magnetic moment is given by $\mathbf{m}_{bead} = V\mathbf{M} = V\Delta\chi\mathbf{H}$ where $\Delta\chi = \chi - \chi_{water}$ is the relative susceptibility of the bead compared to the one of the solution.

The magnetic force applied on these particles can be expressed as the derivative of the magnetic potential energy:

$$\mathbf{F}_{mag} = \nabla(\mathbf{m}_{bead} \bullet \mathbf{B}) \approx (\mathbf{m}_{bead} \bullet \nabla) \mathbf{B} \quad (4)$$

which results in (5) by taking into account (1) and the moment expression under the saturation conditions of the beads ($\mathbf{m}_{bead} \ll \mathbf{m}_{sat}$):

$$\mathbf{F}_{mag} = \frac{V\Delta\chi}{\mu_0} (\mathbf{B} \bullet \nabla) \mathbf{B} \quad (5)$$

Eqn. 5 shows that a magnetic field gradient is required to exert a translation force on a particle.

2.2. Magnetic beads in analytical sciences

Magnetic beads are usually superparamagnetic particles that exhibit a high magnetization in presence of a magnetic field, allowing an easy manipulation of the particles. Once the external magnetic field removed, they present no residual magnetism and can be freely re-suspended.¹¹ A wide range of bioreactive molecules can be adsorbed or coupled to the bead-surface, which provides a high binding surface area. Yet, they have proven to be efficient tools in medical applications such as drug targeting^{12, 13} and bio-separations including protein/peptide isolation, bio-assays, or cell sorting.^{14, 15} Typically, isolation of biomolecules, such as peptides and proteins, is usually performed using a variety of chromatographic, electrophoretic, ultrafiltration and precipitation techniques. The use of magnetic particles for this purpose can simplify considerably the purification steps, limiting as well the volume of eluting or precipitation buffers.¹⁶ Whereas the magnetic beads are nowadays commonly used at laboratory-scale (*i.e.* in test tube), the development of methodologies in microfluidic format has recently emerged decreasing sample/reagent consumption, cost and time consumption.¹⁷⁻²⁰ Such magnetism-based devices have found great applications in biology, as for cell manipulation,²¹⁻²⁶ (bio)chemical reactions such as proteolysis,^{27, 28} bioassay,²⁹⁻³¹ DNA or RNA hybridization.^{32, 33} Magnetic beads appeared as well in microsystems to design mixers, valves or switches.³⁴⁻⁴⁰

2.3. Microfabrication and magnetic actuation

The microfabrication complexity of such magnetism-based devices is highly depending whether the magnetic field actuation is integrated or not to the device. Active magnetic microsystems rely on the use of on-chip micro-electromagnets capable of a local addressability.¹⁸ However, the complex microfabrication processes and the limited field strength (0 – 100 mT) are the weak points of these devices. In contrast, passive magnetic microsystems use external macro-sized permanent magnets or electromagnets.^{28, 30, 41} The process is simplified and larger magnetic fields (> 0.5 T) and forces can be reached. In a recent study, the distribution of magnetic field and force in a microchannel surrounded by permanent magnets was simulated by our group.⁴² It has been shown that the magnetic field and force are restricted to a specific location defined by the magnet geometry and pole orientation (attraction, repulsion, single magnet). The resulting bead capture with these three magnet configurations is illustrated in Figure V-1. One plug of beads is observed at the middle of the magnets when they are placed in attraction while two plugs at the magnet extremities are present in repulsion. With only one magnet, the beads are attracted towards the microchannel sidewall where the magnet is located. In the present chapter, only the case with two permanent magnets in attraction is considered (Figure V-1.A).

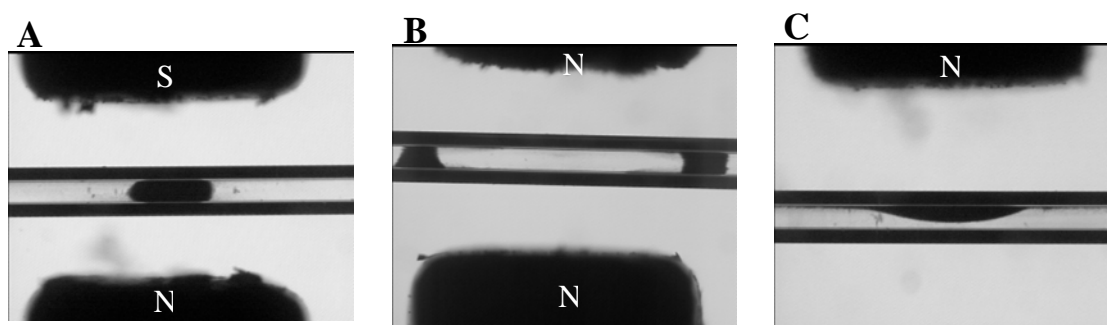


Figure V- 1 Microscope view of the magnetic bead organization in a capillary surrounded by two permanent magnets in A) attraction and B) repulsion configuration or C) only one magnet. The magnet dimensions are 2 x 2 x 8 mm³ with an inter-magnet gap of 1 mm. The capillary is 100 μm i.d. and 375 μm o.d. Magnetic beads of 300 nm diameter (1mg·mL⁻¹) were diluted 10 times in water before injection.

In order to control the magnetic field addressing towards specific locations, magnetic elements can be integrated to the structure, both in active and passive microsystems.^{43, 44} Smistrup *et al.* introduced an on-chip magnetic bead microarray in which an external magnetic field (21 mT) magnetizes soft magnetic elements placed along the microchannel.³² In combination with hydrodynamic focusing, the beads from different incoming streams are captured at the sidewalls and functionalized with two types of magnetic beads carrying different probes to assess DNA hybridization. Alternatively to their work in which the magnetic field value limits the bead trapping at the sidewalls, the present study uses higher field to magnetize the elements leading to full multi-plugs of beads. The fabrication process is also simplified and based on polymer laser-ablation. Indeed, in contrast with intensive clean-room and multi-steps fabrication processes as silicon-based techniques, fast prototyping such as soft lithography⁴⁵ and polymer laser ablation^{46, 47} are quite simple, cheap, and in most cases do not require a heavy clean-room environment. Several groups have used soft lithography to design magnetism-based devices.^{45, 48} Viovy *et al.* introduced a PDMS microchip, based on soft lithography and fast prototyping, with embedded permanent magnets oriented in repulsion from 20° with respect to the microchannel axis.²⁸ The chip was demonstrated to be an efficient reactor to perform protein digestion thanks to the high surface area-to-volume ratio provided by the beads that are organized in columns parallel to the flow, thus limiting the flow resistance.

2.4. Magnetic bead transport in a microfluidic system

The present investigation describes the physical phenomena occurring in a microfluidic system constituted of a microchannel surrounded by two face-to-face permanent magnets in attraction (Figure V-2). The superparamagnetic beads in solution are infused under pressure-driven flow from the microchannel left side. The main forces experienced by the particles are the magnetic force, F_{mag} and the hydrodynamic drag force, F_{drag} . The gravitational force, particle/fluid interactions and inter-particle effects are neglected.

In addition to the magnetic force (eqn. 5), the particles experience a hydrodynamic drag force, defined by the Stokes' equation,

$$F_{drag} = 6\pi\eta Rv \quad (6)$$

with the assumption that the magnetic beads have the approximate shape of a sphere of radius R . η is the fluid viscosity and v the velocity of the bead compared to the surrounding fluid velocity.

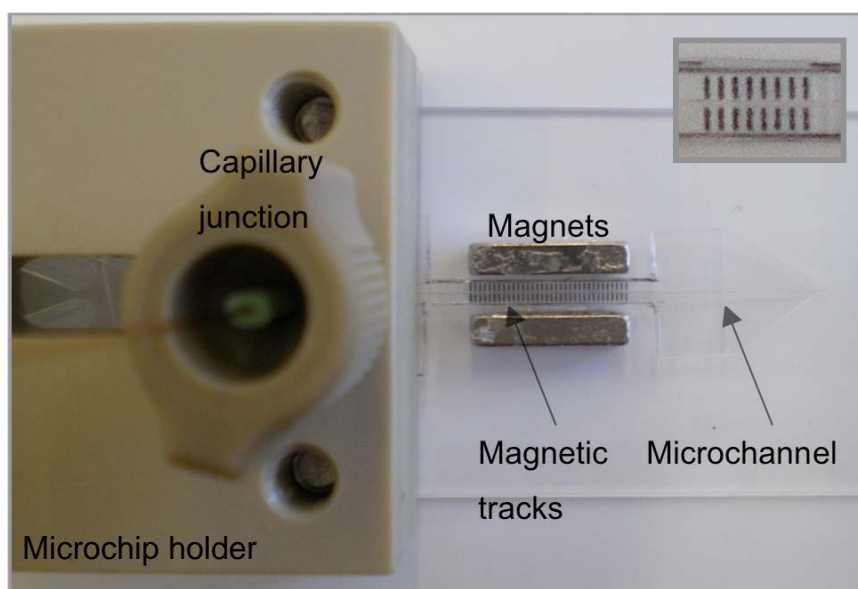


Figure V- 2 Top-view of the microchip with integrated magnetic tracks. The microchannel (100 μm wide, 50 μm deep, 4 cm long) inlet is positioned in a holder with capillary connections. The magnetic track array is composed of 34 tracks spaced by 200 μm and is surrounded by two permanent magnets of 10 mm long fixed in attraction on a glass slide. The inset zoomed picture shows 8 magnetic tracks spaced by 200 μm designed for magnets of 2 mm long.

2.5. Numerical description

Numerical simulations of the magnetic field and force distribution, based on the finite elements (FE) method, were carried out in a 2D geometry, in magnetostatic conditions. The simulations were performed without any flow in the microchannel. The FE formulation was implemented in the commercial software Flux-ExpertTM (Astek, Rhône-Alpes, Grenoble, France) on a Mac Pro with Ubuntu Linux 7.10 operating system.

2.5.1. Numerical model and assumptions

As the different study domains are non conductive (without any free electrical current), the first Maxwell equation writes $\nabla \wedge \mathbf{H} = 0$ and consequently, the magnetic field can be derived from the magnetic scalar potential ϕ ($\mathbf{H} = -\nabla \phi$). From the magnetic induction conservation and equation (3) in which the permanent induction \mathbf{B}_{mag} imposed by the magnet is added, we have:

$$\nabla \cdot \mathbf{B} = \nabla \cdot (-\mu \nabla \phi + \mathbf{B}_{mag}) = 0 \quad (7)$$

which is solved by using a Galerkin formulation (Appendix V-1). In any point of the domain, the flux density vector \mathbf{B} is deduced from the ϕ value.

The following assumptions are made: (i) magnetostatic conditions ($\partial \mathbf{B} / \partial t = 0$), (ii) 2D Cartesian form: the third dimension of the system (*i.e.* the magnet channel and track thickness) is supposed to be at least 10 times larger than its height (*i.e.* magnet gap), so it can be neglected, (iii) no magnetic elements around the magnets, (iv) homogeneous media (μ uniform in each of the different domains), (v) stopped-flow conditions (*i.e.* static bead solution in the microchannel), (vi) the particle-fluid or inter-particle interaction are not considered. (vii) The effect of the beads on the solution permeability ($\mu_{solution}$) is neglected. (viii) The magnetic beads are assumed to be ideal (local $\mathbf{B}_{max} < \mathbf{m}_{sat}$) as there is no quantitative comparison with experimental results.

This numerical model has been previously validated showing a good correlation with published results.^{42, 49}

2.5.2. Geometry and numerical parameters

The reference geometry used for the simulations considers two face-to-face permanent macro-magnets ($L_m = 2$ mm) placed in attraction with an inter-magnet gap $g = 2$ mm, as illustrated in Figure V-2. Consequently, the magnet length over inter-magnet gap ratio $L_m/g = 1$. The microchip presents a width of 1.3 mm in the magnet region and includes at its centre a 100 μm -wide microchannel. The following parameters are applied on the studied geometry: relative permeability of the materials $\mu_r = 1$ in the entire domain, apart from the magnetic tracks where $\mu_r = 4$. Imposed flux density in the magnets: $B_{mag} = \pm 1.3$ T. The beads parameters are fixed at unity: $\Delta\chi = 1$, $V = 1.4 \cdot 10^{-20}$ m³ (for a bead diameter of 0.3 μm). An “air box” is meshed around the magnets to give enough space for the magnetic field rotation from one pole to the other. The size of the mesh elements and of the “air box” has been systematically calibrated.

The numerical investigations concerning the microchip with magnetic tracks were restricted to the design with 2 mm-long magnets as the number of tracks to mesh would be too high for larger magnets.

3. Experimental section

Materials & Chemicals.

Three different magnets were used for this study: a rectangular NdFeB $2 \times 2 \times 8 \text{ mm}^3$ magnet (magnetic remanence of 1.3 T at the pole and a polarization in the longest dimension, from Chen Yang, Finsing, Germany), two rectangular $5 \times 2.5 \times 2 \text{ mm}^3$ and $10 \times 3 \times 2 \text{ mm}^3$ magnets (magnetic remanence of 1.3 T at the pole, with a polarization in the smallest dimension, from Supermagnet, Switzerland). Fused-silica capillaries ($100/375 \text{ }\mu\text{m}$ i.d./o.d.) were obtained from BGB Analytik AG (Böckten, Switzerland). Protein A-coated superparamagnetic beads of uniform size (mean diameter of 300 nm, binding capacity 100 $\mu\text{g/mL}$) were purchased from Ademtech (Pessac, France). The bead suspensions were sonicated and diluted 10 times in water produced by an alpha Q Millipore System (Zug, Switzerland).

Magnetic ink preparation and characterization.

The home-prepared magnetic ink is made of 1 g of carbon ink (Electrador, Electra Polymer & Chemicals Ltd., UK) mixed with 200 mg of $10 \text{ }\mu\text{m}$ iron particles (Merck, Darmstadt, Germany). The density and magnetic permeability of the ink were determined. A density of 4.9679 g/cm^3 was measured on the cured ink with a helium pycnometer (Prof. Heinrich Hofmann, Carlos Morais, Powder technology laboratory, EPFL). The mass magnetization of the ink was measured as a function of the field at 300 K with a SQUID (Prof. Philippe Ansermet, Dr. Simon Granville, Laboratory of Physics of Nanostructures Materials, EPFL). The resulting value of dimensionless magnetic permeability was 4.07. This value was used in the numerical model.

Device microfabrication.

The microfabrication process is based on polymer photoablation and is depicted in Figure V-3.

Step 1. The main microchannel ($100 \text{ }\mu\text{m}$ wide, $50 \text{ }\mu\text{m}$ deep and 4 cm long) is drilled on the topside of a polyethylene-terephthate (PET) sheet of $100 \text{ }\mu\text{m}$ thickness (Melinex sheet from Dupont, Wilmington, DE, USA) by photoablation with an ArF excimer laser (193 nm, Lambda Physik, Göttingen, Germany). Spaced by $650 \text{ }\mu\text{m}$ from the microchannel x -axis, a parallel channel ($50 \text{ }\mu\text{m}$ wide, $100 \text{ }\mu\text{m}$ deep and 1 cm long) is drilled to further facilitate the

microchip lateral sides cutting. Then, rectangular tracks ($100 \times 500 \times 100 \mu\text{m}^3$) perpendicular to the main microchannel are drilled by static laser shoots. The reference design is defined by a channel-track gap of $10 \mu\text{m}$ and an inter-track gap of $200 \mu\text{m}$. Only the photoablation step is made in clean-room environment.

Step 2. The chip is cleaned with MeOH and the lateral sides of the chip are removed to allow the positioning of the permanent magnets close to the magnetic tracks. The chip is laminated and cured 1 hour at 80°C .

Step 3. On the PET chip backside, the microchannel inlets are protected and the tracks are filled with the home-prepared magnetic ink.

Step 4. The backside of the chip is laminated and the chip is cured 30 min at 80°C .

The entire process is achieved in a single day with around 10 microchips per batch.

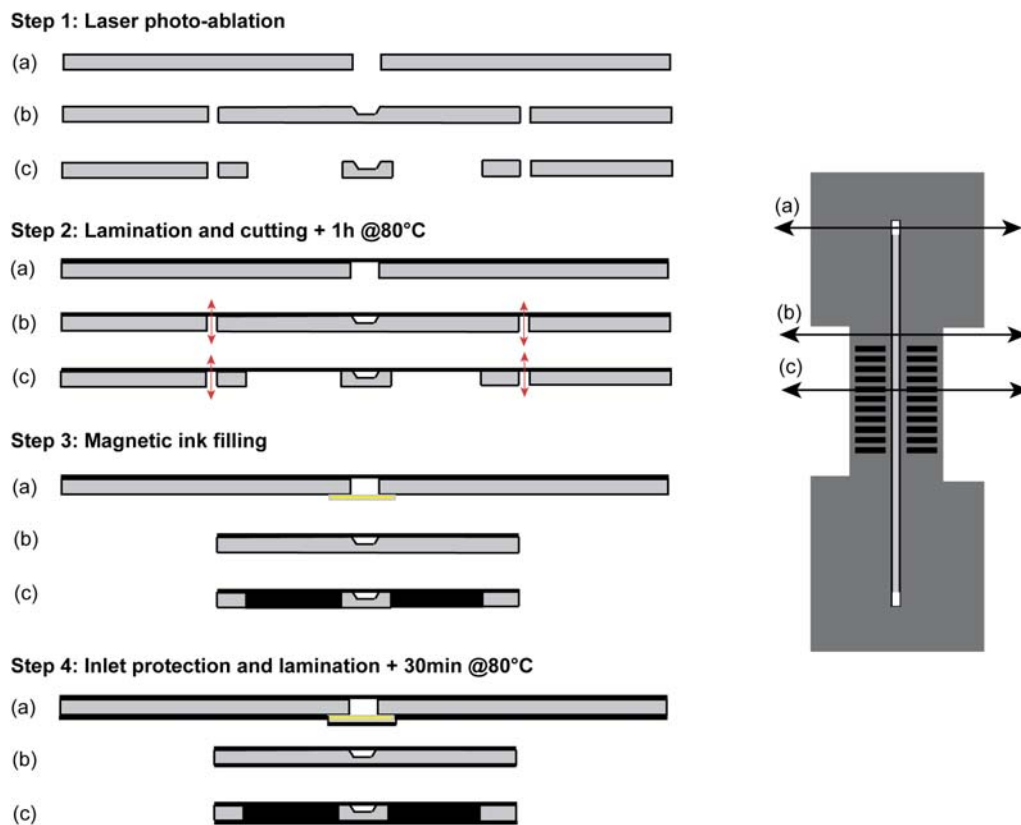


Figure V- 3 Microchip fabrication process.

Microfluidic system operation and cleaning.

The permanent magnets are fixed on a microscope slide in attraction with an inter-magnet gap of 2 mm. The microchip is then positioned in the inter-magnet gap, as illustrated in Figure V-2.

A capillary electrophoresis (CE) PACE MDQ system (Beckman-Coulter, Nyon, Switzerland) embedding an autosampler and UV detector is used for the sample delivery, in pressure mode. The influence of the capillary-to-microchip connections and of the magnetic beads on the pressure drop was evaluated (Figure V-4). The UV detector of the CE allows controlling the good sample delivery. The flow rate is determined by measuring the time for a marker to travel from the injector to the detector at a given applied pressure. It was first evaluated for an open capillary. The deviation from the theoretical Poiseuille equation at high pressure is due to the time delay required to reach the desired pressure. Indeed, it would necessitate a longer injector-detector distance to correctly measure the flow rates at high pressure. In addition, the pressure drop induced by the capillary-microchip connection was evaluated showing as well a good inter-chip reproducibility. Taking into account all these considerations, it was possible to determine the real flow rates applied during this study. The pressure drop induced by the magnetic beads was shown to be negligible.

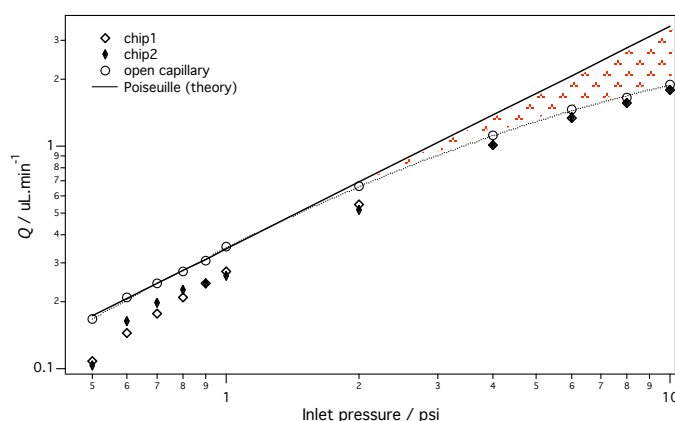


Figure V- 4 Correlation between the applied pressure and delivered flow rate. The values obtained with an open capillary and the capillary connected to the microchip are compared to the ones calculated from the Poiseuille law. The red area corresponds to the deviation of the open capillary with the theoretical values (due to the delay of the gradient of pressure).

The beads are captured at a flow rate of 100 nL/min, optimum to avoid bead sedimentation and unspecific binding during the filling. The time of injection was varied according to the

experiments. For cleaning, the beads are flushed out after magnet removing. The chip is washed with acidic solutions or solvents, and if necessary immersed in ultra-sonic bath.

Imaging of magnetic bead capture / release.

The magnetic beads were observed with a microscope Axiovert 200 (Carl Zeiss, Gottingen, Germany) and a CCD-IRIS camera (Sony, Tokyo, Japan). Images were processed with Igor 6.0 software (WaveMetrics, Portland, OR, USA).

4. Results and Discussions

4.1. Forces and magnet length

Figure V-5.A illustrates the variation of the magnetic force (x -component), along a microchannel surrounded by two permanent magnets of length $L_m = 2, 5$ or 10 mm. The magnets, in attractive configuration, present a symmetry axis at $x = 0$. F_{mag} is positive at the magnet left-edge and negative at the right-edge. For small magnets ($L_m = 2$ mm), the zero- F_{mag} is restricted to a point located at the symmetry axis. When $L_m > 2$ mm, the zero- F_{mag} region becomes larger.

The main forces experienced by a magnetic bead in such a microfluidic system with large magnets ($L_m = 10$ mm) are summarized in Figure V-5.B. The microchannel region between the magnets can be subdivided by three where: (1) F_{mag} and F_{drag} are in the same direction resulting in the acceleration of the beads; (2) $F_{mag} = 0$, leading to the beads slow down; (3) F_{mag} is opposite to F_{drag} . Consequently, if $F_{mag} > F_{drag}$, the beads will be trapped in this area. In stopped-flow conditions, the beads move back to the middle of the magnets, as the negative F_{mag} x -component repels them.

The bead capture, in a microchannel surrounded by two 10 mm-long magnets in attraction, was followed by microscope imaging. The next conditions were fixed for the entire study: *i*) the flow velocity was kept constant for the bead delivery and only the bead injection time was changed according to the experiment; *ii*) the distance between the two magnets was kept constant (inter-magnet gap of 2 mm) to allow the microscopic imaging of the beads. In agreement with the force distribution, the beads are trapped from the magnet end-edge, as illustrated in Figure V-5.C.

As the major magnet length is not optimally exploited in such conditions, our approach was to integrate a magnetic track array in order to distribute the magnetic field all along the microchannel.

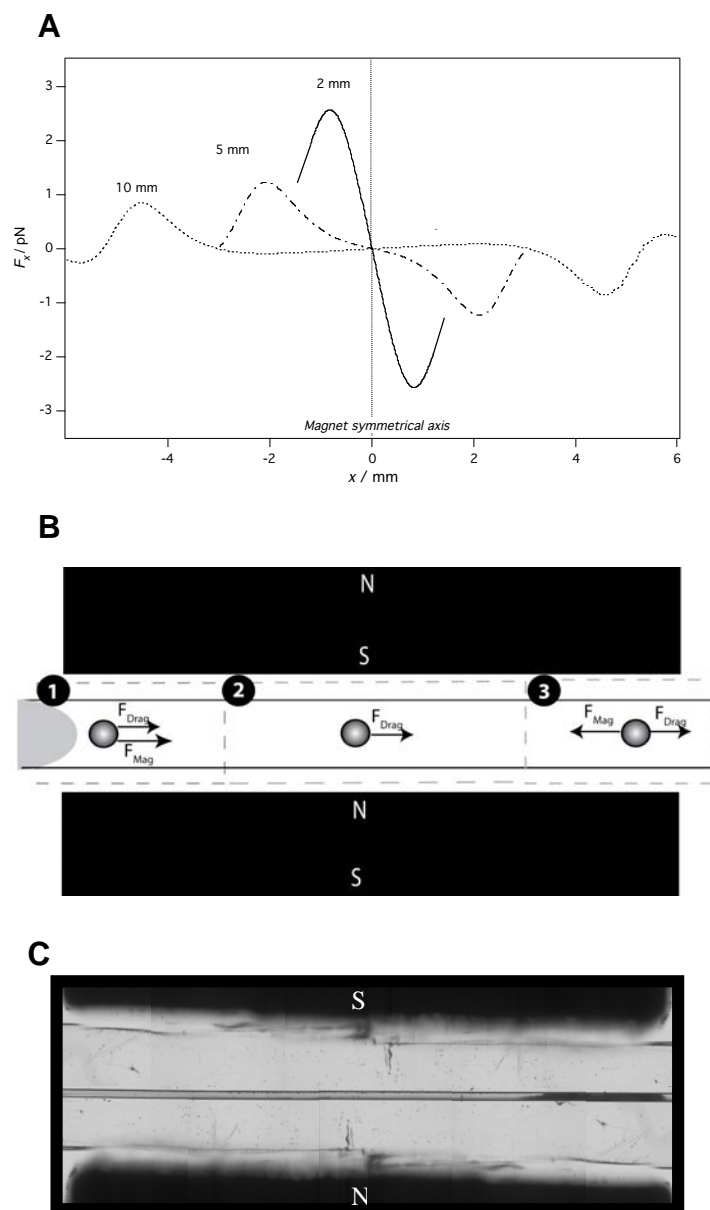


Figure V- 5 A) Variation of the magnetic force (x -component) as a function of the magnet length ($L_m = 2, 5$ and 10 mm). B) Scheme summarizing the main forces, F_{mag} and F_{drag} , experienced by a magnetic bead, with large magnets ($L_m > 2$ mm). C) Microscope picture of the magnetic bead capture in a microchannel surrounded by two magnets of $L_m = 10$ mm.

4.2. Magnetic track integration and field addressing

The microchip design and fabrication process are displayed in Figures V-2 and V-3, and detailed in the *Experimental* section. Briefly, the microchip is constituted of a main microchannel with an array of magnetic tracks integrated perpendicularly and on both side of it in order to address the magnetic field in consecutive locations. The number of tracks is adjusted to fit the magnet length. In the present work, microchip with 8, 17 and 34 tracks were processed to fit with 2, 5 and 10 mm long magnets, respectively. As illustrated in Figure V-2, the microchip is positioned in a holder with capillary connection fittings for sample delivery. The magnetic track region is then positioned between the magnets previously fixed in attraction.

Figure V-6 presents the isovalues of the magnetic field distribution (y -component) obtained by numerical simulations. In the gap between the two magnets in attraction and without magnetic tracks (Figure V-6.A), the magnetic field goes straight from one magnet towards the other and its magnitude along the microchannel ($y = 0$) presents a maximum at the magnet vertical symmetry axis ($x = 0$). Along the microchannel ($y = 0$), the magnitude decreases near the magnet edges due to the enlarging of the field lines at the magnet extremities. The field line curvatures are at the origin of the F_{mag} force maxima in these regions (due to the $B\nabla B$ term in Eqn. 5).¹¹

In the presence of magnetic tracks (Figure V-6.B), the magnetic field lines are focused through the tracks and amplified because of the field line concentration. This configuration is analogous to one with successive micro-magnets positioned along a microchannel where each track is comparable to a single magnet. However, when the external magnetic field is generated by permanent magnets, the magnetic field is not equally distributed between the tracks (as shown by the force in Figure V-7.C). Then, the inner tracks experience a higher magnetic field than the outer ones. However, compared to on-chip micro-electromagnets, the use of macro-sized permanent magnets combined with magnetic tracks enables to reach higher magnetic field values (> 0.5 T).

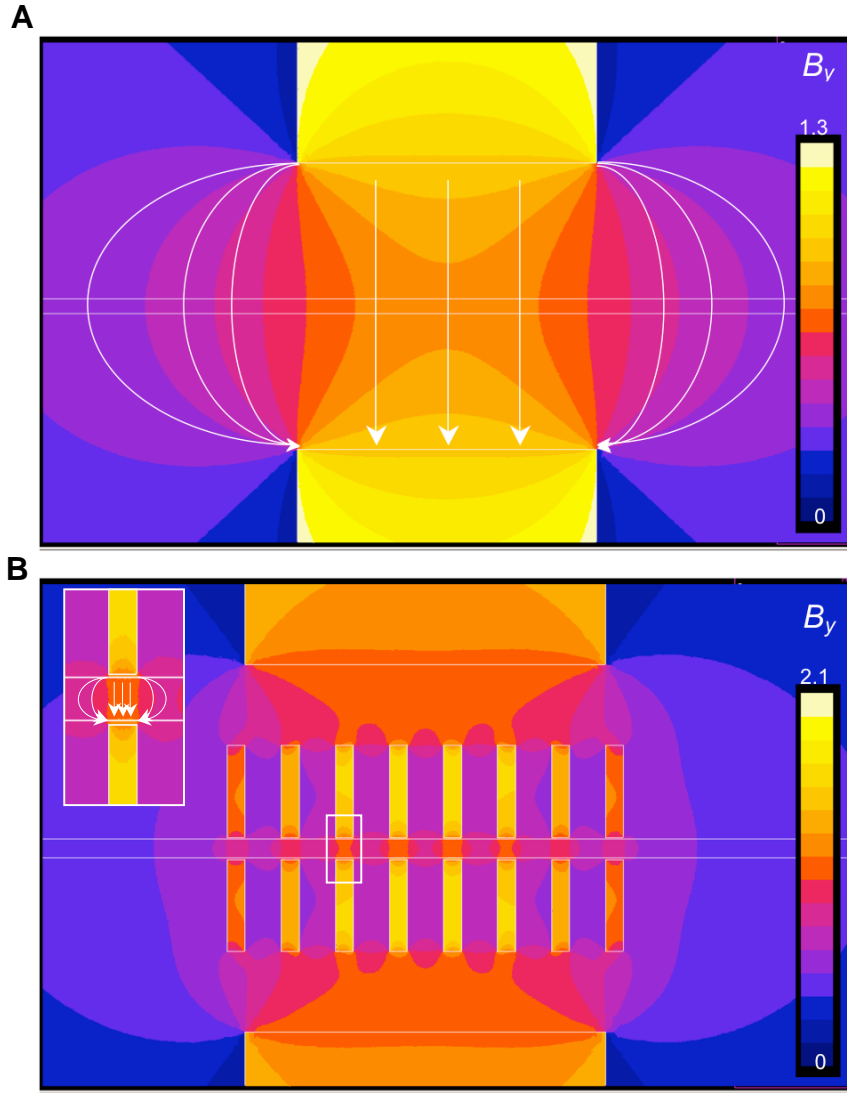


Figure V- 6 Isovalues of the magnetic field distribution (y-component). Microchips A) without and, B) with 8 magnetic tracks are simulated with 2 mm-long permanent magnets. The inter-magnet gap is 2 mm and channel width 100 μm . The white lines underline the curvatures of the magnetic field lines.

4.3. Magnetic force mapping and resulting magnetic bead capture

Figure V-7 shows the magnetic force distribution and the bead capture along the microchannel. Without tracks (Figure V-7.A-B), the negative value of F_{mag} at the magnet end-edge counter-balances the F_{drag} magnitude and enables the magnetic bead trapping (assuming that $F_{mag} > F_{drag}$). For low flow rates (low value of F_{drag}), the starting position of the plug (S) is located approximately at the middle of the magnet, as qualitatively confirmed

on Figure V-7.B. The beads are organized in a single plug growing with time until reaching the point where F_{mag} is not sufficient to retain them. It also confirms the partial bead release outside the end-side (E) of the plug. For the flow velocity value applied here, the region where $F_{mag} > F_{drag}$ (defined as the plug length L_P in dynamic conditions) represents 80 % of the magnet length L_m (Figure V-7.A-B).

Using the magnetic track configuration (Figure V-7.C-D), the magnetic field distribution generates a pattern of successive positive-negative peaks of F_{mag} along the microchannel. The negative peaks located at each track allow to locally trapping the beads, with a F_{mag} x-component amplitude 10 times higher. The first plug is growing from the first magnetic track. When saturation occurs, the beads move to fill the next plug, and so on.

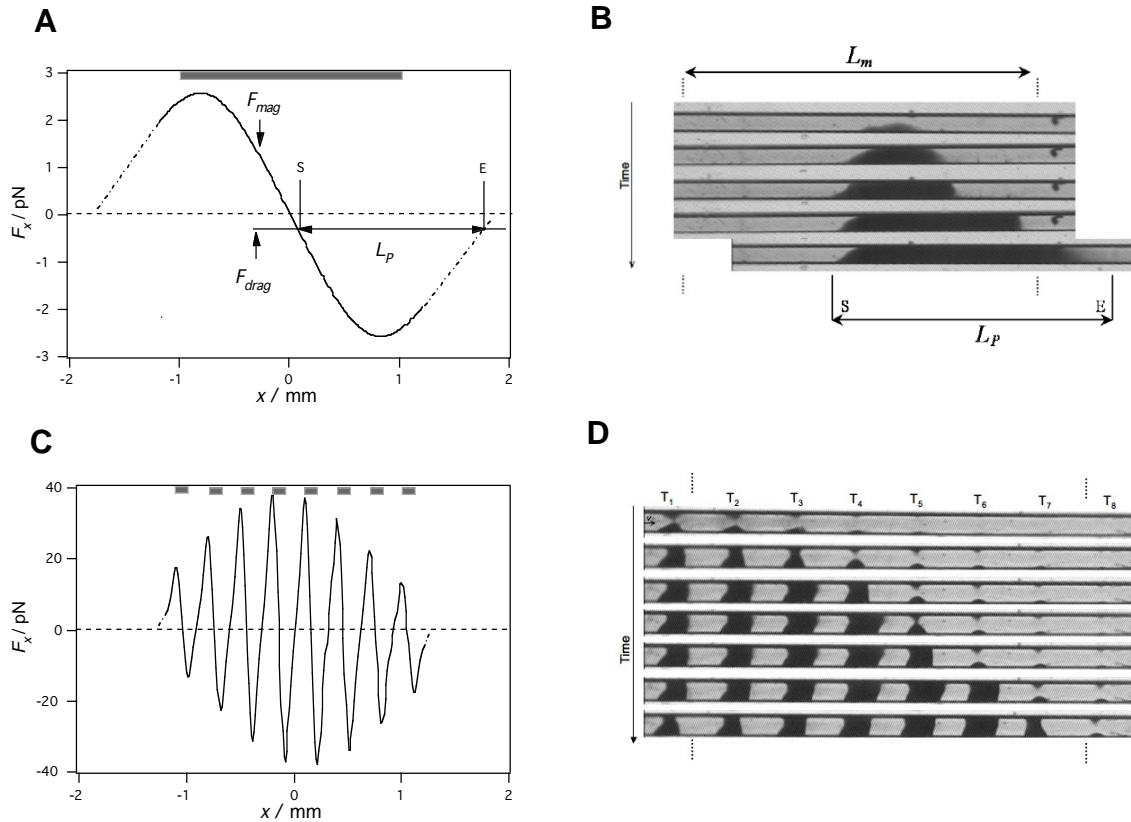


Figure V- 7 Variations of magnetic force (x-component) along the microchannel and microscope imaging of the magnetic bead capture. A-B) Microchips without, and C-D) with magnetic tracks are studied. The vertical dashed lines on the pictures show the position of the permanent magnets extremities with respect to microchannel. S: Start, E: End of the plug of beads. L_P : plug length.

4.4. Design considerations

The influence of the channel-track gap, inter-track gap and magnetic ink permeability values on the magnetic force amplitude is presented in Figure V-8. The results are evaluated as a *gain*, calculated from the ratio of magnetic forces between the chip embedding tracks and not. The position of the permanent magnets with respect to the microchannel remains unchanged. The force is considered at the maximal value at the centre of the microchannel.

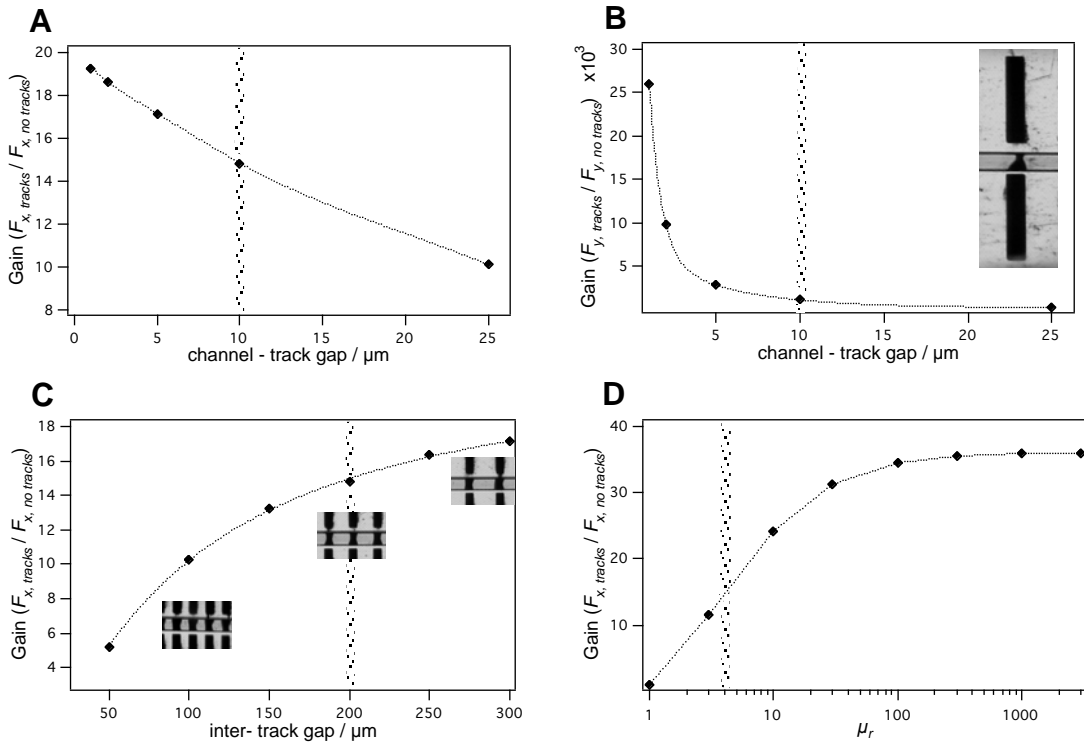


Figure V- 8 Influence of the geometrical parameters and magnetic track permeability on the magnetic force. The gain is expressed as the ratio of magnetic forces between the microchip embedding tracks and not. A-B) Gain (x- and y-component) in function of the channel-track gap value. C-D) Gain (x-component) in function of the inter-track gap value. D) Generalization of the study to other ink permeability values. The picture tags are microscopic images done in parallel to the simulations. The grey region shows the value of the reference design.

First, the channel-track vertical gap was increased from 1 to 25 μm . The gain, in terms of magnetic force, was evaluated for the x - and y -component of the force, as illustrated in Figure V-8.A and 8.B, respectively. The first observation from both figures is that closer the magnetic tracks are from the microchannel, larger is the local magnetic force value. In the presence of magnetic tracks, the minimal F_x gain is 10 for a gap of 25 μm and can reach 19 for a gap of 1 μm (Figure V-8.A). Because of the fixed permanent magnets position, the addition of tracks has a major effect on the y -component of the force with values reaching three orders of magnitude. The F_y gain is of $25 \cdot 10^3$ for a gap of 1 μm and rapidly decreases to $1 \cdot 10^3$ for a 25- μm gap (Figure V-8.B). To illustrate the effect of the track vertical position on the y -component of the force, a chip was designed with an asymmetrical channel-track distance, as shown on the microscope image in Figure V-8.B. When one of the magnetic tracks is closer to the microchannel, the beads start to form a cluster towards its sidewall resulting in an asymmetrical plug. From a microfabrication point of view, the reference design value was fixed at 10 μm to be sure that the lamination layer resists to the flow velocity.

The second studied parameter was the inter-track gap value, which was varied from 50 to 300 μm (Figure V-8.C). The number of tracks was adjusted to fit the magnet length. The tracks were positioned symmetrically from the magnet centre. Therefore, when gap is small, the number of tracks in the area between the two permanent magnets is increased. When the gap is larger, the F_x gain also increases from 5 to 17 and approaches a plateau for a gap value higher than 300 μm . For a gap of 50 μm , the position of the tracks are so close that they can be assimilated to a global magnet without changing significantly the magnetic field lines distribution. On the other hand, with a larger inter-track gap, each track acts as individual small magnet presenting a negative F_{mag} value. Obviously, a compromise between the number of tracks (*i.e.* the number of plugs and by the way the amount of trapped beads) and the intensity of the repelling magnetic force has to be found. It is the reason why, with the flow velocities applied in this study, an inter-track gap of 200 μm appeared as a good compromise for the chip.

In order to extend the present study to other kind of magnetic inks, the effect of the ink properties on the F_x gain was evaluated (Figure V-8.D). The dimensionless relative permeability value was varied from 1 to 3000 and it shows a linear gain increase from 1 to about 20, for $\mu_r = 1$ to 10, respectively. For μ_r values higher than 100, the gain reaches a plateau. The permeability value of the home-prepared magnetic ink was determined to be around 4 that correspond to a gain of 12. Working on the optimization of the ink

composition, a gain three times higher could be reached. In some publications, permalloys are used as magnetic elements.⁴³ They are often made of Nickel (80 %) and Iron (20%), which typically present a relative permeability close to 100, which would provide a gain of 35.

The last parameter to be investigated was the length of the track array. If the tracks are located outside of the inter-magnet region, the magnetic field lines will also be deviated to these outer tracks, decreasing the magnetic field and force of the inner tracks. In addition, these tracks will not efficiently trap beads because of their limited magnetic force amplitude. In the reference design, the channel-track gap is 10 μm , the inter-track gap is 200 μm , and the magnetic tracks fit the permanent magnet length ending with 8, 17 and 34 magnetic tracks for 2, 5 and 10 mm long magnet, respectively.

4.5. Relative quantification of the magnetic bead capture

As the binding surface available for bioassays is directly correlated to the amount of trapped beads, relative quantification was done comparing a multi-plug *vs.* a single plug bead capture (Figure V-9). First, the bead capture was imaged within three microchips with 8, 17 and 34 tracks used with 2, 5 and 10 mm-long magnets, respectively. The magnetic bead injection time was increased (the flow velocity was kept constant). From the microscope images, the surface occupied by the beads was extracted. The resulting surfaces obtained from each experimental condition were then normalized by the maximal occupancy value (*i.e.* value at the plateau) obtained with the 34-track microchip. When the relative occupancy reaches a plateau, all the plugs are saturated with beads. As expected, this saturation value increases with the number of tracks.

Afterwards, the same amounts of beads corresponding to the multi-plug saturation were injected in the respective microchips without magnetic tracks, at the same flow velocity (horizontal lines with grey markers on Figure V-9). The relative occupancy then represents 10%, 29%, 31% of the maximal occupancy for 2, 5 and 10 mm-long magnets, respectively, showing a relevant impact of the magnetic track incorporation. The difference is actually due to a loss of beads during the capture in the absence of tracks. For the magnets of 5 and 10 mm long without tracks, at a given flow rate, approximately 60 % of the beads are lost during the capturing protocol. It is partly due to the magnetic force value, *i.e.* the magnetic force over

drag force ratio, which is lower in the absence of magnetic tracks, as shown in Figures V-7. For the 2 mm-long magnets, the small magnet length limits the amount of trapped beads as the area where F_{mag} competes with F_{drag} has a length which order of magnitude is half of the magnet length (in stopped-flow conditions).

The use of magnetic tracks allows a significant increase of the amount of trapped beads and potentially, the available binding surface for bio-chemical assays. This increase reaches 200% for the 2 and 5 mm long magnets and goes up to 300 % with the largest magnet tested. Obviously, this value depends on the flow rate and amount of injected beads, as well as the track position (*i.e.* the number of tracks and consequently the number of plugs).

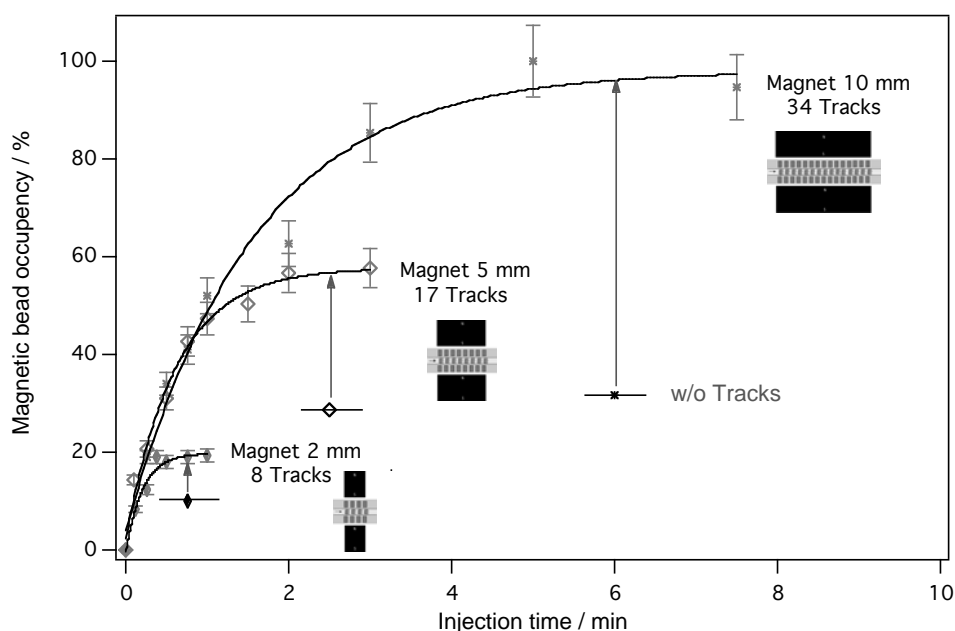


Figure V- 9 Relative quantification of the magnetic bead capture with 2, 5 and 10 mm-long magnets and comparison with microchip without tracks. The magnetic bead injection time is increased, with the injection protocol set at 250 nL/min for injection, and 100 nL/min for the bead flowing and capture.

5. Conclusions

This chapter introduces a simple way to enhance the magnetic bead capture in a microchannel, and consequently the specific binding surface available for bio-chemical assays, by locally addressing the magnetic field through a magnetic track array. Microscope imaging and 2D finite elements simulations were performed considering a microchannel surrounded by two permanent magnets in attraction. Microscope imaging has shown that, for the given flow velocity conditions, the bead capture remains almost constant for a magnet length higher than 5 mm. To enhance the bead capture, 100 μm -wide magnetic tracks perpendicular to the microchannel axis, were integrated to drive the magnetic field towards specific locations. Therefore, in the gap between each opposite track, a repelling magnetic force retains the beads leading to a multi-plug capture.

The influence of geometrical parameters on the magnetic force amplitude, such as the channel-track and inter-track gap values, as well as the magnetic track permeability, were evaluated by numerical simulations, with a microchip operating with 2 mm long magnets. When the inter-track gap is large, the x -component of the force is mainly concerned, leading to an increase of its amplitude (F_x multiplied by 3 for a inter-track gap increasing from 50 to 300 μm). On the other hand, changing the vertical position of the tracks mostly affects the y -component of the force (F_y increased by a factor 25 for a channel-track gap decreasing from 25 to 1 μm). The closer to the microchannel the tracks are, the larger is the y -component force magnitude.

With the multi-plug capture, the amount of trapped beads can be increased from 200 % for the 8- and 17-track to 300 % for the 34-track reference designs. The increase of the bead amount considerably enhances the binding surface available for *in-vitro* applications, such as immuno-affinity separation. Moreover, the negative force retaining the beads is amplified by passing through the tracks (10 times higher for the inner tracks) enabling a capture at higher flow rates. Finally, the precise positioning of the tracks can overcome the difficult symmetrical positioning of the chip in between the magnets.

It would be interesting to further investigate the growth of the plugs in order to understand more deeply the dependence of the plug length with the fluidic and magnetic parameters, and in particular with the F_{mag} over F_{drag} ratio.

Further developments on the present microchip, will be to integrate on-chip electrochemical detection to perform enzyme-based immuno-assays, or to embed a carbon electrode to use it as electrospray emitter in order to follow on-line reactions directly by mass spectrometry.

Another perspective concerns the control of the bead organization to perform mixing applications, as illustrated by the alternated bead clusters (Figure V.10). The implementation of rotating permanent magnets to induce a motion of beads along the microchannel could be an option to investigate in order to increase the mixing of flows.

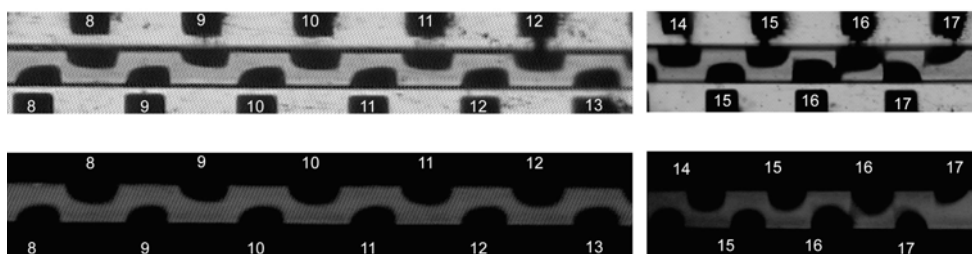


Figure V- 10 Alternated bead clusters showing magnetic bead organization in visible light and under fluorescence. The microchip with two inlets (inlet 1: H_2O , inlet 2: Fluorescein) is made of 17 magnetic tracks and used with permanent magnets of 5 mm long.

REFERENCES

1. M. C. Peoples and H. T. Karnes, Microfluidic immunoaffinity separations for bioanalysis, *Journal of Chromatography B: Analytical Technologies in the Biomedical and Life Sciences*, 2008, 866, 14-25.
2. J. S. Rossier and H. H. Girault, Enzyme linked immunosorbent assay on a microchip with electrochemical detection, *Lab on a Chip - Miniaturization for Chemistry and Biology*, 2001, 1, 153-157.
3. A. Lionello, J. Josserand, H. Jensen and H. Girault, Protein adsorption in static microsystems: effect of the surface to volume ratio, *Lab on a Chip*, 2005, 5, 254-260.
4. A. Lionello, J. Josserand, H. Jensen and H. Girault, Dynamic protein adsorption in microchannels by "stop-flow" and continuous flow, *Lab on a Chip*, 2005, 5, 1096-1103.
5. H. X. Chen, J. M. Busnel, A. L. Gassner, G. Peltre, X. X. Zhang and H. H. Girault, Capillary electrophoresis immunoassay using magnetic beads, *ELECTROPHORESIS*, 2008, 29, 3414-3421.
6. H. X. Chen, J. M. Busnel, G. Peltre, X. X. Zhang and H. H. Girault, Magnetic beads based immunoaffinity capillary electrophoresis of total serum IgE with laser-induced fluorescence detection, *Analytical Chemistry*, 2008, 80, 9583-9588.
7. P. Morier, C. Vollet, P. E. Michel, F. Reymond and J. S. Rossier, Gravity-induced convective flow in microfluidic systems: Electrochemical characterization and application to enzyme-linked immunosorbent assay tests, *ELECTROPHORESIS*, 2004, 25, 3761-3768.
8. M. Abonnenc, L. Dayon, B. Perruche, N. Lion and H. H. Girault, Electrospray micromixer chip for on-line derivatization and kinetic studies, *Analytical Chemistry*, 2008, 80, 3372-3378.
9. L. Dayon, M. Abonnenc, M. Prudent, N. Lion and H. H. Girault, Multitrack electrospray chips, *Journal of Mass Spectrometry*, 2006, 41, 1484-1490.
10. T. C. Rohner, J. S. Rossier and H. H. Girault, Polymer microspray with an integrated thick-film microelectrode, *Analytical Chemistry*, 2001, 73, 5353-5357.
11. S. S. Shevkoplyas, A. C. Siegel, R. M. Westervelt, M. G. Prentiss and G. M. Whitesides, The force acting on a superparamagnetic bead due to an applied magnetic field, *Lab on a Chip - Miniaturisation for Chemistry and Biology*, 2007, 7, 1294-1302.
12. Q. A. Pankhurst, J. Connolly, S. K. Jones and J. Dobson, Applications of magnetic nanoparticles in biomedicine, *Journal of Physics D: Applied Physics*, 2003, 36.
13. A. Ito, M. Shinkai, H. Honda and T. Kobayashi, Medical application of functionalized magnetic nanoparticles, *Journal of Bioscience and Bioengineering*, 2005, 100, 1-11.
14. G. M. Whitesides, R. J. Kazlauskas and L. Josephson, Magnetic separations in biotechnology, *Trends in Biotechnology*, 1983, 1, 144-148.
15. I. Safarik and M. Safarikova, Use of magnetic techniques for the isolation of cells, *Journal of Chromatography B: Biomedical Sciences and Applications*, 1999, 722, 33-53.
16. M. Safarikova and I. Safarik, Magnetic solid-phase extraction, *Journal of Magnetism and Magnetic Materials*, 1999, 194, 108-112.
17. D. Janasek, J. Franzke and A. Manz, Scaling and the design of miniaturized chemical-analysis systems, *Nature*, 2006, 442, 374-380.
18. N. Pamme, Magnetism and microfluidics, *Lab on a Chip - Miniaturisation for Chemistry and Biology*, 2006, 6, 24-38.
19. E. Verpoorte, Chip vision-optics for microchips, *Lab Chip*, 2003, 3.
20. M. A. M. Gijs, Magnetic bead handling on-chip: New opportunities for analytical applications, *Microfluidics and Nanofluidics*, 2004, 1, 22-40.
21. K. H. Man and A. Bruno Frazier, Continuous magnetophoretic separation of blood cells in microdevice format, *Journal of Applied Physics*, 2004, 96, 5797-5802.
22. K. H. Han and A. B. Frazier, Diamagnetic capture mode magnetophoretic microseparator for blood cells, *Journal of Microelectromechanical Systems*, 2005, 14, 1422-1431.

23. N. Pamme and C. Wilhelm, Continuous sorting of magnetic cells via on-chip free-flow magnetophoresis, *Lab on a Chip - Miniaturisation for Chemistry and Biology*, 2006, 6, 974-980.
24. E. P. Furlani, Magnetophoretic separation of blood cells at the microscale, *Journal of Physics D: Applied Physics*, 2007, 40, 1313-1319.
25. J. Jung and K. H. Han, Lateral-driven continuous magnetophoretic separation of blood cells, *Applied Physics Letters*, 2008, 93.
26. B. Y. Qu, Z. Y. Wu, F. Fang, Z. M. Bai, D. Z. Yang and S. K. Xu, A glass microfluidic chip for continuous blood cell sorting by a magnetic gradient without labeling, *Analytical and Bioanalytical Chemistry*, 2008, 392, 1317-1324.
27. L. Korecká, B. Jankovicová, J. Krenková, L. Hernychová, M. Slovákova, A. Le-Nell, J. Chmelik, F. Foret, J. L. Viovy and Z. Bilková, Bioaffinity magnetic reactor for peptide digestion followed by analysis using bottom-up shotgun proteomics strategy, *Journal of Separation Science*, 2008, 31, 507-515.
28. M. Slovákova, N. Minc, Z. Bilková, C. Smadja, W. Faigle, C. Fütterer, M. Taverna and J. L. Viovy, Use of self assembled magnetic beads for on-chip protein digestion, *Lab on a Chip - Miniaturisation for Chemistry and Biology*, 2005, 5, 935-942.
29. S. A. Peyman, A. Iles and N. Pamme, Rapid on-chip multi-step (bio)chemical procedures in continuous flow - Manoeuvring particles through co-laminar reagent streams, *Chemical Communications*, 2008, 1220-1222.
30. F. Lacharme, C. Vandevyver and M. A. M. Gijs, Full on-chip nanoliter immunoassay by geometrical magnetic trapping of nanoparticle chains, *Analytical Chemistry*, 2008, 80, 2905-2910.
31. R. S. Sista, A. E. Eckhardt, V. Srinivasan, M. G. Pollack, S. Palanki and V. K. Pamula, Heterogeneous immunoassays using magnetic beads on a digital microfluidic platform, *Lab on a Chip - Miniaturisation for Chemistry and Biology*, 2008, 8, 2188-2196.
32. K. Smistrup, B. G. Kjeldsen, J. L. Reimers, M. Dufva, J. Petersen and M. F. Hansen, On-chip magnetic bead microarray using hydrodynamic focusing in a passive magnetic separator, *Lab on a Chip - Miniaturisation for Chemistry and Biology*, 2005, 5, 1315-1319.
33. N. Minc, C. Fütterer, K. D. Dorfman, A. Bancaud, C. Gosse, C. Goubault and J. L. Viovy, Quantitative microfluidic separation of DNA in self-assembled magnetic matrixes, *Analytical Chemistry*, 2004, 76, 3770-3776.
34. K. Smistrup and H. A. Stone, A magnetically actuated ball valve applicable for small-scale fluid flows, *Physics of Fluids*, 2007, 19.
35. N. S. Satarkar, W. Zhang, R. E. Eitel and J. Z. Hilt, Magnetic hydrogel nanocomposites as remote controlled microfluidic valves, *Lab on a Chip - Miniaturisation for Chemistry and Biology*, 2009.
36. A. Rida and M. A. M. Gijs, Manipulation of self-assembled structures of magnetic beads for microfluidic mixing and assaying, *Analytical Chemistry*, 2004, 76, 6239-6246.
37. G. H. Seong and R. M. Crooks, Efficient mixing and reactions within microfluidic channels using microbead-supported catalysts, *Journal Of The American Chemical Society*, 2002, 124, 13360-13361.
38. S. L. Biswal and A. P. Gast, Micromixing with linked chains of paramagnetic particles, *Analytical Chemistry*, 2004, 76, 6448-6455.
39. Y. Wang, J. Zhe, B. T. F. Chung and P. Dutta, A rapid magnetic particle driven micromixer, *Microfluidics and Nanofluidics*, 2008, 4, 375-389.
40. S. H. Lee, D. Van Noort, J. Y. Lee, B. T. Zhang and T. H. Park, Effective mixing in a microfluidic chip using magnetic particles, *Lab on a Chip - Miniaturisation for Chemistry and Biology*, 2009, 9, 479-482.
41. M. A. Hayes, N. A. Polson and A. A. Garcia, Active control of dynamic supraparticle structures in microchannels, *Langmuir*, 2001, 17, 2866-2871.
42. A. L. Gassner, M. Abonnenc, J. Morandini, J. Jossierand, J. M. Busnel and H. Girault, Magnetic forces produced by rectangular permanent magnets in static microsystems, *Lab on a Chip*, 2009.

-
43. K. Smistrup, T. Lund-Olesen, M. F. Hansen and P. T. Tang, Microfluidic magnetic separator using an array of soft magnetic elements, *Journal of Applied Physics*, 2006, 99.
 44. E. Mirowski, J. Moreland, S. E. Russek and M. J. Donahue, Integrated microfluidic isolation platform for magnetic particle manipulation in biological systems, *Applied Physics Letters*, 2004, 84, 1786-1788.
 45. A. C. Siegel, S. S. Shevkoplyas, D. B. Weibel, D. A. Bruzewicz, A. W. Martinez and G. M. Whitesides, Cofabrication of electromagnets and microfluidic systems in poly(dimethylsiloxane), *Angewandte Chemie - International Edition*, 2006, 45, 6877-6882.
 46. D. Buerle, Chemical processing with lasers: Recent developments, *Applied Physics B Photophysics and Laser Chemistry*, 1988, 46, 261-270.
 47. D. Buerle, M. Himmelbauer and E. Arenholz, Pulsed laser ablation of polyimide: Fundamental aspects, *Journal of Photochemistry and Photobiology A: Chemistry*, 1997, 106, 27-30.
 48. T. Deng, G. M. Whitesides, M. Radhakrishnan, G. Zabow and M. Prentiss, Manipulation of magnetic microbeads in suspension using micromagnetic systems fabricated with soft lithography, *Applied Physics Letters*, 2001, 78, 1775-1777.
 49. S. Bronzeau and N. Pamme, Simultaneous bioassays in a microfluidic channel on plugs of different magnetic particles, *Analytica Chimica Acta*, 2008, 609, 105-112.

APPENDIX V-1: FINITE ELEMENT FORMULATION

The integral formulation is based on the local form (1), where $B_0 = \mu_0 M_0$ is the magnetic flux density vector imposed in the magnet:

$$\nabla \cdot (-\mu \nabla \phi + B_0) = 0 \quad (1)$$

Equation (1) is derived in the global form (2), using the Galerkin formulation frequently used in the finite element method (multiplication by a projective function α and integration on the domain of study, W). Note that all the gradients are written in the nabla form ∇ .

$$\iint_W \alpha [\nabla \cdot (-\mu \nabla \phi + B_0)] dW = 0 \quad (2)$$

By decomposing the product between α and the divergence in (2), the second order derivative of the unknown ϕ (divergence of $\nabla \phi$) becomes:

$$\alpha \nabla \cdot (-\mu \nabla \phi) = \nabla \cdot (-\alpha \mu \nabla \phi) + \mu \nabla \alpha \cdot \nabla \phi \quad (3)$$

Injecting (3) in (2) and using the Ostrogradsky theorem, the divergence term (second term of (3)) is rejected at the boundary where it equals to zero (no magnetic field crossing the external boundaries of the domain):

$$\iint_W [\mu \nabla \alpha \cdot \nabla \phi + \alpha B_0] dW = 0 \quad (4)$$

Using the function β for the interpolation of the unknown vector ϕ (of the same kind as the projective function α), we obtain the final form (5) where the first term corresponds to the matrix to invert, multiplied by the unknown vector ϕ , the second term being the source term:

$$\iint_W [(\mu \nabla \alpha \cdot \nabla \beta) \phi + \alpha B_0] dW = 0 \quad (5)$$

CHAPTER VI.

Multi-Track electrospray chip

Based on L. Dayon, M. Abonnenc*, M. Prudent*, N. Lion, H.H. Girault, 2006, JMS, 41 (11), 1484-1490. (*Equal authorship)*

1. Introduction

Since the nineties, microtechnologies have offered many options to fabricate devices for applications in the field of analytical sciences and especially in mass spectrometry (MS).

Microfabrication allows a large panel of choices for the design of electrospray (ESI) emitter in terms of material (glass, silica, polydimethylsiloxane, polyethylene terephthalate (PET)), size and shape of the structures.¹ Micro- and nanospray have been widely studied.^{2, 3} They were demonstrated to provide better sensitivity than standard ESI sources commonly used in MS. The advantages of miniaturized ESI microchip emitters are multiple. First, microfabrication enables the incorporation of several ESI emitters on the same chip that is effective for parallel and high throughput analysis. Secondly, on-chip functionalization such as sample preparation and/or separation can be hyphenated with the ESI emitter.

Several groups introduced multi-spray emitter chips some years ago.⁴ In particular, parallel microchannels with reservoirs⁵ or ESI emitter arrays⁶ were positioned on a computer-controlled translation stage for the serial analysis of samples. The emitters were successively aligned in front of the mass spectrometer orifice, as illustrated in Figure VI-1.

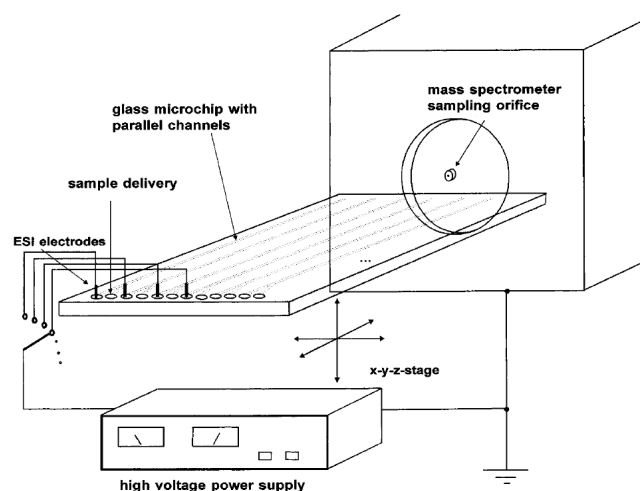


Figure VI- 1 Schematic diagram of the microchip ESI-MS interface. The voltage for ESI was sequentially applied to one well of each channel containing buffer and a platinum electrode. The exit ports of the microchip were aligned sequentially with the orifice of the MS using a 3D stage. Reprinted from Ref ⁶.

Henion's group and Advion Biosciences⁷ developed the TriVersa™ NanoMate™ ESI-Chip with an array of nozzles (Figure VI-2) that were used for high throughput MS quantification of drug from plasma samples.^{8, 9} A robotic probe delivers sample through a conductive pipette tip, which interfaces directly to the back plane of the ESI Chip. This microsystem can be operated as a chip-based infusion (flow rates ranging from 20 to 300 nL·min⁻¹), as interface after a LC/MS separation and allows collecting fractions after splitting flows from a LC setup.

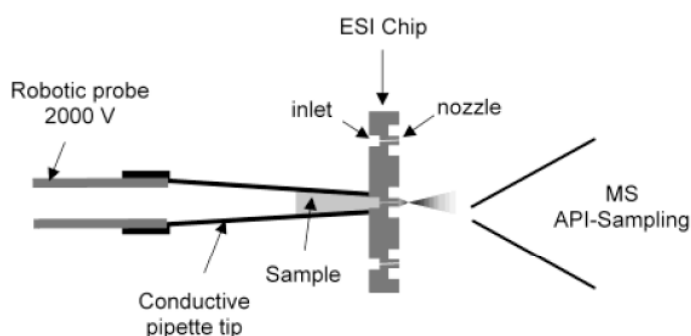


Figure VI- 2 Scheme of the ESI Chip from Advion Biosciences. A robotic probe delivers sample through a conductive pipette tip, which interfaces directly to the back plane of the ESI Chip. Voltage required for nanoelectrospray along with a slight positive pressure (N₂) is delivered to the sample through the robotic probe. Reprinted from Ref ⁸.

Dual sprayer ion source was also reported for the accurate mass measurement of compounds by time-of-flight (TOF) or Fourier transform ion cyclotron resonance (FTICR) MS when internal calibration is required.¹⁰⁻¹³ The two electrospray emitters were positioned orthogonally to each other or in parallel on a rotating platform in front of the mass spectrometer entrance. One sprayer was used to ionize the analyte while the other sprayer provided the calibrant. By switching the voltage between both the emitters, the analyte and calibrant were analyzed sequentially. Such dual sprayers often require a complex apparatus and in most cases, a motorised stage to place the successive emitters in the axis of the mass spectrometer orifice. Other applications of the multi-ESI emitters are the studies of ion/ion interaction by switching the ESI between positive and negative ionization mode¹⁴, mixing and reaction in the Taylor's cone.^{15, 16}

In the present study, a multi-track electrospray chip (MTEC) was designed. The microchannels were patterned by UV-photoablation of PET sheets.^{17, 18} The particularity of the device is to incorporate up to six ESI emitters on a single microchip. The microfabrication protocol is fast and easily flexible as regards the dimensions of the microchannels (typical section of $100 \times 40 \mu\text{m}^2$ and length of 1.5 cm) and the distance between them (4-8 mm). The second key feature of the MTEC set-up is the fixed positioning of the microchip in front of the mass spectrometer. The samples are therefore electrosprayed off-axis of the mass spectrometer orifice. Such a microchip is effective for fast screening applications in analytical chemistry and proteomics. Several proteins and peptides were alternatively electrosprayed from each track by switching the voltage between the microchannels. In addition, a two-track microchip was used for the counting of cysteines in peptides. The serial two-track ESI-MS analysis allows getting the mass of the untagged peptides (reference) and that of the cysteine-derivatized peptides in a single experiment. The relative quantification of a peptide between two samples was also carried out using the two-track version of the MTEC. Finally, the latest improvements concerning the automation of the voltage switch between the channels and the fluidics are presented.

2. Experimental section

Chemicals.

Angiotensin III (RVYIHPF, > 97%, $M = 931.1 \text{ g}\cdot\text{mol}^{-1}$), angiotensin I triacetate salt (DRVYIHPFHL, > 99%, $M = 1269.5 \text{ g}\cdot\text{mol}^{-1}$), Leu-enkephalin (YGGFL, > 99%, $M = 555.6 \text{ g}\cdot\text{mol}^{-1}$) and KCTCCA (70%, $M = 627.8 \text{ g}\cdot\text{mol}^{-1}$) were bought from Bachem (Bubendorf, Switzerland). Bradykinin (RPPGFSPFR, 99%, $M = 1060.2 \text{ g}\cdot\text{mol}^{-1}$) and myoglobin from horse heart (90%) were from Sigma (St Louis, MO, USA) and cytochrome C from horse heart ($\geq 95\%$), 1,4-Benzoquinone (BQ) ($\geq 98\%$, $M = 108.1 \text{ g}\cdot\text{mol}^{-1}$) and acetic acid (> 99.5%) from Fluka (Büchs, Switzerland). Keratin K18 (RPVSSAApSVYAGAC, > 95%, $M = 1418.5 \text{ g}\cdot\text{mol}^{-1}$) was bought from AnaSpec (San José, CA, USA). Methanol (> 99.8%) was from Riedel-de-Haën (Seelze, Germany). Water (UV-HPLC) and acetonitrile (HPLC-gradient grade) were from Panreac Quimica S.A. (Barcelona, Spain). All the chemicals were used without any further purification.

The spray medium was MeOH / H₂O / AcOH (50% / 49% / 1%). The concentration of the peptides and proteins was 50 μM and 5 μM respectively. Cysteines in KCTCCA were derivatized by mixing the peptide at 50 μM in the acidic spray medium with 5% (*V/V*) of BQ at 100 mM in CH₃CN.¹⁹ The reaction was performed at room temperature for 60 min. For quantification experiments, KCTCCA concentration was 12.5, 25 and 50 μM . All solutions were prepared freshly every day.

Microchip device.

The MTEC was microfabricated according to a simple procedure.^{18, 20} A PET polymer sheet of 100 μm thickness (Melinex[®] sheet from Dupont, Wilmington, DE, USA) was ablated by the UV-light of an excimer laser (193 nm, Lambda Physik, Göttingen, Germany). The microchannel pattern (Figure VI-3) was drilled by translation of the *xy*-table, moving the sample during irradiation. The depth of the microchannel was adjusted by setting the speed of the *xy*-table. At the ends of the microchannel, reservoirs were made by static laser shootings that drilled the PET sheet right through. The MTEC device was obtained by drilling on a single PET sheet several parallel microchannels at a distance d from one to another. The microchannel shape was inspected and the dimensions were controlled using a microscope enabling the measurement of length, width and depth of the structure. After laser ablation, the chip was cleaned with MeOH or isopropanol and dried under nitrogen. The PET substrate

was then laminated to close the structures. Microchannels with two reservoirs at their extremities were obtained. In the lamination process, a thin PET foil coated with a melting adhesive layer of polyethylene (PE) (PET of 25 μm thickness with a 10 μm thick adhesive PE from Morane, Oxon, UK) was rolled onto the PET sheet with a heated roller (130 $^{\circ}\text{C}$ and 3 bars for 3 s). The chip was put at 80 $^{\circ}\text{C}$ for 45-60 min between glass plates to allow adhesion of the lamination layer on the structure. The final V-shaped nozzles were obtained by cutting the microchip (*i.e.* one extremity of the microchannel) with scissors. The microchannel section was $100 \times 40 \mu\text{m}^2$ and the distance d between successive parallel microchannels was 4 or 8 mm. The microchannel length was 1-1.5 cm. For the gravity-controlled flow experiments (“Proof-of-concept” section), a polycarbonate well (diameter $f = 6.5 \text{ mm}$) was fixed at the inlet (*i.e.* reservoir) of each microchannel (Figure VI-3). In the last part of this chapter, the MTEC was inserted in a holder with capillary connections to be operated under controlled-flow. A syringe pump is therefore used to control the infusion flow rate.

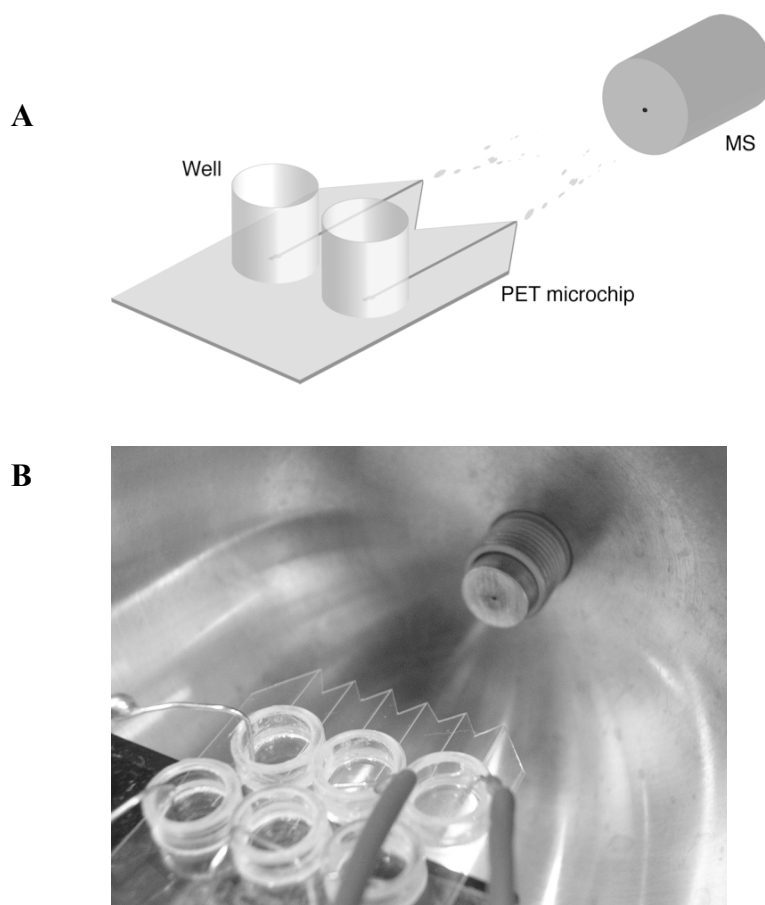


Figure VI- 3 Multi-track electrospray chip. (MTEC). A) Schematic representation of a two-track chip. B) Picture of a MTEC comprising 6 microchannels

Mass spectrometry.

A LCQ DUO ion trap mass spectrometer (Thermo Electron, San José, USA) was used for ESI-MS. The heated capillary was kept at 200 °C. The maximal injection time (IT) is set at 200 ms with 3 micro-scans. The ESI interface was removed and the MTEC was mounted on a plate fixed on the probe slide adapter of the mass spectrometer. The MTEC was centred in front of the mass spectrometer orifice (Figure VI-3). For a chip with an even number of tracks, the microchannels are thus all positioned parallel but off-axis of the mass spectrometer orifice. Samples were loaded (sample volume $V = 50$ nL) in the wells, providing a typical flow rate lower than $100 \text{ nL} \cdot \text{min}^{-1}$.²¹ In each well, a platinum wire electrode was immersed. The high potential (4 kV) was applied to the sample using the mass spectrometer internal voltage. It was switched manually to the following sample using an external source of voltage (4 kV) at time intervals $\Delta t = 30, 15$ or 6 s. After another Δt , the next serial electrospraying was achieved using the mass spectrometer internal voltage again, *etc.* The distance from the outlet of the microchannel to the entrance of the mass spectrometer varied between 1.5-2 cm in order to optimize the signal and the trap injection time. Optimization of mass spectrometer parameters was realized on the analyte of interest. Each experiment was repeated and reproduced with different chips.

Under controlled-flow, a flow rate of $250 \text{ nL} \cdot \text{min}^{-1}$ was applied to the channels. The spray voltage (4 kV) can be applied to the embedded carbon electrodes or to the conductive capillary coating (Chapter III). In the last part of this chapter, the voltage switch between each channel is controlled by a LabView interface (Appendix VI-1).

A Micromass LCT ESI-TOF (Waters AG, Baden-Dättwil, Switzerland) was used to test the MTEC with an orthogonal ESI source.

3. Results and Discussions

3.1. Proof-of-concept

3.1.1. Sample screening

3.1.1.1. Two-track microchip

The MTEC was first evaluated in the simple case of a chip comprising two parallel microchannels distant from $d = 8$ mm, which was appropriate to prevent from solution mixing (Figure VI-3.A). Peptide samples were sequentially electrosprayed. Angiotensin III and bradykinin (or Leu-enkephalin) were put in the different reservoirs of the microchannels. The voltage provided by the MS was applied to the first sample (Angiotensin III) during 30 s. While the voltage of the MS was switched to 0 V, an identical voltage was applied with an external source to the second sample (bradykinin or Leu-enkephalin) during 30 s. The switching sequence was repeated ten times (data not shown). The stability and reproducibility of the experiments were demonstrated. The chips were re-used after washing with the spray medium. Protein samples of myoglobin and cytochrome C were successively electrosprayed as described above. The mass spectra were recorded on half a sequence ($\Delta t = 30$ s), one sequence ($2\Delta t = 60$ s) or several sequences of voltage switch in order to split or gather the MS data from each sample (Figure VI-4). The total ion current (TIC) was monitored. It is representative of the voltage switch and traduces the sample ionization efficiencies. Myoglobin was shown to ionize better than cytochrome C during the ESI-MS analysis.

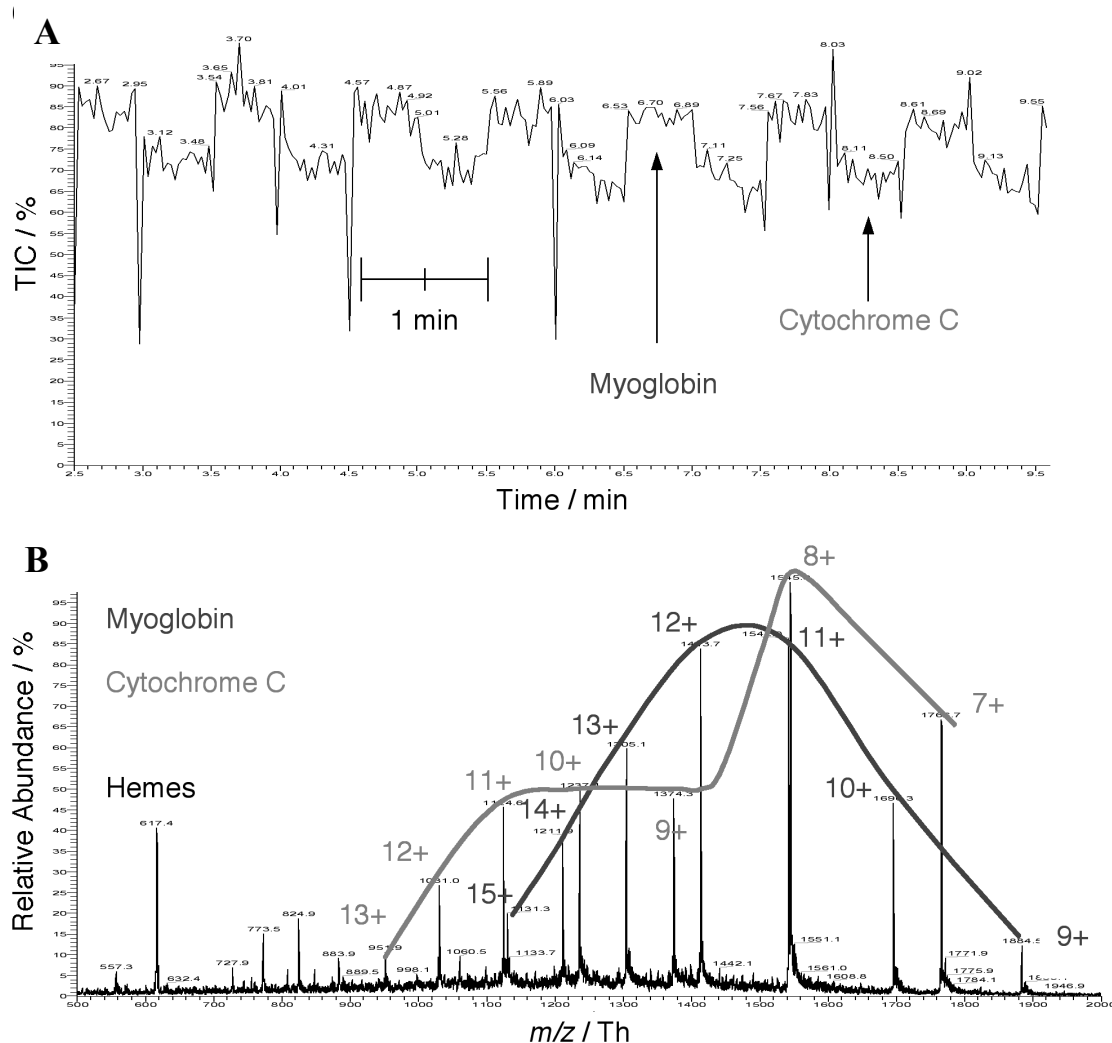


Figure VI-4 A) Total ion current (TIC) and B) cumulative mass spectrum of myoglobin and cytochrome C. The average cumulative mass spectrum was obtained by integration of the scans on 8 min. Each switch was done after $\Delta t = 30$ s. The TIC signal clearly shows the difference in ionization efficiency of the two proteins.

3.1.1.2. Six-track microchip

A MTEC emitter with six microchannels was microfabricated (Figure VI-3.B) and tested with peptide samples (Figure VI-5). No mixing of the sample solutions was detected although d was decreased to 4 mm. Solutions of KCTCCA, angiotensin III, Leu-enkephalin, angiotensin I, Keratin K18 and bradykinin were placed respectively in the six microchannel reservoirs and sequentially electrosprayed by successive application of the voltage (from the mass spectrometer or the external source). The TIC was recorded during 12 min. The superposition of the mass spectra shown in Figure VI-5.B demonstrates that the MTEC device allows rapid screening of all six samples.

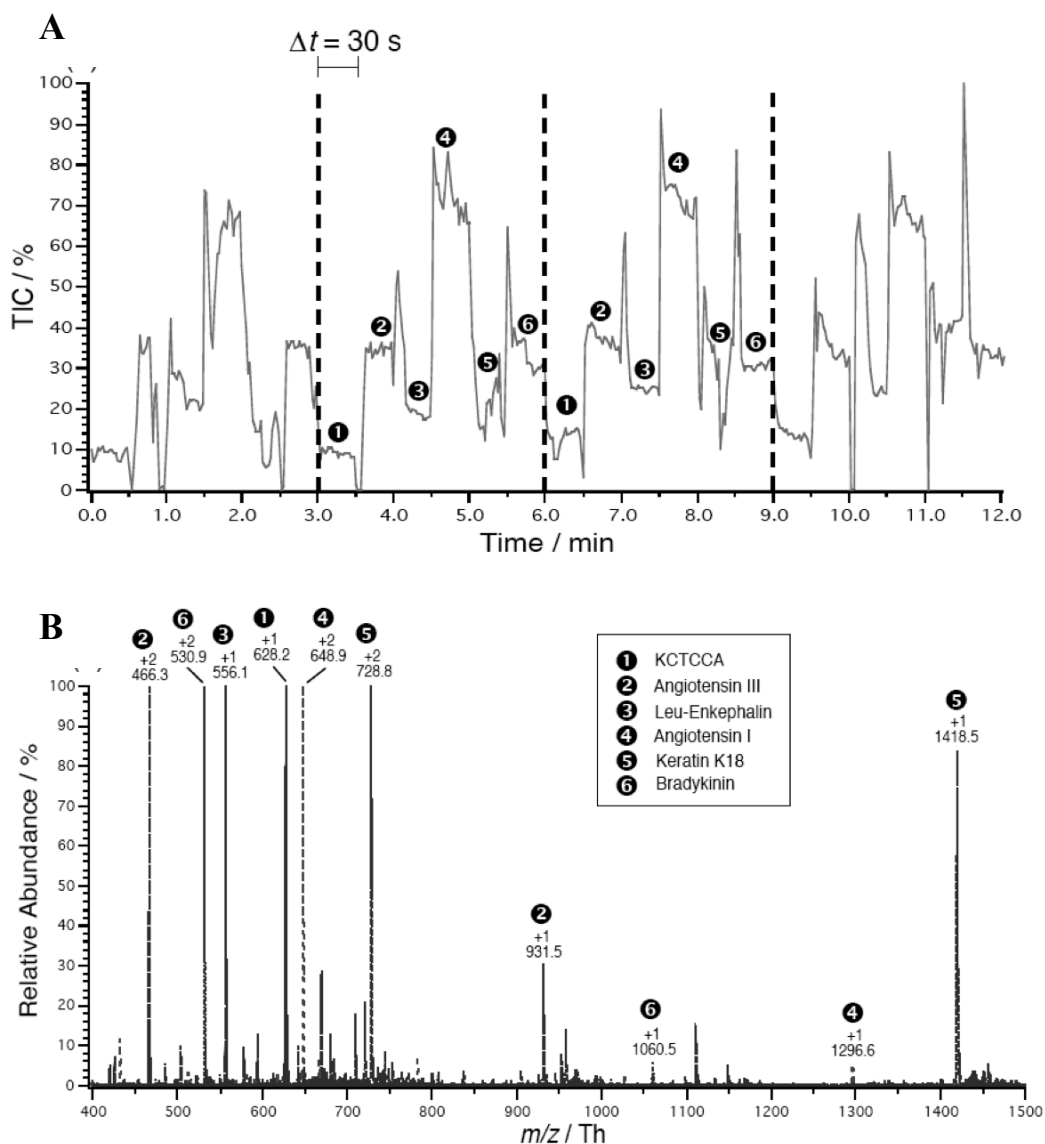


Figure VI- 5 Screening of KCTCCA (①), angiotensin III (②), Leu-enkephalin (③), angiotensin I (④), keratin K18 (⑤) and bradykinin (⑥) performed successively with a six-track microchip. Each sample was analysed during 30 s. A) Total ion current signal on 12 min corresponding to four screening sequence of the six samples. B) Superposed mass spectra of the six compounds.

A rapid screening of samples was performed using the MTEC device. This multi-microchannel chip is used without alignment of the microchannel nozzles with the orifice of the mass spectrometer. Therefore, there is no requirement of a 3D stage during the experiment. The efficiency of the ESI was shown to vary according to the position of the microchannel from the axis of the MS orifice. The MS analysis (*i.e.* the electrospraying of the solution) was achieved up to 15 mm from the axis. This study demonstrates that the MTEC can be used to introduce an internal mass calibrant. In TOF- or FTICR-MS, the MTEC set-up can thus be advantageously employed to achieve high mass measurement accuracy.

3.1.2. Counting of cysteine residues in peptides.

The MTEC was further used for the counting of cysteines in peptides. 1,4-Benzoquinone was employed as reagent to chemically label the cysteines of KCTCCA in the ESI medium.¹⁹ After complete derivatization, a two-track chip ($d = 8$ mm) was positioned in front of the mass spectrometer (Figure VI-3.A). One reservoir was filled with the KCTCCA solution and the second with the labelled peptide at the same concentration (50 μ M). The solutions were electrosprayed successively (Figure VI-6.A). The collection of mass scans on a selected time window gives access to the peptide, the tagged peptide or both (Figure VI-6.C, 6.D and 6.B respectively). When monitoring the whole sequence ($2\Delta t$), the number of cysteines in the peptide can be easily determined (Figure VI-6.B). From the mass of the peptide to that of the tagged peptide, the number of mass shifts due to the tag enables the counting of cysteine residues.²² In addition, the TIC signal clearly indicates that the quinone-tagged KCTCCA ionizes slightly better than KCTCCA (Figure VI-6.A). This tag-induced ionization effect has been already observed in the case of β -lactoglobulin A.²³ The voltage switch interval Δt was reduced from 30 s to 15 s and 6 s (Figure VI-6.A). When switching every 6 s, the analysis of both samples was still perfectly achieved (Figure VI-6.C-D).

Moreover, the MTEC device serves for counting of specific amino acid residue. The counting of cysteines in a peptide was demonstrated. Although the technique requires a separation of the initial sample, the information provided by the knowledge of the content of a rare amino acid like cysteine was shown to improve protein identification by constraining the data base search during peptide mass fingerprinting.^{22, 24, 25} Using the MTEC, the sample is rapidly

(few seconds) compared to its tagged analogues by switching the voltage. By comparison of the two mass signals, the amino acid content is assessed through the detected mass shift. The counting strategy may therefore be applied to the counting of many other amino acids when quantitatively and specifically modified by a mass tag.^{19, 26, 27} By extension to synthetic chemistry, these data highlight the potential of the MTEC for the high throughput screening of reactions in solutions.

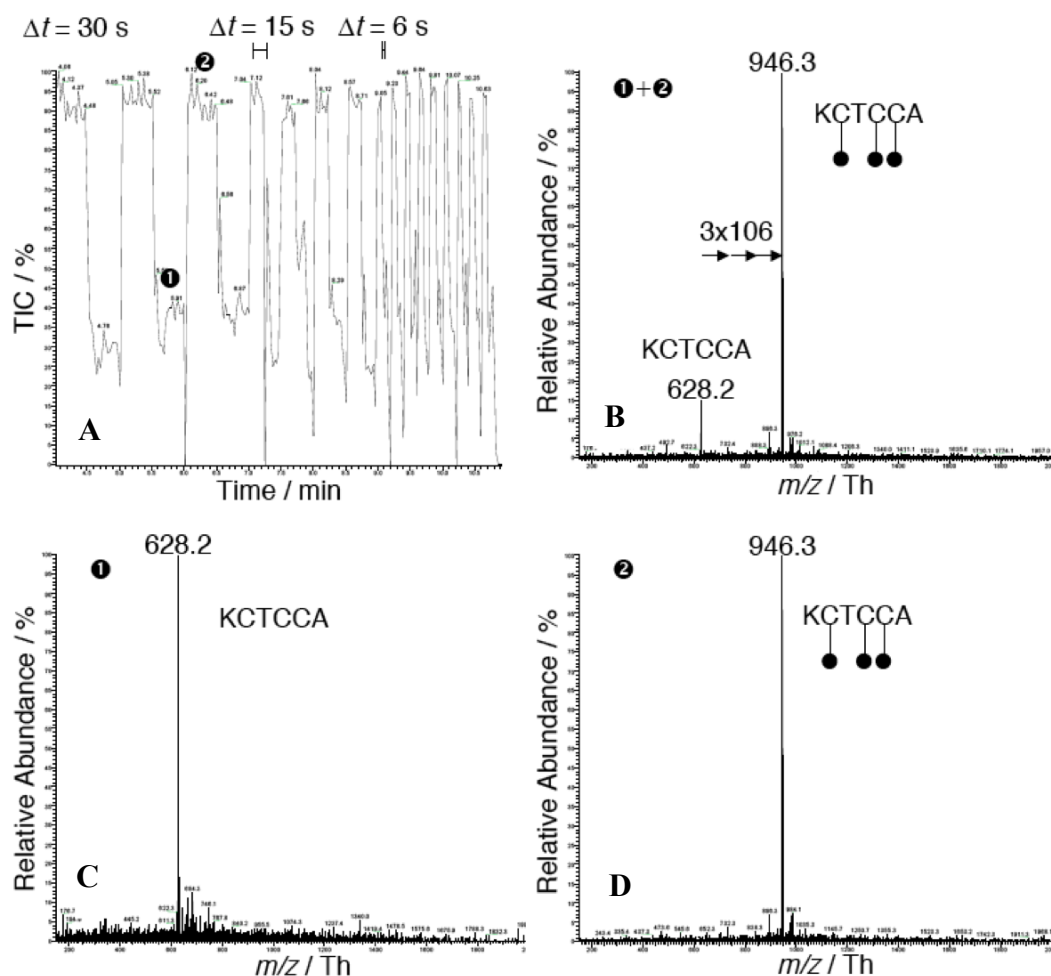


Figure VI- 6 Two-track electrospraying of KCTCCA and its cysteinyl-tagged analogue. A) Total ion current signal with decreasing switch time interval Δt . B) Mass spectrum of both species (①+②) averaged on 12 s ($\Delta t = 6$ s). C) Mass spectrum of KCTCCA (①), averaged on 6 s. D) Mass spectrum of cysteinyl-tagged KCTCCA (②), averaged on 6 s.

Lastly, the voltage switch was reduced to 6 s, still allowing a valuable analysis of the samples. The decrease of the analysis time offers an enhancement of the dynamic potential of the MTEC. However, the switching time interval remains too large at present for the

accumulation of two ion populations in the trap of a mass spectrometer. A.I. Nepomuceno *et al.* accomplished accumulation of the analyte and the internal calibrant by decreasing the switching time to 50 ms.¹¹

3.1.3. Relative quantification

The two-track chip (Figure VI-3.A) was used to electrospray two KCTCCA samples at different concentrations. When using the two-track version of the MTEC, both the symmetric microchannels were located at equal distance from the axis of the mass spectrometer orifice, providing identical spraying conditions. Experiments with two samples of KCTCCA at 12.5 μM / 50 μM , 25 μM / 50 μM and 50 μM / 50 μM were carried out. The MS data provides the relative quantification of the samples (Figure VI-7). The ion count (IC) relative to KCTCCA and its mass peak intensity traduce the relative amount of the peptide in the sample. For 12.5 μM / 50 μM (theoretical ratio of 0.25) the averaged mass peak intensity ratio of the two samples is 0.22 (Figure VI.7-C) while it is 0.52 for 25 μM / 50 μM (theoretical ratio of 0.5) (Figure VI.7-B). The control experiment with KCTCCA at 50 μM / 50 μM confirms an equivalent ESI efficiency in both the microchannels (Figure VI.7-A); the averaged peak intensity ratio of the two identical samples is 0.94 (theoretical ratio of 1). These data were confirmed by a series of measurements with angiotensin III (data not shown).

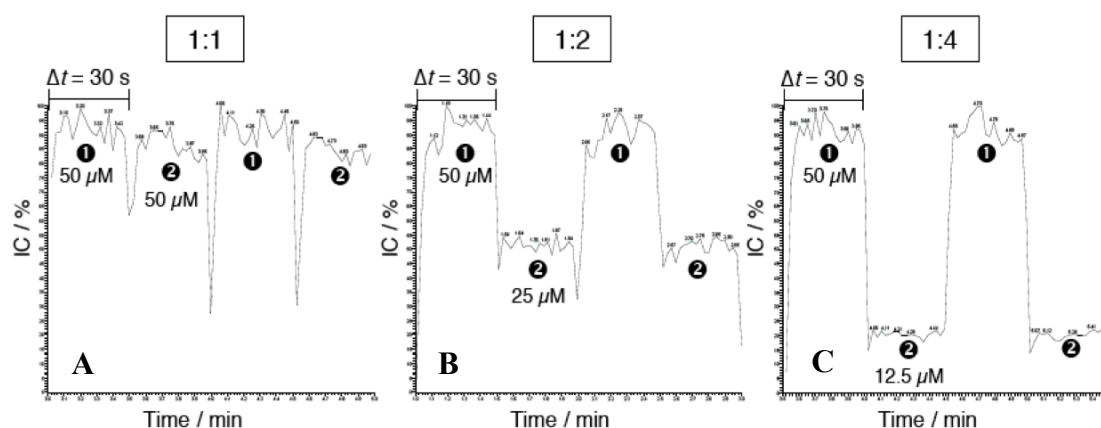


Figure VI- 7 Relative quantification of KCTCCA in two samples using a two-track microchip. A) Ion count (IC) signal at $m/z = 628.2$ Th for KCTCCA 50 μM (●) and 50 μM (●) (ratio of 1). B) IC signal at $m/z = 628.2$ Th for KCTCCA 25 μM (●) and 50 μM (●) (ratio of 0.5). C) IC signal at $m/z = 628.2$ Th for KCTCCA 12.5 μM (●) and 50 μM (●) (ratio of 0.25).

Another remarkable result obtained with the MTEC concerns the direct comparison of ionization efficiency of molecules and the relative quantification of samples. When a symmetric chip is used (*i.e.* when sample solutions are electrosprayed at a symmetric position from the axis of the MS orifice), the relative ionization efficiency of two samples can be probed. All results clearly show that the IC signal varies according to the sample. Besides, the separation of the flow stream of the analytes prevents from preferential ionization and subsequent signal suppression of certain molecules as well as difference in concentration and various electrospraying conditions.²⁸ When two samples ionize similarly (for example, the same peptide but at a different concentration), the relative quantification is directly achieved by comparison of the IC or the mass peak intensities of the two samples on the averaged mass spectra. The relative quantification of KCTCCA samples was clearly demonstrated. These results are very promising for the development of micro total analysis system (μ TAS) for the evaluation of up- and down-regulation of proteins.²⁹

3.2. Latest developments on the MTEC

Further developments concerning the automation of the voltage switching between each track were done. A switching box was configured in order to alternate the applied voltage sequentially from one channel to another (up to 8 tracks are configurable). The general setup is illustrated in Figure VI-8. The minimal switching time is 254 ms (time required for a software code loop execution) and up to the infinity. It is important to precise that the maximal injection time of the MS was set at 200 ms. The elapsed time of an analysis with the LCQ Ion Trap is around 1.6 s. The analysis time can be a limiting factor in the present experiment if the switching time is too fast (< 1 s) compared to the analysis time.

Another setup improvement concerns the control of the flow in the microchannel by the use of capillary connections. A holder with six microfluidic connections was designed with an inter-channel distance of 4 mm. In the experiments detailed below, the sample delivery was fixed at $250 \text{ nL} \cdot \text{min}^{-1}$ for each track, and applied continuously during the entire analysis. The voltage was set at 4 kV and applied to either the silver capillary coating or the embedded carbon electrode (see Chapter III).

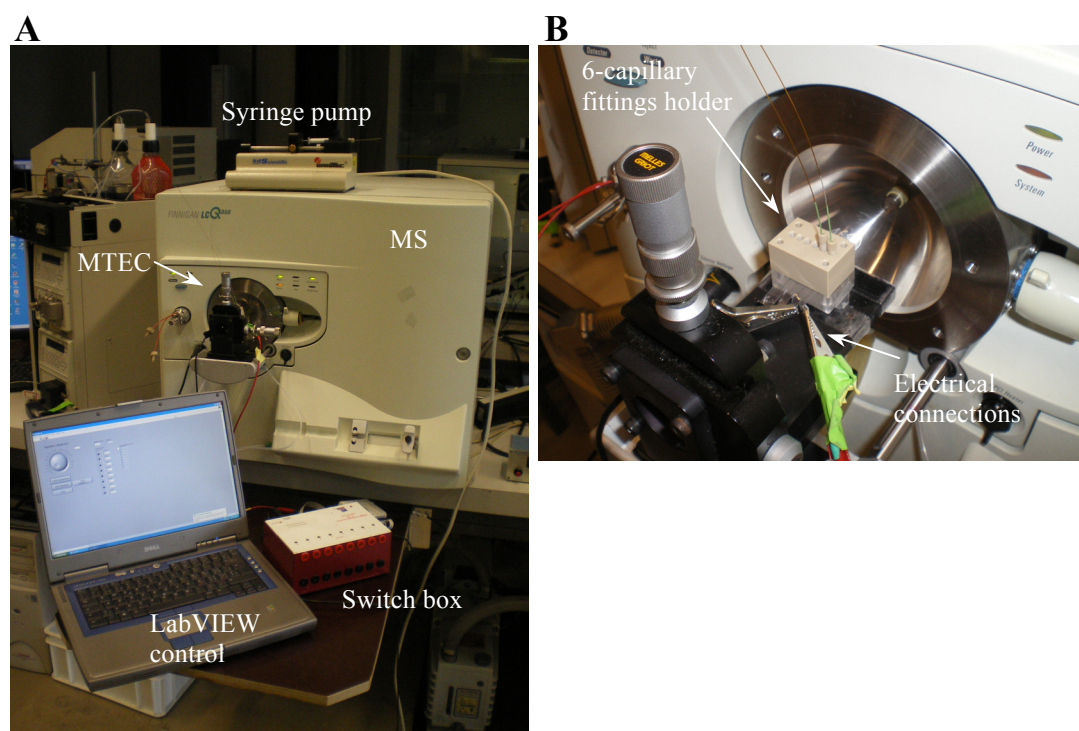


Figure VI- 8 A) General setup of the automated MTEC with a 8-channel switch box with LabView control. B) The MTEC is operated under controlled flow. The chip is inserted in a holder with capillary connections and positioned in a fixed position in front of the MS inlet.

First, the switch box was tested with a microchip composed of two microchannels fed with different peptide solution (KCTCCA 50 μM and Angiotensin III 50 μM in spray medium). The two channels were aligned symmetrically and off-axis with respect to the MS inlet and maintain at the same position during the entire analysis. Every 2 minutes of monitoring, the switch time was decreased starting from $\Delta t = 10$ s and down to $\Delta t = 0.5$ s. From $10 \text{ s} > \Delta t > 2$ s, the spray is stable as shown in Figure VI-9. For switch times equal or lower than 1 s, it is more difficult to maintain a continuous spray between switching. The ion counts detected are then lower. This is likely due to the delay to establish a stable electrospray, the trap infusion time and the analysis time inherent of the mass spectrometer.

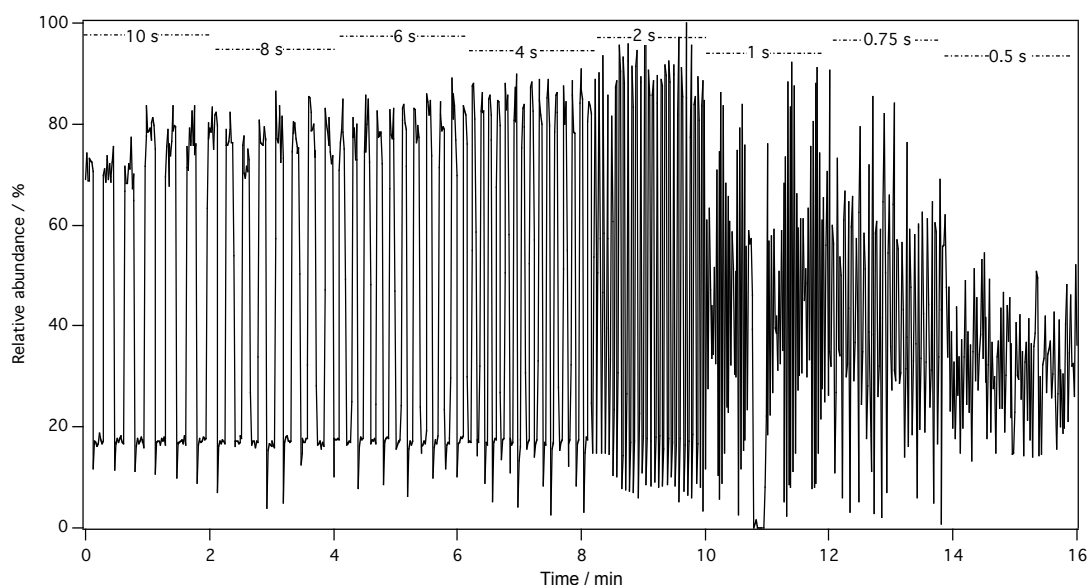


Figure VI-9 Total ion current signal with decreasing switch time interval Δt (1: KCTCCA 50 μ M, 2: Angiotensin III 50 μ M in MeOH:H₂O:AcOH 50:49:1).

Finally, the MTEC was evaluated in front of an orthogonal ESI source, such as the one of the ESI-TOF mass spectrometer (Figure VI-10.A). A great application of the MTEC concerns the infusion of an internal calibrant in parallel to the sample of interest to achieve higher mass accuracy measurements. In Figure VI-10.B, the stability of the spray was evaluated over a range of emitter – MS inlet distance. The distance indicated in the figure corresponds to the distance from an initial emitter position fixed at $d_0 = 1$ cm from the MS inlet (*i.e.* minimal distance at which a spray is observed). Then, the emitter was moved at a distance d with respect to the d_0 position. Over a distance of 3 – 4 mm, the TIC recorded is almost constant. As the microchannels are spaced by 4 mm, with such an ESI source, two channels can be easily used, in a fixed manner, in order to infuse a calibrant or to analyze two samples in parallel without any apparent effect of the sprayer position.

The switch box therefore simplifies considerably the operation of the MTEC device enabling to easily decrease the switch time under the second.

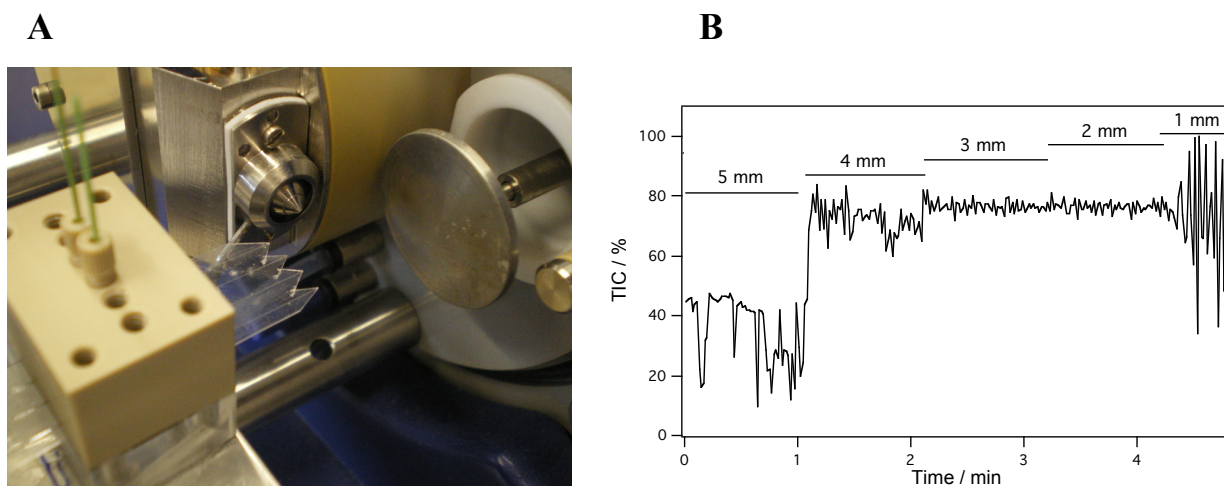


Figure VI- 10 MTEC in front of a 90° - electrospray source of a TOF mass spectrometer. A) General setup. B) Influence of the emitter – MS inlet distance (d) on the TIC. The emitter is moved from the indicated distance respect to the initial position at $d_0 = 1$ cm.

4. Conclusions

The MTEC is constituted of an array of parallel microchannels that operate sequentially as ESI emitters. Its microfabrication is relatively cheap and fast. The drilling/design of a MTEC with six microchannels lasts 20 min. The lamination and curing steps are batch processed (~60 min). The device is highly reproducible and robust. The advantage of such a technology is that it allows the screening of samples in a very short time. As the ESI can occur out from the axis of the mass spectrometer, there is no requirement to move the MTEC in front of the apparatus when switching the voltage (*i.e.* the sample). Moreover, the device is set to offer multiple applications: internal mass calibration, reaction evaluation (*e.g.* the counting of cysteine residues in biomolecules), ionization efficiency probing and relative quantification of analyte.

The ultimate developments of the MTEC include the embedding of electrodes in the microchannels and operation under controlled flow conditions.²⁰ The decrease of the voltage switching time down to 1 s was easily assessed with the automated switch. The study of gas phase chemistry is a nice perspective for the MTEC. However, the voltage switching time has to be compatible with the injection time of the mass spectrometer. Indeed, both ions coming from the different tracks must be captured at the same time in the trap (*i.e.* the switching time must be lower than the injection time in the trap). Another great application would be to couple the device with liquid chromatography that was already assessed with a single emitter microchip (Chapter IV) and then to compare two parallel LC/MS analysis.

The implementation of differential functionalization of the MTEC channels to screen a biological sample followed by an on-line mass spectrometric detection could benefit of such a flexible system. As example the microchannels can be functionalized with different type of antibodies to evaluate the presence or not of given antigens in a biological sample.

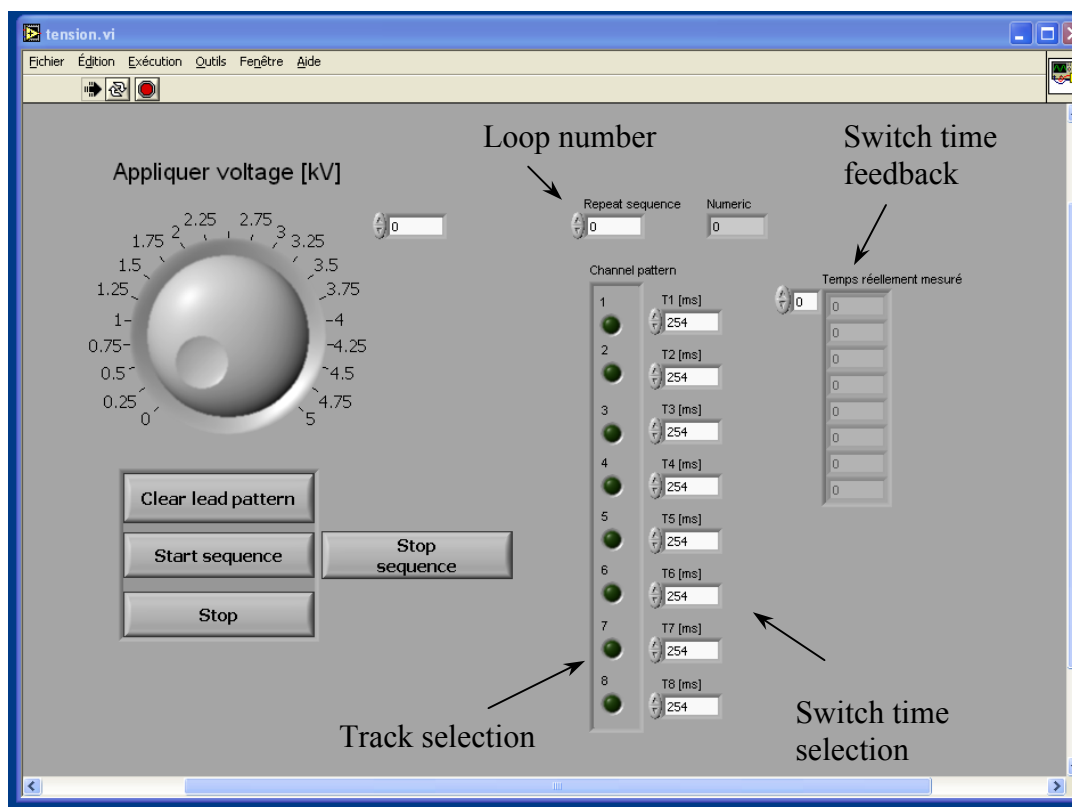
Finally, it would be interesting to investigate the MTEC as a tool to deposit differently charged polyelectrolytes onto a conductive substrate to make multi-layer films. Typically, the 2-track device can be use both in positive (track 1) and negative (track 2) ionization mode in order to assemble successively layer-by-layer positively and negatively charged polyelectrolytes, without any cross-contamination. Obviously, in this specific application, the translation and alignment of the substrate, easy with a controlled translation stage, is mandatory to obtain homogeneous multi-layers.^{30, 31}

REFERENCES

1. N. Lion, T. C. Rohner, L. Dayon, I. L. Arnaud, E. Damoc, N. Youhnovski, Z. Y. Wu, C. Roussel, J. Josserand, H. Jensen, J. S. Rossier, M. Przybylski and H. H. Girault, Microfluidic systems in proteomics, *Electrophoresis*, 2003, 24, 3533-3562.
2. G. T. T. Gibson, S. M. Mugo and R. D. Oleschuk, Nanoelectrospray emitters: Trends and perspective, *Mass Spectrometry Reviews*, 2009, DOI 10.1002/mas.20248.
3. T. Sikanen, S. Franssila, T. J. Kauppila, R. Kostianen, T. Kotiaho and R. A. Ketola, Microchip technology in mass spectrometry, *Mass Spectrometry Reviews*, 2009, DOI 10.1002/mas.20238.
4. F. Foret and P. Kusy, Microfluids for multiplexed MS analysis, *Electrophoresis*, 2006, 27, 4877-4887.
5. Q. Xue, F. Foret, Y. M. Dunayevskiy, P. M. Zavracky, N. E. McGruer and B. L. Karger, Multichannel microchip electrospray mass spectrometry, *Anal. Chem.*, 1997, 69, 426-430.
6. H. H. Liu, C. Felten, Q. F. Xue, B. L. Zhang, P. Jedrzejewski, B. L. Karger and F. Foret, Development of multichannel devices with an array of electrospray tips for high-throughput mass spectrometry, *Anal. Chem.*, 2000, 72, 3303-3310.
7. <http://www.advion.com/biosystems/chip-based-nanoelectrospray.php>.
8. J. M. Dethy, B. L. Ackermann, C. Delatour, J. D. Henion and G. A. Schultz, Demonstration of direct bioanalysis of drugs in plasma using nanoelectrospray infusion from a silicon chip coupled with tandem mass spectrometry, *Anal. Chem.*, 2003, 75, 805-811.
9. G. A. Schultz, T. N. Corso, S. J. Prosser and S. Zhang, A fully integrated monolithic microchip electrospray device for mass spectrometry, *Anal. Chem.*, 2000, 72, 4058-4063.
10. Y. Satomi, Y. Kudo, K. Sasaki, T. Hase and T. Takao, Accurate mass measurement in nanoelectrospray ionization mass spectrometry by alternate switching of high voltage between sample and reference sprayers, *Rapid Communications in Mass Spectrometry*, 2005, 19, 540-546.
11. A. I. Nepomuceno, D. C. Muddiman, H. R. Bergen Iii, J. R. Craighead, M. J. Burke, P. E. Caskey and J. A. Allan, Dual electrospray ionization source for confident generation of accurate mass tags using liquid chromatography Fourier transform ion cyclotron resonance mass spectrometry, *Anal. Chem.*, 2003, 75, 3411-3418.
12. F. Zhou, W. Shui, Y. Lu, P. Yang and Y. Guo, High accuracy mass measurement of peptides with internal calibration using a dual electrospray ionization sprayer system for protein identification, *Rapid Communications in Mass Spectrometry*, 2002, 16, 505-511.
13. J. C. Wolff, C. Eckers, A. B. Sage, K. Giles and R. Bateman, Accurate mass liquid chromatography/mass spectrometry on quadrupole orthogonal acceleration time-of-flight mass analyzers using switching between separate sample and reference sprays. 2. Applications using the dual-electrospray ion source, *Anal. Chem.*, 2001, 73, 2605-2612.
14. Y. Xia, X. R. Liang and S. A. McLuckey, Pulsed dual electrospray ionization for ion/ion reactions, *J. Am. Soc. Mass Spectrom.*, 2005, 16, 1750-1756.
15. N. Lion, Ecole Polytechnique Fédérale de Lausanne, 2006.
16. Y. R. Chen, M. C. Tseng and G. R. Her, Design and performance of a low-flow capillary electrophoresis-electrospray-mass spectrometry interface using an emitter with dual beveled edge, *Electrophoresis*, 2005, 26, 1376-1382.
17. R. Srinivasan and V. Maynebant, Self-developing photoetching of poly(ethylene-terephthalate) films by far ultraviolet excimer laser-radiation, *Appl. Phys. Lett.*, 1982, 41, 576-578.
18. M. A. Roberts, J. S. Rossier, P. Bercier and H. Girault, UV laser machined polymer substrates for the development of microdiagnostic systems, *Anal. Chem.*, 1997, 69, 2035-2042.
19. L. Dayon, Ecole Polytechnique Fédérale de Lausanne, 2006.
20. T. C. Rohner, J. S. Rossier and H. H. Girault, Polymer microspray with an integrated thick-film microelectrode, *Anal. Chem.*, 2001, 73, 5353-5357.

21. P. Morier, C. Vollet, P. E. Michel, F. Reymond and J. S. Rossier, Gravity-induced convective flow in microfluidic systems: Electrochemical characterization and application to enzyme-linked immunosorbent assay tests, *Electrophoresis*, 2004, 25, 3761-3768.
22. L. Dayon, C. Roussel, M. Prudent, N. Lion and H. H. Girault, On-line counting of cysteine residues in peptides during electrospray ionization by electrogenerated tags and their application to protein identification, *Electrophoresis*, 2005, 26, 238-247.
23. L. Dayon, C. Roussel and H. H. Girault, Probing cysteine reactivity in proteins by mass spectrometric EC-tagging, *J. Proteome Res.*, 2006, 5, 793-800.
24. S. Sechi and B. T. Chait, Modification of cysteine residues by alkylation. A tool in peptide mapping and protein identification, *Anal. Chem.*, 1998, 70, 5150-5158.
25. D. R. Goodlett, J. E. Bruce, G. A. Anderson, B. Rist, L. Pasa-Tolic, O. Fiehn, R. D. Smith and R. Aebersold, Protein identification with a single accurate mass of a cysteine-containing peptide and constrained database searching, *Anal. Chem.*, 2000, 72, 1112-1118.
26. H. Mirzaei and F. Regnier, Structure specific chromatographic selection in targeted proteomics, *J. Chromatogr. B*, 2005, 817, 23-34.
27. A. Leitner and W. Lindner, Current chemical tagging strategies for proteome analysis by mass spectrometry, *J. Chromatogr. B*, 2004, 813, 1-26.
28. N. B. Cech and C. G. Enke, Practical implications of some recent studies in electrospray ionization fundamentals, *Mass Spectrom. Rev.*, 2001, 20, 362-387.
29. E. Bonneil, S. Tessier, A. Carrier and P. Thibault, Multiplex multidimensional nanoLC-MS system for targeted proteomic analyses, *Electrophoresis*, 2005, 26, 4575-4589.
30. S. Tan, B. Su, M. Hojeij and H. H. Girault, Porphyrin "Mille-Feuilles" photo-electrodes, *Journal of Electroanalytical Chemistry*, 2008, 621, 322-329.
31. M. Hojeij, B. Su, S. Tan, G. Meriguet and H. H. Girault, Nanoporous photocathode and photoanode made by multilayer assembly of quantum dots, *ACS Nano*, 2008, 2, 984-992.

APPENDIX VI-1: SWITCH BOX LABVIEW INTERFACE



CHAPTER VII.

Membrane desorption electrospray ionization (M-DESI) mass spectrometry

1. Introduction

Since the introduction of desorption electrospray ionization (DESI)³ in 2004, and the direct analysis in real time (DART)⁵ in 2005, this new field, namely “ambient desorption ionization” for mass spectrometric analysis, has developed rapidly. Analyte desorption always accompanies the ionization step and, little or no sample preparation is required. The different ambient desorption ionization techniques have been reviewed recently and are listed in Table VII-1.^{7, 8} They can be classified in two groups, the ESI-related and APCI^a-related techniques. In ESI-related ambient techniques, analytes are first desorbed or sampled from solid or liquid sample and then, transported into the mass spectrometer in evaporating charged solvent droplets. DESI and DeSSI⁹ use solvent spray to desorb/ionize the compounds, while nitrogen gas is used in ND-EESI.¹⁰ These ESI-related methods may include a separate sudden desorption by the use of a laser, as in ELDI,¹¹ LAESI¹² and MALDESI.¹³ Pneumatically-assisted electrosprays are employed to sample liquids directly, as in EESI¹⁴ or FD-ESI.¹⁵ SSP¹⁶ uses a liquid junction created between the probe and the liquid surface. Soluble compounds are then collected by solvent flow, which is subsequently delivered into an electrospray emitter. ESI-related techniques are characterized by a large mass range and complex mass spectra (multi-charged species, adducts and unsolvated

^a APCI is the acronym for “atmospheric pressure chemical ionization”.

aqueous clusters). In APCI-related techniques, gas-phase chemical reactions are used together with a desorption step to ionize condensed-phase analytes directly from surfaces. These methods rely on some form of electrical discharge, whether that is a photoionization method (DAPPI)¹⁷, or dielectric barrier (DBDI)¹⁸, corona (DART, DAPCI, ASAP)^{19,20} or glow (HAPGDI, PADI)^{21,22} discharge. In APTDI,²³ reagents for chemical ionization are produced by heating organic or inorganic salts. APCI-related ionization techniques are typically characterized by ionization of both polar and non-polar small molecules and produce relatively simple mass spectra.

TECHNIQUE	ACRONYM	DATE
Desorption Electrospray Ionization	DESI	2004
Surface Sampling Probe	SSP	2004
Direct Analysis in Real Time	DART	2005
Ambient Solid Analysis Probe	ASAP	2005
Electrospray Laser Desorption/Ionization	ELDI	2005
Fused Droplet Electrospray Ionization	FD-ESI	2005
Desorption Atmospheric Pressure Chemical Ionization	DAPCI	2005
MALDI Assisted Electrospray Ionization	MALDESI	2006
Extractive Electrospray Ionization	EESI	2006
Desorption Sonic Spray Ionization	DeSSI	2006
Helium Atmospheric Pressure Glow Discharge Ionization	HAPGDI	2006
Atmospheric Pressure Thermal Desorption Ionization	APTDI	2006
Plasma-Assisted Desorption/Ionization	PADI	2007
Dielectric Barrier Discharge Ionization	DBDI	2007
Neutral Desorption Extractive Electrospray Ionization	ND-EESI	2007
Laser Ablation Electrospray Ionization	LAESI	2007
Desorption Atmospheric Pressure Photo Ionization	DAPPI	2007
Transmission Mode Desorption Electrospray Ionization	TM-DESI	2008

Table VII- 1 Ambient desorption ionization techniques. Adapted from Ref⁷.

In this chapter, a brief overview of the desorption electrospray ionization (DESI) method is given. Then, a DESI alternative, so-called membrane - desorption electrospray ionization (M-DESI) is introduced enabling to screen rapidly a mesh membrane placed vertically and in-axis between the ESI emitter and the MS inlet. At this stage, preliminary results are shown with a discussion about the actual issues and perspectives of this technique.

2. Desorption electrospray ionization (DESI)

Desorption electrospray ionization was introduced for the first time by Cooks in 2004.³ A typical DESI experiment is illustrated in Figure VII-1 where an electrospray emitter is positioned at a given angle relative to the surface and the mass spectrometer inlet.

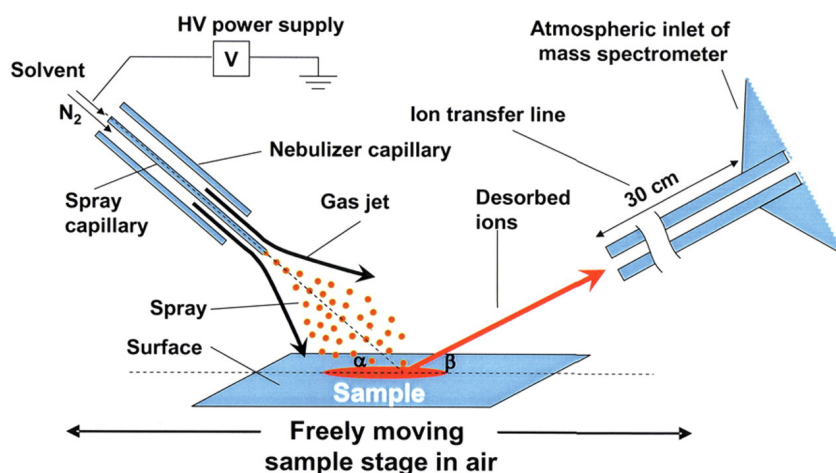


Figure VII- 1 Schematic setup of a DESI MS experiment. The sample solution was deposited and dried onto a PTFE surface, and methanol:water (1:1 containing 1% acetic acid or 0.1% aqueous acetic acid solution) was sprayed at a flow rate from 3 to 15 $\mu\text{l}\cdot\text{min}^{-1}$ under the influence of a high voltage (4 kV). The nominal linear velocity of the nebulizing gas was set to 350 $\text{m}\cdot\text{s}^{-1}$. Reprinted from Ref ⁶.

The signal intensity monitored by MS depends strongly on geometrical parameters, such as the α and β angles in Figure VII-1, the electrospray emitter - surface distance, and the surface - MS inlet distance.

The impact of emitted parent droplets onto the surface has been recently simulated with angles $\alpha = 55^\circ$ and $\beta = 10^\circ$ and, $\alpha = \beta = 90^\circ$, showing that the generation of offspring droplets strongly depends on the spray incidence angle.^{24, 25} Typically, for $\alpha = 55^\circ$, the averaged droplet size was found to be $\approx 1 \mu\text{m}$ at the near-surface region. Further away from the surface (takeoff angle $\gg 10^\circ$), offspring droplets are known to be significantly larger. As a consequence, the best signal intensity in DESI experiments is obtained with the electrospray emitter fixed at an angle $\alpha = 55^\circ$, and the MS inlet at $\beta = 10^\circ$ with respect to the surface.

More recently, an enclosed geometry-independent DESI source has been introduced where $\alpha = \beta = 90^\circ$ (Figure VII.2).⁴ The main advantage of this configuration is the non-dependence of signal strength on the geometry. Moreover, the spectral characteristics are similar to those observed in DESI. It was demonstrated to be a suitable tool for rapid analysis of dried or frozen samples from standard 96-well plates.

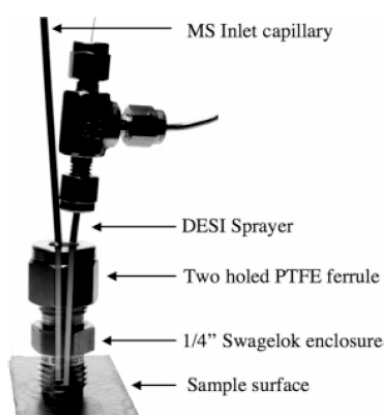


Figure VII- 2 Enclosed desorption electrospray ionization source with a 90° collection angle. The enclosure was simply a stainless $\frac{1}{4}$ -in. Swagelok connector with a custom-made two-holed PTFE ferrule. The enclosure was pressed down firmly on the surface during the combined spray sampling and ionization step. Reprinted from Ref ⁴.

Mechanistic hypothesis.

In DESI, parent charged droplets formed during electrospray present a diameter of less than $10\ \mu\text{m}$ and are directed towards a surface where their impact (or that of the desolvated ions formed from the initial droplets, depending on conditions selected) causes the release of analytes from the surface, in ambient environment.²⁶ Till now all the mechanisms involved in DESI are not well identified and several studies are still going on. Based on experimental results and simulations, two mechanisms were proposed, the “droplet pick-up” mechanisms and gas-phase ionization processes. These two ion formation mechanisms are summarily illustrated in Figure VII-3 where Type I ions are formed by the “gas-phase charge transfer” mechanism, and Type II ions by “droplet pick-up”.

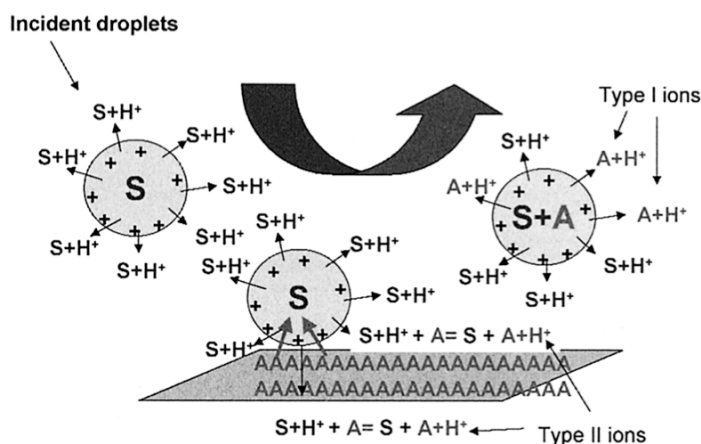


Figure VII- 3 General scheme for two ion formation mechanisms in DESI-MS. Type I ions are formed by charge (e.g., proton) transfer when primary ions or multiply charged incident droplets impact the surface and react with the analyte present at the surface. Type II ions are formed when charged droplets impact the surface, dissolve the analyte, and leave the surface as secondary charged microdroplets, which are desolvated in the mass spectrometer inlet to give gas phase ions. (S) Surface; (A) analyte. Reprinted from Ref ².

According to the “droplet pick-up” hypothesis, surface analytes dissolve or otherwise collect in a localized solvent layer formed by the first droplets. Later-arriving droplets impact this surface solvent-layer and break it up, creating numerous offspring droplets containing the material originating from the solvent layer including the dissolved analytes. Analyte desorption thus occurs by momentum transfer in the form of charged sub- μm droplets that are then, ionized by ESI-mechanism. However, for some analytes such as, cholesterol, carotene or TNT, the ionization mechanisms seem to be different. This set of compounds is preferentially ionized when the potential difference between the sprayer and the surface is set to 2 kV. Charge transfer between solvent ions and analyte molecules then includes the exchange of a proton or an electron between a gas-phase ion and a surface molecule.

Surface characteristics, applications and figures of merit of DESI.

The surface characteristics in terms of chemical composition, porosity, texture, and electrical conductivity was reported to influence DESI analysis.²⁷⁻³¹ The roughness of the surface, in addition to low gas and solvent flow rates, help to avoid the “splashing of solvent” where samples are removed from the surface by the spray. Moreover, the surface must be chosen in function of the physico-chemical properties of the compounds to analyze. For the DESI analysis of small molecules, thin-layer chromatography (TLC) plates, PTFE-printed slides,

porous wafers (pSi) or nano-porous alumina surfaces have been employed.^{28, 32-34} Glass, polymethylmethacrylate (PMMA), polytetrafluoroethylene (PTFE) sheets, stainless steel were widely used for proteins, peptides or small molecules. Moreover, DESI can be applied to both conductive and insulated surfaces. Various applications in imaging studies of surfaces,³⁵⁻³⁷ metabolomic discovery,³⁸⁻⁴⁰ analysis of pharmaceuticals,^{41, 42} polymers,⁴³ proteins/peptides,^{44, 45} bacteria,^{46, 47} explosives,^{19, 48, 49} chemical warfare,^{47, 50-52} forensic^{30, 52-54} established the DESI as a powerful tool in actual ionization techniques. The sensitivity of a DESI analysis coupled to linear ion trap mass spectrometers is typically in the range of low femtomoles for small molecules, as explosives or pharmaceuticals. Furthermore, the studies of biopolymers (peptides or proteins) report similar levels. Great improvements in the reproducibility of quantitative results have also been made, showing RSD < 5%.^{7, 27, 55}

3. Membrane - Desorption Electrospray Ionization (M-DESI)

As mentioned above, the sensitivity of a DESI analysis is strongly geometry-dependent. While in DESI the sample is deposited onto a continuous plane surface placed at given angles with respect to the ESI emitter and MS inlet, we investigated in this chapter, the feasibility to desorb/ionize analytes directly from a membrane positioned vertically and *in-axis* in front of the mass spectrometer inlet, as illustrated in Figure VII-4. The spray incidence angle is therefore reduced to 0°. The desorption efficiency depends on geometrical parameters that are the ‘electrospray emitter – membrane’ and ‘membrane – MS inlet’ distances, as well as on the mesh membrane characteristics (fiber material, mesh size...). The present chapter presents some preliminary results on the M-DESI mass spectrometry method.

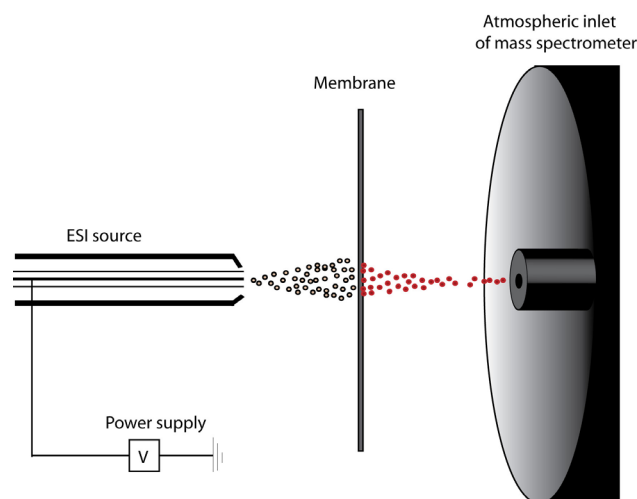


Figure VII- 4 Principle of the M-DESI. The sample is deposited onto a membrane, The membrane is positioned in-axis between the electrospray emitter and the MS inlet. By passing through the membrane, the sprayed solution desorbs/ionizes the sample that is directly analyzed by MS.

Within the same investigation period, Brodbelt's group published an identical desorption technique, so-called *Transmission Mode-DESI* (TM-DESI).^{56, 57} Their investigations are quite similar than those presented in this chapter, with a step forward in the characterization.

3.1. Experimental section

Chemicals.

Angiotensin I triacetate salt (DRVYIHPFHL, > 99%, $M = 1269.5 \text{ g}\cdot\text{mol}^{-1}$), angiotensin III (AVYIHPF, > 99%, $M = 931.1 \text{ g}\cdot\text{mol}^{-1}$), and KCTCCA peptide (70%, $M = 627.8 \text{ g}\cdot\text{mol}^{-1}$) were from Bachem (Budendorf, Switzerland). Cytochrome C from horse heart ($\geq 95\%$) and acetic acid (> 99.5%) were from Fluka (Büchs, Switzerland). Methanol (> 99.8%) was from Riedel-de-Haën (Seelze, Germany). Water (UV-HPLC) was from Panreac Quimica S.A. (Barcelona, Spain). All chemical were used without any further purification.

Sample preparation.

The electrospray solution was MeOH/H₂O/AcOH (50/49/1, v/v/v). The peptides and proteins are diluted either in H₂O or ESI buffer depending on the experiments. The concentrations tested for the peptides and proteins are 10 and 50 μM . The membranes are rinsed with H₂O/MeOH mixtures (50/50, v/v) and allow to dry before use.

Mass spectrometry.

All experiments were performed with a LCQ DUO ion trap mass spectrometer (Thermo Electron, San José, USA). In some experiments, a MS inlet extension (Figure VII-5) was used because of the entrance of the LCQ DUO ion trap that is localized in a cavity. The heated capillary was kept at 200 °C, and the spray voltage at 4 kV. The maximal ion accumulation time was 200 ms and the signal averaging set to 3 microscans. With this instrument, the ESI source can be operated both with a co-axial sheath gas (surrounding the capillary tip in the ESI source) and/or an auxiliary gas (few cm away from the ESI emitter and enables focusing the spray when operated in normal conditions). However, the auxiliary gas was shown to reduce the ESI response in presence of the membrane. Consequently, only the co-axial sheath gas was used in the experiments presented in this chapter.



Figure VII- 5 Picture of the MS inlet extension added to the LCQ ion trap mass spectrometer.

Setup.

The setup is illustrated in Figure VII-6. The membrane is first tightened in a custom-made membrane-holder (Figure VII-6.C). Then, this membrane-holder is fixed in a larger holder, fitting the standard ESI source of the MS, by offering the possibility to move the membrane along the *x*-axis by rotation. In addition, when the membrane holder is not centred with respect to the ESI capillary emitter, it enables to scan the membrane by rotation. The ESI solution is delivered to the ESI source by a capillary with the flow rate controlled by a syringe pump. The voltage is applied by the MS power supply.

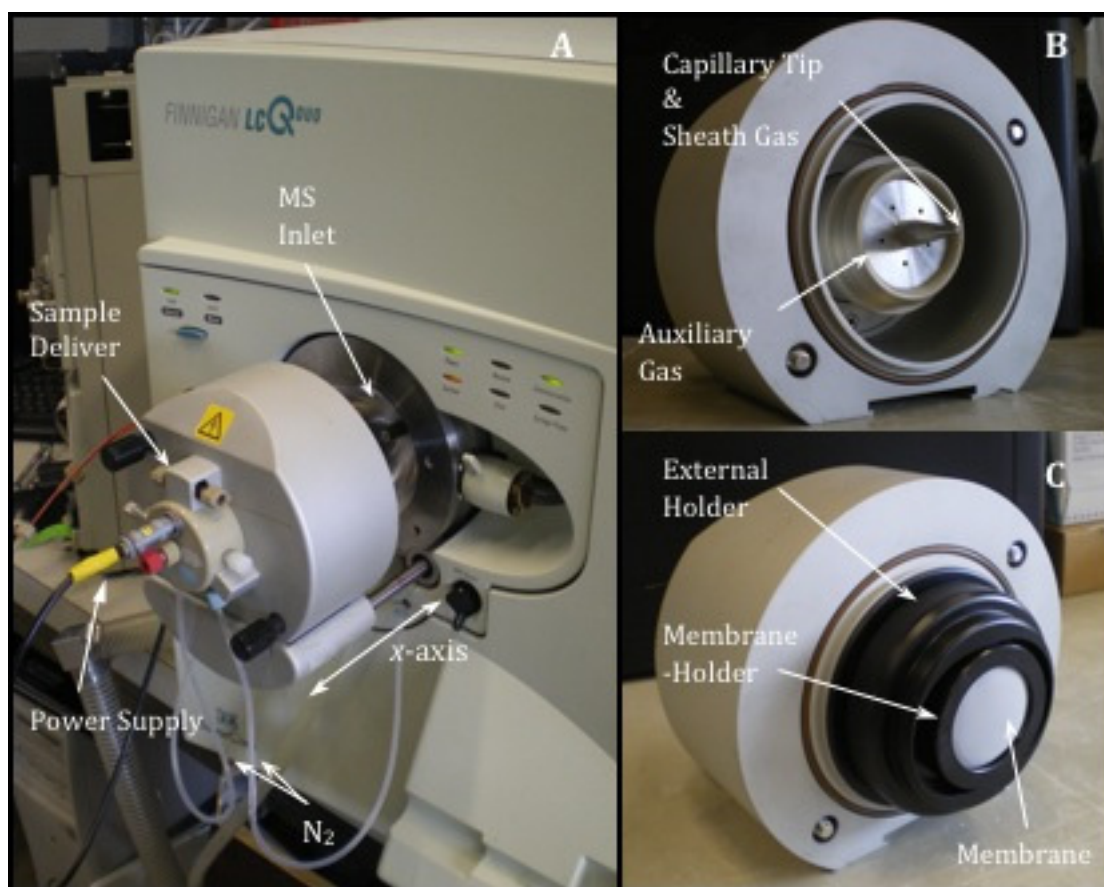


Figure VII- 6 A) General view of the M-DESI setup including the electrospray ionization source with the power supply connection, the capillary for the sample delivery and the nitrogen connections (auxiliary and sheath gas). The ionization source can be moved along the *x*-axis with respect to the MS inlet. B) Electrospray ionization source with the capillary tip and co-axial sheath gas. Around the capillary outlet, 5 outlets for the auxiliary gas enable to focus the spray. C) The membrane is fixed in a custom-made membrane-holder that is then positioned in a larger holder fitting the ESI source. The external holder can be extended along the *x*-axis by rotation.

Mesh membrane (or tissue) considerations.

In the first set of experiments, a cleaning lens tissue from Kodak was used as membrane because of its large open area. However, as its characteristics were not known, rapidly we switched to commercial mesh tissues.

Open mesh tissues were kindly provided by Sefar (Heiden, Switzerland). As illustrated in Figure VII-7, the tissues are characterized by the fiber material, the mesh opening (w), the yarn diameter (d), and the open area (a_0) that characterizes the permeability to the air of the membrane.

The open area is defined as:

$$a_0 [\%] = \frac{w^2 \times 100}{(w + d)^2} \quad (1)$$

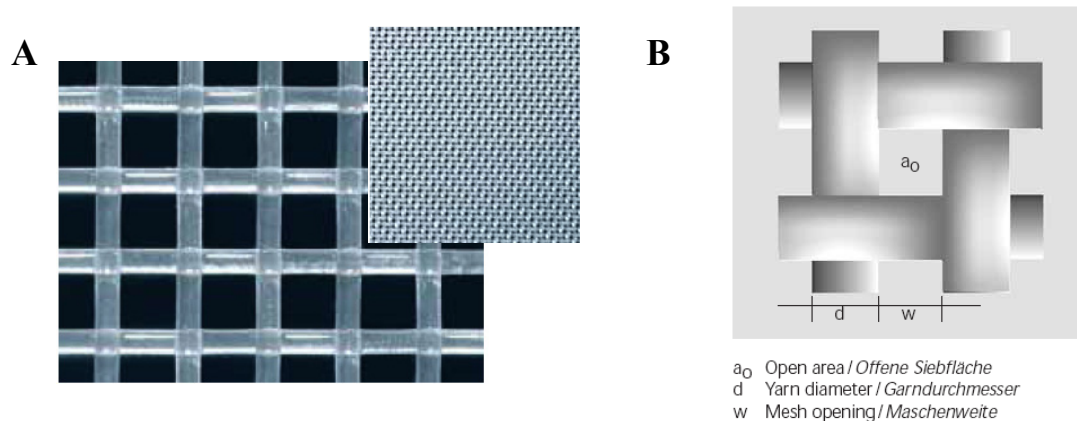


Figure VII- 7 A) Open mesh membrane. B) Geometrical parameters of the mesh. Reprinted from ¹.

Membrane properties.

An important consideration of the M-DESI concerns the tissue properties, and particularly its resistance to acid, base and solvents. Various fiber materials are available and made of polyamide (PA 6.6 and PA 6, *i.e.* nylon), polyethylene terephthalate (PET), ethylene monochlor trifluor ethylene (E-CTFE) and ethylene tetrafluor ethylene (ETFE). Their properties are listed in Table VII.2. E-CTFE and ETFE fibers are similar to PTFE (or Teflon) that is a material often used as surface in standard DESI-MS experiments. Obviously, the solution in which samples are suspended and deposited onto the

membrane, as well as the spray solution have to be chosen according to the membrane characteristics. Typically, when the membrane is hydrophilic, if a well-concentrated spot is desired, the sample would need to be suspended in a sufficiently apolar solvent.

MATERIAL PROPERTIES	<i>Unit</i>	PA 6.6	PA 6	PET	E-CTFE	ETFE
Specific gravity	<i>g/mm³</i>	1.14	1.14	1.38	1.69	1.75
Tensile strength	<i>daN/mm²</i>	41-67	41-67	45-75	28	40-50
Relative strength at wet conditions	%	85-90	85-90	100	100	100
Elongation at break	%	20-35	20-60	15-30	25	25
Moisture absorption at 20°C/65% r.h.	%	3.5-4	3.5-4.5	0.4	0.1	0
Working temperature dr	°C	115	115	150	140	150
Stability to light		poor	poor	poor	good	good
Abrasion resistance		good	good	limited	limited	good
Acid resistance		limited-poor	limited-poor	good	good	good
Alcaline resistance		good	good	limited	good	good
Stability to solvents		limited	good	good	good	good
Hydrolysis resistance		good	good	limited	good	good

Table VII- 2 Properties of the fiber materials. PA (Polyamide), PET (polyethylene terephthalate), E-CTFE (ethylene monochlor trifluor ethylene), and ETFE (ethylene tetrafluor ethylene). Adapted from Ref ¹.

The membranes kindly provided by Sefar are listed in Table VII.3 and some of them were used in this study. Membranes made of PET exist with approximate mesh openings of 10, 50, 100 and 250 μm , and were used for the majority of the characterization experiments.

	Mesh opening (w)	Open area (%)
PA 6.6	10	3
	100	32
PA 6	500	38
PET	10	2
	54	24
	100	32
	250	39
E-CTFE	250	39
ETFE	300	36

Table VII- 3 Characteristics (mesh opening and open area) of the tissues.

3.2. Results and Discussions

3.2.1. M-DESI of proteins and peptides

In order to demonstrate the feasibility to analyze a sample by M-DESI, a protein (cytochrome C) and a peptide (Angioten I) were deposited onto different membranes. As prospective experiment, a cleaning lens tissue (e.g. Kodak tissue) was manually tightened between the electrospray emitter and the MS inlet. Because of the inlet design of our MS, an extension tube of 10 cm long was used (Figure VII-5).

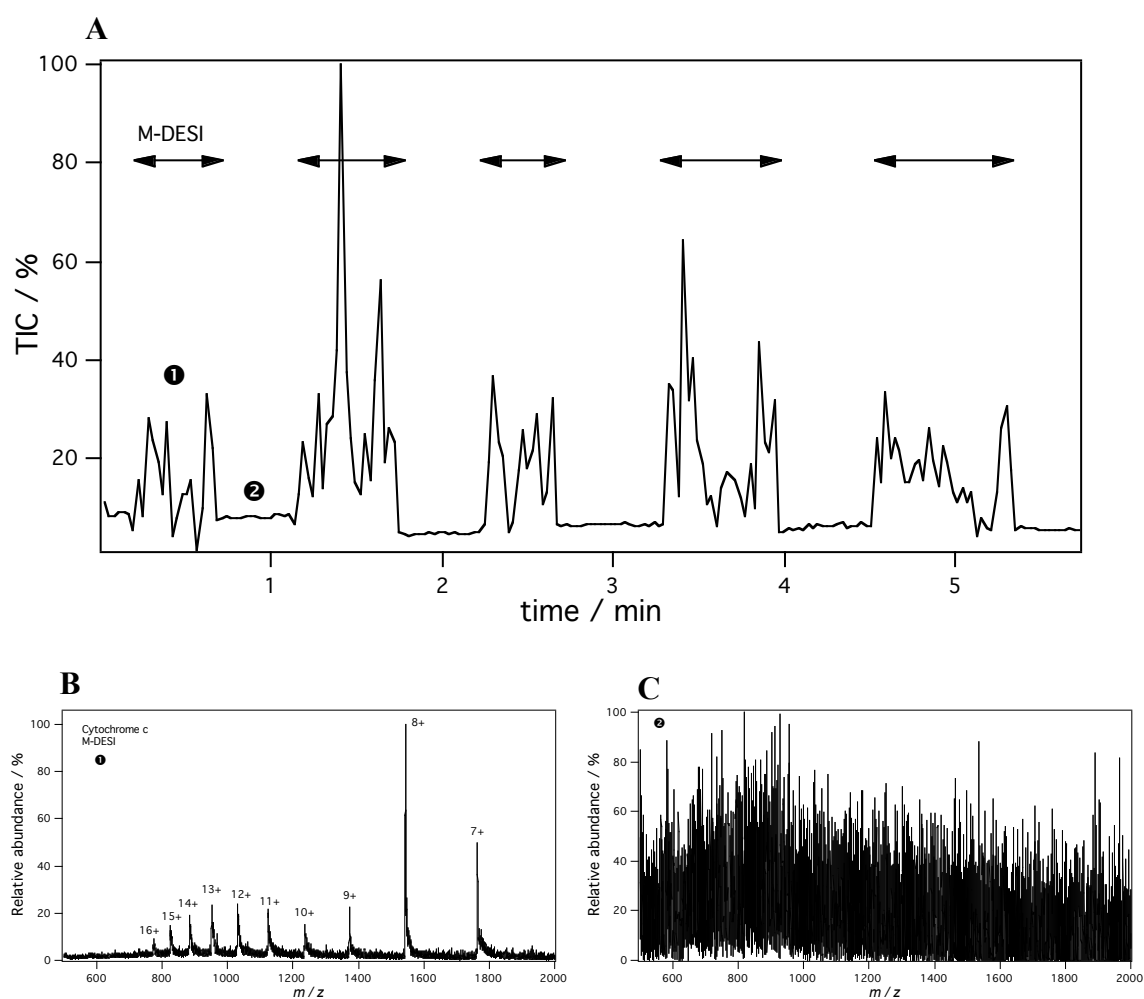


Figure VII- 8 M-DESI mass spectrometry of cytochrome c. A) Total ion current when ① the membrane is in-axis or ② removed. B) Average mass spectra in presence of the membrane. C) Mass spectrum without membrane. 2 μL of cytochrome c ($0.1\text{mg}\cdot\text{mL}^{-1}$ in water) was spotted on a Kodak tissue. Spray voltage: 4 kV. ESI spraying solution: $\text{MeOH}:\text{H}_2\text{O}:\text{AcOH}$ 50:49:1), Sheath gas: 40 a.u..

Figure VII-8 demonstrates the desorption of cytochrome c from a membrane placed between the ESI emitter and the MS inlet extension. The membrane was alternatively positioned in-axis between the ESI emitter and the MS inlet extension and removed. In presence of the membrane with the deposited sample aligned in front of the electrospray emitter, the protein was rapidly desorbed and ionized. Control experiment without the membrane shows a background mass spectrum, proving that the detected cytochrome c was desorbed from the membrane and not provided by the electrospray. In presence of a membrane, the total ion current (TIC) is less stable in comparison to the TIC without membrane. The multiply charged species of cytochrome c suggests that the ionization process during desorption is similar to the electrospray process. This “proof-of-concept” experiment was not optimum because the membrane was held manually and a custom-made extension was used. Indeed, a loss of signal intensity of a factor 10 was measured when using such an extension.

The same experiment was repeated with the Angiotensin I. Figure VII-9 shows average mass spectra obtained from the M-DESI MS analysis. The peptide was efficiently desorbed and mostly observed as singly charged. The signal decay was found to be in the order of few seconds once the membrane is placed in-axis.

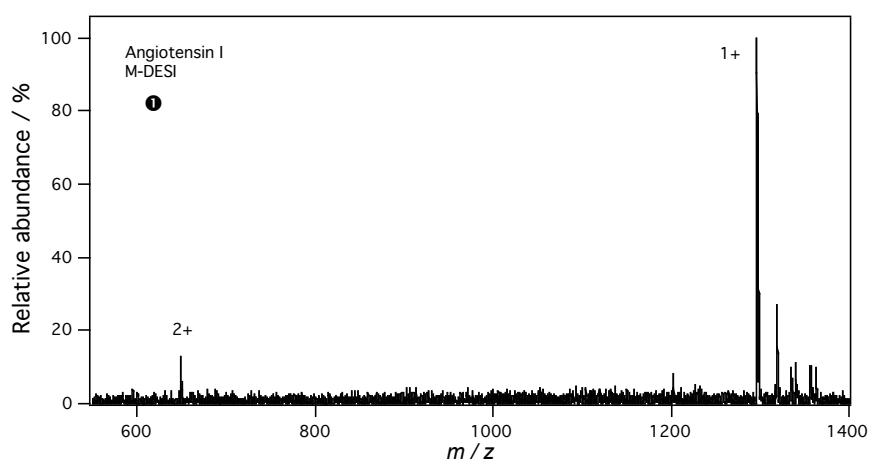


Figure VII- 9 M-DESI of Angiotensin I from a membrane placed in-axis between the ESI emitter and MS inlet extension. 2 μL of Angiotensin I ($0.1 \text{ mg}\cdot\text{mL}^{-1}$ in water) was spotted on a Kodak tissue. Spray voltage: 4 kV. MS buffer: MeOH:H₂O:AcOH 50:49:1). Sheath gas: 40 a.u..

Finally, four different samples (cytochrome c, Myoglobin, Angiotensin I, and KCTCCA) were deposited onto the same membrane that was then, scanned by aligning successively the spots in the electrospray axis. All proteins were successfully analyzed by MS using this M-DESI method. This preliminary work opens the door to the possible screening of samples from a membrane, which can be interesting after separation for instance.

The preliminary experiments described above were performed holding the membrane manually and without knowledge of the open area of the membrane. Obviously, the geometrical positioning was not accurate. In order to control these parameters, two separate holders were designed, one to tighten the membrane, as illustrated in Figure VII-6.C, and the other to fit the ESI source and maintain the membrane-holder complex. The investigations presented below were then achieved using custom-made holder to fix the membrane and without MS inlet extension.

3.2.2. Mesh size and spray transmission

The membranes are defined by their mesh dimensions, as explained in the experimental section of this chapter. The open area a_0 (eqn. 1) of the membrane highly influences the spray transmission. When the open area is small, the sprayed solution cannot pass through the mesh membrane. In contrast, when the open area is too large, the number of fibers on which the sample is allowed to dry is reduced. A compromise has to be found between the surface of the fibers and the open area.

Mesh opening	10 μm	50 μm	100 μm	250 μm
Open area	3%	24%	32%	39%
ESI response (position 1)¹	1%	33%	42%	81%
ESI response (position 2)²	17%	49%	52%	89%

¹ The ESI response was calculated as the average from 3 replicate analyses divided by the response of a standard ESI experiment, i.e. without membrane. Position 1: capillary tip - membrane distance = 15 mm

² Position 2: capillary tip - membrane distance = 5 mm

Table VII- 4 Influence of the mesh opening on the spray transmission through the membrane.

The spray transmission through membranes of different open area is presented in Table VII-4. A solution of Angiotensin III (10 μM in ESI solution) was sprayed through the membranes at a flow rate of 4 $\mu\text{L}\cdot\text{min}^{-1}$, a voltage of 4 kV, a sheath gas of 40 a.u., and with the ESI source closed. The spray transmission was normalized with the ESI response obtained without membrane. Two distances between the membrane and the ESI emitter, *i.e.* 5 mm and 15 mm were tested, corresponding to position 2 and 1, respectively. As the ESI source was closed in this experiment, the membrane - MS inlet distance also changed, from 13 to 3 mm for position 2 and 1, respectively. When the open area of the membrane decreases, the spray transmission becomes more difficult. As example, in position 2 only 17% of the sprayed solution passes through the 10 μm -membrane while 89% transmission was obtained for the 250 μm -membrane. The observed signal loss can be attributed to the sample adsorption onto the membrane. In addition, when comparing the results between position 1 and 2, the MS signal was higher when the membrane was closer to the ESI emitter.

The membrane with an open mesh of 100 μm was taken as reference membrane in this study.

3.2.3. Gas flow considerations

One major issue of our setup concerns the application of the co-axial gas flow to aid the spray transmission through the membrane. Unfortunately, the exact correspondence of the gas arbitrary units is not provided by the manufacturer of the MS. The spray transmission was evaluated by spraying a solution of Angiotensin III (10 μM in ESI solution) through a 100 μm – PET membrane, at 4 $\mu\text{L}\cdot\text{min}^{-1}$, and with 4 kV. The ESI response representative of the spray transmission was recorded by MS while changing the gas flow. Below gas values of 40 a.u., the signal recorded was rather low, meaning that the spray transmission was not efficient and most of the sample probably adsorb to the membrane. For gas flows ranging from 40 to 60 a.u., the transmission is maximal and equivalent for each of the gas flow values tested. At higher values, the signal slightly decreases. Consequently, in our study, gas flows from 40 to 60 a.u. were used preferentially.

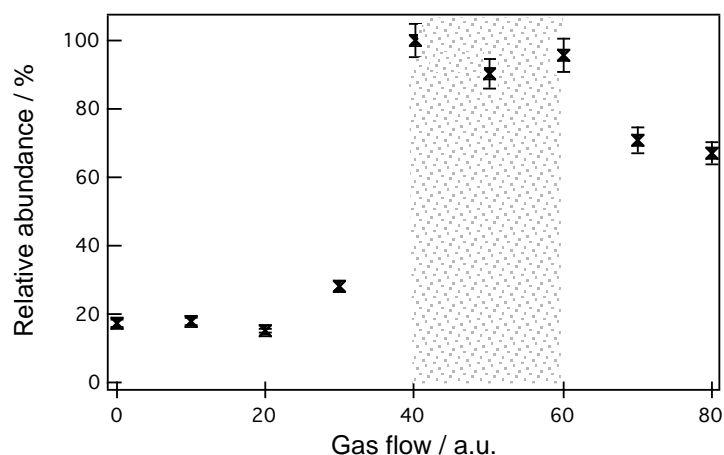


Figure VII- 10 Influence of the gas flow on the spray transmission. A solution of Angiotensin III 10 μM in ESI solution was sprayed at $4 \mu\text{L}\cdot\text{min}^{-1}$ through a PET 100 μm membrane, at a voltage of 4 kV.

3.2.4. Areas of the deposited sample and of the spray impact onto a membrane

Because of the coloured heme of the cytochrome c, this protein was used to evaluate easily the dimensions of both the deposited spots and the spray impact area.

	Volume	Sample area
1	1 μL	1.5 mm^2
2	2 μL	2 mm^2
3	4 μL	2.5 mm^2
4	6 μL	3.5 mm^2
5	8 μL	4 mm^2
6	10 μL	4.5 mm^2



Table VII- 5 Areas of the sample spot on the membrane as a function of the deposited volume. Volumes of cytochrome c solution ($0.1 \text{ mg}\cdot\text{mL}^{-1}$ in water) from 1 to 10 μL were deposited onto the membrane and allowed to dry. A PET membrane of 100 μm was used.

First, different volumes of the protein solution were deposited onto the membrane. Obviously, the dimensions of the spots depend on the properties of the membrane and of the solution in which analytes are suspended and deposited. Here, we used a PET membrane. Different volumes from 1 to 10 μL of cytochrome c ($0.1 \text{ mg}\cdot\text{mL}^{-1}$ in water)

were deposited onto the 100 μm – membrane. The samples were allowed to dry several minutes. Then, the areas of each spot were measured (Table VII-5). In the adjacent figure, one can see that the final spots present lozenge – shapes due to the sample diffusion along the enlaced fibers of the membrane. The spot areas range from 1.5 to 4.5 mm^2 according to the deposited volume.

The second important parameter is the area of the spray impact onto the membrane. A solution of cytochrome c ($0.1 \text{ mg}\cdot\text{mL}^{-1}$ in ESI solution) was sprayed through the 100 μm - membrane during 2 min, at different flow rate and sheath gas flow. The electrospray voltage was 4 kV. As before, the impact area was determined by measuring the dimensions of the red area onto the membrane. Increasing the solution flow rate, or the gas flow, extends the impact area of the spray onto the membrane, which is not totally circular. As example, the spray impact area changed from 0.14 to 0.55 mm^2 by increasing the gas from 40 to 60 a.u., at a fixed flow rate of 4 $\mu\text{L}\cdot\text{min}^{-1}$. The spot n°5 (adjacent figure of Table VII-6) results from four 90° rotations of the membrane with the holder positioned slightly off-axis with respect to the emitter. The spot is larger than in static conditions. Such a rotation might be use to desorb/ionize samples from a larger membrane area.

	Flow rate	Gas flow	Spray impact area
1	8 $\mu\text{L}\cdot\text{min}^{-1}$	40 a.u.	0.55 mm^2
2	8 $\mu\text{L}\cdot\text{min}^{-1}$	60 a.u.	1.25 mm^2
3	4 $\mu\text{L}\cdot\text{min}^{-1}$	60 a.u.	0.55 mm^2
4	4 $\mu\text{L}\cdot\text{min}^{-1}$	40 a.u.	0.14 mm^2
5 ^a	4 $\mu\text{L}\cdot\text{min}^{-1}$	40 a.u.	1.67 mm^2

^a 4x 90° - holder rotation



Table VII- 6 Areas of the spray impact onto the membrane. A concentrated solution of cytochrome c ($0.1 \text{ mg}\cdot\text{mL}^{-1}$ in ESI solution) was electrosprayed during 2 min through the membrane, changing the solution flow rate and the gas flow. The impact zone is recognized by the presence of the red protein deposit onto the membrane. A PET membrane of 100 μm was used.

As illustrated in these two experiments, the sample deposition and spray impact areas onto the membrane are quite limited. In order to get an optimal signal, the sample spot

must be perfectly aligned in the emitter axis, and this is actually the tricky part of the M-DESI method. However, one could see an advantage of the small spray impact in case of surface scanning that would increase the resolution.

3.2.5. Geometry considerations.

The main advantage of the custom-made holder is the possibility to entirely close the ESI source of the instrument, as in normal use. In this position, the membrane is placed at 1 cm from the mass spectrometer inlet. Figure VII-11 reports the influence of the membrane – MS inlet distance on the signal intensity. A solution of Angiotensin III (10 μM in ESI solution) was sprayed through the membrane at 4 $\mu\text{L}\cdot\text{min}^{-1}$, with an applied voltage of 4 kV and a sheath gas of 40 a.u.. PET membranes of 10, 50 and 100 μm mesh size, corresponding to open area of 2%, 24%, 32%, respectively, were tested. The signal intensity of the transmitted protein is at least 10 times larger when the source is closed, *i.e.* with the minimal membrane - MS inlet distance. Then, the signal decreases progressively once the membrane is far away.

Although working with the ESI source close is not practical for membrane alignment, it presents the most efficient spray transmission with the actual setup.

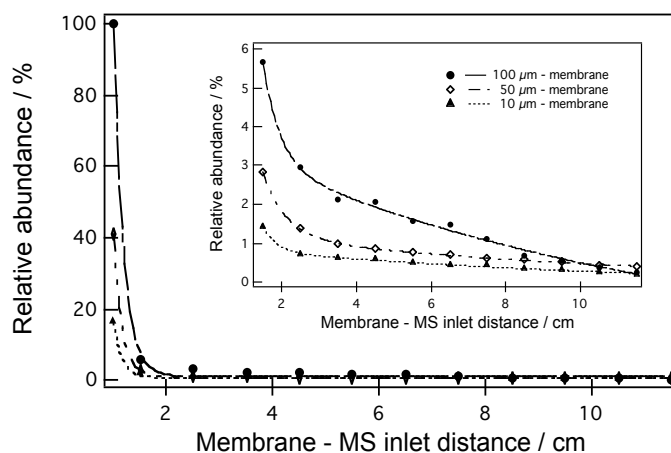


Figure VII- 11 Influence of the membrane – MS inlet distance on the electrospray transmission. The inset figure is a zoomed graph of the same experiment. The ESI emitter – MS inlet was 3mm.

3.2.6. Remarks on the membrane properties

Up to now, membranes composed of PET and PA have been tested with apparently no difference on the peptide/proteins desorption in terms of signal intensity by MS. However, a more precise and quantitative analysis of the sample desorption in function of the membrane properties and the solvent should be performed. For example, the desorption efficiency might be evaluated by quantifying the remaining sample onto the membrane after a DESI-MS experiment by fluorescence microscopy or spectroscopy.

4. Conclusions & Perspectives

The investigation of a new desorption/ionization method inspired from DESI was presented in this chapter. The novelty compared to DESI is that the sample is desorbed from a mesh membrane positioned vertically and in-axis between the electrospray emitter and the mass spectrometer entrance. The feasibility of the method has been demonstrated with proteins and peptides and the first characterizations were carried out on commercial mesh tissues of different open areas.

To hold the membrane, a custom-made holder was designed to fit with the ESI source of our LCQ ion trap mass spectrometer. However, the main issue of the actual setup remains the MS inlet located inside a cavity. The use of a mass spectrometer with a more accessible MS inlet would considerably facilitate the manipulation and alignment of the membrane.

Moreover, the present study was made with sample dried onto a membrane, for desorption experiments. Some trials were also made with wet sample (drop sample), leading to an easier and more rapid analysis. However, a comparison between dry and wet sample analysis need to be more in-depth studied.

Among the surfaces used in DESI, some are conductive. Typically, for small compounds, a potential difference between the ESI emitter and the surface was demonstrated to enhance the analyte detection. It would be interesting to test membranes composed of fibers with a conductive coating, and to evaluate the effect of applying a voltage to the membrane.

Regarding the potential applications, the M-DESI can be suitable to rapidly screen samples after their deposition onto a membrane. The membrane alignment, positioning and translation are therefore the main issue of this application. The direct perspective is to use the M-DESI

to scan a membrane after protein blotting. Indeed, in gel electrophoresis, the standard procedure consists in extracting the proteins from a gel by blotting onto a membrane (as a PVDF membrane). The proteins are visualized either by staining, immuno-blotting or electrochemistry. The blotting on a mesh membrane and its direct detection by MS would be a smart application for the M-DESI. As an alternative, the proteins could be separated directly on the membrane and analyze on-line by M-DESI MS.

Finally, one could imagine performing reactions, as immuno-affinity or oxido-reduction reactions, onto the membrane and then, analyzing the products by M-DESI.

REFERENCES

1. <http://www.sefar.ch>.
2. <http://cshprotocols.cshlp.org>.
3. Z. Takats, J. M. Wiseman, B. Gologan and R. G. Cooks, Mass spectrometry sampling under ambient conditions with desorption electrospray ionization, *Science* (New York, NY), 2004.
4. A. Venter and R. G. Cooks, Desorption electrospray ionization in a small pressure-tight enclosure, *Analytical Chemistry*, 2007, 79, 6398-6403.
5. R. B. Cody, J. A. Laramée and H. D. Durst, Versatile new ion source for the analysis of materials in open air under ambient conditions, *Analytical Chemistry*, 2005, 77, 2297-2302.
6. Z. Takats, J. M. Wiseman, B. Gologan and R. G. Cooks, Mass spectrometry sampling under ambient conditions with desorption electrospray ionization, *Science* (New York, NY), 2004, 306, 471-473.
7. A. Venter, M. Nefliu and R. Graham Cooks, Ambient desorption ionization mass spectrometry, *TrAC - Trends in Analytical Chemistry*, 2008, 27, 284-290.
8. G. J. Van Berkel, S. P. Pasilis and O. Ovchinnikova, Established and emerging atmospheric pressure surface sampling/ionization techniques for mass spectrometry, *Journal of Mass Spectrometry*, 2008, 43, 1161-1180.
9. R. Haddad, R. Sparrapan and M. N. Eberlin, Desorption sonic spray ionization for (high) voltage-free ambient mass spectrometry, *Rapid Communications in Mass Spectrometry*, 2006, 20, 2901-2905.
10. H. Chen, S. Yang, A. Wortmann and R. Zenobi, Neutral Desorption Sampling of Living Objects for Rapid Analysis by Extractive Electrospray Ionization Mass Spectrometry, *Angewandte Chemie - International Edition*, 2007, 46, 7591-7594.
11. J. Shiea, M. Z. Huang, H. J. Hsu, C. Y. Lee, C. H. Yuan, I. Beech and J. Sunner, Electrospray-assisted laser desorption/ionization mass spectrometry for direct ambient analysis of solids, *Rapid Communications in Mass Spectrometry*, 2005, 19, 3701-3704.
12. P. Nemes and A. Vertes, Laser ablation electrospray ionization for atmospheric pressure, in vivo, and imaging mass spectrometry, *Analytical Chemistry*, 2007, 79, 8098-8106.
13. J. S. Sampson, A. M. Hawkrige and D. C. Muddiman, Generation and Detection of Multiply-Charged Peptides and Proteins by Matrix-Assisted Laser Desorption Electrospray Ionization (MALDESI) Fourier Transform Ion Cyclotron Resonance Mass Spectrometry, *Journal of the American Society for Mass Spectrometry*, 2006, 17, 1712-1716.
14. H. Chen, A. Venter and R. G. Cooks, Extractive electrospray ionization for direct analysis of undiluted urine, milk and other complex mixtures without sample preparation, *Chemical Communications*, 2006, 2042-2044.
15. I. F. Shieh, C. Y. Lee and J. Shiea, Eliminating the interferences from TRIS buffer and SDS in protein analysis by fused-droplet electrospray ionization mass spectrometry, *Journal of Proteome Research*, 2005, 4, 606-612.
16. M. J. Ford and G. J. Van Berkel, An improved thin-layer chromatography/mass spectrometry coupling using a surface sampling probe electrospray ion trap system, *Rapid Communications in Mass Spectrometry*, 2004, 18, 1303-1309.
17. M. Haapala, J. Pöl, V. Saarela, V. Arvola, T. Kotiaho, R. A. Ketola, S. Franssila, T. J. Kauppila and R. Kostianen, Desorption atmospheric pressure photoionization, *Analytical Chemistry*, 2007, 79, 7867-7872.
18. N. Na, M. Zhao, S. Zhang, C. Yang and X. Zhang, Development of a Dielectric Barrier Discharge Ion Source for Ambient Mass Spectrometry, *Journal of the American Society for Mass Spectrometry*, 2007, 18, 1859-1862.
19. Z. Takats, I. Cotte-Rodriguez, N. Talaty, H. Chen and R. G. Cooks, Direct, trace level detection of explosives on ambient surfaces by desorption electrospray ionization mass spectrometry, *Chemical Communications*, 2005, 1950-1952.

20. C. N. McEwen, R. G. McKay and B. S. Larsen, Analysis of solids, liquids, and biological tissues using solids probe introduction at atmospheric pressure on commercial LC/MS instruments, *Analytical Chemistry*, 2005, 77, 7826-7831.
21. W. C. Wetzel, F. J. Andrade, J. A. C. Broekaert and G. M. Hieftje, Development of a direct current He atmospheric-pressure glow discharge as an ionization source for elemental mass spectrometry via hydride generation, *Journal of Analytical Atomic Spectrometry*, 2006, 21, 750-756.
22. L. V. Ratcliffe, F. J. M. Rutten, D. A. Barrett, T. Whitmore, D. Seymour, C. Greenwood, Y. Aranda-Gonzalvo, S. Robinson and M. McCoustra, Surface analysis under ambient conditions using plasma-assisted desorption/ionization mass spectrometry, *Analytical Chemistry*, 2007, 79, 6094-6101.
23. H. Chen, Z. Ouyang and R. G. Cooks, Thermal production and reactions of organic ions at atmospheric pressure, *Angewandte Chemie - International Edition*, 2006, 45, 3656-3660.
24. A. B. Costa and R. G. Cooks, Simulation of atmospheric transport and droplet-thin film collisions in desorption electrospray ionization, *Chemical Communications*, 2007, 3915-3917.
25. A. B. Costa and R. Graham Cooks, Simulated splashes: Elucidating the mechanism of desorption electrospray ionization mass spectrometry, *Chemical Physics Letters*, 2008, 464, 1-8.
26. A. Venter, P. E. Sojka and R. G. Cooks, Droplet dynamics and ionization mechanisms in desorption electrospray ionization mass spectrometry, *Analytical Chemistry*, 2006, 78, 8549-8555.
27. D. R. Ifa, N. E. Manicke, A. L. Rusine and R. G. Cooks, Quantitative analysis of small molecules by desorption electrospray ionization mass spectrometry from polytetrafluoroethylene surfaces, *Rapid Communications in Mass Spectrometry*, 2008, 22, 503-510.
28. T. J. Kauppila, N. Talaty, P. K. Salo, T. Kotiaho, R. Kostainen and R. G. Cooks, New surfaces for desorption electrospray ionization mass spectrometry: Porous silicon and ultra-thin layer chromatography plates, *Rapid Communications in Mass Spectrometry*, 2006, 20, 2143-2150.
29. A. K. Sen, R. Nayak, J. Darabi and D. R. Knapp, Use of nanoporous alumina surface for desorption electrospray ionization mass spectrometry in proteomic analysis, *Biomedical Microdevices*, 2008, 10, 531-538.
30. Z. Tats, J. M. Wiseman and R. G. Cooks, Ambient mass spectrometry using desorption electrospray ionization (DESI): Instrumentation, mechanisms and applications in forensics, chemistry, and biology, *Journal of Mass Spectrometry*, 2005, 40, 1261-1275.
31. M. Volny, A. Venter, S. A. Smith, M. Pazzi and R. G. Cooks, Surface effects and electrochemical cell capacitance in desorption electrospray ionization, *Analyst*, 2008, 133, 525-531.
32. R. Nayak, J. Liu, A. K. Sen and D. R. Knapp, Dual desorption electrospray ionization-laser desorption ionization mass spectrometry on a common nanoporous alumina platform for enhanced shotgun proteomic analysis, *Analytical Chemistry*, 2008, 80, 8840-8844.
33. G. J. Van Berkel, M. J. Ford and M. A. Deibel, Thin-layer chromatography and mass spectrometry coupled using desorption electrospray ionization, *Analytical Chemistry*, 2005, 77, 1207-1215.
34. G. J. Van Berkel and V. Kertesz, Automated sampling and imaging of analytes separated on thin-layer chromatography plates using desorption electrospray ionization mass spectrometry, *Analytical Chemistry*, 2006, 78, 4938-4944.
35. J. M. Wiseman, D. R. Ifa, Q. Song and R. G. Cooks, Tissue imaging at atmospheric pressure using Desorption Electrospray Ionization (DESI) mass spectrometry, *Angewandte Chemie - International Edition*, 2006, 45, 7188-7192.
36. D. R. Ifa, N. E. Manicke, A. L. Dill and R. G. Cooks, Latent fingerprint chemical imaging by mass spectrometry, *Science (New York, NY)*, 2008, 321, 805.
37. V. Kertesz and G. J. Van Berkel, Scanning and surface alignment considerations in chemical imaging with desorption electrospray mass spectrometry, *Analytical Chemistry*, 2008, 80, 1027-1032.

38. T. J. Kauppila, J. M. Wiseman, R. A. Ketola, T. Kotiaho, R. G. Cooks and R. Kostianen, Desorption electrospray ionization mass spectrometry for the analysis of pharmaceuticals and metabolites, *Rapid Communications in Mass Spectrometry*, 2006, 20, 387-392.
39. H. Chen, Z. Pan, N. Talaty, D. Raftery and R. Graham Cooks, Combining desorption electrospray ionization mass spectrometry and nuclear magnetic resonance for differential metabolomics without sample preparation, *Rapid Communications in Mass Spectrometry*, 2006, 20, 1577-1584.
40. Z. Pan, H. Gu, N. Talaty, H. Chen, N. Shanaiah, B. E. Hainline, R. G. Cooks and D. Raftery, Principal component analysis of urine metabolites detected by NMR and DESI-MS in patients with inborn errors of metabolism, *Analytical and Bioanalytical Chemistry*, 2007, 387, 539-549.
41. H. Chen, N. N. Talaty, Z. Takats and R. G. Cooks, Desorption electrospray ionization mass spectrometry for high-throughput analysis of pharmaceutical samples in the ambient environment, *Analytical Chemistry*, 2005, 77, 6915-6927.
42. J. P. Williams and J. H. Scrivens, Rapid accurate mass desorption electrospray ionisation tandem mass spectrometry of pharmaceutical samples, *Rapid Communications in Mass Spectrometry*, 2005, 19, 3643-3650.
43. A. T. Jackson, J. P. Williams and J. H. Scrivens, Desorption electrospray ionisation mass spectrometry and tandem mass spectrometry of low molecular weight synthetic polymers, *Rapid Communications in Mass Spectrometry*, 2006, 20, 2717-2727.
44. M. S. Bereman, L. Nyadong, F. M. Fernandez and D. C. Muddiman, Direct high-resolution peptide and protein analysis by desorption electrospray ionization Fourier transform ion cyclotron resonance mass spectrometry, *Rapid Communications in Mass Spectrometry*, 2006, 20, 3409-3411.
45. Y. S. Shin, B. Drolet, R. Mayer, K. Dolence and F. Basile, Desorption electrospray ionization-mass spectrometry of proteins, *Analytical Chemistry*, 2007, 79, 3514-3518.
46. A. U. Jackson, S. R. Werner, N. Talaty, Y. Song, K. Campbell, R. G. Cooks and J. A. Morgan, Targeted metabolomic analysis of *Escherichia coli* by desorption electrospray ionization and extractive electrospray ionization mass spectrometry, *Analytical Biochemistry*, 2008, 375, 272-281.
47. Y. Song and R. G. Cooks, Reactive desorption electrospray ionization for selective detection of the hydrolysis products of phosphonate esters, *Journal of Mass Spectrometry*, 2007, 42, 1086-1092.
48. I. Cotte-Rodríguez, Z. Takas, N. Talaty, H. Chen and R. G. Cooks, Desorption electrospray ionization of explosives on surfaces: Sensitivity and selectivity enhancement by reactive desorption electrospray ionization, *Analytical Chemistry*, 2005, 77, 6755-6764.
49. D. R. Justes, N. Talaty, I. Cotte-Rodriguez and R. G. Cooks, Detection of explosives on skin using ambient ionization mass spectrometry, *Chemical communications (Cambridge, England)*, 2007, 2142-2144.
50. I. Cotte-Rodriguez and R. G. Cooks, Non-proximate detection of explosives and chemical warfare agent simulants by desorption electrospray ionization mass spectrometry, *Chemical Communications*, 2006, 2968-2970.
51. P. A. D'Agostino, C. L. Chenier, J. R. Hancock and C. R. Jackson Lepage, Desorption electrospray ionisation mass spectrometric analysis of chemical warfare agents from solid-phase microextraction fibers, *Rapid Communications in Mass Spectrometry*, 2007, 21, 543-549.
52. P. A. D'Agostino, J. R. Hancock, C. L. Chenier and C. R. J. Lepage, Liquid chromatography electrospray tandem mass spectrometric and desorption electrospray ionization tandem mass spectrometric analysis of chemical warfare agents in office media typically collected during a forensic investigation, *Journal of Chromatography A*, 2006, 1110, 86-94.
53. D. R. Ifa, L. M. Gumaelius, L. S. Eberlin, N. E. Manicke and R. G. Cooks, Forensic analysis of inks by imaging desorption electrospray ionization (DESI) mass spectrometry, *Analyst*, 2007, 132, 461-467.
54. L. Nyadong, M. D. Green, V. R. De Jesus, P. N. Newton and F. M. Fernandez, Reactive desorption electrospray ionization linear ion trap mass spectrometry of latest-generation

- counterfeit antimalarials via noncovalent complex formation, *Analytical Chemistry*, 2007, 79, 2150-2157.
55. N. E. Manicke, T. Kistler, D. R. Ifa, R. G. Cooks and Z. Ouyang, High-Throughput Quantitative Analysis by Desorption Electrospray Ionization Mass Spectrometry, *Journal of the American Society for Mass Spectrometry*, 2009, 20, 321-325.
56. J. E. Chipuk and J. S. Brodbelt, Transmission Mode Desorption Electrospray Ionization, *Journal of the American Society for Mass Spectrometry*, 2008, 19, 1612-1620.
57. J. E. Chipuk and J. S. Brodbelt, The Influence of Material and Mesh Characteristics on Transmission Mode Desorption Electrospray Ionization, *Journal of the American Society for Mass Spectrometry*, 2009, 20, 584-592.

CHAPTER VIII.

Conclusions & Perspectives

Designing a fully integrated miniaturized analytical platform for proteomic studies is a great challenge for any analytical chemist. One could imagine a complete platform combining sample preparation, separation, reactor and detection units all integrated in a microsystem or coupled to a dedicated instrument such as a mass spectrometer.

Actual mass spectrometry-based proteomic studies rely indeed on the development of analytical methodologies and instrumentation progress. The sensitivity of protein identification can be enhanced in several ways using, for example, sample pre-fractionation, pre- or post-column modification of proteins/peptides, or high-resolution mass spectrometry to name just a few. In this context, the primary objective of this work was to investigate operational units of miniaturized systems with the long term goal to combine them in a fully integrated proteomic platform.

Chemical labeling of peptides was demonstrated in the past to enhance peptide ionization and subsequently, their detection by MS, or to insure the protein identification score by adding information about the peptidic sequence, as the number of rare amino acids like cysteines. One of the first objectives was to develop an electrospray microchip emitter including an efficient on-chip post-column peptide derivatization unit to be used directly in a LC-MS workflow. Two directions were investigated to enhance on-chip chemical reactions by passive mixing. The first method consists in optimizing a classical sandwich mixer-reactor using finite-element simulations. The diffusive properties ratio of the molecules to react was demonstrated to be an important factor to take into account in such a mixer-reactor. In

addition, confining the reaction as close as possible to the walls by decreasing the outer flow rate significantly increases the reaction extent.

The second method explored as an alternative to the sandwich mixer-reactor was to passively perturb the flow directly onto the electrospray emitter microchip. For this, a mixing unit made of parallel grooves as well as a microchannel junction to provide the chemical reagent were added to the device demonstrating a good mixing efficiency within the short residence time in the microchannel. This last device was implemented in a LC-MS workflow to achieve post-column modification of peptides. The on-line derivatization of tryptic cysteinyl peptides with benzoquinone was successfully demonstrated with this electrospray micromixer chip, showing a more confident and accurate protein identification by peptide mass fingerprinting when adding information on the peptidic sequence. This work showed good promise as interface between LC and MS because of its ability to maintain a continuous spray despite the evolution of the eluent and without the need of gas flow.

Another line of investigation relies on the immobilization of the stationary phase to perform on-chip reactions. Magnetic beads have proven to be efficient tools to reversibly immobilize a stationary phase. A novel design of polymer chip with an integrated magnetic track array was conceived to enhance the bead trapping along the microchannel by controlling the magnetic field distribution. This first study was of great interest for applications such as on-chip affinity separation, purification of biological sample or pre-concentration just before mass spectrometry analysis.

In the light of high-throughput analysis, multiplexing of MS analysis was investigated as well. An electrospray microchip integrated up to 6 parallel channels enabled to successively screen different samples and perform relative quantification. Many developments on the multi-track electrospray chip are conceivable. One could imagine immobilizing differently coated magnetic beads into the parallel channels to screen a sample with different antibody-coated beads for allergen studies (Figure VIII-1).

As a further development, the on-line LC-MS post-column derivatization method could be implemented on a multi-track electrospray device. The flow coming from the HPLC system can be divided on-chip into two sub-flows, one part of the analytes could be subjected to on-line quantitative tagging while the other part serves as blank. The analysis time will then be reduced to a single run for routine cysteine counting in peptides when successively electrospraying both samples in parallel. In addition, the multi-track electrospray chip can be

used for high mass accuracy measurements with a reference channel (as with TOF, FT-ICR or Orbitrap mass spectrometers). Outside of the MS field, multi-track electrospray devices can be very useful tools for layer-by-layer deposition onto a surface, without any cross-contamination.

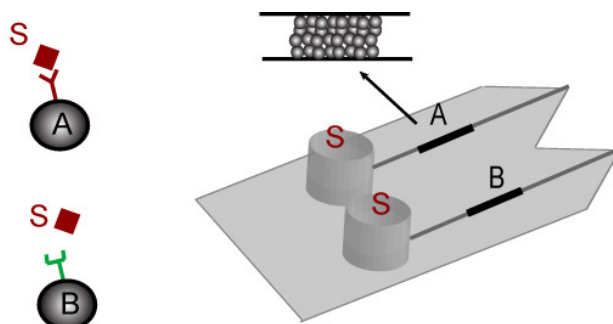


Figure VIII- 1 Illustration of the use of the “multi-track” electrospray chip (MTEC) to screen a biological sample (S) by various antibody-coated magnetic beads in parallel channels. Immobilized antigen could further be detected after elution by on-line mass spectrometry.

Finally and in parallel to the development of miniaturized analytical devices, a novel ionization method has been investigated to enable rapid and sensitive analyte identification after chromatographic separation. The method so-called membrane desorption electrospray ionization (M-DESI) presents the advantage of an in-axis analyte desorption over the traditional DESI. Preliminary results were presented in this thesis opening the door to a full range of applications. Among all of them, reactive desorption occurring between a reactant deposited onto the membrane and another provided by the spray could be investigated. Similarly, reactions occurring on the membrane might be directly probed by rapid desorption/ionization mass spectrometry. Moreover, the study of proteins separated by gel electrophoresis and blotted on the membrane would benefit of a fast scanning identification by mass spectrometry (Figure VIII-2). Paper chromatography or electrophoresis directly on a membrane could also be hyphenated to this ionization technique.

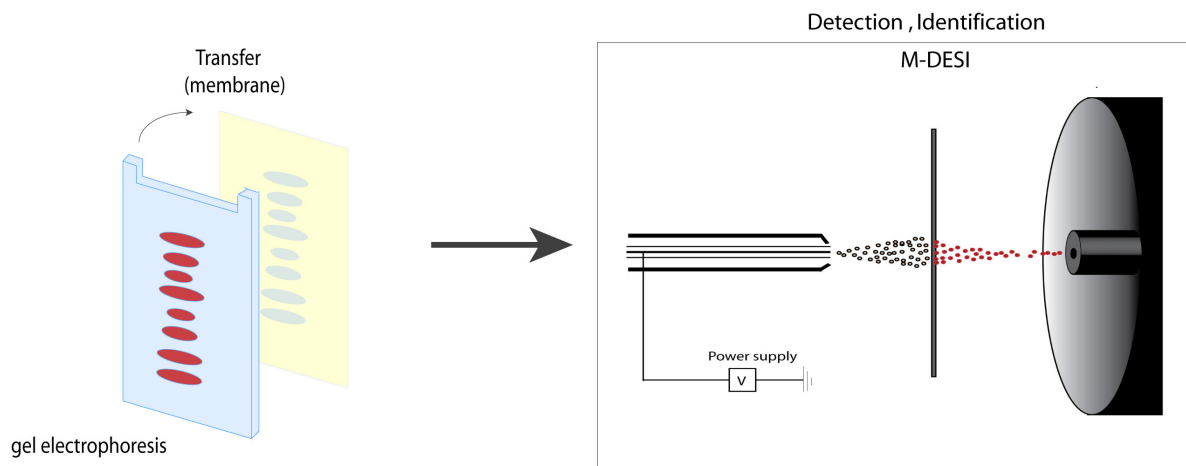


Figure VIII- 2 Illustration of the potential application of the membrane desorption electrospray ionization (M-DESI) to screen a membrane after gel electrophoresis blotting.

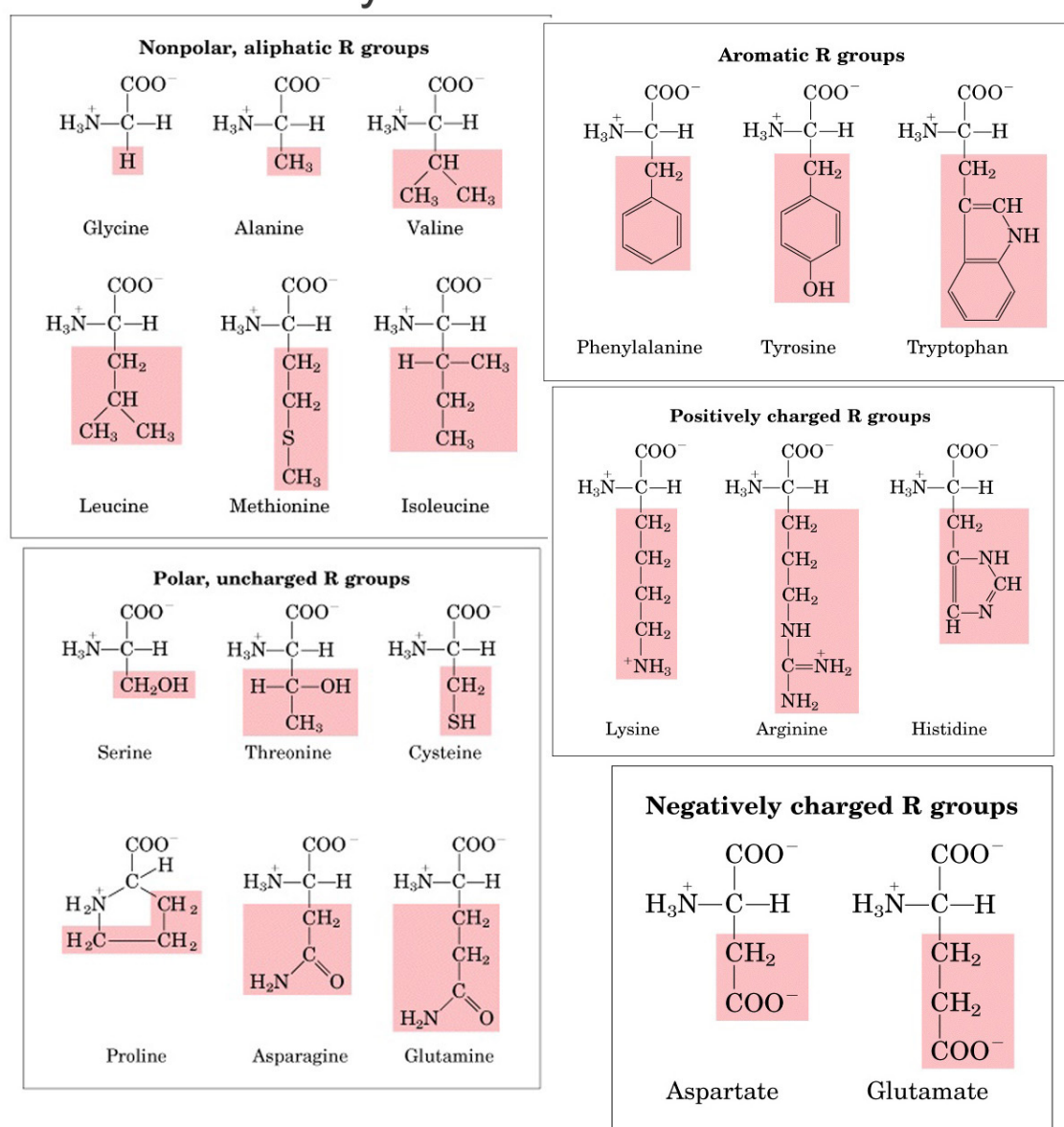
From a more general point of view, it is interesting to put this work in perspective to other fields of application, and not to restrict it to protein studies. The scientific community is now facing up new challenges in “systems biology” by considering the biological problematics at a system-level. The understanding of biological interactions between different levels, *i.e.* between gene -, transcript -, protein -, metabolite- level..., is therefore of major importance, and relies mainly on cascades of regulation processes. The study of post-translational modification is among the most studied regulation process, and was a great defy for analytical chemists. Glycosylations as example are involved in several biochemical processes and cellular communications, and present a large complexity because of the fine structural change between glycans. Mass spectrometry – based analytical methodologies are now viewed as an evident tool in glycobiology and are actually in transition towards miniaturized analytical platforms^a. Last but not least, miniaturized analytical systems can also present a great potential in metabolite studies that are indeed of major importance in the understanding of cellular pathways under normal or adverse conditions. Over the last years, the general opinion was aware about the impact of chemical or physical agents on human health but also on the environment, and the need of a strict regulation on it. Miniaturized analytical and portable devices dedicated to rapid point-of-care analysis or to in-lab characterization and quantitation of metabolites could be a great perspective to this thesis work. Analytical

^a Chip-mass spectrometry for glycomic studies, L. Bindila, J. Peter-Katalinic, Mass spectrometry reviews, 2009, Vol. 28, 223-253.

microsystems are on the slope of enlightenment and have still to demonstrate all their potentiality in biological science.

APPENDIX I.

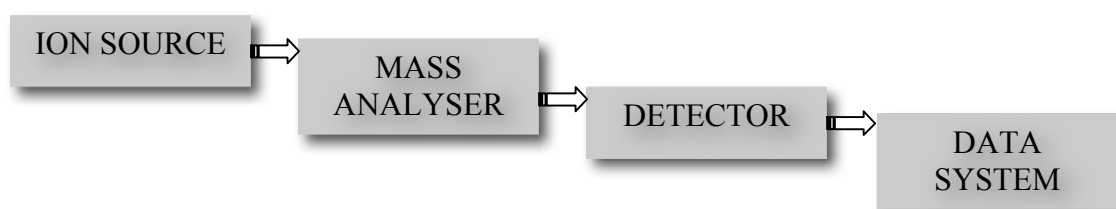
Amino acids



APPENDIX II.

Basics of a mass spectrometer

A mass spectrometer is a powerful analytical instrument that enables the transfer of ions from liquid or solid phase to gas phase, and subsequently their separation and detection according to their m/z ratio. The mass spectrometer can be divided in four basic parts: the ion source, the mass analyzer, the detector and the data system. The types of MS differ by their physical principles, their performance standards, their mode of operation, and their ability to support specific analytical strategies.^{1, 2}



Units of a mass spectrometer

Ionization source

In the source region, molecules are ionized and then, accelerated into the mass analyzer. Various ionization techniques are coupled to mass spectrometry, and are chosen in accordance to the nature of the molecules to analyze. *Electron ionization* (EI) and *chemical ionization* (CI) are generally used for gases and vapor. Two techniques often used with liquid and solid biological samples are *electrospray ionization* (ESI) and *matrix-assisted laser desorption/ionization* (MALDI). *Inductively coupled plasma* (ICP) sources are used primarily for metal analysis on a wide array of sample types. Others include *fast atom bombardment*

(FAB), *thermospray*, *atmospheric pressure chemical ionization* (APCI), *secondary ion mass spectrometry* (SIMS) and *thermal ionization*. Most recently ambient desorption ionization (DI) techniques also appeared in the MS field, as the *desorption electrospray ionization* (DESI) technique.

Mass analyzers

The mass analyzer is the heart of the MS. In this part, the ions are separated, either in space or in time, according to their mass to charge ratio. All mass spectrometers are then based on dynamics of charged particles in electric and magnetic fields in vacuum. The high vacuum system maintains a low pressure, which minimizes ion-molecule reactions, scattering, and neutralization of the ions. There are many types of mass analyzers, using either static or dynamic fields, and magnetic or electric fields.

Quadrupole analyzers use the stability of the trajectories in oscillating electric fields to separate ions according to their m/z ratios. In ion trap (IT) mass analyzers, ions are trapped and can therefore be accumulated over time in a physical device. IT uses an oscillating electric field to store ions. They are characterized by MS/MS capabilities with unmatched sensitivity and fast data acquisition. However, IT analyzers have limited resolution, low-ion trapping capacity, and limited mass accuracy. The development of linear ion trap (LIT) analyzers with higher ion trapping capacities has expanded the dynamic range and the overall sensitivity of this technique.

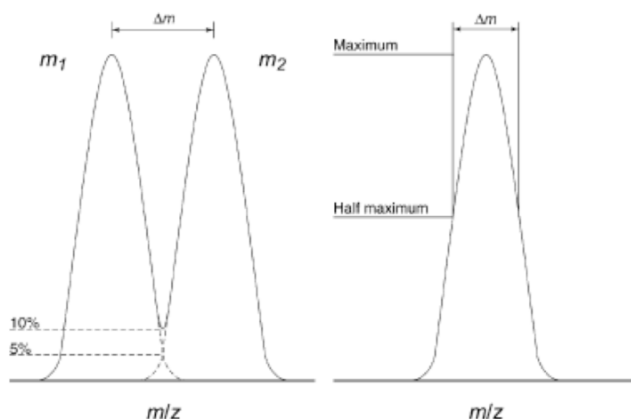
In time-of-flight (ToF) and hybrid ToF instruments (Q-Q-ToF, ToF-ToF), the m/z ratio of an analyte ion is deduced from its flight time through a tube of specified length that is under vacuum.

Fourier transform - ion cyclotron instrument (FT-ICR) with external ion source represents a breakthrough in terms of resolving power and mass accuracy. The development of LIT-ICR hybrid instruments allows full parallel MS and MS/MS acquisition.

Finally, orbitrap mass analyzers are one of the last developed mass analyzer and are actually experiencing a widespread success. In orbitrap, ions are separated in an oscillating electric field and present characteristics almost similar to an FT-ICR instrument in terms of resolution and mass accuracy.

The performance of a mass analyzer is evaluated according to the following parameters, the m/z range (or mass range), the mass resolving power, the mass resolution, the mass precision (repeatability) and finally, the mass accuracy.

Explicitly, the mass accuracy (ppm) and resolution of the mass analyzers are defined by the following relationships:



$$\text{Mass Accuracy} = \frac{m_{\text{observed}} - m_{\text{theory}}}{m_{\text{theory}}} \times 10^6 \quad (\text{ppm})$$

$$\text{Resolution} = \frac{m}{\Delta m}$$

where m is the m/z of the peak of interest and Δm is the peak width in term of m/z .

Resolution can be measure using the “10% valley” definition, as most commonly applied when using magnetic-sector instrument, or by using the full width at half maximum (FWHM) definition, which is typically used during the analysis of data acquires as from IT or TOF mass spectrometers. In the next Table, the FWHM is considered in the calculations.

The following Table presents some characteristics of the mainly used mass spectrometers:

	Mass range	Mass Accuracy (ppm)	Resolution	Cost
Quadrupole or Ion trap	< 2000 or 4000	200 - 300	3000-5000	Low
TOF	unlimited	20 - 100	10^4 - 10^5	medium
Orbitrap	< 6000	1 - 50	10^5	medium/high
FT-ICR	<4000	1 - 50	10^5 - 10^7	high

Detector and data system.

After separation in the mass analyzer, ions are transferred towards the detector. Several types of detectors exist as Faraday cylinder, electron multipliers, microchannel plates, photons multipliers, etc. Finally, the signal is transmitted to the data system that insures three main functions: 1) the control of the mass spectrometer, 2) the acquisition of the data from the mass spectrometer, and 3) the interpretation of the data.

REFERENCES

1. B. Domon and R. Aebersold, *Science (New York, NY)*, 2006, 312, 212-217.
2. R. De Hoffmann and V. Stroobant, *Wiley*, 3rd edition. 2007.

CURRICULUM VITAE

PERSONAL

Mélanie ABONNENC

Citizenship: French

Date of birth: 26th October 1980

ACADEMIC

- 2006–2009** **PhD student: “ Miniaturized analytical systems for mass spectrometry – based protein studies”.** Supervisor: Prof. Hubert Girault.
Laboratoire d'Electrochimie Physique et Analytique.
Ecole Polytechnique Fédérale de Lausanne (Lausanne, CH)
- 2003** **MSc sin Bioinformatics for Genomics and Post-genomics, with Honours.**
Blaise Pascal University (Clermont-Ferrand, FR)
- 2001** **Bachelor's degree in Cellular and Molecular Biology, with Honours.**
Joseph Fourier University (Grenoble, FR)

PROFESSIONAL EXPERIENCE

- 2006–2009** **ECOLE POLYTECHNIQUE FEDERALE DE LAUSANNE, Lausanne, Switzerland**
 Teaching assistant.
- 2003 - 2005** **SILICON BIOSYSTEMS, Bologna, Italy**
 Marie Curie Fellow: Development of biological and *in-silico* protocols for the validation of an individual cell-sorting lab-on-a-chip prototype.
- 2003** **BIOCHIP LABORATORY, CEA Grenoble, France**
 Master's degree training (6 months): Development of *in-silico* procedures and conception of a graphical user interface for an individual cell sorting system. (*European project MeDICS*).
- 2002** **DNA BIOCHEMISTRY LABORATORY, University hospital, Grenoble, France.**
 Bachelor's degree training (1 month): Optimization of a denaturing HPLC (DHPLC) system for high throughput screening of genetic mutations.
- 2000 & 2001** **FRUIVAL, Portes-lès-Valence, France**
 Summer work: Laboratory assistant (control and quality insurance).

SKILLS / QUALIFICATIONS

- Mass spectrometry** ESI-Ion Trap, ESI-TOF, MALDI-TOF, LC-MS
- Separation techniques** HPLC, IEF (IPG, OFF-GEL), SDS-PAGE and western blot
- Microfabrication** Laser photoablation: Fabrication of polymer microchip with the following functionalities: electrospray emitters, micromixers, magnetic bead trapping.
- Biology** Knowledge in cellular and molecular biology. Techniques of cell culture and molecular biology.
- Others**
- Management of trainees at different levels (BSc, MSc) on analytical instrumentation (mass spectrometry, IEF) and cellular biology.
 - Referee for the Lab-on-a-Chip journal

COMPUTER SKILLS	Operating systems MacOS X, Windows, Linux Softwares Microsoft Office, Papers, Endnote, Igor, Flux-Expert Bioinformatics Mascot, Profound
LANGUAGES	French (mother tongue), English (Fluent), Italian (Fluent), Spanish (basic)
PEER-REVIEWED PUBLICATIONS	<p>Magnetic track array for efficient bead capture in microchannels. M. Abonnenc, A.L. Gassner, J. Morandini, J. Josserand, H. H. Girault, Anal. Bioanal. Chem., Accepted for publication, 2009.</p> <p>Magnetic forces produced by rectangular permanent magnets in static microsystems. A.L. Gassner, M. Abonnenc, H.X. Chen, J. Morandini, J. Josserand, J.S. Rossier, J.M. Busnel, H.H. Girault, Lab Chip, 2009, DOI: 10.1039/B901865D.</p> <p>Sandwich mixer-reactor: Influence of the diffusion coefficient and flow rate ratios. M. Abonnenc, J. Josserand, H.H. Girault, Lab Chip, 2009, 9, 440-448.</p> <p>Electrospray Micromixer Chip for On-line Derivatization and Kinetic Studies, M. Abonnenc, L. Dayon, B. Perruche, N. Lion, H.H. Girault, Anal.Chem., 2008, 80 (9), 3372-3378.</p> <p>Multitrack electrospray chips, L. Dayon*, M. Abonnenc*, M. Prudent*, N. Lion, H.H. Girault, J. Mass. Spectrom., 2006, 41(11): 1484-1490. (* equal authorship)</p> <p>Electronic sorting and recovery of single live cells from microliter sized sample. A.B. Fuchs, A. Romani, D. Freida, G. Medoro, M. Abonnenc, L. Altomare, I. Chartier, D. Guergour, C. Villiers, P.N. Marche, M. Tartagni, R. Guerrieri, F. Chatelain, N. Manaresi. Lab Chip, 2006, 6 (1):121-126.</p> <p>Dielectrophoresis-based 'Lab-on-a-chip' devices for programmable binding of microspheres to target cells. M. Borgatti, L. Altomare, M. Abonnenc, E. Fabbri, N. Manaresi, G. Medoro, A. Romani, M. Tartagni, C. Nastruzzi, S. Di Croce, A. Tosi, I. Mancini, R. Guerrieri, R. Gambari. Int. J. Oncol., 2005, vol. 27, no. 6, pp. 1559-1566</p> <p>Teaching cells to dance: The impact of transistor miniaturization on the manipulation of populations of living cells. M. Abonnenc, L. Altomare, M. Baruffa, V. Ferrarini, R. Guerrieri, B. Iafelice, A. Leonardi, N. Manaresi, G. Medoro, A. Romani, M. Tartagni, P. Vulto. Solid-State Electronics, 2005, 49 (5), 674-683.</p>
NON PEER-REVIEWED PUBLICATIONS	<p>Method for selective cell lysis based on dielectrophoresis. G. Medoro, M. Abonnenc, A. Fittipaldi, A. Simoncelli, A. Romani, R. Guerrieri, N. Manaresi. In Proceedings of the 10th International Conference on Miniaturized Systems for Chemistry and Life Sciences (MicroTAS 2006)</p> <p>A Dielectrophoretic Microchip for Controlled Cell Targeting With Functionalized Microspheres. M. Abonnenc, M. Borgatti, A. Romani, L. Altomare, E. Fabbri, I. Mancini, G. Medoro, D. Freida, M. Tartagni, C. Nastruzzi, R. Gambari, O. Baricordi, R. Rizzo, R. Guerrieri, N. Manaresi. NanoBioTechnology, vol. 1, no. 3, September 2005</p> <p>Electronic sorting and recovery of single live cells from microliter sized samples. A.B. Fuchs, D. Freida, M. Abonnenc, G. Medoro, L. Altomare, A. Romani, I. Van Uitert, M. Tartagni, R. Guerrieri, F. Chatelain, N. Manaresi. The 9th International Conference on Miniaturized Systems for Chemistry and Life Sciences (MicroTAS), Proceedings of. October 2005</p> <p>Dielectrophoretic cage-speed separation of bio-particles. G. Medoro, P. Vulto, L. Altomare, M. Abonnenc, A. Romani, M. Tartagni, R. Guerrieri, N. Manaresi. Proceedings of IEEE Sensors 1, art n° M2L-D.4, 76-79.</p>

NON PEER-REVIEWED PUBLICATIONS

Method for selective cell lysis based on dielectrophoresis. G. Medoro, M. Abonnenc, A. Fittipaldi, A. Simoncelli, A. Romani, R. Guerrieri, N. Manaresi. In Proceedings of the 10th International Conference on Miniaturized Systems for Chemistry and Life Sciences (MicroTAS 2006)

A Dielectrophoretic Microchip for Controlled Cell Targeting With Functionalized Microspheres. M. Abonnenc, M. Borgatti, A. Romani, L. Altomare, E. Fabbri, I. Mancini, G. Medoro, D. Freida, M. Tartagni, C. Nastruzzi, R. Gambari, O. Baricordi, R. Rizzo, R. Guerrieri, N. Manaresi. NanoBioTechnology, vol. 1, no. 3, September 2005

Electronic sorting and recovery of single live cells from microliter sized samples. A.B. Fuchs, D. Freida, M. Abonnenc, G. Medoro, L. Altomare, A. Romani, I. Van Uitert, M. Tartagni, R. Guerrieri, F. Chatelain, N. Manaresi. The 9th International Conference on Miniaturized Systems for Chemistry and Life Sciences (MicroTAS), Proceedings of. October 2005

Dielectrophoretic cage-speed separation of bio-particles. G. Medoro, P. Vulto, L. Altomare, M. Abonnenc, A. Romani, M. Tartagni, R. Guerrieri, N. Manaresi. Proceedings of IEEE Sensors 1, art n° M2L-D.4, 76-79.

New perspectives and opportunities from the wild west of microelectronic biochips. N. Manaresi, M. Abonnenc, V. Auger, P. Vulto, A. Romani, L. Altomare, M. Tartagni, R. Guerrieri. Proceedings – Design, Automation and Test in Europe, art. N° 1395738, 1092-1093.

PATENTS

Method for the selection and/or the processing of particles, in particular cells (Patent WO2007119154). M. Abonnenc, N. Manaresi, G. Medoro.

Methods and apparatuses for selection and/or processing of particles, in particular for selective and/or optimized lysis of cells (Patent WO2007116312). N. Manaresi, G. Medoro, M. Abonnenc.

ORAL PRESENTATIONS

Sandwich mixer-reactor: Influence of the diffusion coefficient and flow rate ratios. M. Abonnenc, J. Josserand, H.H. Girault, SCS fall meeting 2009, Lausanne.

Polymer microchip with integrated magnetic tracks for multi-plug bead capture: characterizations, advantages, and applications. M. Abonnenc, A-L. Gassner, J. Josserand, H.H. Girault. MSB 2009, Boston.

Electrospray micromixer for on-chip real-time LC-MS derivatization of tryptic peptides. M. Abonnenc, L. Dayon, B. Perruche, J. Josserand, N. Lion, H.H. Girault. MSB 2008, Berlin.

Induction of Biologically Significant Interactions Between Individual Cells and Microbeads on a Dielectrophoretic Microchip. M. Abonnenc, M. Borgatti, A. Romani, L. Altomare, E. Fabbri, G. Medoro, D. Freida, M. Tartagni, C. Nastruzzi, R. Gambar, R. Guerrieri, N. Manaresi. NanoBioEurope 2005, Münster.

POSTER PRESENTATIONS

On-chip mixing for chemical tagging of peptides during electrospray mass spectrometry. M. Abonnenc, L. Dayon, J. Josserand, B. Perruche, N. Lion and H. H. Girault. SMAP 2007, Pau, France

New designs of polymer electrospray microchip for MS-based proteomics. M. Abonnenc, L. Dayon, M. Prudent, N. Lion, H.H. Girault. 2nd summer school on Mass Spectrometry in Biotechnology and Biomedicine (MSBM), 2007, Dubrovnik, Croatia.